# Development of Technology for Production of Iron – Multiwall Carbon Nanotubes Composite as a Conducting Magnetic Material

## Ph.D. Thesis

**Akshay Kumar**
**(2012RMT9007)**


**Department of Metallurgical and Materials Engineering**
**Malaviya National Institute of Technology Jaipur, India**

**December, 2017**

# Development of Technology for Production of Iron – Multiwall Carbon Nanotubes Composite as a Conducting Magnetic Material

This thesis is submitted as a partial fulfilment
of the Ph.D. programme in Engineering

**Akshay Kumar**
**(2012RMT9007)**


**Department of Metallurgical and Materials Engineering**
**Malaviya National Institute of Technology Jaipur, India**
**December, 2017**

***This thesis is dedicated to***

*My Parents: Sh. Rajendra Singh &Smt. MunniDevi*

*My Wife: Jyoti*

*My Daughter Jiya*

*For their unconditional love, motivation and especially never ending patience*

**MALAVIYA NATIONAL INSTITUTE OF TECHNOLOGY JAIPUR**
**DEPARTMENT OF METALLURGICAL AND MATERIALS ENGINEERING**

# CERTIFICATE

This is to certify that the thesis entitled **"Development of Technology for Production of Iron – Multiwall Carbon Nanotubes Composite as a Conducting Magnetic Material**" is being submitted by me to the Malaviya National Institute of Technology Jaipur for the award of the degree of **Doctor of Philosophy** in Metallurgical and Materials Engineering is a bonafide record of original research work carried out by me. The content of the thesis has been checked using software "Turnitin" for Plagiarism.

I have incorporated all the suggestions/queries/changes raised by the Examiner in the Thesis Evaluation Reports.

**(Akshay Kumar)**

This is to certify that above statement made by the candidate is true to our knowledge.

**M.K Banerjee**
**MoS Chair Professor**
**(Supervisor)**

**Prof. Upender Pandel**
**(Co-Supervisor)**

Ph.D. viva-voce examination of Mr. Akshay Kumar, Research Scholar, was held on 27-12-2017 in Department of Metallurgical & Materials Engineering, MNIT Jaipur. The candidate defended the viva-voce successfully to the satisfaction of Oral Defense Committee. The Committee recommends for the award of Ph.D. Degree.

**Signature of Supervisors** **Signature of External Examiner**

# ACKNOWLEDGEMENTS

First of all, I would like to express my deep gratitude and sincere thanks to my supervisors **MoS Chair Professor M.K.Banerjee** and **Professor UpenderPandel** for their full support, guidance and freedom for work to accomplish the challenges in my research. It is great honor for me to work under their guidance.

My special thanks go to**Dr. Ajaya Kumar Pradhan** Assistant professor, Department of Metallurgical and Materials Engineering MNIT Jaipur, for their consistent help and encouragement throughout my Ph.D. work.

I would like to express my sincere thanks to **Dr. Vishnu Kumar Sharma, Dr. S.K Gupta and Prof Awadhesh Bhardwaj** for being in my DREC committee as well as for their encouragement, analytical insights and recommendations.

I acknowledge **Material Research Centre, MNIT Jaipur** for providing the characterization facilities.

I express my deep appreciation to my friends and co-workers **Mr.Anil Kumar, Mr. MukeshKumar Chowrasia, Mr. Sachin Rathi, Mr. Arun Kumar, Mr. Avnish Gautam, Mr. OrnovMaulik,** and all the post graduate students of the department of Metallurgical and Materials Engineering, MNIT Jaipur for their moral support and help. I would like to extend my sincere thanks to all the faculty and staff members of MNIT, Jaipur for their support during my Ph.D. I would like to thank my parents and my family members for their unconditional love and support. Without them, this thesis would not be possible.

**(Akshay Kumar)**

# *CHAPTER ONE*

## *Introduction*

In this chapter, general introduction about metal matrix (Fe-MWCNTs) nanocomposite and the work carried out in the Ph.D. thesis has been dealt. The importance of the metal matrix composites, their advantages, and applications are introduced in this chapter. Especially, research questions on the Fe-MWCNTs nanocomposites are narrated. In the end, the motivation, objective for the work undertaken, the methodology adopted, and the results are given in brief.

## 1.1 Introduction

Since discovery of carbon nanotubes in early 1990s, the excellent properties of nanotubes have enticed the researchers to make use of this unique material as reinforcement to develop nanocomposites based on various matrices. The use of carbon nanotubes in polymer matrix composites has been a fascinating development in composite science and engineering. This has stimulated the scientists to make use of the properties of carbon nanotubes by way of using them as reinforcement in metal matrix composites [1-9]. However, introducing carbon nanotubes as effective dispersoids in metal matrices is much more difficult than in polymer matrix. Thus, successful fabrication of metal matrix-CNT composites has become a matter of technological challenge to materials engineers and scientists. Intense tendency towards agglomeration of reinforcing nanotubes poses difficulty in mixing these materials with metals; agglomerating tendency of nanotubes is inherited from the Vander Waals forces of attraction among them coupled with its tubular structure of high aspect ratio; thus, production of metal-CNT composite with uniform dispersion of reinforcement is a challenging task. Use of liquid metallurgy has been unsuccessful due to poor wettability of CNTS; also, large density differential between CNT and matrix metal restricts attainment of homogeneous distribution of reinforcing nanotubes within the metal matrix [10].There are reports on successful production of metal-CNT nanocomposites by the employment of essentially a high-energy ball milling (HEBM) technique, commonly referred as mechanical alloying route [11-13]. Following the reported success in fabrication of such composites through mechanical alloying route, wide usage of the technique with different modifications in pretreatment of nanotubes are documented in literature [14-15]. Although there are good number of research reports in synthesizing the carbon nanotube reinforced composites of different metal matrices, information on successful fabrication of iron matrix- multiwall carbon nanotube (MWCNT) reinforced nanocomposites is not abundant in literatures. In view of this it appears that a study on structural evolution in high energy ball milled iron-MWCNT composites of different compositions is warranted. Hence attempts are made to fix the processing conditions in MA route of synthesizing iron-MWCNT composites so

that evolution of means to evade the probable damage in MWCNT structure during ball milling is possible.

It is well known that high energy ball milling of MWCNT leads to a considerable damage to its structure [15]. In fact, prolonged ball milling causes significant physical damage of MWCNTs, thereby making them shortened collapsed of tubular structure and even completely amorphous [16-17]. Accelerated damage of the structure of MWCNT is stated to take place if MWCNTs undergo ball milling with metals like iron [18-19]. The above-mentioned damage, induced by MA technique of production of metal-MWCNT composite degrades the mechanical and physical properties of the composites and thus poses limitation in the functionalities of the composites. Although success in fabrication of metal-MWCNT is recorded elsewhere, the desirable properties as expected due to reinforcement with MWCNT are not yet reproducibly achieved. This deficiency is attributed to difficulty in securing a good interfacial bonding between metal matrix and MWCNTs [18]. Density function theory has been used to simulate the interfacial bonding behavior in metal-CNT composites [20-21]. Effectiveness in interfacial bonding may be enhanced in transition metal-MWCNT composite. Transition metals have 3d vacant orbital and therefore when mixed with MWCNT under high energy collisions, there is a possibility of 3d-2p hybridization between iron and carbon of MWCNT which when happens, leads to an excellent interfacial bonding between the matrix and reinforcing MWCNT [14]. It is therefore envisaged that if the parameters of ball milling are properly controlled, it can lead to optimal damage of outer walls of MWCNT, producing amorphous carbon. These loosely held carbon atoms can undergo hybridization and ensure good interfacial bonding. Also controlled HEBM can give rise to uniform dispersion of well embedded MWCNT composites. Majority of the researches on MWCNT reinforced metal matrix nanocomposites have aimed to secure improvement in mechanical properties. The effect of iron nanoparticles filling within MWCNTs or forming layers of iron nanoparticles on MWCNTs has been amply studied by the researchers [22-25]. However, focused attempt to tailor the dispersion of MWCNTs within iron matrix by way of HEBM for improving the physical properties is not yet documented in literature.

Since transition metal like iron is an excellent material for application in electromagnetic and also since the author is not aware of any systemic study to control the dispersion of MWCNT in iron matrix along with insurance of good interfacial bonding, attempts are made in this investigation to study the feasibility of achieving a good interfacial bonding in an iron-2wt.%MWCNT by evolution of optimal processing conditions. Also, study is done to understand the genesis and nature of structural damage of MWCNT high energy ball milled with iron. Moreover, the effect of process parameters on the magnetic properties of the nanocomposite produced by HEBM is also examined in Chapter five of this thesis.

It has been reported that if a contaminating phase, expectedly, arising out of a reaction between matrix and MWCNT during high energy ball milling, is formed at the interface, the potentials of MWCNT reinforcement for enhancing the properties cannot be appropriately harnessed [14]. However, a different opinion is advocated by other school of thought which claims that the formation of aluminum carbide at the interface in aluminum-MWCNT composite is aiding to securing a good interfacial bonding owing to diminution of wettability angle of reinforcement with the aluminum matrix[15]. In contrast, opposite view that reaction product at the interface is not a necessary condition to secure good interfacial bonding and hence to improve the properties is also reported [26].

Transition metals are known to be very important structural materials for different engineering industries. Again, as mentioned earlier these metals are amenable to 3d-2p hybridization which is stated to help in getting a good interfacial bonding [26]. Also, a number of transition metals are strong carbide formers; thus, formation of transition metal-MWCNT composite by high energy ball milling is conducive to carbide formation of respective metal. In case of iron as the matrix metal the scenario is different. Research report of fabrication of HEBM and spark plasma sintered Titanium- MWCNT composite have shown that there was no carbide formation at the interface [27]. Effect of carbide at the interface on the mechanical properties of metal-MWCNT composites have so far attracted maximum attention of the researcher. Besides being an important structural material for extraordinary mechanical properties, iron as a transition metal, is also useful in

electromagnetic as well as permanent magnets for engineering applications. Unlike other transition metals iron can dissolve carbon to a large extent and at the same time it is a very good carbide former due to its high chemical affinity for carbon.

It has been reported in the previous chapter that when the milling time is higher than one hour, structural degradation of MWCNT in an iron-2wt.%MWCNT composite takes place significantly by way of carbide formation at the interface.

Spark plasma sintering (SPS) technique is considered to be a very efficient consolidation technique of high energy ball milled composite powders [28]; this is possible due to the rapid heating and cooling from the sintering temperature after holding for a short time. Spark plasma sintering not only enables to achieve the theoretical density of the composites due to being sintered at high pressure but also, retards grain growth. In the case of iron as the matrix metal, the probability of damage of MWCNT structure during SPS may not be ignorable due to the reason of high solubility of carbon in iron, possible pressure aided phase transformation of BCC iron, carburizing of iron and hence formation of carbides.

It is anticipated that the amount of MWCNT added to iron matrix is equally a deciding factor as regard to the quantum of damage to take place for a specific milling time. It is experienced that milling time of 1h can avoid extensive damage of MWCNT in iron matrix composite; however, it is not known if a composite containing higher percentage of MWCNT can survive damage under the same milling condition. Hence it is considered meaningful to study the effect of MWCNT content on the physical and mechanical properties of Fe-MWCNT composites fabricated by high energy ball milling for 50 min followed by spark plasma sintering. So attempts are made to understand the evolution of structure of iron - MWCNT composites of varying MWCNT content when it is synthesized by MA route at a fixed milling time followed by spark plasma consolidation technique. Moreover, in view of its importance, the properties of the composites, both mechanical and physical, are tried to be correlated with the processing and structures. The outcome of this part of investigation is elaborated in Chapter six of this thesis.

It is found that, the matrix metals of high affinity with carbon for the formation of its carbide, requires special attention for avoidance of contamination at the interface; development of their composites with MWCNT as reinforcements is a matter of technological concern. As mentioned earlier, there are varying opinions regarding beneficial or detrimental effect of interfacial carbide on the bonding quality between metal and MWCNT; it cannot be refuted that carbides present at the interface always signifies structural damage of MWCNT, which, undoubtedly, disallows achieving the maximum possible advantage accruable from the use of MWCNT as reinforcement. Hence, surface treatment of MWCNT has been carried out by a number of workers, for the sake of alleviating with such difficulty, that are normally emanated from the structural damage of MWCNT at its surface.

Iron is an excellent magnetic material suitable for many applications; again, MWCNT possesses unique electrical properties. It may be expected that suitably produced iron matrix- MWCNT nanocomposite can have extraordinary combination of magnetic and electrical properties. It is reported elsewhere that surface treatment of MWCNT by silver coating may be accomplished for use as reinforcing material for nickel based composites. Such silver coated MWCNT used as reinforcement in nickel matrix composites have significantly enhanced its electrical conductivity and mechanical property. It seems worthy to investigate into the effect of silver doping on the structure and physical properties of Fe-MWCNT composites of varying MWCNT content under optimized high energy ball milling conditions. In anticipation of the formation of a silver layered reinforcing MWCNT in the matrix of iron based HEBM composites, the present investigation is carried out to probe into the effect of MWCNT percent on the structure and properties of silver doped composites. Further, effort is also exerted to understand the role of silver doping in influencing the interfacial structure and hence the final properties of Fe-MWCNT composites. The details of this research are narrated in Chapter 7.

It is shown in the previous chapter that high energy ball milling of iron-2wt.% MWCNT experiences unwanted interfacial reaction after 1 h of high energy ball milling. Also, the effect of the amount of MWCNT on the structure and

properties of iron-MWCNT composites is already investigated and described in the previous chapters. The above study has shown that beyond a limiting value of ~3wt% of MWCNT, appreciable damage of the MWCNT structure is caused due to high energy ball milling of iron-MWCNT composite for 50 min. It is further observed by the present author and also by the other investigators [26-28] that higher milling time yields a better dispersion of MWCNT and helps to avoid agglomeration tendency of MWCNT at its higher concentration.

It is apparent that the role of milling time in excess of one hour may give more insight into the structure and property evolution in iron matrix composites reinforced with varying percentage of MWCNT. There is no report about the effect of MWCNT content on the structural integrity of reinforcing phase when it is ball milled with iron matrix for more than 1h milling time, viz., and 2h. For this reason effort is made to examine the effect of MWCNT content onto the structural stability and the achievable properties of Fe-MWCNT composite after 2h milling.

Spark plasma sintering method of consolidation of composite powder produced by high energy ball milling has helped to achieve theoretical density due to being sintered under pressure. In general, good structural stability can be obtained by spark plasma sintering. In the case of iron as matrix metal, the problem arising out of high diffusivity of carbon in iron even at the low sintering temperature must be paid due attention for securing a structurally sound nanocomposite. A high thermodynamic driving force for dissolution of carbon in iron in a situation of high carbon potential can induce damage of MWCNT even during spark plasma sintering process. So, the Fe-MWCNT nanocomposite produced by HEBM followed by SPS is not free from the risk of extra structural damage, which may appreciably deteriorate its physical and mechanical properties. Since there is no document on the systematic study for gaining the knowledge about the structural damage if caused by spark plasma sintering of 2h ball milled Fe-MWCNT composites, it is considered important to carry out detailed investigation in the matter.

Therefore, attempts are made to study the effect of MWCNT content on the structure and properties of iron matrix composites after they are spark plasma sintered following high energy ball milling for 2h. The details of results of this

investigation along with adequate explanations are presented in Chapter 8 of the thesis being submitted.

## 1.2 Objectives of the Research Work

The main objectives of present work have outlined as follows

- Effect of high energy ball milling on the structure of iron –multiwall carbon nanotubes (MWCNTs) composite.
- Development of a novel MWCNTs reinforced iron matrix nanocomposite through powder metallurgy route.
- Effect of MWCNTs content on the structure and properties of spark plasma sintered iron-MWCNTs composites synthesized by high energy ball milling.
- Effect of silver doping on the structure and properties of spark plasma sintered $Iron_X$- wt.% MWCNT composites (x=1,2,3 and 4 wt.%) synthesized by high energy ball milling
- Effect of fabrication process on structure and properties of Iron-x wt.% MWCNTs composites (x=0.5,1, 2 and 3wt%)

## REFERENCES


[1] S. Iijima, Helical microtubules of graphitic carbon, Nature 354 (1991) 56–58.

[2] V. N. Popov, Carbon nanotubes properties and application, Mater. Sci. Eng. 43 (2004) 61-10.

[3] S.C.Tjong, Recent progress in the development and properties of novel metal matrix nanocomposites reinforced with carbon nanotubes and grapheme nanosheets, Mater. Sci.Eng. 74 (2013) 281-350.

[4] S.R. Bakshi, D. Lahiri, A. Agarwal, Carbon nanotube reinforced metal matrix composites - a review, Int. Mater. Rev. 55 (2010) 41-64.

[5] J.Z. Liao, M.J. Tan, I. Sridhar, Spark plasma sintered multi-wall carbon nanotube reinforced aluminum matrix composites, Mater. Des. 31 (2010) 96–100.

[6] R. Pérez-Bustamante, C.D. Gómez-Esparza, I. Estrada-Guel, M. Miki-Yoshida, L. Licea-Jiménez, A.S. Pérez-García, R. Martínez-Sánchez, Microstructural and mechanical characterization of Al-MWCNT composites produced by mechanical milling, Mater. Sci. Eng. A. 502 (2009) 159–163.

[7] A. M. K. Esawi, K. Morsi, A. Sayed, M. Taher, S. Lanka, Effect of carbon nanotube (CNT) content on the mechanical properties of CNT-reinforced aluminium composites, Compos Sci Technol. 70 (2010) 2237–2241.

[8] H. Kwon, D.H. Park, J.F. Silvain, A.Kawasaki, Investigation of carbon nanotube reinforced aluminum matrix composite materials, Compos. Sci. Technol. 70 (2010) 546–550.

[9] C. Suryanarayana, N. Al-Aqeeli, Mechanically alloyed nanocomposites, Prog. Mater. Sci. 58 (2013) 383–512.

[10] H. T. Son, T.S. Kim, C. Suryanarayana, B.S. Chun, Homogeneous dispersion of graphite in a 6061 aluminum alloy by ball milling, Materials Science and Engineering A348 (2003) 163-169.

[11] D. Jeyasimman, K. Sivaprasad, S. Sivasankaran, R. Narayanasamy, Fabrication and consolidation behavior of Al 6061 nanocomposite powders reinforced by multi-walled carbon nanotubes, Powder Technology 258 (2014) 189–197.

[12] A.M.K. Esawi, K.Morsi, A. Syed, M. Taher, S. Lanka, The influence of carbon nanotube (CNT) morphology and diameter on the processing and properties of CNT reinforced aluminum composites, Compos. A: Appl. Sci. Manuf. 42 (2011) 234–243.

[13] W.U. Yufeng, G.Y. Kim, A.M. Russell, Effects of mechanical alloying on Al 6061- CNT composite fabricated by semi-solid powder processing, Mater. Sci. Eng. A 538(2012) 164–172.

[14] B. Chen, J. Shen, X. Ye, H. Imai, J. Umeda, M. Takahashi, K. Kondoh, Solid-state interfacial reaction and load transfer efficiency in carbon nanotubes (CNTs)-reinforced aluminum matrix composites, Carbon 114 (2017) 198-208.

[15] W. Zhou, S. Bang, H. Kurita, T. Miyazaki, Y. Fan, A. Kawasaki, Interface and interfacial reactions in multi-walled carbon nanotube reinforced aluminum matrix composites, Carbon 96 (2016) 919-928.

[16] J. Liao, M. J. Tan, Mixing of carbon nanotubes (CNTs) and aluminum powder for powder metallurgy use, Powder Technology 208 (2011) 42–48.

[17] S. Khurram, M. Munir, M.Qian, LI .Yuncang, T.D. Oldfield, P. Kingshott, D.M. Zhu, C. Wen, Quantitative Analyses of MWCNT-Ti Powder Mixtures using Raman Spectroscopy: The Influence of Milling Parameters on Nanostructural Evolution, Advanced Engineering Materials17 ( 2015) 1660-1669.

[18] J.Y. Suh, D.H. Bae, Mechanical properties of Fe-based composites reinforced with multi-walled carbon nanotubes, Materials Science& Engineering A 582 (2013) 321–325.

[19] Y.B Li, B.Q.Wei, J. Liang, Q. Yu, D.H Wu, Transformation of carbon nanotubes to nanoparticles by ball milling process. Carbon 37 (1999) 493-7.

[20] Y. He, J. Zhang, Y. Wang, Z.Yu, Coating geometries of metals on single-walled carbon nanotubes, Appl. Phys. Letter96 (2010)063108-3.

[21] S. Yuan, Y. Kong, F. Wen, F. Li, $Fe_4$ cluster adsorbed on single-wall carbon nanotubes: A density functional study, Computational Mater. Science 42 (2008) 83-9.

[22] S.F. Boi, J.Guo, M. Lan, T. Yu, S. Wang, Y. He, J. Wen, G. Xiang, Tuning high magnetizations in foam-like carbon-based films completely filled with α-Fe**,**Carbon 101(2016) 28-36.

[23] T. Peci, M. Baxendale, Length and a-Fe content control of self-organised ferromagnetic nano wires encapsulated by multiwalled carbon nanotubes by low flow-rate CVD, Carbon 98 (2016) 519-525.

[24] F.C. Dillon, A. Bajpai, A. Koos, S. Downes, Z. Aslam, N.Grobert, Tuning the magnetic properties of iron-filled carbon nanotubes**,** Carbon50 (2012) 3674-81.

[25] S. Hudziak, A.Darfeuille, R. Zhang, T. Peijs, G. Mountjoy, G. Bertoni, M. Baxendale, Magnetoresistive phenomena on Fe-Filled carbon nanotube/ elastomer composites, Nanotechnology21 (2010)125505-8.

[26] K.S. Munir, Y. Li, D. Liang, M. Qian, W. Xu, C. Wen Effect of dispersion method on the deterioration, interfacial interactions and re-agglomeration of carbon nanotubes in titanium metal matrix composites, Materials and Design 88 (2015) 138–148.

[27] F. C. Wang,Z. H. Zhang, Y.J. Sun, Y. Liu, Z. Y. Hu, H. Wang, A. V. Korznikov, E. Korznikova, Z.F.Liu, S. Osamu, Rapid and low temperature spark plasma sintering synthesis of novel carbon nanotube reinforced titanium matrix composites, Carbon 95 (2015) 396-407

[28] K. S. Munir, Y. Zheng, D. Zhang, J.Lin, Y. Li,C. Wen, Improving the strengthening efficiency of carbon nanotubes in titanium metal matrix composites, Materials Science & Engineering A 696 (2017) 10–25.

# *CHAPTER TWO*

## *Literature Review*

This chapter covers the literature review for the metal matrix nanocomposites, including the methods adopted for the synthesis of metal matrix nanocomposites. Various routes used to the MWCNT for better dispersion of MWCNT in metal matrix are also explained in detail with suitable illustrations. Emphasis has been given on the structure of the metal matrix-MWCNT composites obtained via various routes and its correlations with the physical and mechanical properties of the composites. The possible applications of metal matrix nanocomposites in the areas needing consideration for mechanical strength, hardness, usage as sensors, electronic devices, data storage device and as super paramagnetic materials are also described in detail.

## 2.1 Introduction

Composite materials consist of a matrix inside which one or more distinct reinforcement phases are distributed. The discovery of carbon nanotubes (CNTs) is believed to be responsible for triggering the nanotechnology revolution. Carbon nanotubes are unique nanostructure materials with extraordinary mechanical, thermal and electrical properties. These properties have inspired the development of nanocomposites with extraordinary properties. The reinforcement (CNT) phase is added with the aim to improve the specific property such as strength, stiffness, toughness, thermal conductivity, electrical conductivity, magnetic property, coefficient of thermal expansion, electromagnetic shielding, damping and wear resistance [1].The challenges faced and the techniques to overcome them for successful commercialization of carbon nanotubes reinforced metal matrix nanocomposites is described elsewhere [2,3].

## 2.2 Carbon Nanotubes

Carbon is unique element that exists in two crystalline forms, diamond and graphite. The new additions to the carbon allotropes family are fullerenes, the closed-cage carbon molecules, for example $C_{60}$ and nanotubes of graphite, popularly known as carbon nanotubes. Discovered in1985 at Rice University, the fullerenes are closed-shell configuration of $sp^2$ hybridized carbon cluster[3]. The famous $C_{60}$, also known as "Bucky ball," is the most thoroughly studied member among the fullerenes and consists of 12 pentagonal and 20 hexagonal rings fused together forming a cage-like structure. This was followed by the discovery of carbon nanotubes which opened up an era in nanoscience and nanotechnology. Carbon nanotubes were discovered by Japanese scientist Sumio-Iijima during the examination of carbon soot produced by arc evaporation of graphite in helium atmosphere [4]. The nanotubes observed in high-resolution transmission electron microscopy (HRTEM) were multi-walled and had a diameter in the range of 4 to 30 nm and length up to 1 μm. Carbon nanotubes are the grapheme sheets of hexagonal carbon rings rolled into long cylinders with both ends capped by fullerene like structures. It was later reported about the synthesis of nanotubes having single walls

[5-6].Table 2.1 shows some of the physical parameters given for the isomers made possible by the different hybridizations of carbon [7].

**Table 2.1**Parameters of carbon atom in various materials [7]

| **Dimension** | **0-D** | **1-D** | **2-D** | **3-D** |
|---|---|---|---|---|
| | $C_{60}$ | Carbon nanotube | Graphite | Diamond |
| Hybridization | $sp^2$ | $sp^2$ | $sp^2$ | $sp^3$ |
| Density (g/cm3) | 1.72 | 1.2-2.0 | 2.26 | 3.515 |
| Bond Length(Å) | 1.4 | 1.44 | 1.42 | 1.54 |
| Electronic Properties | Semiconductor Eg=1.9eV | Metal or semiconductor | Semi-metal | Insulator Eg=5.47eV |

The physical characteristic that predominantly determines the behavior of CNTs is the structure of the carbon atoms within the graphitic sheet. For example, the chirality of the CNT, the twist or wrap-angle of the nanotube with respect to its central axis, determines the electrical characteristics of the tube. The mechanical strength of CNTs is estimated to be higher than 1TPa in the tensile direction [8]; it is also largely affected by the arrangement of the carbon atoms and the general defectiveness of this structuring. CNTs can be grouped into two categories based upon the number of layers of graphite carbon that comprise their sidewalls.

## 2.3 Processing routes

### *2.3.1 Powder Metallurgy Route*

Powder metallurgy (PM) is one of the most common and economic route for the fabrication composite material. This route not only produces products with good dimensional precision, but also imparts good mechanical and physical properties in them. Powder metallurgy route can be sub divided in to four different methods depending on type of pressure and heat shown in figure2.1&figure2.2 shows subdivisions of PM route which can be employed for the fabrication of Fe-CNT composite products.

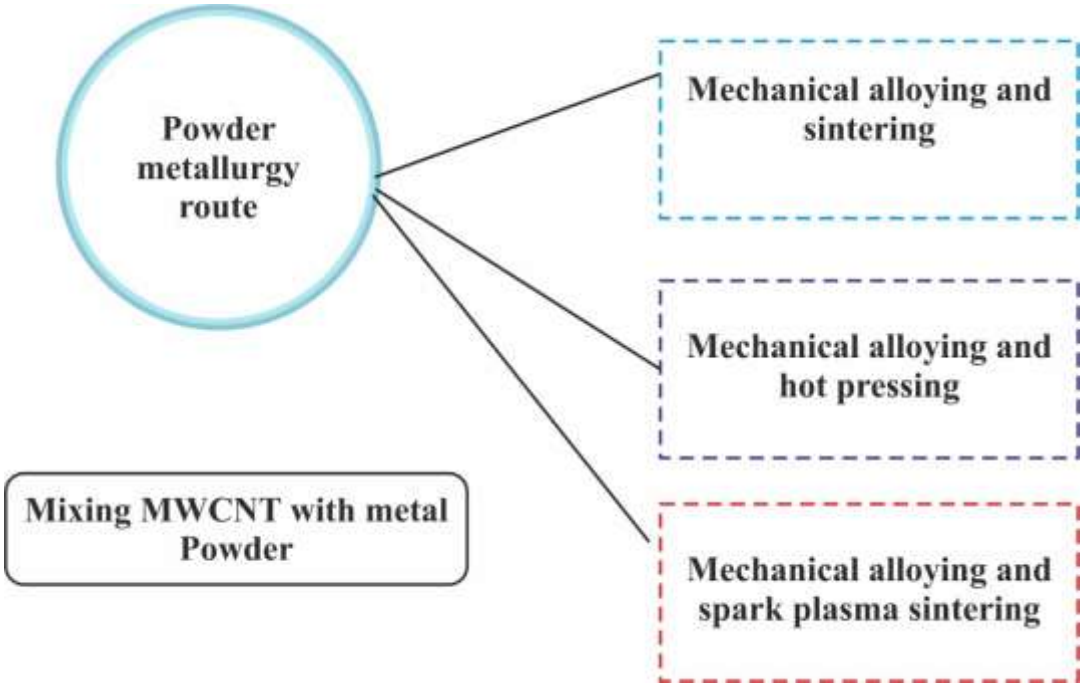


**Figure2.1** Subdivisions of powder metallurgy route

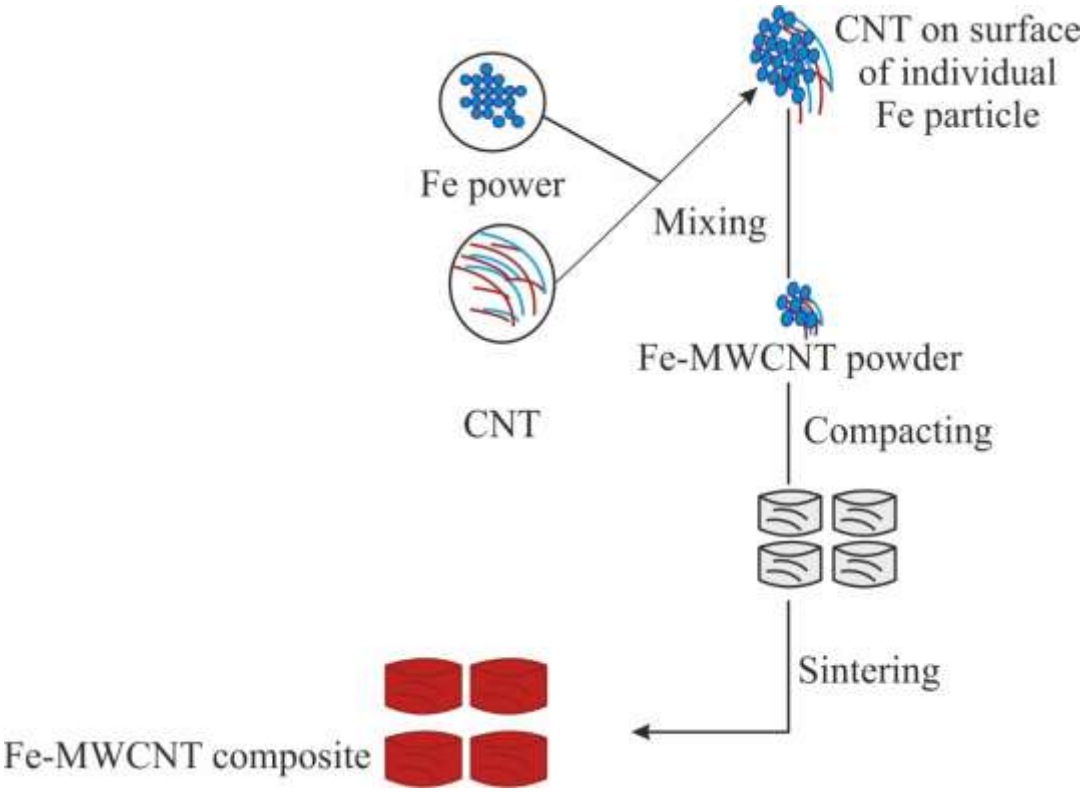


**Figure2.2** PM route for Fe-MWCNT nanocomposites.

### *2.3.2 Fabrication and characterization of aluminum-CNT composites using different techniques*

Powder metallurgy (PM) route can be used to synthesize lightweight aluminum matrix nanocomposites by reinforcing it with optimum percentage of CNTs. Many deficient properties of aluminum such as: hardness, strength, stiffness, wear resistance, corrosion and oxidation resistance etc. can be improved by this process. Zare *et al.* [9], have achieved uniform distribution of CNTs without agglomeration in aluminum, 2mg powder using ultrasonic and ball mill attrition. Liao *et al*. [10] have conducted a study on the CNT dispersion in aluminum powder by different mixing techniques, i.e. (i) high energy ball milling, (ii) low energy ball milling and (iii) a polyester binder-assisted (PBA) technique. The results have shown that the separation of CNTs was affected by both the powder mixing operation and the secondary processing. Secondary processing with a large enough deformation has the capability to homogeneously redistribute the reinforcements. However, the amount defects in the CNTs have been observed to increase after mixing and sintering due to the physical compression force. On the other hand, graphitic structures have not been damaged during the secondary processing, due to the protective action of the soft matrix. However, CNTs are subjected to substantial compressive stress not only during mixing but also while sintering, due to the constraints from the consolidation and shrinkage from thermal mismatch. Jin-long *et al*. [11] have fabricated aluminum matrix composites reinforced with CNT by a powder metallurgy method. The hardness of the composites has been observed to increase with the increase in CNT content up to 2.0 wt.% and then it has been observed to decrease. They have also found that within the range of CNT content between 1.0% to 2.0%, both friction coefficient and wear rate of the composites decrease with the increase in CNT content and the composite containing 2.0% CNT is observed to exhibit lowest coefficient of friction and wear rate. Narayanasamy *et al*.[12] have described the consolidation behavior of Al 6061alloy matrix nanocomposites reinforced with multi-walled carbon nanotubes. They have successfully prepared Al 6061 nanocomposites containing various weight percentages of MWCNTs (0, 0.5, 1.0, 1.5 and 2.0) by high-energy ball milling with milling time up to 30h. The milled powders are consolidated by cold uniaxial

compaction followed by sintering at different temperatures (450 °C, 525 °C and 600°C) under a reducing atmosphere ($N_2$) in order to evaluate the materials' sinter ability. The structural evolution of MWCNTs before and after milling is investigated by Raman spectroscopy as shown infigure2.3.The results have revealed that the MWCNTs sustained less structural damage even after 2 h of mechanical milling.

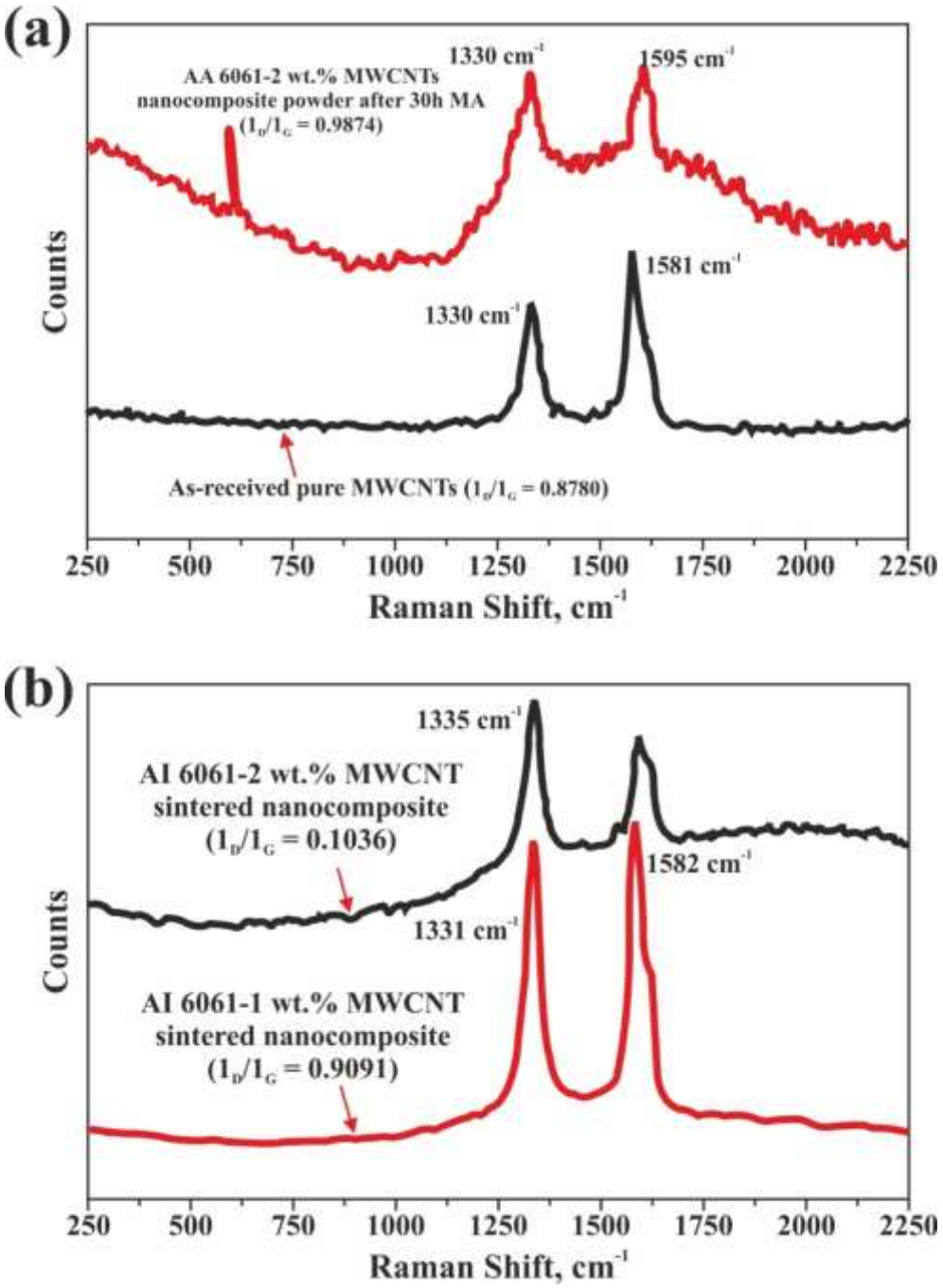


**Figure 2.3**Raman spectra for (a) as-received MWCNTs and Al 6061-2 wt.% MWCNT nanocomposites powders after 30 h of MA, (b) Al 6061-1 wt.% MWCNTs and Al 6061-2 wt.% MWCNTs sintered nanocomposites at $525^0$C [12].

Vickers hardness of the sintered composites has been observed to increase linearly with the addition of MWCNTs to Al 6061 matrix. A hardness value of ~76 HV (818 MPa) and a green compression strength of ~161 MPa have been observed in the case of Al 6061-2 wt.% MWCNT nanocomposites and these were attributed to grain refinement, aluminum carbide formation and work hardening.

### *2.3.3 Flake powder metallurgy*

In a recent study Zhiqiang Li *et al.* [13] have used flake powder metallurgy (flake PM) to achieve uniform distribution of CNTs in Al-CNT composites. The structural integrity of the CNTs is maintained in the composites as CNTs are not affected by the high energy physical force such as impact of balls during ball-milling. They have concluded that a strong and ductile Al-CNT composite might be fabricated using this process, with tensile strength up to 435 MPa and ultimate strain up to 6%. These values have surpassed the strength values of materials produced by conventional methods. In order to produce a material with high tensile strength and ductility, Al-CNT nanolaminates composites with alternating layers of Al (400 nm) and CNTs (50 nm) are fabricated by Jiang *et al*.[14] using flake PM. In comparison to conventional homogeneous nanocomposites composed of the same constituents, the final bulk products with high level ordered nanolaminates have been observed to exhibit high tensile strength up to 375 MPa and high strain (12%). They have attributed this enhancement to the enhanced dislocation storage capability and two-dimensional alignment of CNTs.

### *2.3.4 Effect of CNTs size and structure on the composite*

Lin Wang *et al.* [15] have described that the shape and size of the CNT used in the composite would have a great influence on the particle size after milling. They used small diameter MWCNT's (20 nm diameter) with a curly structure and milled them with pure Al powder after sonication using the same milling conditions as used by Esawi *et al.* [16] for comparison purposes. The resulting particle size of both the Al-CNT and the pure aluminum are observed to be different from the results reported by [16]. Particle size of pure Al increased from 29.3 microns to 106 microns after 72 h of milling**,** figure2.4 (a) and the particle size of Al-CNT has not been observed to increase or decrease after 72 h of milling shown in figure2.4

(b).The particle size values reported by them are 1-2 nm after 48 h of milling in case of the 2 wt.% Al-CNT composite. They have shown that the difference in results may be due to the difference in size and structure of the MWCNT used in both the experiments.

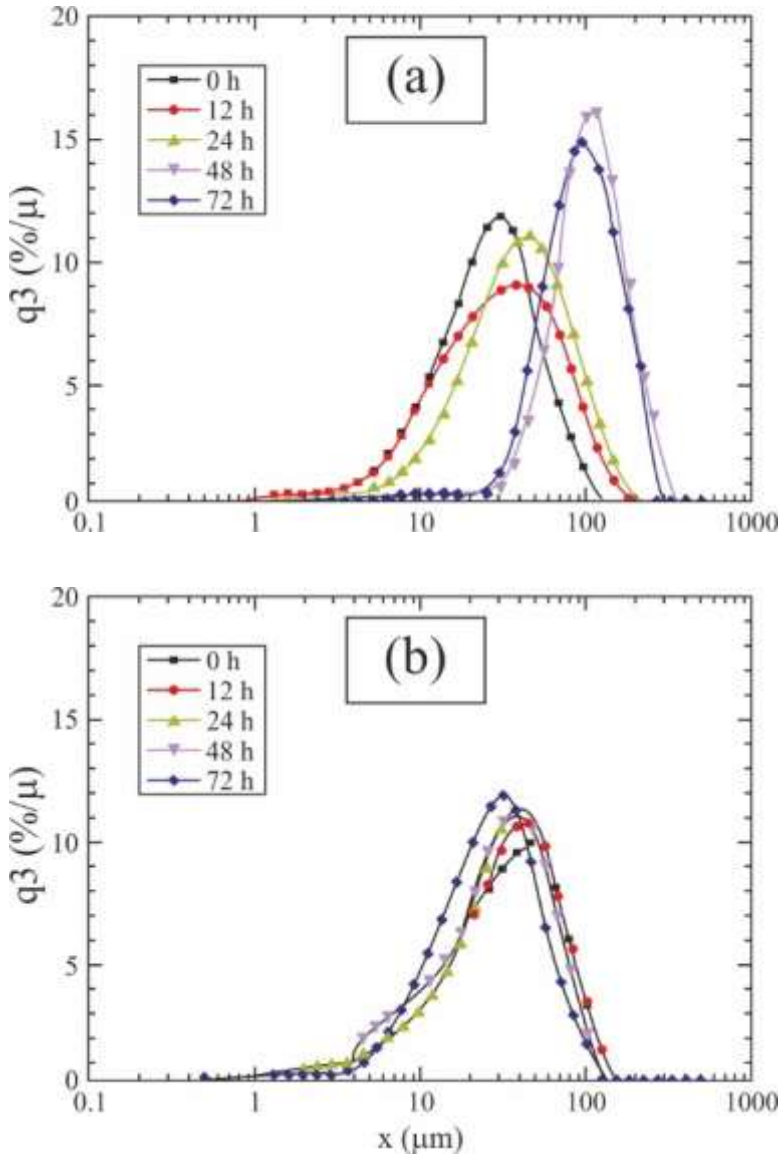


**Figure2.4 (a)** Pure Al powder distribution, **(b)** Al-CNT mixture powders [15]

Lin Wang [15] have argued that smaller diameter CNT increases the total surface area of the CNT that comes in contact with Al, which in turn has reduced the contact area between the Al particles themselves during ball milling, and this hinders the cold welding of Al particles together. Furthermore, based on the concept of mechanics of materials, they have explained that the bending stiffness and critical

buckling load are small in their case in comparison to the case of Esawi due to the smaller diameter CNT's which would encourage the CNT's to be deformed, and entrapped laterally just beneath the surface of the Al particles as shown in figure2.5.

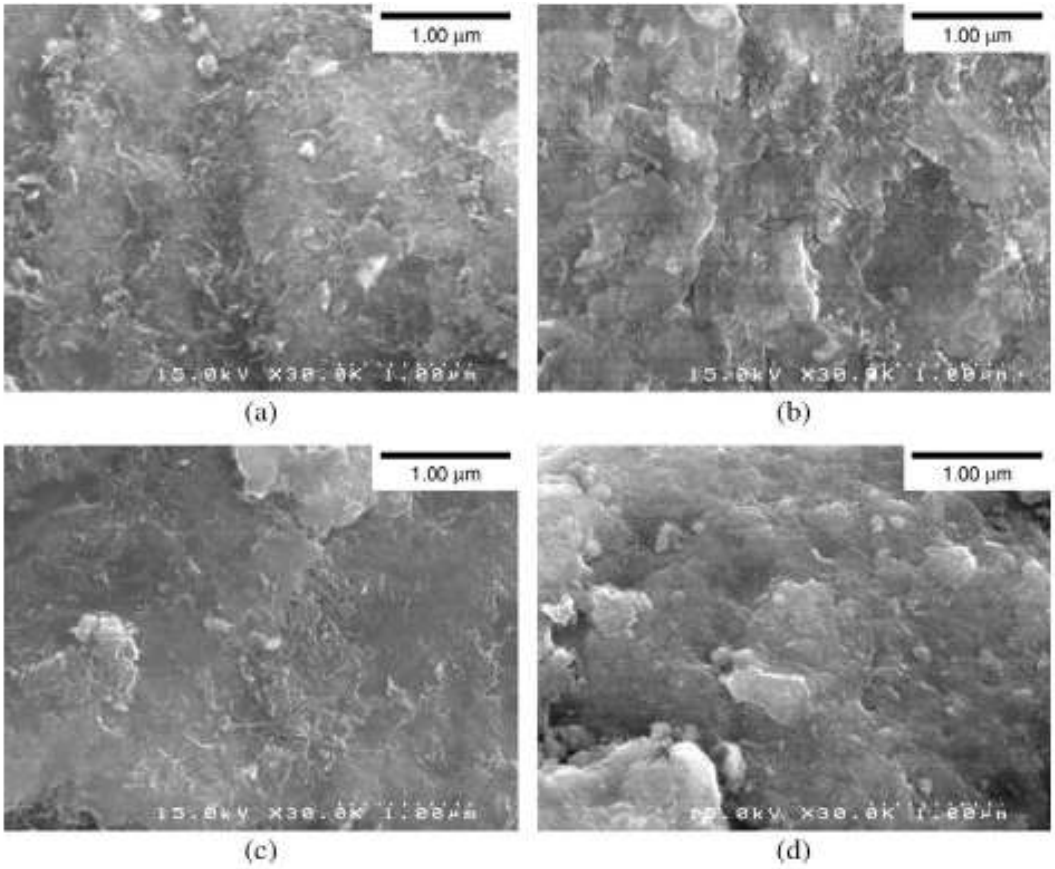


**Figure2.5**The development in particle morphology after (12, 24, 48, and 72 h) [15]

### *2.3.5 Spark plasma sintering to produce Al-CNT Composites*

In spark plasma sintering technique, a pulsed direct current is passed through the powder, producing rapid heating and thus greatly enhancing the sintering rate. This method is, generally, suitable for consolidation of nano powders as this does not allow sufficient time for grain growth. Morsi *et al*.[17]have used the SPS technique for the heat treatment and consolidation of SPEX milled Al-CNT powders (well dispersed CNTs in an Al matrix with 2.5 and 5 wt.% CNT content).They have used CNTs with average diameter of 30nm and99.7% pure Al powder with average diameter of 45µm. The authors reported that SPEX milling results in powders with varying size and morphology. They have found that crystallite size of Al in the 2.5

wt.%CNT containing composite powder after 90 min milling is 88 nm in comparison to 52 nm for the 5.0 wt.% CNT after 2 h, milling indicating a grain refining effect of the addition of CNTs. In addition, annealing experiments are also conducted on the Al-5 wt.% CNT powder at temperatures ranging from 300$^{o}$C to 500$^{o}$C. XRD scans have revealed that aluminum carbide is present in the sample annealed at 500$^{0}$C, and also in the sample annealed at 400$^{o}$C even though in traces. The authors have shown the presence of CNT in the deep etched plasma sintered microstructure in figure 2.6. They have also reported that the Vickers hardness increases from 91 to 107 HV with the increase in CNT content from 2.5 wt.% to 5 wt.% [17].Other researchers have investigated the consolidation of the same Al-CNT composites using a novel process, spark plasma extrusion (SPE) process. In comparison to SPS, SPE has the added advantage of allowing the production of powder-based materials of extended geometries and bulk deformation under the influence of electric current which may yield materials with unique properties [18]. The authors have successfully spark plasma extruded 60 min milled Al and 90 min milled Al-CNT powders. In addition, the Al-CNT composite displayed higher hardness (~33%) and compressive strength (~10%) than the pure Al counterpart under the investigated processing parameters, which is claimed to be due to the strengthening effects of CNTs and reduced Al crystallite size in the composite powder in comparison to the milled pure Al powder [18, 19].

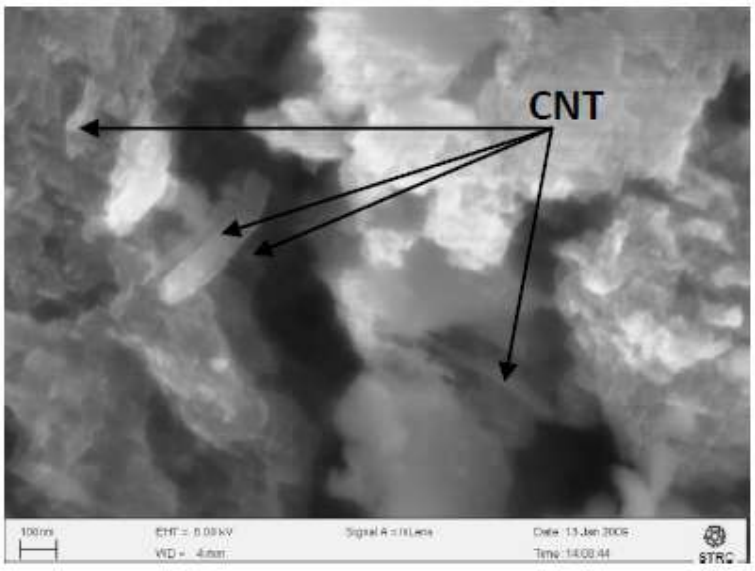


**Figure2.6**FESEM micrograph of deep-etched spark plasma sintered 5 wt.% CNT–Al samples showing nanotubes [17].

Kwon*et al.* [20] has also used SPS followed by extrusion to process their material. They have reported that their product exhibits a tensile strength that is much higher than pure Al. They have prepared the powder mixture by using nano scale dispersion (NSD) method that was first used by Noguchi *etal.*[21]. In this process, natural rubber (NR) is used as a mixing medium for the dispersion of CNT with metal powder. The authors have used 99.8% pure gas atomized Al powder, 5 vol.% MWCNT with an average diameter of 20nm, along with natural rubber in the process. The mixture is put in a furnace under argon atmosphere at a temperature of 500 $^0$C for 2 h to evaporate the natural rubber. The obtained powder is then put in a carbon mold and sintered at 600 $^0$C for 20 min under 50MPa of pressure. Finally, the sintered billet (15mm diameter, 30mm length) is extruded at 400$^0$C with an extrusion ratio of 20:1figure2.7 is a schematic representation of the process steps [20].

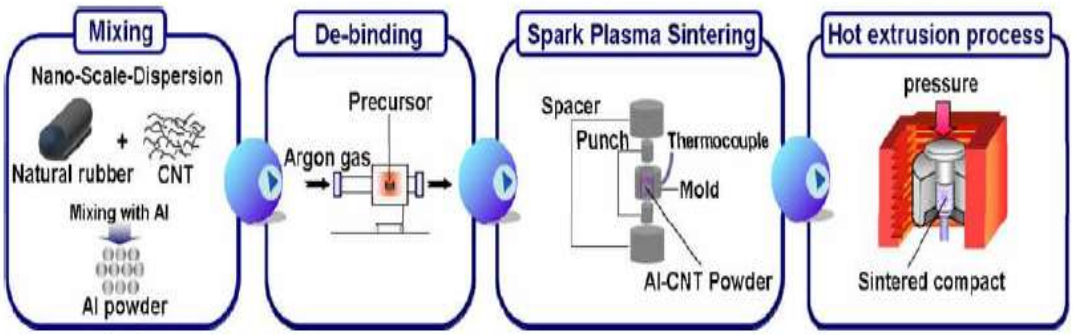


**Figure2.7**Mixing, SPS, and hot extrusion steps [20]

FESEM is used to examine the dispersion of CNT in the matrix after the debinding process. Images shown in figure 2.8 (b) indicate that the CNTs are condensed on the surface of the Al particles by the capillary effect of the melting NR. Figure2.8 (a) shows that the Al particles have preserved their spherical structure despite the heat treatment. Also, the authors have reported some agglomerations of CNT on the surface of the Al particles and this is clearly seen in figure2.8(c).TEM images showed the presence of different phases at the grain boundary interface which are found out to be CNTs, amorphous carbon, graphite, and Al carbide from EDS and SAD pattern analysis. [20].

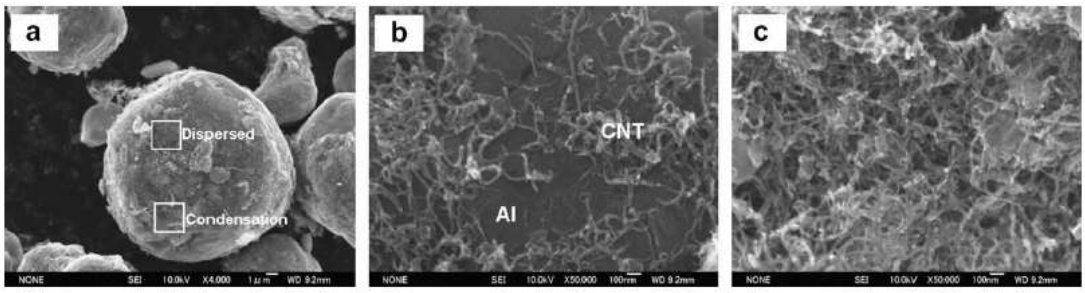


**Figure 2.8(a)** Al-CNT powder mixture, (b) uniformly dispersed Al-CNT phase, (c) agglomerations of CNTs on Al particles [20].

They have reported an ultimate tensile stress value of 190MPa at 11% elongation for the 5 vol.% CNT sample, and 90MPa for the pure Al sample. These results which are achieved without any work hardening are remarkable and outstanding compared to other reports, and it has been attributed to the formation of Al carbide which enhanced the bonding between Al and CNTs [20].

## 2.4 Interfacial Al-CNT reactions

Multi-walled Al-CNT composites, with aluminum (Al) carbide nanostructures at the CNT-Al interface are prepared by F.Housaer *et al.* [22] they have studied the effects of the sintering temperature and the consolidation technique on the composite interfaces. The CNT/Al powder was placed in a carbon mold with a diameter of 20mmand sintered using two different powder metallurgy techniques: hot-pressing and Spark Plasma Sintering. The samples were prepared by hot-pressing at 580, 600, 620 and 645 °C. XRD patterns of Al-CNT composite prepared by hot-pressing at various temperatures are shown infigure2.9. At sintering temperature 580 °C, only peaks corresponding to aluminum are notable. At 600 °C, two additional peaks (32.0° and 55.3°) can be seen. For higher sintering temperature (620 and 645 °C), these two peaks significantly grow and also two others (31.2° and 36.0°) have been observed to emerge. All these additional peaks are due to the $Al_4C_3$ phase. Thus, this study shows that the amount of $Al_4C_3$ phase depends on the sintering temperature. In particular, $Al_4C_3$ phase is detectable from the sintering temperature 600 °C and its amount increases with temperature. For Samples sintered by SPS at 580 °C and 600 °C corresponding XRD pattern are shown in figure2.10.

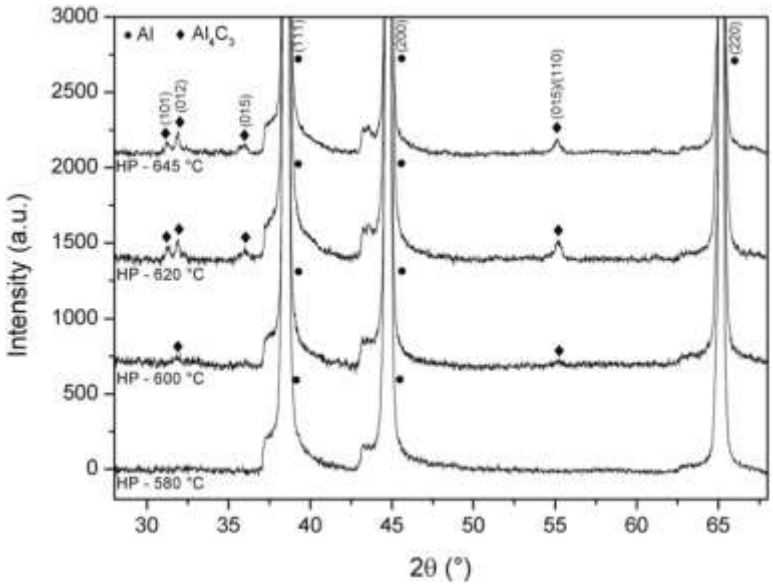


**Figure2.9**XRD patterns of Al-CNT composites hot-pressed at various temperatures.

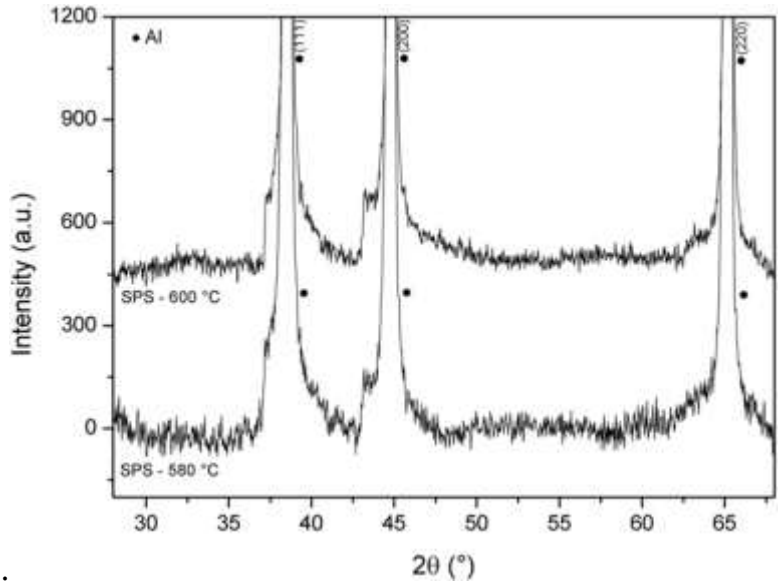


.

**Figure 2.10** XRD patterns of Al-CNT composites sintered by SPS at 580 °C and 600 °C.

Authors have claimed that the sample sintered by SPS, does not develop $Al_4C_3$ unlike the hot-pressed sample. The only exception is the presence of very few $Al_4C_3$ particles at matrix grain boundaries of both samples after TEM study. This implies that many CNT are present at matrix grain boundaries and only few $Al_4C_3$ crystals are formed. Thus, it is possible to control the interfaces in Al-CNT composites by controlling the temperature and the time of sintering. In particular flash sintering technique such as SPS, which limits the growth of $Al_4C_3$ is an

interesting alternative for preparing Al-CNT composites with enhanced physical properties. A. Kawasaki *et al.* [23], have studied the interfacial reaction between the MWCNT reinforcement and the Al matrix by precisely controlling the heat treatment. The thermal expansion response of multi-walled carbon nanotube (MWCNT) reinforced Al matrix composites is employed to study the improvement of the load transfer at the interface between the MWCNTs and the Al matrix. Aluminum carbide ($Al_4C_3$) nanostructure at the end of the MWCNTs, incorporated in the Al matrix, is produced by appropriate heat-treatment. The strain contrast around the $Al_4C_3$particles is observed in the high-resolution transmission electron microscopy (HRTEM).This has revealed the evidence of a trace of friction, which would lead to the enhancement of the anchoring effect from the Al matrix. This anchoring effect of $Al_4C_3$ may hinder the local interfacial slippage and constrain the deformation of the Al matrix. As a result, the thermal expansion behavior has become linear and reversible under cyclic thermal load. It is concluded that the formation of $Al_4C_3$ could effectively enhance the load transfer in Al -MWCNT composites. The yield strength of the Al-MWCNT composites is observed to increase substantially when the appropriate quantity of $Al_4C_3$ produced at the MWCNT-Al interface by the precisely controlled heat-treatment.

## 2.5 Copper-CNT Composites

Copper is an element with the symbol Cu and atomic number 29. It is a ductile metal with very high thermal and electrical conductivity. Pure copper is soft and malleable; a freshly exposed surface has a reddish-orange color. It is used as a conductor of heat and electricity, a building material, and a constituent of various alloys. The main areas where copper is found in humans are liver, muscle and bone. In sufficient concentration, Cu compounds are poisonous to higher organisms and are used as bacteriostatic substances, fungicides and wood preservatives.

### *2.5.1 Ball milling of composite powder*

Hongqi Li *et al*. [24] have studied the Cu-CNT powder mixture ball milled for five h in an argon atmosphere with ball to powder ratio (BPR) 6:1. By studying the powder morphology, they have reported about the various stages through which particle undergoes during ball milling. Size of particle increased from nanometer to

micrometer after 5h of ball milling and particle have been observed to have smooth flat surface. It is assumed that initially the particles are deformed into flat plate like structure which resulted in work hardening. Then they are fractured due to impact by balls. Lastly particle size is increased due to cold welding. All these stages result in dispersion of CNTs in matrix homogenously.

### *2.5.2 Processing of Cu-CNT canned powder via compaction and sintering of green compact*

Sintering is a process in which the green compact is heated in an inert atmosphere up to 70-85% of the matrix melting point. During this process, the surface of the particles is partially melted and gets bonded with the surrounding particles resulting in a stronger compact. Van Trinh Pham *et al.*[25] have studied the effect of three different sintering temperatures on Cu-CNT composite. The three temperatures are 850°C, 900°C and 950°C and sintering is carried for 2 h. They have concluded that the sintering of the composite at 900°C with 3wt.%CNT results in best hardness values. Ke Chu *et al.* [26] have prepared Cu-Cr/CNT and Cu-CNT composites by hot pressing at 750°C. The hardness of Cu-CNT is found to be 135 Hv which is two times higher than that of the pure Cu. Tensile strength of Cu-CNT composite is observed to increase from 168 MPa to 296 MPa which is 128 MPa higher than that of the pure Cu sample. Both hardness and tensile strength values are for the 10 vol.% CNT addition. The reason for these remarkable results is homogenous dispersion of CNT in the Cu matrix. However, a decrease in both hardness and yield strength were observed for 15vol.%CNT reinforcement. This is the reported agglomeration of CNT at the Cu grain boundaries. On the other hand Cu-Cr/CNT composite is observed to result in remarkable improvement in mechanical properties. It has resulted in a Hardness value of 157 Hv and yield strength of 388 MPa i.e. approximately 128% and 135%corresponding increase as compared to Cu-CNT composite. The authors have reported that the reason for such high strength is due to the good interfacial bonding by formation of $Cr_3C_2$ layer between Cu-Cr and CNT at the interface.

### *2.5.3 Spark plasma sintering Cu-CNT nanocomposite*

High density Cu-CNT nanocomposites have been successfully prepared by high energy ball milling followed by spark plasma sintering. Niraj Nayan *et al*. [27] have studied the Cu matrix composites reinforced with 0.2, 5 and 10 vol. % of single walled carbon nanotubes (SWCNT) and 5 and 10 vol. % of multi-wall carbon nanotubes (MWCNT) processed by high energy attritor milling of pure copper powder with carbon nanotubes (CNT) and subsequently consolidated by spark plasma sintering (SPS). Microstructural characterization has shown a network of CNT along the grain boundaries and the presence of porosities at the grain boundaries as well as at the triple junctions. By covering the particle boundaries, the higher volume fraction of CNT makes the sintering difficult as compared to the single phase copper or low volume fraction CNT composites. Raman spectroscopy study has indicated that there is an increase in number of defects in the nanotube after milling and sintering of the composite. Mechanical properties evaluation has shown that the SWCNT composites result in higher strength and deformability compared to MWCNT reinforced composites. The failure strain has been observed to decrease with the increase in volume percent of CNT due to clustering of CNTs.

## 2.6 Molecular level mixing

Dong. H. Nam *et al*.[28] have treated CNTs in two different aspects. One batch is treated with acid which they called as ATCNT and the other batch is coated with poly-vinyl-alcohol (PVA) and is called as PCNT. Both ATCNT and PCNT are reinforced in Al-Cu matrix. They have combined molecular-level-mixing and mechanical alloying methods to prepare the Al-Cu/CNT composites. With the addition of 4vol.% of ATCNT and PCNT the yield strength has been observed to be376 MPa and 384 MPa respectively. Whereas the cases of Al-Cu sample the yields strength is observed to be only 110 MPa. The ultimate tensile strength values of ATCNT and PCNT reinforced composites are observed to be 494 MPa and 470 MPa, respectively. These values are almost two times higher than that of Al-Cu matrix, which possesses an ultimate tensile strength of 237 MPa. From the above results it is clear that with different types of treatment of CNT there might not be substantial variation in mechanical properties in the composite. However elastic

moduli have shown different resulted-Cu/PCNT hasshownalmost30% increase to 93 GPa whereas Al-Cu/AT-CNT has shown an increase to only 73 GPa.

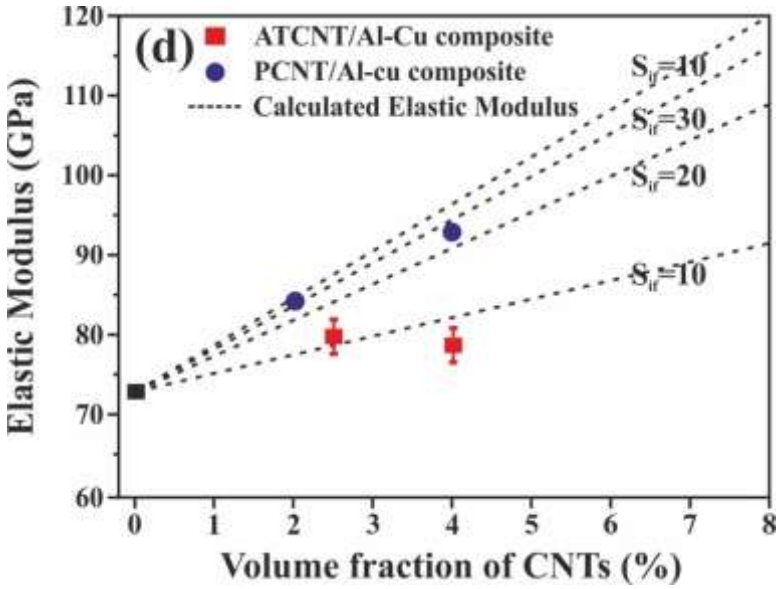


**Figure2.11**Elastic modulus of PCNT/Al–Cu and ATCNT/Al–Cu composites with volume fraction of CNTs and comparison with the calculated elastic modulus [28].

Kyung Tae Kim *et al.* [29] have prepared Cu-CNT composite by molecular-level-mixing method. They have studied the thermal expansion behavior of the prepared composite. The results of thermal expansion in 5 vol.% and 10 vol.% CNT reinforced composites are observed to be 14 $K^{-1}$ and 12.1 $K^{-1}$ respectively which are lower when compared to the pure Cu sample which has a CTE value of 17 ppm $K^{-1}$. This reveals that addition of CNT increases the stiffness of the composite.

## 2.7 Fe-CNT Composites

S.K. Pradhan *et al.*[30] have studied the carbide preparation in a conventional route. Through, mechanical milling of the powder ingredients at room temperature, one can easily produce nanocrystalline metal carbides. It is supported by the result that preparation of nanocrystalline $Fe_3C$ was possible by mechanical milling of α-Fe and graphite powders under inert atmosphere at room temperature. Mössbauer spectra of ball-milled powder clearly reveal that the $Fe_3C$phase is initiated at 3h of milling and the stoichiometric $Fe_3C$ is formed after 5h of milling. The phase transformation kinetics studied through Rietveld method reveals that a

small number of carbon atoms diffuse into α-Fe matrix and $Fe_3C$ phase is formed through the solid-state reaction of nanocrystalline graphite and α-Fe powders during ball milling. D.H. Bae [31] has studied the reinforcing efficiency of multi-walled carbon nanotubes (MWCNTs) in Fe matrix through powder metallurgy routes. For the preparation of composites Fe powder containing MWCNTs are first mechanical milled and hot pressed at $570^0$C for 2 h under140MPa, pressure. In this process, the MWCNTs have been observed to provide a high reinforcement factor of 0.6 and a yield stress of 2.2GPa at the 4 vol.% MWCNTs. On the other hand, for the composites produced by compaction and then sintering at $850^0$C, the dispersed MWCNTs decompose and form a Fe–C interstitial alloyed phase, in which the composite shows a relatively low yield stress of 450 MPa at the 8.3vol.% Fe–C phase. For the composite sintered at high temperature at $1150^0$C, the reinforcement factor is found to be 0.2 and the yield stress is about 280MPa at the 9.2 vol.% $Fe_3C$. These results demonstrate that MWCNTs with a high aspect ratio and a strong bonding character with the matrix have a great role in reinforcing the Fe-based composites.

## 2.8 Physical properties of carbon nanotube reinforced metal matrix nanocomposite

### *2.8.1 Electroless deposition process*

Byung K Lim *et al*. [32] have coated CNT with Cu by Electroless process and then have consolidated the samples at 550°C using SPS process. They have observed a decrease in electrical conductivity by increasing the CNT volume fraction in the Cu matrix. Agglomeration of CNT at the matrix grain boundaries, which results in scattering of charges is reported to be the reason for decrease in electrical conductivity.

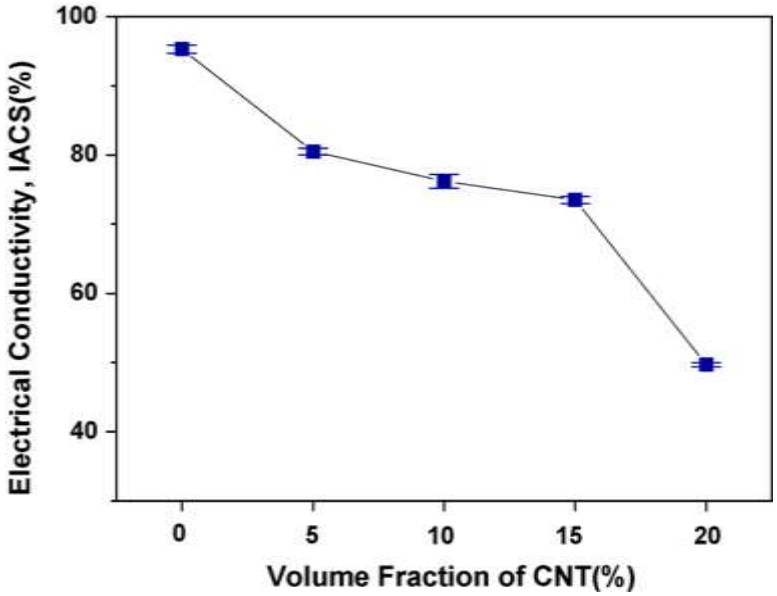


**Figure 2.12** The standard IACS % electrical conductivity for the sintered Cu and the Related Cu- CNT nanocomposites [32].

CNT have acted like barrier instead of charge carrier due to improper alignment CNT along the path of moving charges, and due to poor wettability with matrix. Also, the porosity content has been observed to increase with the increase in CNT content. All these factors are believed to be responsible for the decrease in electrical conductivity with the increase in CNT content in the composite. Y.D. Wang *et al*. [33] have reported smaller crystallite size and higher lattice micro-strain in the carbon nanotube reinforced Cu matrix composite coating, prepared by electrochemical deposition under ultrasonic field, in comparison to pure Cu coating. It has been observed that the as deposited coatings retain a good fraction of the electrical conductivity in comparison to pure copper. It is believed to be due to the dominating effect of the beneficial factor over the detrimental factors, as explained further. The SWCNT acts as scattering centers for electrons and hence increase the resistivity at lower temperature. Furthermore the grain refinement and the increase in micro-strain in the Cu matrix also play important role in increase of electron scattering. The value of temperature coefficient of resistivity, α, which illustrates the electron-phonon interaction [34], is $6.20\pm0.20\times10^{-1}\Omega$.m at 293 K for the composite which is slightly lower than that of OFHC Cu ($6.80\times10^{-11}\Omega$.m). This slight difference may be explained by the following three factors: First, the electrical conductivity of SWNTs is $10^{8}$ $S\cdot m^{-1}$[35,36] which is same or even better than that

of pure Cu; Second, the high surface area of the nanotubes create a large interface-to-volume ratio at the Cu-SWNT interfaces, resulting in large scattering during electron transfer and, hence, leading to an increase in resistivity [37]; third the majority of the SWNTs are distributed at the grain boundaries and form a network leading to the continuity of the nanotube phase, which provides an interlinked electrical pathway for the reduction in resistivity [38].It is believed that the third factor, plays an important role in the decrease in electrical resistivity at room temperature for the SWNT-doped Cu.

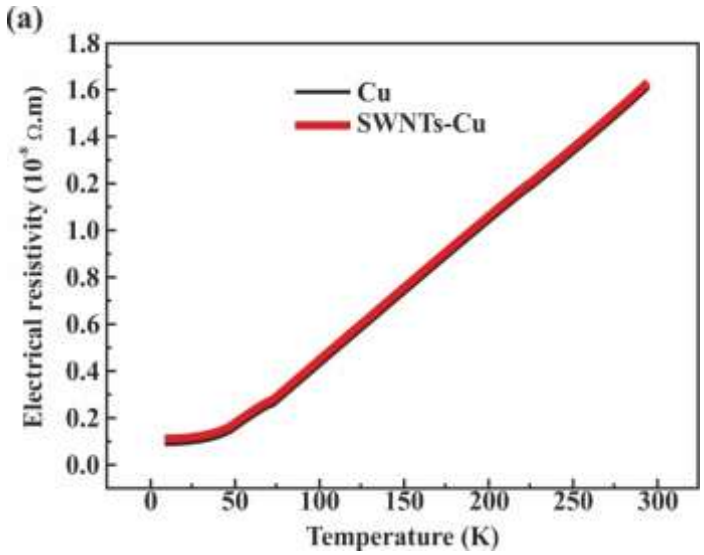


**Figure 2.13(a)** Dependence of electrical resistivity (r) for the as-deposited Cu-SWNT in temperature range of 10 to 300 K (in red line). For comparison, electrical resistivity data of OFHC Cu [38] are also included (in black line).

Sheikh M. Uddin *et.al* [39] has prepared the CNT reinforced copper and copper alloy (bronze) composites by hot-press sintering method of powder metallurgy. Conductivity of bronze composites reinforced with both MWNTs and SWNTs are investigated. The conduction of electricity essentially occurs through the outermost nanotubes. In the case of MWCNTs, the interactions with the internal coaxial nanotubes may lead to variations in the electronic properties. However, metallic SWCNTs can sustain huge current densities (max.109 A/cm$^2$) without being damaged, i.e. about three orders of magnitude higher than that of copper[40]**.**Figure 2.14shows that the electrical conductivity of Bronze -CNT composites has increased up to 10% by the addition of 0.1 wt.% MWCNTs whereas it has increased up to

20% by addition of same amount of SWCNTs. Addition of CNT contents does not always increase the electrical conductivity rather it, decreases after a certain limit.

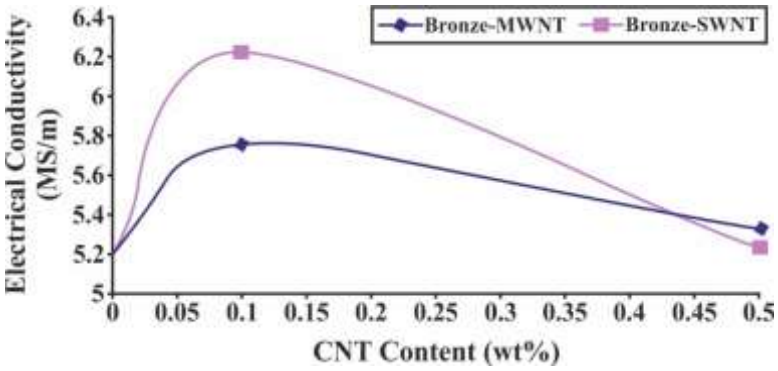


**Figure2.14**Electrical conductivity of Bronze -CNT composites with the addition of MWCNTs and SWCNTs.

The electrical conductivity of the hot forged copper is found to be 98 % IACS. However the conductivity has been observed to decrease with the increase MWCNTs in the copper matrix. At high temperature, the thermal conductivities of the nanocomposites decreased due to the scattering of phonons. The incorporation of MWCNTs in the copper matrix has shown no enhancement in the electrical conductivity. This is mainly due to the presence of interfaces and due to the grain refinement caused by the MWCNTs [41]. Zhong Zheng *et al.*[42] have reported four technical difficulties in preparing Cu/CNT composites(a) interfacial interaction between carbon nanotubes/Cu (b) proper dispersion of CNTs in the matrix (c) densification of composites, and (d) the orientation of CNTs. Thus, Ni-Cu bilayers on SWCNTs are prepared through electroless plating to build up strong interaction between CNTs and Cu matrix. Powders are mixed through ultrasonic assisted mechanical agitation to disperse SWCNTs homogeneously in the Cu matrix. Hot forging is employed to densify the composite samples and die stretching is employed to align the SWCNTs. By these method SWCNTs are observed to be uniformly dispersed in the dense composites and aligned along the stretch direction. The hardness and tensile strength are found to increase by 67.3% and30.4% respectively by the addition of 5 vol.% SWCNTs. However the composite is observed to be anisotropic in strength and conductivity.

## 2.9 Electrical Conductivity of carbonyl iron-carbon nanotubes

Guoxiu Tong *et al.*[43] have studied the conductivity (σ) of CIPs-CNTs composites as a function of the weight fraction of CNTs. The conductivity of the CNTs is 100.50 S $cm^{-1}$, which is almost three orders of magnitude higher than that (0.049 S $cm^{-1}$) of the CIPs. In general, the electrical conductivity of the insulating materials can be improved by the addition of CNTs [44, 45]. By the addition of2.2 vol.% CNTs the conductivity of CIPs-CNTs composites has been observed to increases lightly0.068 S $cm^{-1}$. Also, it is observed that the σ of CIPs-CNTs composites increases by nearly two orders of magnitude when increase the vol. % of WCNTs is 4.4. The σ of CIPs-CNTs composites further increases by nearly three times from 4.18 to 13.54 ($Scm^{-1}$) as MWCNTs content increase from 4.4 % to 6.6 %. The aforesaid conductive behavior can be interpreted as follows. The conduction mechanism of the CIPs-CNTs composites may be classified into two types. One is ohmic conduction due to the metallic contact between CNTs bundles and CIPs as well as among the CIPs and, the other is non-ohmic conduction owing to existing small gaps between the CNTs bundles. At relatively low MWCNTs content (e.g., 2.2 %), the increase in conductivity of the CIPs-CNTs composites principally depends on the ohmic conduction between the CNT bundles and the CIPs. With the increase in CNT content up to (4.4 %) the gap between the adjacent CNTs bundles decreases significantly and the conductive network forms locally. The conductivity behavior of the composites is largely dependent upon interaction between the CNTs and CIPs matrix, the properties of the CNTs themselves (diameter, length, specific surface area, and surface conductivity), and the dispersion and relative concentrations of the CNTs within the matrix.

## 2.10 Magnetic properties of materials

Magnetic materials have revolutionized our lives. These materials are used in electronic, computer and telecommunication industries. The magnetic properties of the materials are measured from certain defined points and the derivatives obtained from the variation of magnetization with magnetic field as shown in figure 2.15. Magnetic materials are broadly classified into two main groups with either hard or soft magnetic characteristics [46].

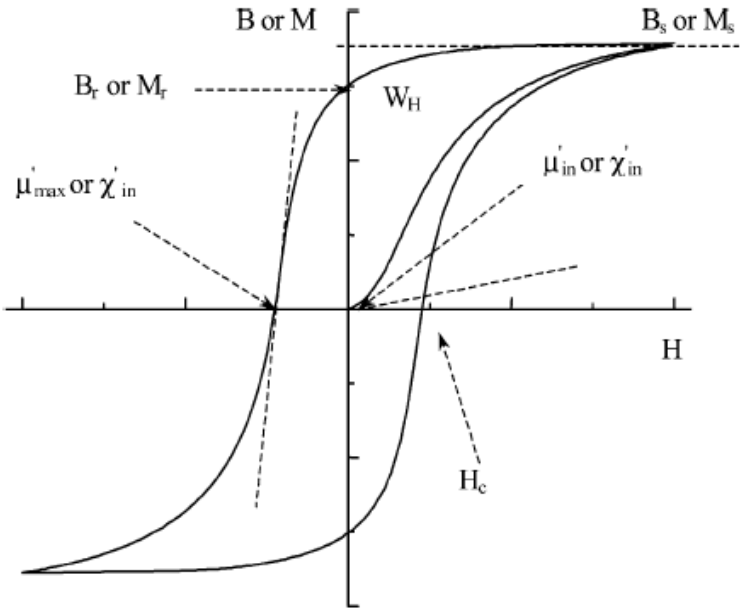


**Figure2.15**Magnetic properties of materials as defined on the BH plane or flux density B versus magnetic field H, (or the MH plane of magnetization M versus magnetic field H). These include coercivity Hc, remanence $B_R$ ($M_R$), hysteresis loss $W_H$, initial permeability $\mu_{in}$ (initial susceptibility $\chi_{in}$), maximum differential permeability $\mu_{max}$ (maximum differential susceptibility $\chi_{in}$) and saturation flux density Bs (saturation magnetization Ms).

### *2.10.1 Soft magnetic materials*

The important characteristics of magnetically soft materials are their high permeability, high saturation induction, low hysteresis energy loss and low eddy-current loss in alternating-flux applications. These groups of materials include high-purity iron, low-carbon iron, iron -copper, iron–nickel alloys, iron–cobalt alloys and ferrites. During the last few decades different aspects of processing (milling time, particle size effect, annealing temperature and time), properties, effect of additives, alloying elements for these materials are discussed by many researchers [47–58]. Iron-based alloy powders are one of the main components of the soft magnetic composites (SMCs).

### *2.10.2* **Magnetic properties of Fe- Cu system**

Majumdar.*et.al* [59] have reported the dependence of the magnetic properties on the Fe content in $Fe_{100-x}Cu_x$ (x =10 to 50) alloys. The solid solutions are obtained by high energy ball milling of Fe and Cu powders.

Their investigation leads to the following conclusions.

- The X-ray diffraction patterns of the ball milled powder indicate that the formation of Fe-Cu solid solution over a wide range is possible. Between 20 and 34% of Cu, a two-phase region is observed consisting of f.c.c. and b.c.c. solid solutions. Combined analysis by TEM and Mossbauer spectroscopy indicates that two iron-rich alloys with Cu content not more than 20% has formed. The b.c.c. phase is predominantly α- Fe with very little copper in the solid solution.
- In all mechanically alloyed samples with copper content varying from 10 to 50%, the presence of a small amount of γ-iron is observed.
- The magnetization is found to decrease with milling time for all compositions except $Fe_{50}Cu_{50.}$The decrease in magnetization with the increasing copper concentration is due to the dilution of the magnetic moment due to iron.

M. Barzegar Vishlaghi *et al.*[60] have observed that that the addition of CNT suppresses the solid solubility of Fe in Cu matrix. As the dispersion and implantation of CNTs in the metal matrix improved, particles size is observed to become smaller and their shape becomes more granular. The saturation magnetization and coercivity of the composite samples increased with the addition of CNT probably due to the presence of undissolved Fe in the nanocomposites and homogeneity of microstructure. Electrical resistivity of nanocomposites is observed to be higher than that of matrix alloy. The increment is found to be more when the milling time of CNTs and metal powder is short.

J.Z. Jiang.*et al.*[61]has studied the effect of temperature on magnetic property of Fe-Cu solid solution. The thermal stability of the Fe–Cu solid solutions and the magnetic properties of these alloys have also been studied by several groups [62-68]. The saturation magnetization ($M(T)$) of the as-milled fcc-$Fe_{50}Cu_{50}$ alloy as a function of temperature [66], measured in 1 *T* field, is shown in figure 2.16. The magnetization decreases with increasing temperature up to about 510 K. With further increase in temperature, the magnetization increases.

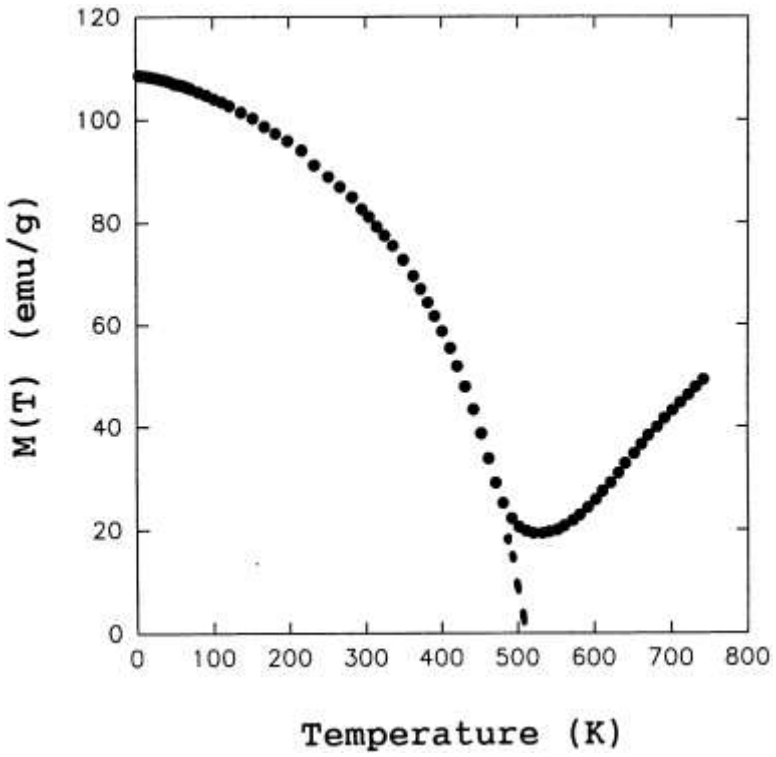


**Figure2.16**The saturation magnetization of an as-milled fcc-$Fe_{50}Cu_{50}$sample as a function of temperature in 1 *T* field [66].

Evangelia Dislaki *et al.* [69] have studied $FexCu_{1-x}$ films over a wide composition range ($0 \leq x \leq 86$) prepared from an aqueous sulfate electrolytic solution using three different complexing agents and variable plating conditions.

Hysteresis loops of deposits with diverse atomic percent of Fe are recorded by VSM. The results of these measurements obtained by applying field parallel to the film plane are presented in figure2.17. It is evident the graph that the saturation magnetization, $M_S$, decreases monotonically with the decrease in Fe content. Importantly, films with 6 at% Fe exhibit ferromagnetic behavior albeit with a very low saturation magnetization (4 emu $g^{-1}$). This is probably due to the occurrence of phase separation since fully alloyed fcc films with 6 at% Fe are typically paramagnetic at room temperature although an enhanced magnetization is expected at low temperature for fcc-CuFe clusters with very small sizes [70, 71].

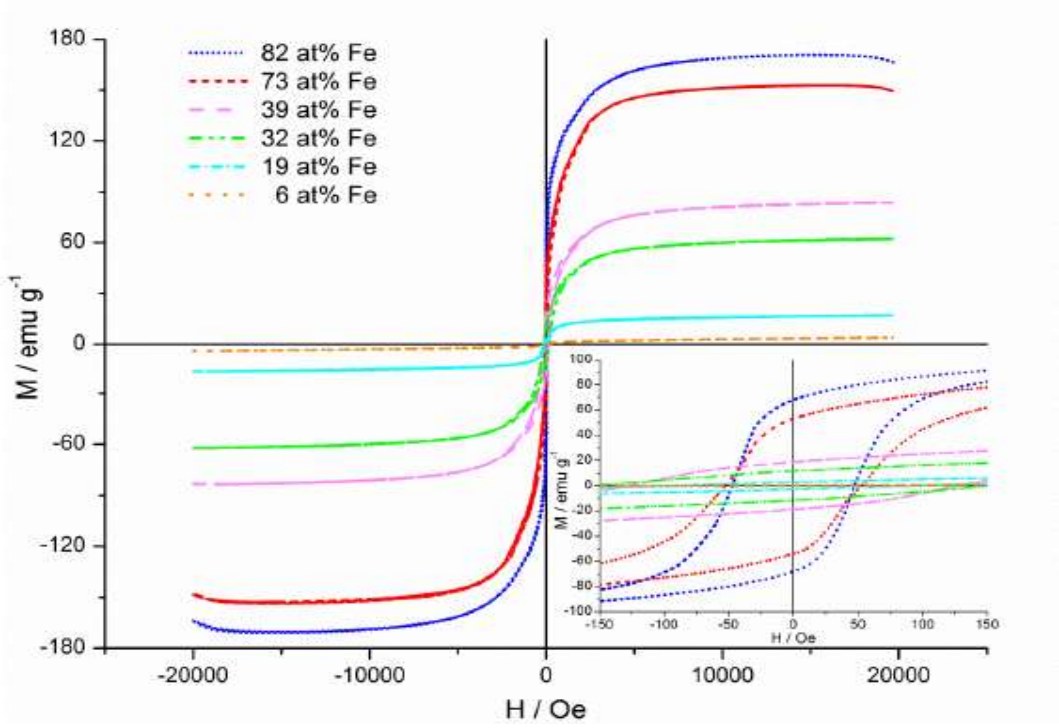


**Figure2.17** Magnetic hysteresis loops obtained from films of varying Fe content. The inset shows a magnified detail at low fields [69].

## 2.11 Fe–Co alloys

The Fe–Co-based soft magnetic alloys have the highest saturation magnetization [72]. These alloys exhibit high saturation magnetization Ms and high Curie temperatures (Tc = $900^0$C)which make them potential candidates for the high temperatures applications such as new generation turbine engines as well as in recording media. The iron–cobalt alloys, with slightly improved permeability have been preferred for their high magnetic saturation of flux density [72]. To process Fe-Co alloys with good soft magnetic properties, the following points are considered to be important [73].

(a) The microstructure of mechanically alloyed powders and its effect on the magnetic properties

(b) Strain relaxation and micro structural evolution after heat treatment

(c) The effects of elemental additions on microstructures of the alloys.

Young Do Kim *et al.*[74] have studied two powder mixtures of Fe and Co-produced by MA and MCA. The alloy powder, synthesized by MCA process through ball milling and hydrogen reduction of $Fe_2O_3$ and $Co_3O_4$powders have

shown ordered BCC structure with the grain size of 40 nm.Figure2.18 shows the magnetization curve for Fe–Co alloy powders, produced by MA and MCA process. The spontaneous magnetization for both the alloy powders is almost the same at about215emu/g. However, the coercive force has shown different values such as 97 Oe for MA powder and 43 Oe for MCA powder. The coercive force is known to be strongly dependent on the grain size, internal strain and dislocation density [75].

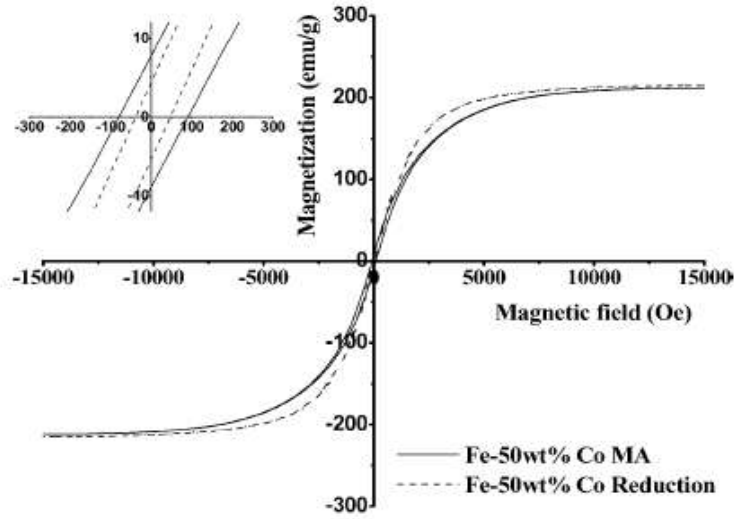


**Figure2.18**Room temperature magnetization versus applied magnetic field curve for the synthesized powders. Inset shows enlargement of the plot near the origin [75].

The MCA powder has exhibited a low coercivity force of 43 Oe and good permeability as compared to MA powder. Enhanced magnetic properties of the MCA powder are explained by the formation of ordered structure and relaxation of internal strain. H. Shokrollahi *et.al* [76] have investigated the effect of different heating rates on both micro structural and magnetic properties of milled nanostructured $Fe_xCo_{1-x}$ ($x$ = 0.8, 0.7, 0.6, 0.5 and 0.3) powders.Figure2.19shows the saturation magnetization as a function of Co concentration for different milling times and heating rates. By milling for 8h the $M_S$ shows a significant increase due to proper alloying of the powder and then shows only a slight increase as the milling time increased from8 to 45 h. due to the reduction in magneto crystalline anisotropy caused by the grain refinement. On annealing, with decreasing the heating rate from 30 to 2°C/min, the $M_S$ (all range of composition) improves nearly by 6%. Low

heating rates (2°C/min) lead to decrease in micro strains (0.03%) and atomic fraction of grain boundaries (7%), both of which increase the $M_S$.

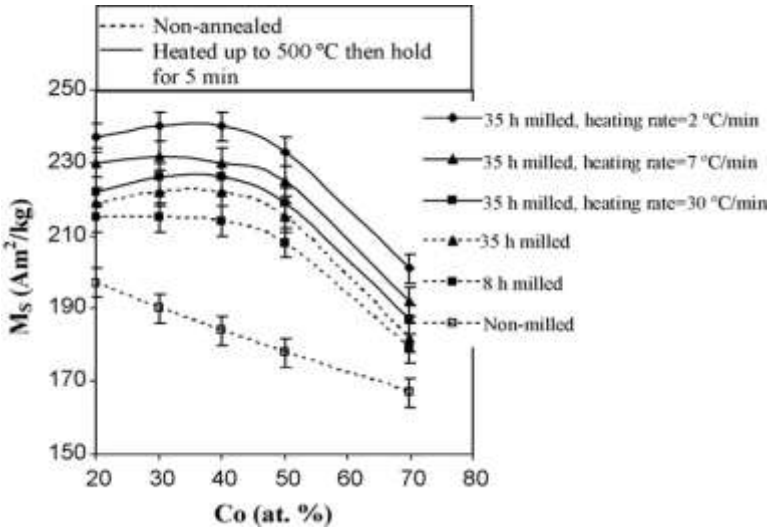


**Figure2.19**$M_S$ of Fe–Co powder mixtures versus Co concentration for as-milled and annealed alloys [76].

By milling for 3 h the coercivity has been observed to reach a maximum due to the introduction of strain and defects and due to the reduction in crystallite size. By milling for 3-35 h the coercivity reduces further due to the effect of very fine crystallite size. For long milling times, $H_C$ decreases slightly due to the stress relief caused by the increase in temperature. During annealing, two stages are normally observed. During the first stage, the coercivity of $Fe_{70}Co_{30}$ powders increases to 55 Oe due to the increase in the crystallite size ($D > L_{ex}$). During the second stage an increase in the $H_C$ (to 8 Oe) is observed due to the decrease in the crystallite size ($D < L_{ex}$) occurs. A. Zelenakova *et al*.[77] have studied the $Fe_{100-x}Co_x$ (x = 30, 45, 50, 60 wt.%) alloys with average grain size of 10nm prepared by mechanical alloying of the elemental Fe and Co powders using a high-energy ball mill. The lattice parameter, saturation magnetization and coercivity are analyzed as a function of the Co content. The average hyperfine magnetic field value of about 35 T suggests that the disordered BCC Fe–Co solid solution is formed after 30 h of milling. The ordering (transformation from α-BCC to B2 structure) is confirmed below the temperature $720^0$C after cooling from DSC analysis in all compositions with the exception of $Fe_{70}Co_{30}$.

## 2.12 Magnetic property of Carbon coated nanoparticles of Fe, Co, Ni

Xiang cheng Sun *et al*. [78] have studied the carbon encapsulated nanoparticles of Fe, Ni, and Co, with average particle sizes of 15, 11.5 and 10.5 nm, respectively synthesized by modified arc-discharge method.

The magnetic measurement of the three as-made nanoparticles Fe(c), Co(c) and Ni(c), indicates that the values of saturation magnetic moment are 37.6, 55.5 and 15.7% of the bulk ferromagnetic elements counterparts, respectively. The comparison values of remanent magnetization (*M*r) and saturation magnetization (*M*s) have indicated that the encapsulated Fe and Co nanoparticles are shown to be ferromagnetic with a ratio of remnant to saturation magnetization *M*r/*M*s 0.3 whereas, the encapsulated Ni nanoparticles exhibits super paramagnetic behavior at room temperature shown in figure2.20. It is concluded that the magnetic behavior of the three carbon encapsulated nanoparticles have originated from the nature of their nanocrystalline structure (i.e. size effect, defect).

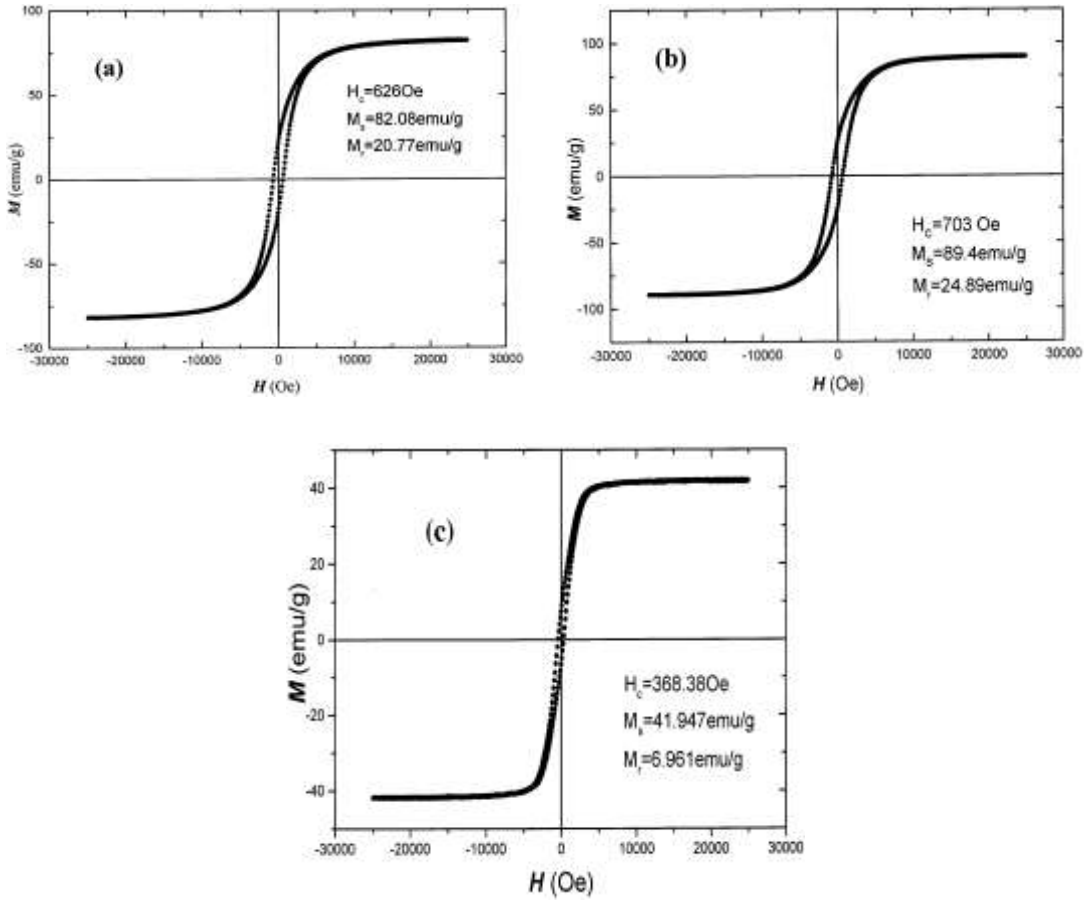


**Figure2.20**The VSM measurements curves for carbon encapsulated Fe (a), Co (b), Ni (c) nanoparticles at room temperature [78].

A. El-Gendy *et al.*[79]have studied the synthesis of carbon coated nanoparticles by two different methods such as arc-discharge and high temperature annealing of mixtures of carbon-based materials and metal powders [80, 81]. High pressure chemical vapor deposition (HPCVD) method has been applied to synthesize metallic nanoparticles coated with carbon. TEM images of the carbon coated nanoparticles are shown in figure2.21(I and II) and the resulting size distribution based on the TEM analysis presented in figure2.21 (III). In a few of the cases, as highlighted in figure2.21A (I and III) carbon particles without metallic cores have also been formed. In the cases of Co-C and Ni-C, the carbon shells are similar to that in the case of Fe-C, but the core size distribution is found to be slightly different. For Co-C and Ni-C it is observed that the core size distribution in the range of 4-100 and 10-50 nm, with average diameters 27 and 20 nm, respectively figures2.21B (III), C (III)

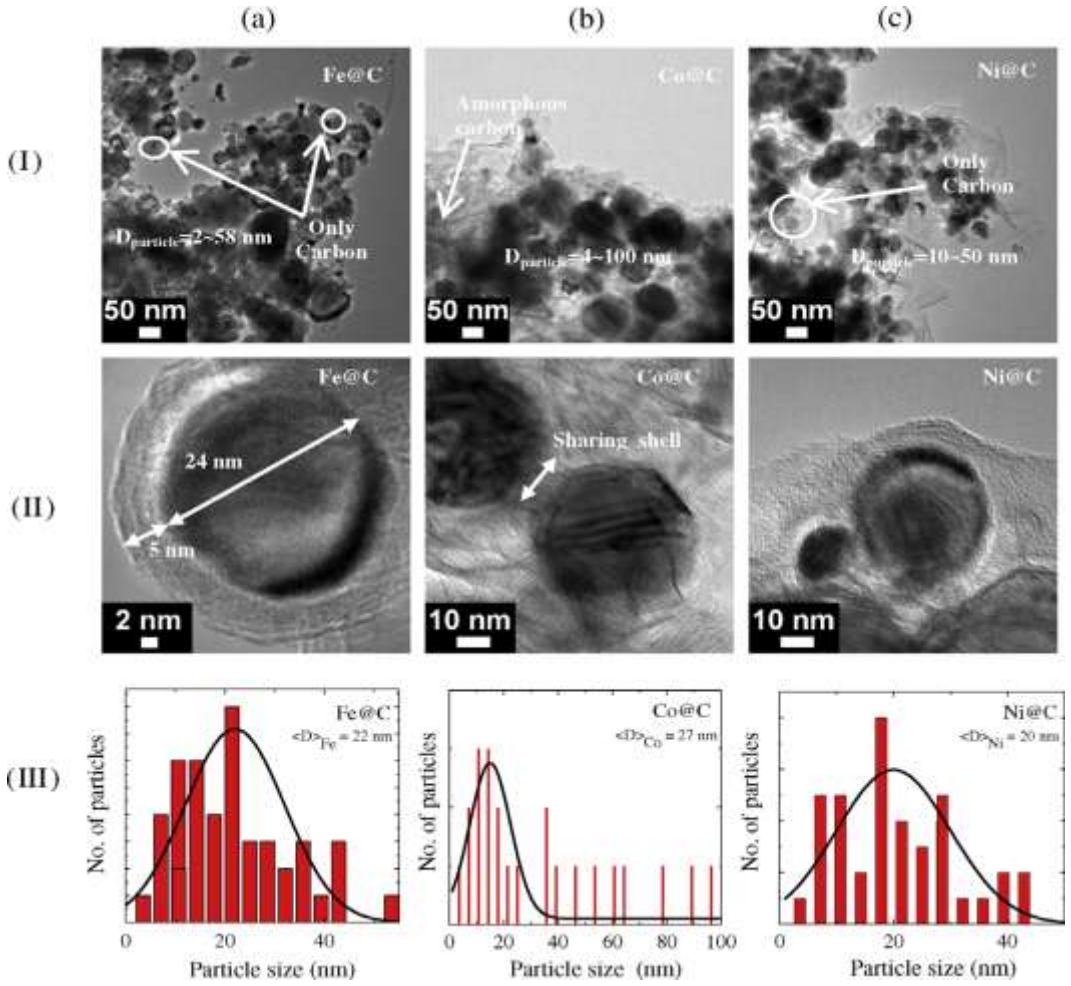


**Figure2.21** TEM images and average size distribution of Fe-C (A (I, II, III)), Co-C (B (I, II, III)) and Ni-C (C (I, II, III)).

In figure 2.22, the full hysteresis loops of the magnetization in an external field up to 1T are presented for the three materials under study. For all samples, the data imply a ferromagnetic behavior as indicated by the open hysteresis loops, i.e. the presence of a remanent magnetization Quantitative analysis yields the saturation magnetization Ms79 ± 5, 158 ± 7 and 32 ± 7 emu/gms respectively whereas the remanent magnetization values are found to be 15.7, 20.9 and 2.3 emu/gms.

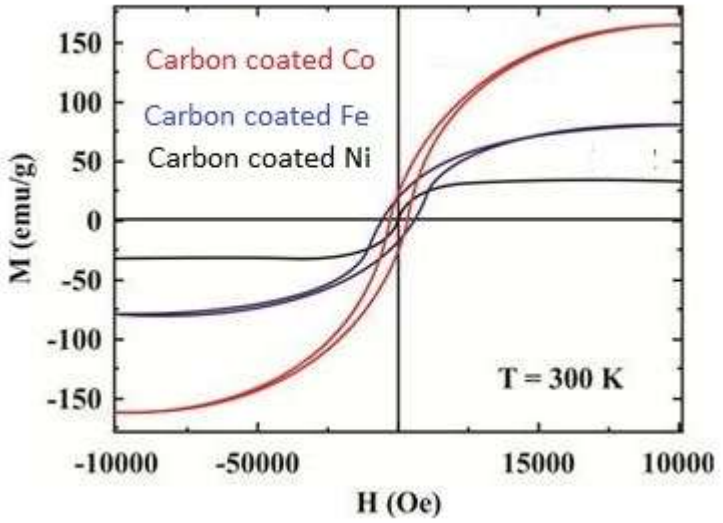


**Figure 2.22** Hysteresis loops at room temperature of Fe-C, Co-C, and Ni-C powder samples.

The magnetization is expected to be insignificant due to the rather large size of the metallic cores. In addition the small diamagnetic response of the carbon shells are also neglected [82, 83]. The mass ratio is about 36%, 97%, and 55% of the total sample mass of Fe-C, Co-C, and Ni-C, respectively. Dongping Sun *et al*.[84]have described a technique that uses a facile strategy to prepare carbon coated Fe, Co and Ni nanoparticles (denoted as Fe-C, Co-C, and Ni-C, respectively) by direct pyrolys is of bacterial cellulose (BC) which involves adsorption of corresponding metal nitrates under an inert atmosphere. Fe-C cores have been observed to have an average size of 60 nm with a narrow range of distribution from 2 to 6 nm. In the case of Co-C and Ni-C, the core size distribution is found to be in the range of 20-100 and 3-40 nm, with average diameters of 40 and 30nm, respectively.

Magnetic properties of the Fe-C, Co-C, and Ni-C are investigated at room temperature using a vibrating sample magnetometer. As shown in figure2.23, the saturation magnetization (*M*s)values are 89.927, 142.525 and 52.191 emu/gms for Fe-C, Co-C, and Ni-C, respectively, while the relative remanent magnetization (*M*r) values found to be 6.74, 11.6 and nearly zero emu/gms.

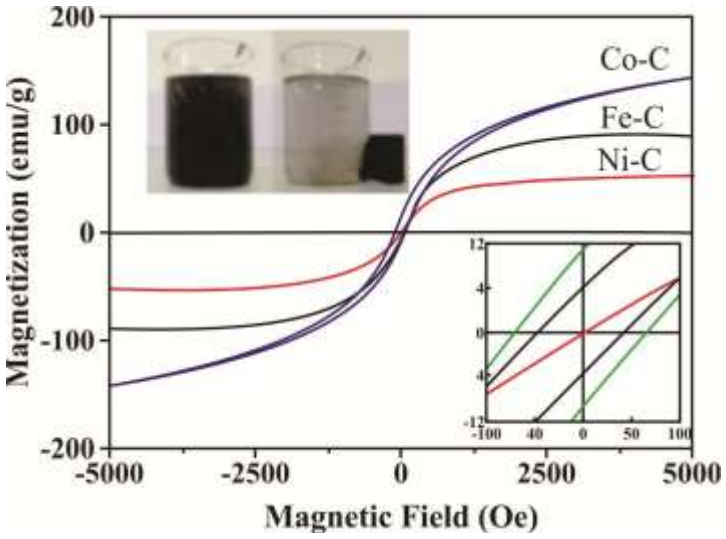


**Figure2.23**Hysteresis loops at room temperature for Fe-C, Co-C, and Ni-C powder samples [84].

Magnetic measurements have revealed that Fe-C and Co-C materials exhibit typical ferromagnetic properties while Ni-C shows super paramagnetic property at room temperature. The size dependence of the coercivity is connected with the domain structure and the grain size. In bulk samples, where the particle size strongly exceeds the domain wall width, magnetization reversal occurs due to domain wall motion.

### *2.12.1 Magnetic property of Fe–Co–Ni alloy with mechanical alloying*

Duan Yuping *et al.*[85] have investigated the precursor of $Fe_{50}Co_{40}Ni_{10}$(wt. %) powdersprepared by mechanical alloying (MA), and the evolution of structure, magnetic properties and absorbing ability are discussed systematically as a function milling time. Moreover, the magnetic property is calculated in a theoretical perspective using the first principles of the density functional theory (DFT), and the effects of the changed electronic structure on the saturation magnetization are investigated.

As shown in figure 2.24, the powders after milling for 25 h have shown a maximum $M_S$ of 153emu/g. The milling process has resulted in the increase of $H_C$ and $M_r$, and the maximum values are found to be 134 Oe and 17.28 emu/g for the powders after 90 and 40 h milling, respectively.

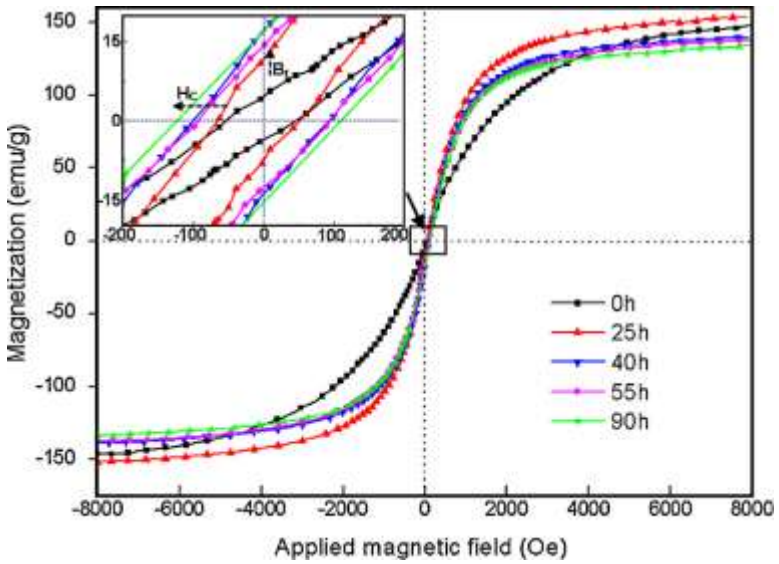


**Figure2.24** Hysteresis loops of Fe-Co-Ni powders milled for different times (0-90 h)[85].

The $M_S$ increases slightly from 147 emu/g to153 emu/g at the early stage of milling i.e. up to 25 h. This trend is attributed to the formation of solid solution of α Fe (Ni, Co) and to the charge transference between Fe, Ni and Co atoms [86].In order to explore the relationship between the variations in $M_S$ and the electron distribution, the models of α-Fe, α-Fe (Ni) and α-Fe (Co) are built and the corresponding properties, such as electron distribution and Bohr magnetron are calculated using first principle of density functional theory (DFT) within the generalized gradient approximation (GGA). The hysteresis loop for equiatomic FeNiCo mechanically alloyed powders is obtained after different intervals of milling. The maximum saturation magnetization is calculated as the magnetic moment per unit weight of the sample. It can be seen from figure2.25that the *M*s reaches its maximum value of 125.58 emu/gms at 25 h of milling.

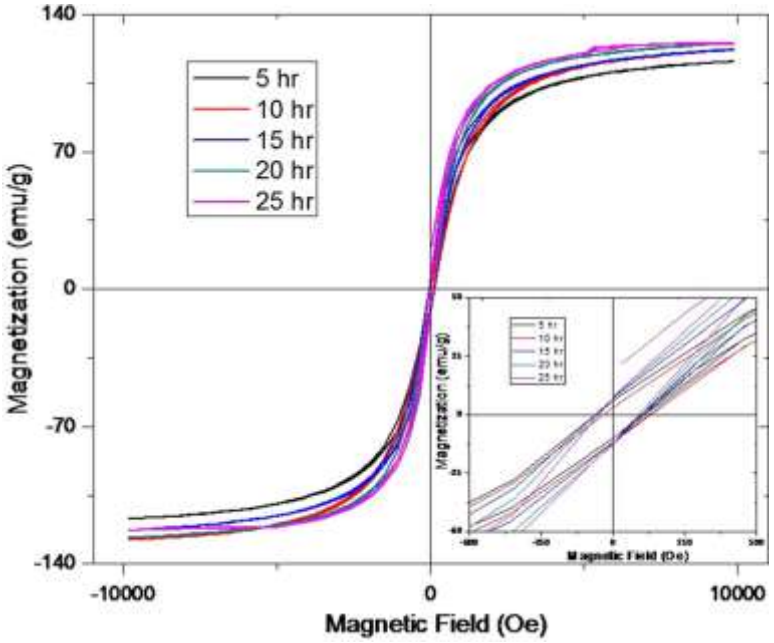


**Figure 2.25**Typical magnetic hysteresis loops for equiatomic Fe-Ni-Co powders milled for different periods (5–25 h).

Similar study is also conducted by Hossein Raanaei *et al* [87] on a nanostructured Fe-Co-Ni alloy with$Fe_{50}Co_{30}Ni_{20}$ composition and processed by mechanical alloying. The initial powder is milled for 2, 4, 8, 16, 32 and 48 h. The variation in magnetic behavior with the milling time is shown in figure 2.26 & figure 2.27.The *Ms* Value increases from 110 to 136 emu/gms after 4 h milling and then decreases sharply to 119 and 56 emu/gms for the samples milled for 8 and 16 h.

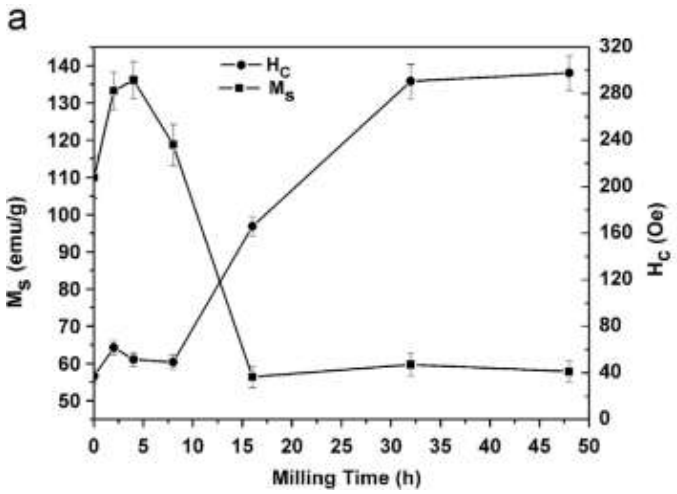

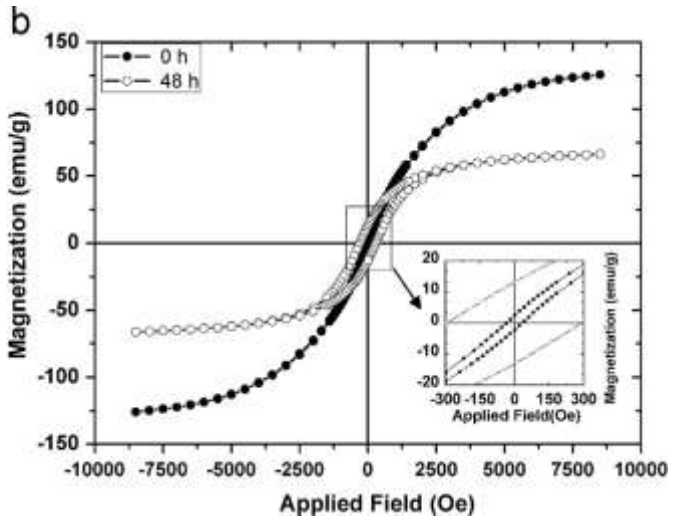


**Figure 2.26 (a)** Evolution of saturation magnetization and coercivity vs. milling time and**(b)** the measured hysteresis loops of the unmilled and 48 h milled samples [87].

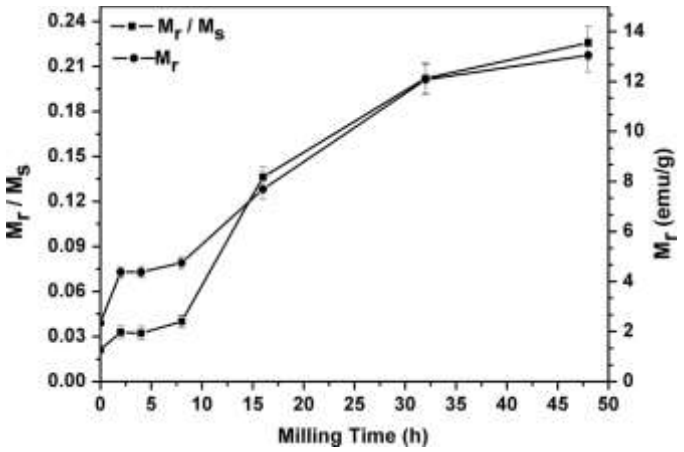


**Figure 2.27** Variations of Mr and *M*r/*M*s with milling time[87]

The variation in *M*s in the period of (2-16h) is also a signature of formation of BCC Fe (Co,Ni) solid solution considering the change in crystallite size depicted in figure 2.28.

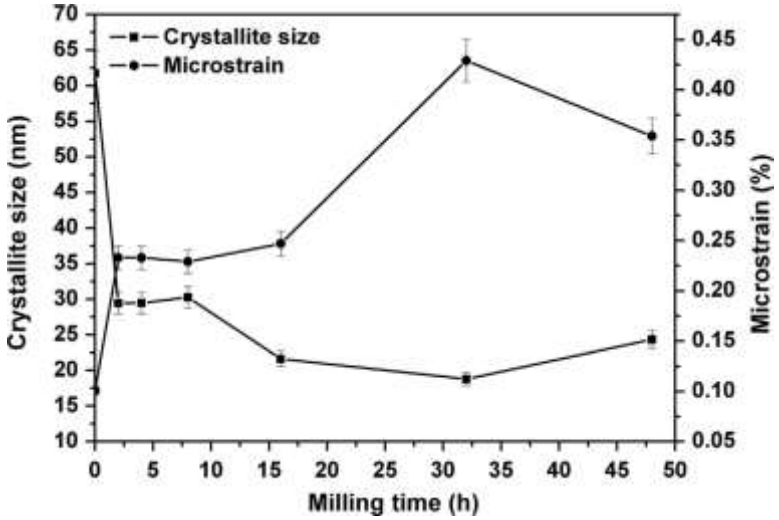


**Figure2.28**Crystallite size and lattice strain as a function of milling time [87].

The following are proposed as the reasons for the decrease in *Ms*:

(a) Large amount of magnetic atoms placed in disordered grain boundaries.

(b) The presence of nickel atoms in the alloy can reduce the value of hyperfine magnetic field.

(c) The increase in internal strain of the powders with the increases in milling time along with the introduction of point defects and dislocations.

## 2.13 Magnetism in Fe-CNT nanocomposites

H. Terrones *et al.* [89] have studied the carbon nanotubes filled with ferromagnetic nanowires of Fe, FeCo and FeNi through chemical vapor deposition method. Due to the bamboo-like morphology of carbon nanotubes, it is possible that the linear reduction of the coercive field could be a combined effect of both the mechanisms magneto elastic and thermal fluctuations. Hysteresis loops measured for samples consisting of randomly oriented flakes of aligned MWCNTs filled with Fe located at their tips figure 2.29 revealed that the magnetization reversal mechanism could take place via nucleation and the subsequent propagation of a reverse magnetic domain.It is found that the coercive field is up to 0.23 T (2300 Oe) at 4 K, which is much larger than the *Hc* for bulk Fe (e.g., tenths of Oe).

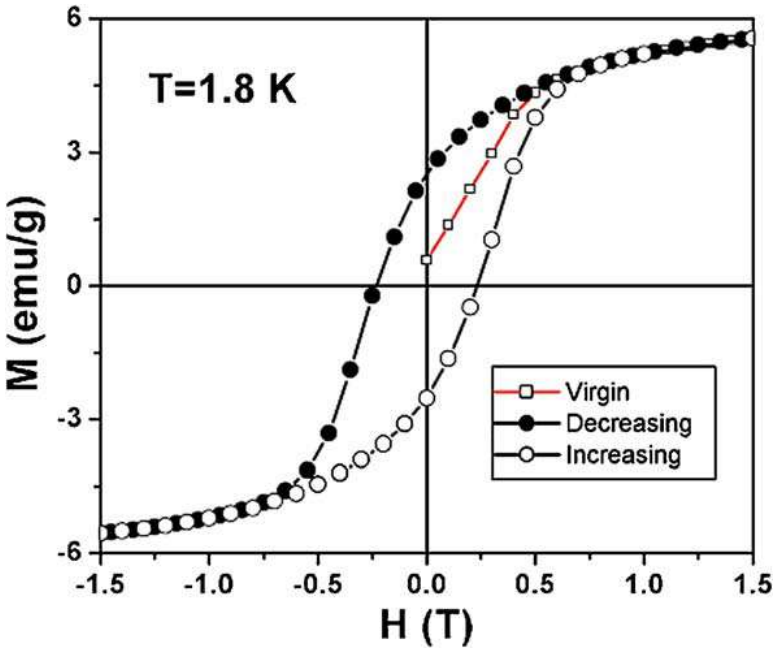


**Figure 2.29** Hysteresis loop of flakes of aligned Fe-partly-filled by MWNTs, randomly oriented and measured at 1.8 K[89].

These sudden changes in the hysteresis loops are attributed to the formation of unusual remanent spin configurations. Bingjing Hea *et al.* [90] have studied the magnetic property of the MWNT-$Fe^{2+}$ composite. The nanotube-based composite MWNT-$Fe^{2+}$ is prepared through the coordination action of the carboxylic acid groups from the oxidized multi-walled carbon nanotubes (MWNTs). The magnetic behavior of this composite is measured as a function of the magnetic field strength at 5K as a function of temperature (5–300 K) at 30 KOe. A hysteresis loop at 5K with a small coercivity of 260 Oe is observed. The experimental results have shown that the MWNT-$Fe^{2+}$ composite possess special ferromagnetic interaction between nanotubes and iron ions.

The hysteresis loop displays a characteristic behavior of a ferromagnet with a coercive field of 260 Oe and a remnant magnetization of 0.016 emu/g. The curve shows a slow increase with the increasing applied field as shown in figure 2.30. This behavior explained that the anisotropy and size distribution of the MWNTs block the orientation of magnetic moments, which lead to slow saturation of the magnetization [91].

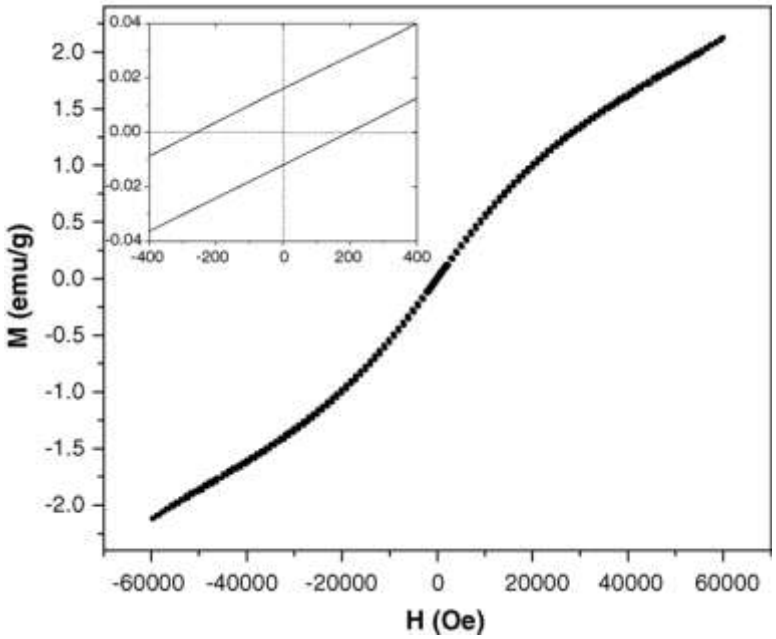


**Figure2.30**Hysteresis loop at 5K for MWNT-$Fe2^{+}$. (Inset shows expanded view of the region from-400 to +400 Oe)[90].

## REFERENCES


[1] A. Agarwal, S.R. Bakshi, D. Lahiri, Carbon Nanotubes - Reinforced Metal Matrix Composites, CRC Press, Taylor and Francis Group LLC (2011).

[2] C.N.R. Rao and A. Govindaraj, Nanotubes and Nanowires,The Royal Society of Chemistry Publishing Cambridge 2005.

[3] H.W. Kroto, J.R. Heath, S. C. O. Brien, R.F. Curl, R.E. Smalley,$C_{60}$: Buckminsterfullerene,Nature 318 (1985) 162-163.

[4] S. Iijima, Nature, Helical microtubules of graphite carbon, Nature 354 (1991)56-58.

[5] S. Iijima, T. Ichihashi, Single shell carbon nanotubes of 1nm diameter,Nature363(1993) 603-605.

[6] D.S. Bethune, C.H. Kiang, M.S. de Vries, G. Gorman, R. Savoy, J. Vazquez, and R. Bayers, Electrical conductivity of individual carbon nanotubes,Nature363 (1993)603-605.

[7] C. Klinke, J.M.Bonard, K. Kern,Comparative study of the catalytic growth of patterned carbon nanotube films, Surface Science 494 (2001) 195-201.

[8] D.Ugarte,Curling and closure of graphitic networks under electron-beam irradiation,Nature 359 (1992)707-709.

[9] Z.Y. Liu, B.L. Xiao, W.G. Wang, and Z.Y. Ma, Singly dispersed carbon nanotube - aluminum composites fabricated by powder metallurgy combined with friction stir processing, Carbon 50 (2012) 1843-1852.

[10] J.Lio, M. J. Tan, Mixing of carbon nanotubes (CNTs) and aluminum powder for powder metallurgy use, Powder Technology 208 (2011) 42-48.

[11] D. Jeyasimman, K. Sivaprasad, S. Sivasankaran, R. Narayanasamy, Fabricationand consolidation behavior of Al 6061 nanocomposite powders reinforced by multi-walled carbon nanotubes, Powder Technology 258 (2014) 189–197.

[12] L.Jiang, Z.Li, G.Fan, L. Cao, D. Zhang, The use of flake powder metallurgy to produce carbon nanotube (CNT)/aluminum composites with a homogenous CNT distribution, Carbon 50 (2012) 1993- 1998.

[13] L. Jiang, Z. Li, G. Fan, L.Cao, D. Zhang, Strong and ductile carbon nanotube/aluminum bulk nanolaminated composites with two-dimensional alignment of carbon nanotubes, Scripta Materialia 66 (2012) 331–334.

[14] L. Wang, H. Choi, J-M Myoung, W. Lee, Mechanical alloying of multi-walled carbon nanotubes and aluminum powders for the preparation of carbon/metal composites, Carbon47(2009) 3427-3433.

[15] A. Esawi, K. MorsiDispersion of Carbon Nanotubes (CNTs) in Aluminum Powder, CompositesPart A 38 (2006) 646–650.

[16] K.Morsi, A.M.K. Esawi, P. Borah, S. Lanka, A. Sayed, Characterization and Spark Plasma Sintering of Mechanically Milled Aluminum (Al) - Carbon Nanotube (CNT) composite powders, Journal of Composite Materials 44 (2010) 1991-2003.

[17] K. Morsi, A.M.K. Esawi, S. Lanka, A. Sayed, M.Taher, Spark Plasma Extrusion (SPE) of Ball-milled Aluminum and Carbon Nanotube Reinforced Aluminum Composite Powders, Composites Part A 41 (2010) 322–326.

[18] K. Morsi, A.M.K, Esawi, P.Borah, S.Lanka, A. Sayed, Spark Plasma Extrusion of single and dual matrix carbon nanotube-aluminum composites, Materials Science and Engineering A 527 (2010) 5686-5690.

[19] H. Kwon, M. Estili, K. Takagi, T. Miyazaki, A. Kawasaki, Combination of Hot Extrusion and Spark Plasma Sintering for Producing Carbon Nanotube Reinforced Aluminum Matrix Composites, Carbon47 (2009)570-577.

[20] N. Tooru, B.Junichi, Latest Trends in Automobile Material: Iron and Steel, Metals and Ceramics. Development of Carbon Nanotube-Aluminum and Expectations as Lightening Members, Eng Mater 8 (2004) 36-39.

[21] F. Housaer, F. Beclin,M. Touzin, D. Tingaud, A. Legris, A. Addad, Interfacial characterization in carbon nanotube reinforced aluminum matrix composites, Materials Characterization 110 (2015) 94–101.

[22] W.Zhou, T. Yamaguchi, K. Kikuchi, N. Nomura, A. Kawasaki, Effectively enhanced load transfer by interfacial reactions inmulti-walled carbon nanotube reinforced Al matrix, Composites Part A 125 (2017) 369-376.

[23] H. Li, A. Misra, Y. Zhub, Z. Horitac, C. C. Koch, T. G. Holesinger. Processing and Characterization of Nanostructured Cu-carbon Nanotube Composites, Materials Science and Engineering A 523 (2009) 60-64.

[24] V.M. Pham, H.T Bui, B.T Tran, X.T Than, V.C. Nguyen, D.P. Doan, N.M. Phan, The Effect of Sintering Temperature on the Mechanical Properties of a Cu/CNT Nanocomposite Prepared via a Powder Metallurgy Method, Advances in Natural Science Nanoscience and Nanotechnology 2 (2011) 015006 -10.

[25] K.Chu, J. Cheng,J. Li-kun, L.Wensheng, Improvement of Interface and Mechanical Properties in Carbon Nanotube Reinforced Cu–Cr Matrix Composites, Materials and Design, 45(2013) 407-411.

[26] N. Nayan, A.K. Shukla, P. Chandran, S. R. Bakshi, S.V.S.N. Murty,B. Pant, P.V. Venkita Krishnan Processing and characterization of spark plasma sintered copper/carbon nanotube composites, Materials Science & Engineering A 682 (2017) 229–237.

[27] H. Dong, I.Seung, Y.Byung, M. Hoon, Do.S. Han, S.H.Hong, Synergistic Strengthening by Load Transfer Mechanism and Grain Refinement of CNT/Al–Cu Composites,Carbon 50 (2012) 2417-2423.

[28] K.T Kim, J. Ecket,G.Liu,M.P. Jin, K.L Byung,H.H.Soon, Influence of Embedded-Carbon Nanotubes on the Themal Properties of Copper Matirix Nanocomposite Processed by Molecular-Level Mixing,SciptaMaterialia 64(2011) 181-184.

[29] B. Ghosh, S.K. Pradhan, Microstructure characterization of nanocrystalline $Fe_3C$ synthesized by high-energy ball milling, Journal of Alloys and Compounds 477 (2009) 127–132.

[30] J.Y. Suh, D.H. Bae Mechanical properties of Fe-based composites reinforced with multi-walled carbon nanotubes, Materials Science & Engineering A582(2013)321–325.

[31] Walid, M. D., Byung, K. L., Chan, B. M, Dong, H. N. Soon, H. H, Electrical and Mechanical Properties of Carbon Nanotube Reinforced Copper Nanocomposites Fabricated by Electroless Deposition Process, Materials Science and Engineering A 513 (2009)247–253.

[32] L.Yang,Y.D.Wang,Y.Ren,C.S.He, J.N.Deng, J.Nan, J.G.Chen, L.Zuo, Single-walled carbon nanotube-reinforced copper composite coatings prepared by electro deposition under ultrasonic field, Material Letters 62 (2008) 47-50.

[33] Y. Ren, C.H. Rüscher, C. Haas, G.A. Wiegers, Electrical transport and optical properties of the incommensurate intergrowth compounds (SbS)1.15(TiS2)*n* with *n* = 1 and 2,J. Phys. Condens. Matter 14 (2002) 8011.

[34] T.W. Ebbesen, H.J. Lezec, H. Hiura, J.W. Bennett, H.F. Ghaemi, T. Thio, Electrical Conductivity of individual carbon nanotube, Nature 382 (1996) 54.

[35] H.J. Dai, E.W. Wong, C.M. Lieber, Science 72 (1996) 523.

[36] R.A. Ma, J. Wu, B.Q. Wei, J. Liang, Processing and properties of carbon nanotubes–nano-SiC ceramic,J. Mater. Sci. 33 (1998) 5243-5246.

[37] G.D. Zhan, J.D. Kuntz, J.E. Garay, A.K. Mukherjee, Electrical properties of nanoceramics reinforced with ropes of single-walled carbonnanotubes,Appl. Phys. Lett. 83 (2003) 1228.

[38] S. M. Uddin, T. Mahmud, C.Wolf, C. Glanz, I. Kolaric, C. Volkmer, H.Höller, U. Wienecke, S. Roth, H. J. Fecht, Effect of size and shape of metal particles to improve hardness and electrical properties of carbon nanotube reinforced copper and copper alloy composites, Composites Science and Technology 70 (2010) 2253–2257.

[39] C.T White,T.N Todorov. Armchair carbon nanotubes as long ballistic conductors, Nature 393 (1998) 393 240.

[40] P. G. Koppad, H.R. A. Rama, K.T. Kashyap, On shear-lag and thermal mismatch model in multiwalled carbon nanotube/copper matrix nanocomposites, Journal of Alloys and Compounds 549 (2013) 82–87.

[41] S. Zhao, Z. Zheng,Z. Huang,S. Dong,P. Luo, Z, Zhang, Y. Wang, Cu matrix composites reinforced with aligned carbon nanotubes: Mechanical, electrical and thermal properties, Materials Science&EngineeringA675(2016)82–91.

[42] G Tong, W, Wu, Q, Hua, Y. Miao, J. Guan, H. Qian, Enhanced electromagnetic characteristics of carbon nanotubes/carbonyl iron Powders complex absorbers in 2–18GHz ranges, Journal of Alloys and Compounds 509 (2011) 451- 456.

[43] Y.J. Kim, T.S. Shin, H.D. Choi, J.H. Kwon, Y.C. Chung, H.G. Yoon, Electrical conductivity of chemically modified multiwalled carbon nanotube/epoxy composites, Carbon 43 (2005) 23-30.

[44] X.S. Fang, Y. Bando, U.K. Gautam, C.H. Ye, D. Golberg, Inorganic semiconductor nanostructures and their field-emission applications,J. Mater. Chem. 18 (2008) 509-522.

[45] D.C. Jiles Recent advances and future directions in magnetic materials, Acta Materialia 51 (2003) 5907–5939.

[46] I. Chicinas, V. Pop, O. Isnard, Magnetic properties of Ni3Fe intermetallic compound obtained by mechanical alloying, J. Mag. Mater 885 (2002)242-245.

[47] A. Bahrami, H. R. Madaah Hosseini, P. Abachi, S. Miraghaei, Structural and soft magnetic properties of nanocrystalline $Fe_{85}Si_{10}Ni_5$ powders prepared by mechanical alloying, Mater Lett60 (2006) 1068-1070.

[48] H. Jeon, J. Kim, J.Y Chung, Y.D Kim, Formation of nanocrystalline Fe–Co powders produced by mechanical alloying, Mater SciEng A 291 (2000) 17-21.

[49] H. Moumeni, S. Alleg, J.M Greneche, Structural properties of $Fe_{50}Co50$ nano structured powder prepared by mechanical alloying, Journal of Alloys and Compounds386 (2005) 12-19.

[50] H.Shokrollahi, K. Janghorban, Influence of additives on the magnetic properties microstructure and densification of Mn–Zn soft ferrites, Mater Sci Eng B 141 (2007) 91-107.

[51] H. Shokrollahi, K. Janghorban, R. Koohkan, S. Sharafi, Preparation of nanocrystalline Fe- Ni powders by mechanical alloying used in soft magnetic composites, Journal of Magnetism and Magnetic Materials320 (2008) 1089-1094.

[52] Shokrollahi H. Magnetic properties and densification of manganese–zinc soft ferrites ($Mn_{1x}Zn_xFe_2O_4$) doped with low melting point oxides, Journal of Magnetism and Magnetic Materials 320 (2008) 463-474.

[53] B. Hashemi, H. Shokrollahi, Kh. Gheisari, S. Javadpour, Magnetic losses of 3the soft magnetic composites consisting of iron and Ni-Zn ferrite, Journal of Magnetism and Magnetic Materials 320 (2008) 1544-1548.

[54] H. Shokrollahi, K. Janghorban, The effect of compaction parameters and particle size on magnetic properties of iron-based alloys used in soft magnetic composites, Materials Science and Engineering B 134 (2006) 41-43.

[55] H.Shokrollahi, K. Janghorban, Influence of $V_2O_5$ addition on the grain growth and magnetic properties of Mn-Zn high permeability ferrites, Journal of Magnetism and Magnetic Materials 308 (2007) 238–242.

[56] Sparchez Z, Chicinas I, Isnard O, Pop V, Popa F. Mechanical alloying of $Ni_3Fe$ in the presence of $Ni_3Fe$ nanocrystalline germs, Journal of Alloys and Compounds 434–435 (2007) 485–488.

[57] H.Shokrollahi, K. Janghorban, Different annealing treatments for improvement of magnetic and electrical properties of soft magnetic composites, Journal of Magnetism and Magnetic Materials 317 (2007) 61–67.

[58] B. Majumdar, M. Manivel Rajab, A. Narayanasamyb, K. Chattopadhyay, Structural and magnetic investigations on the metastable phases of the mechanically alloyed Fe-Cu system, Journal of Alloys and Compounds 248 (1997) 192-200.

[59] M.Barzegar A. Ataie, Role of Intensive Milling on Microstructure and Physical Properties of Cu80Fe20/10CNT Nanocomposite, Journal of Ultrafine Grained and Nanostructured Material47(2014) 37-42.

[60] J.Z. Jiang, C. Gente, R. Bormann Mechanical alloying in the Fe-Cu system, Materials Science and Engineering A242 (1998) 268–277.

[61] P.H. Shingu, K.N. Ishihara, K. Uenishi, J. Kuyama, B. Huang, S. Nasu, in: A.H. Clauer. J.J. de Barbadillo (Eds.), Solid State Powder Processing, The Minerals, Metals and Materials Society, Warrendale, PA, 49 (1990)21.

[62] K. Uenishi, K.F. Kobayashi, S. Nasu, H. Hatano, K.N. Ishihara, P.H. Shingu, Z. Metallkd Mechanical alloying in the Fe-Cu system,J. Appl. Phys. 83 (1992) 132.

[63] E. Ma, M. Atzmon, F.E. Pinkerton, Thermodynamic and magnetic properties of metastable $Fe_xCu_{100-x}$ solid solutions formed by mechanical alloying, J. Appl. Phys. 74 (1993) 955-962.

[64] A. Hernando, P. Crespo, J.M. Barandiaran, A.G. Escorial, R. Yavari, Magnetic properties of mechanically alloyed Fe-Cu,J. Magn. Magn. Mater. 124 (1993) 5-8.

[65] J.Z. Jiang, Q.A. Pankhurst, C.E. Johnson, C. Gente, R. Bormann,Magnetic properties of mechanically alloyed FeCu, J. Phys. Condens. Matter 6 (1994) 227-232.

[66] O. Drbohlav, A.R. Yavari, Magnetic properties of mechanically alloyed nanocrystalline fcc $Cu_{50}Fe_{50}$ during thermal decomposition, Journal of Magnetism and Magnetic Materials 137 (1994) 243-248.

[67] O. Drbohlav, A.R. Yavari, Mechanical alloying and thermal decomposition of ferromagnetic nanocrystalline f.c.c.-$Cu_{50}Fe_{50}$,Acta Mater 43 (1995) 1799-1809.

[68] E. Dislaki, J. Sorta, E.Pellicer, Parametric aqueous electro deposition study and characterization of Fe–Cu films Electrochemical,Acta231 (2017)739-748

[69] P. Gorria, D. Martínez-Blanco, J. A. Blanco, A. Hernando, J.S Garitaonandia, L.F. Barquín, J.Campo, R. I Smith, Invar effect in fcc-FeCu solid solutions, Physical Review *B*69 (2004) 214421-5.

[70] C. Cutrano, Ch.E. Lekka, Structural, magnetic and electronic properties of Cu-Fe nanoclusters by density functional theory calculations, Journal of Alloys and Compounds 707 (2017) 114-119

[71] T. Sourmail, Near equiatomic FeCo alloys: constitution, mechanical and magnetic properties, Prog Mater Sci 50 (2005) 1-84.

[72] H. Jeon, J. Kim, J.Y. Chung, Y.D,Kim, Formation of nanocrystalline Fe–Co powders produced by mechanical alloying, Mater Sci Eng A 291 (2000) 17-21.

[73] B.H. Lee, B. S. Ahn, D. G. Kim, S.Tag Oh, H.Jeon,J.Ahn, Y.D. Kim Microstructure and magnetic properties of nanosized Fe–Co alloy powders synthesized by mechano-chemical and mechanical alloying process, Materials Letters 57 (2003) 1103– 1107.

[74] C. Kuhrt, L. Schultz, Formation and magnetic properties of nanocrystalline mechanically alloyed Fe –Co and Fe – Ni, J. Appl. Phys. 73 (1993) 6588–6590.

[75] H. Shokrollahi The magnetic and structural properties of the most important alloys of iron produced by mechanical alloying, Materials and Design 30 (2009) 3374–3387.

[76] A. Zelenakova, D. Oleksakova, J. Degmova, J.Kovac, P. KollaR, M. Kusy, P. Sovak Structural and magnetic properties of mechanically alloyed FeCo powders, Journal of Magnetism and Magnetic Materials 316 (2007) 519–22.

[77] X.Sun, A. Gutierrez, M.J.Yacaman, X. Dong, S.Jin, Investigations on magnetic properties and structure for carbon encapsulated nanoparticles of Fe, Co,Ni, Materials Science and Engineering A 286 (2000) 157–60.

[78] A.A. El-Gendy, E.M.M. Ibrahim, V.O. Khavrus, Y. Krupskaya, S. Hampel, A. Leonhardt, B. B. Chner, R. Klingeler The synthesis of carbon coated Fe, Co and Ni nanoparticles and an examination of their magnetic properties, Carbon 47 (2009)2821-2828.

[79] J.J Henry, S.A Majetich, Morphology, structure, and growth of nanoparticles produced in a carbon arc, Phys Rev B 52 (1995) 12564–71.

[80] P.J.F Harris, S.C Tsang, A simple technique for the synthesis of filled carbon nanoparticles, Chem Phys Lett 293 (1998) 53–8.

[81] J. Heremans, C.H Olk, D.T Morelli, Magnetic susceptibility of carbon structures, Phys Rev B 49 (1994) 15122–5.

[82] K.Lipert, F. Kretzschmar, M. Ritschel, Leonhardt A, Klingeler R, Bu¨ chner B. Nonmagnetic carbon nanotubes, J Appl Phys 105 (2009) 1–4.

[83] B. Ma, Y. Huang, C. Zhu, C. Chen, M. Fan,D.Sun, A facile method to synthesize carbon coated Fe, Co and Ni and an examination of their magnetic properties, Journal of Alloys and Compounds 687 (2016) 741-745.

[84] D.Yuping, Z. Yahong, W. Tongmin, G. Shuchao, L. xin, L. Xingjun, Evolution study of microstructure and electromagnetic behaviors of Fe-Co-Ni alloy with mechanical alloying, Materials Science and Engineering B 185 (2014) 86–93.

[85] L. Karimi, H. Shokrollahi, Structural, microstructural and magnetic properties of amorphous/nanocrystalline $Ni_{63}Fe_{13}Mo_4Nb_{20}$ powders prepared by mechanical alloying, J. Alloys Compd. 509 (2011) 6571–77.

[86] H.Raanaei, H. Eskandari, V.M. Hosseini Structural and magnetic properties of nanocrystalline Fe–Co–Ni alloy processed by mechanical alloying, Journal of Magnetism and Magnetic Materials398 (2016)190–195.

[87] E. Jartych,on the magnetic properties of mechano synthesized Co–Fe–Ni ternary alloys, Journal of Magnetism and Magnetic Materials323(2011)209–216.

[88] H. Terrones, F. López-Urías, E. M. Sandoval, J.A. R. Manzo, A. Zamudi, A.L. Elías, M. Terrones Magnetism in Fe-based and carbon nanostructures: Theory and applications, Solid State Sciences 8 (2006) 303–320.

[89] B. He, M.Wang, W. Sun, Z.Shen Preparation and magnetic property of the MWNT-Fe2+ composite, Materials Chemistry and Physics 95 (2006) 289–293.

[90] X.K. Wang, R.P.H. Chang, A. Patashinski, J.B. Ketterson, Magnetic susceptibility of buck tube, J. Mater. Res. 9 (6) (1994) 1578–1582.

[91] A.S. Kotosonov, Texture and magnetic anisotropy of carbon nanotubes in cathode deposits obtained by the electric-arc method, JETP Lett. 70 (7) (1999) 476–480

# *CHAPTER THREE*

## *Methodology*

In this chapter, description about the raw materials used for the current research is elaborately made. Also detailed account of various experimental techniques used, experimental conditions employed and parameters fixed for individual experimentation is provided. The methods adopted for synthesis of Fe-MWCNT nanocomposites are narrated and the implication of selection of specific fabrication parameters is also discussed. Details about the methodology adopted for various characterization techniques like X-Ray Diffraction(XRD), Fourier transform infrared spectroscopy (FT-IR), Raman spectroscopy, DC electrical conductivity, Optical microscopy, Vickers micro hardness, Scanning Electron Microscopy(SEM), Transmission Electron Microscopy(TEM), Vibrating sample magnetometer (VSM), INSTRON and X-ray Photoelectron spectroscopy(XPS)that are used in the research work, are presented in this chapter.

## 3.1 Introduction

Mechanical alloying route is one of the mostwidely used processing techniques for the synthesis of Fe-MWCNT metal matrix nanocomposites.The selection of processing technique mainly depends upon the reinforcement material, the matrix material, and the application. The processing of nanocomposites is the most important step, as it controls the microstructure which in turn decides various properties of the materials. In the prsent research, all samples of Fe-MWCNTs metal matrix nanocomposites are prepared under argon atmosphere.

## 3.2 Materials

The following chemical are used to prepare all the samples; Iron power (Fe; 99% purity, size 325 mesh Sigma-Aldrich) is used as the matrix material. Steric acid ($CH_3(CH_2)_{16}COOH$; 99%.purity) is used as the PCA. The MWCNTs (density 2.16 g/cc) purchased from Nanoshel (with diameter and length are (16-20 nm) and (3-8 μm), respectively) is used as the filler to enhance the physical and mechanical property of Fe-MWCNT metal matrix nanocomposites.

## 3.3 Synthesis of Fe-MWCNTx(x=0.5, 1 and 2 wt.%)

High energy ball milling of mixture of iron powder and MWCNT was carried out by the use of both solid and liquid process control agent (stearic acid and ethanol respectively). MWCNT content has been varied from 0.5 wt.% to 2 wt.%. After sonication of MWCNT in 50 ml of ethanol for 10 min, iron powders were added and ultra-sonication of the suspension is continued for 5 min. Evaporation of ethanol is accomplished by heating the mixture at 50°C for 30 min. The mixture is then subjected to high energy ball milling (HEBM) for 2 h with ball to powder ratio 6:1 (BPR) at a vial speed of 200rpm. Stearic acid is used as process control agent for all compositions of composite. Also, ethanol as liquid process control agent (PCA) has been tried in high energy ball milling of iron-1 wt.% MWCNT powder mix with ball to metal ratio of 6:1 at a milling speed of 200 rpm. The morphology of the as milled alloys powders are discussed in details.

## 3.4 Synthesis of Fe-2wt% MWNTs powder

In this part, ball milling was performed with 2 wt.% CNTs concentration in addition to a pure Fe sample as a reference. High energy ball milling of a mixture of

the iron powder and 2 wt.% MWCNT has been carried out in a Planetary Ball Mill. The Fe-2 wt.% MWNTs powders were taken in 250 ml tungsten carbide vial. The air inside the vial was flushed out by passing pure Argon gas. Tungsten carbide balls (ball: powder = 6:1) were used for milling the mixture at a vial speed of 200 rpm for various periods of time. In order to avoid sticking and agglomeration of iron powder, 1 wt.% stearic acid has been used as the process control agent (PCA). Samples milled under argon atmosphere were collected at regular intervals of milling viz.10, 20, 30, 40, 60 & 90 min for characterizing the Fe-based MWCNT nanocomposites. The morphology of the as milled alloys powders were discussed in details.

## 3.5 Synthesis of Fe –MWCNT$_X$ powder (X= 1%, 2%, 3% and 4 wt.% MWCNTs)

The Fe-MWCNT composite were obtained by homogeneously mixing the Fe powder with various weight fractions MWCNTs (1%, 2% 3% and 4 wt.%). Fe-MWCNTs powder has been synthesized by mechanical alloying followed by spark plasma sintering. Fe-MWCNT powder was placed in 250ml tungsten carbide jar under argon atmosphere. The ball to powder ratio and the milling speed were maintained as 6:1 ad 200 rpm respectively. During milling process one weight percent stearic acid was added as a process control agent (PCA) to prevent the excessive sticking and agglomeration of Fe powders. Sample 1 wt.% MWCNT to 4wt.%MWCNT were milled for 50 min.

### *3.5.1 Spark plasma sintering (SPS) of Fe –MWCNT$_X$ powder (X= 1%, 2%, 3% and 4 wt.% MWCNTs)*

The Fe-MWCNT milled powders were (total four sample with different wt.% of MWCNT) densified by a spark plasma sintering (SPS) equipment, Dr. Sinter (Model SPS 625IIT Kharagpur).The milled powders were filled in a die cavity having diameter of 20 mm. Graphite foil was used to prevent the sticking of alloy powders from the die walls.

As milled powder Fe-1 wt.% MWCNT,Fe-2 wt.% MWCNT,Fe-3 wt.% MWCNT,Fe-4 wt.% MWCNT after 50 min of milling were sintered at $650^0$C.The holding time at the sintering temperature, the heating rate and applied load were 10 min, $100^0$C/min and 50MPa, respectively. The results showed the CNT particles

segregated to the grains boundaries and negligible quantity of porosity in the microstructure for all the samples.Thefinal products of approximately 20mm×5mm height were polished with SiC emery paper to remove surface contamination from the graphite die and foil before measuring the D.C electrical conductivityand other property characterization. TheSpark plasma sintering (SPS) process is shown in figure3.1.

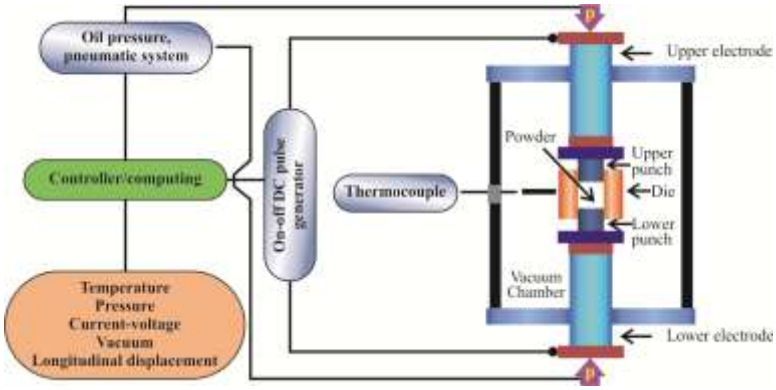


**Figure 3.1** Schematic diagram of spark plasma sintering set up.

### 3.6 Synthesis of Fe–MWCNT$_X$ -Ag$_Y$ powder (X= 1%, 2%, 3% and 4 wt.% MWCNTand Silver dopedY = 0.1 wt.% for each sample)

In this processes doping 0.1 wt.% of silver in Fe-MWCNT nanocomposite is done by mechanical alloying route. The milling process has been carried out at the room temperature using tungsten carbide vial (jar) and balls during high energy ball milling in planetary mill of make, Fritsch Pulversitte-6Gramny. The Fe - MWCNT-Agcomposites were obtained by homogeneously mixing the Fe powder with various weight fractions MWCNTs (1 %, 2%, 3% and 4 wt.%) and adding by measured quantity of silver as dopant (y=0.1 wt.%) in each batch. Fe-MWCNT-Ag powder was placed in 250ml Tungsten carbide jar under argon atmosphere. The ball to powder ratio and the speed were maintained as 6:1 ad 200 rpm respectively. During milling process one weight percent stearic acid was added as a process control agent (PCA) to prevent the excessive sticking and agglomeration of Fe powders. The Fe-MWCNT-Ag powder was milled only 50 min.

### *3.6.1 Spark plasma sintering (SPS) of Fe –MWCNT$_X$-Ag$_Y$-powder (X= 1%, 2%, 3% and 4 wt.% MWCNTs and silver doped Y=0.1 wt.% for each sample)*

The Fe-MWCNT-Ag milled powders were (total four sample with different wt. % of MWCNT with0.1 wt.% of silver) has been densified by a spark plasma sintering (SPS) equipment, Dr. Sinter (Model SPS -625IIT Kharagpur).The milled powders were filled in a die cavity having diameter of 20 mm. Graphite foil was used to prevent the sticking of alloy powders from the die walls. The milled powders of Fe-MWCNT-Agafter 50 min of milling were Spark Plasma Sintered at $650^0$C.The holding time at sintering temperature, the heating rate and applied load were 10 min, $100^0$C/min and 50MPa, respectively. The results showed that the CNT particles were concentrated at the grain boundaries and porosity content has been negligibly small as seen in the microstructures of all the samples. Measurement of electrical conductivity of sintered samples Fe-MWCNT-Ag was carried out.

## 3.7 Synthesis of Fe- MWCNTx powders(X=0.5 1, 2, and 3 wt.%of MWCNTs)

The milled powders were filled in graphite die cavity having diameter of 20 mm. Graphite foil was used to prevent the sticking of alloy powders from the die walls. The powders of Fe-MWCNT after high energy ball milling for 2h were subjected to SPS at $700^0$C.The holding time at sintering temperature, the heating rate and applied load were 10 min, $100^0$C/min and 60MPa, respectively. After spark plasma sintering, the finished samples of approximately diameter and height 20mm× 5mm were polished with SiC paper to remove surface contamination from the graphite die; after then the mechanical and physical properties of Fe-MWCNTs naocomposite have been studied.

## 3.8 Characterization Techniques and Processes

Many characterization techniques are used for the understanding the behavior of iron-MWCNT composites with or without silver doping. The processes are shown schematically in figure 3.2

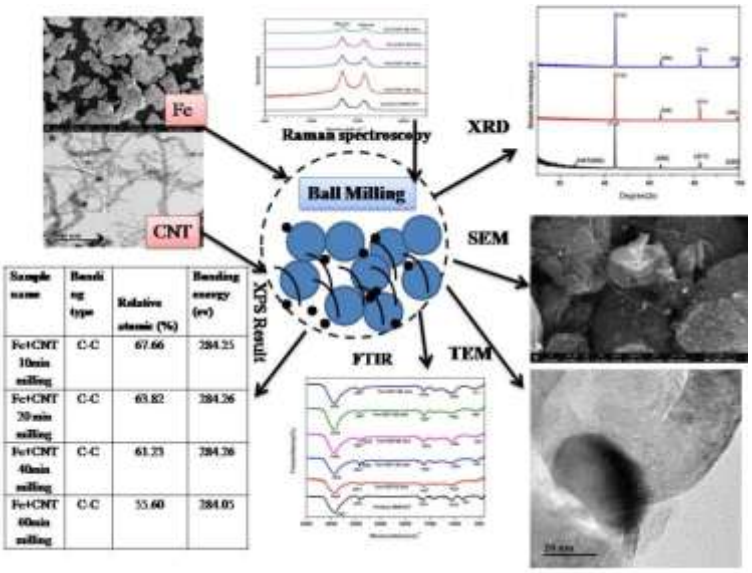


**Figure 3.2**The milling processes of Fe-MWCNT nanocomposites and characterization technique.

### *3.8.1 X-ray Diffractometry (XRD)*

Information related to the crystallinity of the samples of Fe-MWCNTs is collected with the help of X-ray Diffraction study conducted with XRD of make Panalytical X-'pert pro; Cu Kα radiation (wavelength = 1.54 Å) was used for diffraction study. The XRD data were collected in the 2θ range 20 to 100° with scan speed $2^0$/min., step size 0.04° and counting time 30s. The slit size used for the present experiments has been 10 mm x 15mm and the penetration depth of X-ray was maintained at about 15 µm. The detection limit of minor phase is less than 1 wt.%. The XRD experiment has been carried out for long enough time to secure a high signal to noise ratio; this enables to achieve a detection limit less than 1 wt.% even for MWCNT of low atomic scattering factor.

### *3.8.2 Fourier Transform Infrared (FTIR) Spectroscopy*

Fourier transform infrared (FTIR) spectroscopy (Perkin Elmer, 4000–400 $cm^1$) is a technique which is used to obtain an infrared spectrum of absorption or emission of a solid. FTIR spectroscopy at the same time collects high spectral resolution data over a wide spectral range. This confers an important advantage over a dispersive spectrometer which measures intensity over a narrow range of wavelengths at a time. The bonding characteristics of all Fe-MWCNTs

nanocomposites samples are studied with Fourier transform infrared spectroscopy by the use of KBr as binder.

### *3.8.3 Raman Spectroscopy*

Raman scattering occur with a change in vibrational, rotational or electronic energy of a molecule. If the scattering is elastic, the process is called Rayleigh scattering. If it's not elastic, the process is called Raman scattering. Raman spectroscopy is carried out to get information about the structural integrity of the as-received MWCNT and the Fe-MWCNT nanocomposites after high energy ball milling before and after SPS. Raman spectra of nanocomposites milled for various times were recorded under Argon ion laser excitation at 514 nm at a very low power (< 1mW) to avoid excessive heating. Raman spectroscopy was carried out at room temperature in AIRIX STR 500 CONFOCAL MICRO Raman Spectrometer.

### *3.8.4 Scanning Electron Microscopy (SEM)*

The morphology of Fe-MWCNT nanocomposites is examined using FESEM (Nova Nano450SEM, FEI, North America) operated at 15-20 kV. Energy dispersive X-ray spectroscopy (EDS) detector (Bruker, Germany) is employed for the determination phase composition and for elemental mapping.

### *3.8.5 Optical Microscopy*

Optical microscopy is carry out to reveal the morphology of phase present. Carl Zeiss LSM 780.Optical microscope was used to carry out to microstructural analysis and used to analyze microstructure at different magnification level like 25X, 100X, 200X.

### *3.8.6 Transmission Electron Microscopy (TEM)*

It is considered to be a valuable characterization tool that provides a wealth of information about the internal structure of Fe-MWCNT composites, and is very helpful in detecting the presence of nanostructures, and any contamination at the matrix-MWCNT interface. The microstructures of Fe-MWCNT mixture in powder form, and in solid from after SPS have been investigated by high resolution transmission electron microscopy (HRTEM) of make FEI: TECNAI $G^2$ operated at

200 kV. Samples for TEM study have been prepared by dispersing a small amount material in isopropyl alcohol and then a single drop of the suspension is put on a 300-mesh carbon coated copper grid with the help a micropipette in order to find out the information about samples in powder form. In order to dry the copper grid, it is kept for overnight and then used for TEM analysis. In case solid samples, sample preparation by ion milling as well as by twin jet polishing techniques were carried and the thickness of the final sample was such as to be perfectly electron transparent.

### *3.8.7 Thermal analysis*

Properly cleaned sample pieces of 10mg weight are used for Differential Scanning Calorimetry (DSC) (Netzsch Model no. DSC 404 F3)analysis. Nitrogen gas is used for controlled atmospheric conditions and the heating rate is kept 10° K/min. Baseline is corrected before acquiring the DSC curve for each samples.

### *3.8.8 X-ray photoelectron spectroscopy (XPS)*

XPS study is performed in an Omicron Nanotechnology XPS system from Oxford Instruments (model ESCA+). Aluminum source is used for XPS study under high vacuum with monochromatic Al-Kα radiation having source energy of 1486.7eV and a 124-mm hemispherical electron analyzer is used for the study. The present study has envisaged the availability of carbon atoms through controlled damage of MWCNT in Fe-MWCNT nanocomposites so that iron - carbon bond formation by p-d hybridization becomes possible at the interface. XPS study is employed as an aid to assess the degree of damage in MWCNT due to high energy ball milling.

### *3.8.9 Vibrating Sample Magnetometer (VSM)*

Vibrating Sample Magnetometer (VSM) model EZ9 Microsence Company is employed at an applied magnetic field range -20Oe to + 20Oe for studying the room temperature magnetic properties of Fe-MWCNT nanocomposites powder obtained by high energy milling with or without sintering.

### *3.8.10 Current-Voltage Measurements*

The DC electrical conductivityof Fe-MWCNT nanocomposites pellets are measured using Electrometer (B 1500A Agilent Technology).Silver paste is applied on the cross-sectional faces of the pellets prior the electrical conductivity measurements. Standard two-probe set up is used for these measurements. The equations 3.5 and 3.6are used to calculate the DC electrical conductivity of Fe-MWCNT nanocomposites.

$$\rho = RA/ \quad (3.5) \text{ ---------- } (3.5)$$

$$\sigma = 1/ \quad (3.6) \text{ ---------- } (3.6)$$

where$\rho$ (ohm. m) is the resistivity of the Fe-MWCNT pellet, $R$ (ohm) is the resistance of the Fe-MWCNT pellet; $A$ ($m^2$) is the area of the pellet, $L$ (m) is the thickness of the Fe-MWCNT pellet and $\sigma$ (S/m) is the conductivity.

### *3.8.11 Vickers Micro-Hardness Testing*

The surfaces of the specimens are ground and polished before testing. The measurements are performed at room temperature with a UHL VMHT (WalterUhlGmbh, Germany) micro hardness tester. The load of 300 gf and dwell time of 15 sec is applied to measure the hardness of the bulk nanocomposites pellets. Ten different indentations are made at different sites on each of the samples and the average of ten consistent values is taken as the reportable result.

### *3.8.12 Compression Test*

The compressive test of Fe-MWCNT composites of varying amounts of reinforcement has been carried out at room temperature in an Instron testing machine (model - 8800) under a constant crosshead speed and with an initial strain rate of 0.05 $s^{-1}$.To conduct the compressive tests the samples are per prepared in a cylindrical from with a height and diameter 5×5 mm. The engineering stress – engineering strain diagrams are used to assess the compressive strength of the materials.

The methodology adopted in research work summarized with flow diagram shown in figure 3.3.

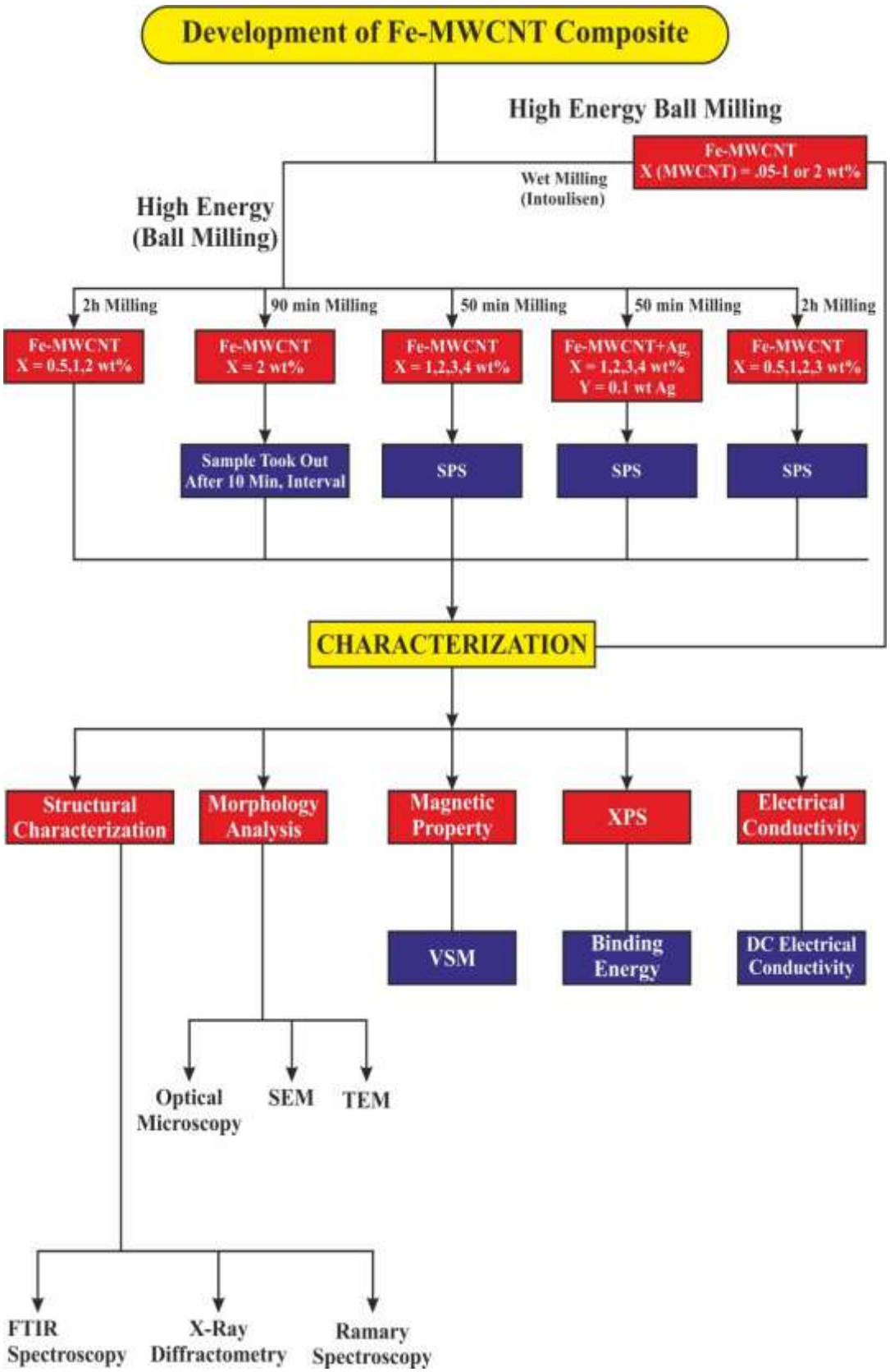


**Figure 3.3** Schematic representation of the methodologies used in the present investigation

# *CHAPTER FOUR*

## *Effect of High Energy Ball Milling on The Structure of Iron –Multiwall Carbon Nanotubes (MWCNT) Composite*

This chapter describes the results of study on the possible loss in structural integrity when high energy ball milling is employed to produce iron matrix MWCNT reinforced composite. The damage caused to MWCNT due to harsh ball milling condition and its influence on interfacial bonding is reported. Different amount of MWCNT is used to find the optimal percentage of MWCNT for avoidance of the formation of chemical reaction product at the matrix - reinforcement interface. Effect of process control agent is assessed by the use of different materials for the purpose. It is observed that ethanol as a process control agent (PCA) causes degradation of MWCNT reinforcements after milling for 2h whereas solid stearic acid used as process control agent, allows satisfactory conservation of MWCNT structure. It is further noted that at a high MWCNT content (~ 2 wt.%), high energy ball milling leads to synthesis of iron and carbon and forms iron carbide (cementite) at the iron-MWCNT interface. At low percentage of MWCNT, dissolution of carbon in iron takes place and the extent of damage of reinforcement in iron matrix composite becomes negligibly small; however, under the present ball milling condition (ball to metal ratio~ 6:1 and 200 rpm vial speed) iron-1 wt.% MWCNT composite of good interfacial bonding can retain the tubular structure of reinforcing MWCNT.

## 4.1 Introduction

Due to attractive physical and mechanical properties, carbon nanotubes have attracted special attention of the researchers to explore its employment in a number of useful applications [1, 2].Nonlinear vibration properties of multiwall carbon nanotubes, its buckling behavior under load and other physical and mechanical behavior of MWCNT have been elegantly studied by previous workers [3-5].There are reports on the capability of magnetic particle filled CNTs to absorb microwaves [6, 7].Success in the development of CNT reinforced polymer matrix composites, has stimulated new researches for development of nanocomposites based on metal matrix. It is known that high aspect ratio along with Vander Waals forces among CNTS make it difficult to disperse CNTs uniformly within a metal matrix. Several fabrication methods are so far tried for production of uniformly distributed Metal-MWCNT nanocomposites [8]. However, it is reported that mechanical alloying route has been successful in fabrication of aluminum- MWCNT composites with reasonably good distribution of reinforcing material [9-11]. Poor interfacial bonding and agglomerating tendency of MWCNTs are considered to be responsible for causing problems in securing reproducibility in structure and properties of metal matrix MWCNT reinforced composites. In spite of success in production of metal-MWCNT composite, fabrication of iron matrix-MWCNT composites by high energy ball milling bears the risk of damage at the surface of MWCNT. This is because the solubility of carbon atoms in iron is quite high. Also, iron has high affinity for carbon to form its carbide. Hence mechanical alloying can lead to the formation of carbide at the matrix-MWCNT interface through mechano-chemical synthesis of MWCNT and the matrix metal. While some researchers believe this reaction to be a genuine danger in harnessing the potential advantage of MWCNT as reinforcement, there are others who opine that the formation of carbide in aluminum-MWCNT interface reduces the wettability angle and thus aids in achieving a better interfacial bonding. Since attempt to produce iron-MWCNT composite through mechanical alloying route is scarce in literature, it seems worthy to study structural evolution in high energy ball milled iron-MWCNT nanocomposite containing varying amounts of MWCNT. Attempts are also made to evolve means for conservation of graphite structure of MWCNT.

## 4.2 Experimental work

### *4.2.1 Materials*

The materials used for the present study are the multiwall carbon nanotubes (MWCNT) and iron powders of predetermined sizes and shapes. The purity of iron powder (Sigma Aldrich) is greater than 99% and its size is -325 mesh (~ 44micron). The iron powders of irregular shape, make up the metal matrix; MWCNTs fabricated by chemical vapor deposition (CVD) technique has the purity 98 wt.%; its diameter is about 10- 20nm and length ranges from 3-8 μm. Scanning Electron microscopy and high resolution transmission electron microscopy (HRTEM) are used to examine the morphology of as received iron powder and the MWCNT used in the present study (figure 4.1).

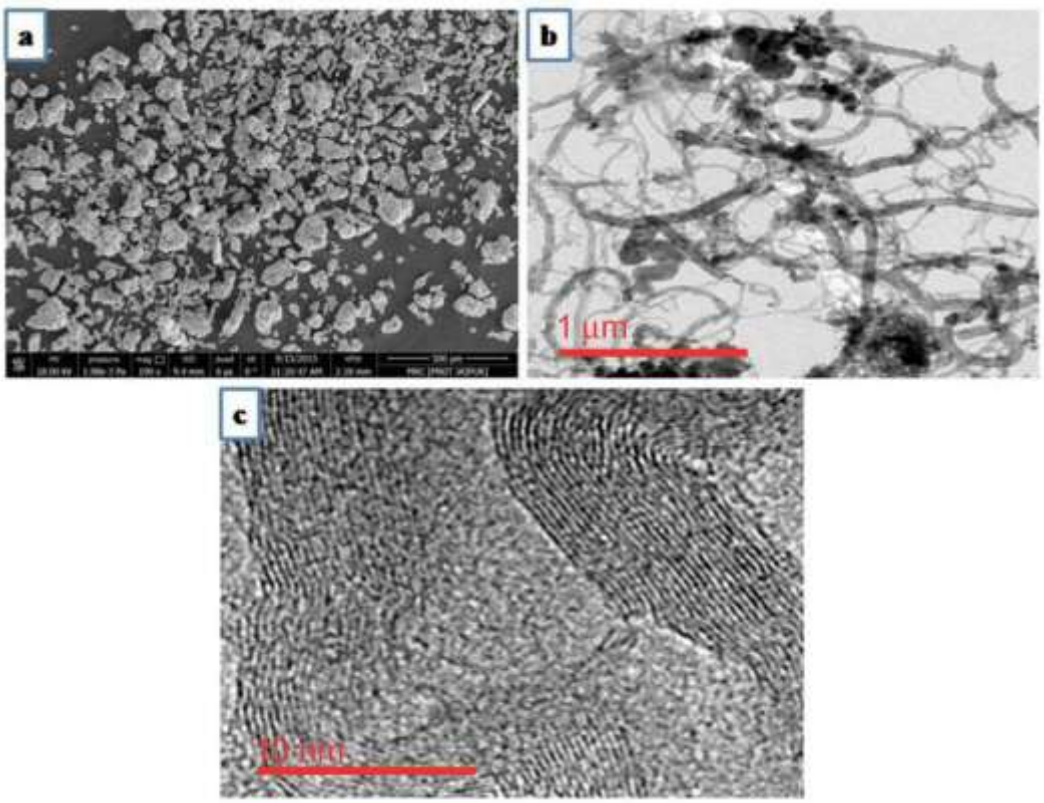


**Figure4.1** (a) SEM image of as received pure iron powder (b) TEM image of as received MWCNT and (c) HRTEM image of MWCNT.

### *4.2.2 Method of preparation*

High energy ball milling of mixture of iron powder and MWCNT was carried out by the use of both solid and liquid process control agent (stearic acid and ethanol respectively). MWCNT content has been varied from 0.5 wt.% to 2 wt.%.

After sonication of MWCNT in 50 ml of ethanol for 10 min, iron powders were added and ultra-sonication of the suspension is continued for 5 min. Evaporation of ethanol is accomplished by heating the mixture at 50°C for 30 min. The mixture is then subjected to high energy ball milling (HEBM) for 2h by following procedure described in Methodology chapter. Both stearic acid and ethanol are used as process control agents.

### *4.2.3 Characterization of ball milled composites*

Microstructural study of nanocomposites of different MWCNT content was conducted by field emission scanning electron microscope of model, NOVA NANOSEM 450, at an accelerating voltage of 15KV. X-ray diffraction study was carried with the aid of Xpert-Pro Pan Analytical model XRD system as per procedure described in earlier chapter. High resolution transmission electron microscope (Tecnai $G^2$20 FEI S Twin) is employed for microstructural study at high resolution. Raman spectroscopy has been carried out with experimental composites by following the method described in Chapter three.

## 4.3 Result and Discussion

### *4.3.1 SEM Analysis*

The microstructures of HEBM nanocomposite are shown in figure 4.2 and figure 4.3. Figure 4.2 reveals that in Fe-1 wt.% MWCNT nanocomposite, MWCNT are embedded in the matrix of iron particles which have been flattened due to high energy ball milling for 2 h. It is also observed that the MWCNTs have become shorter in length due to ball milling. This observation is in agreement with previous investigations [12].

In case of nanocomposite containing 2 wt.% MWCNT, it does not seem that flattening of iron particles has been as good as in 1wt.% MWCNT containing nanocomposites figure 4.3(a). Increasing the MWCNT content is known to exhibit higher tendency for agglomeration due to Vander Waal's forces of attraction. Also, higher MWCNT content within metal matrix puts more resistance to deformation of

metal particles because of the fact that a higher amount of MWCNT in the nanocomposite would share higher amount of energy imposed onto the system during high energy ball milling. At the same time, high population density of MWCNT restricts the radial flow of metallic materials and so metal particles have become constrained in flattening at higher concentration of MWCNTs (2 wt.%). Moreover, the microstructures in figure 4.2(b) and figure 4.3(b) show that the interfacial bonding is apparently good after 2h ball milling.

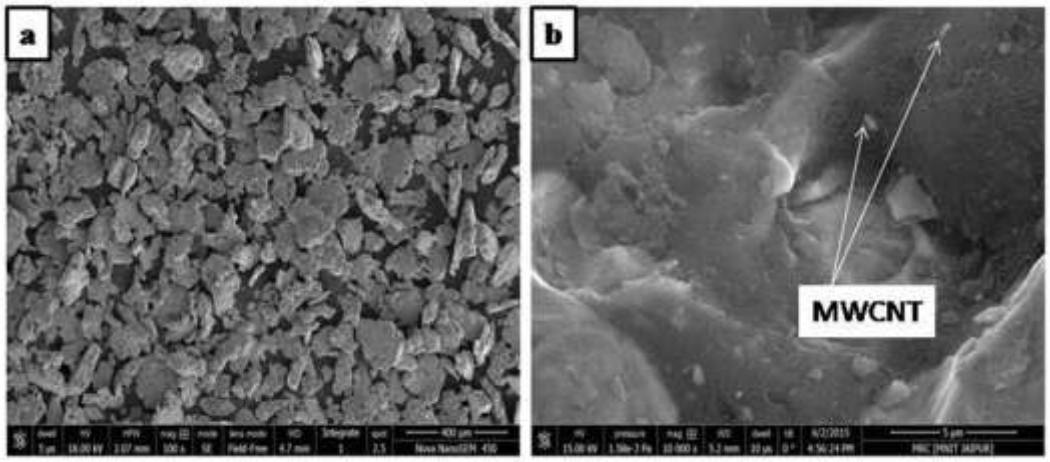


**Figure 4.2** SEM image of Fe-1wt% MWCNT nanocomposite, (a) Flattening of metal particles and (b) At higher magnification; MWCNTs are embedded at places (white arrow).

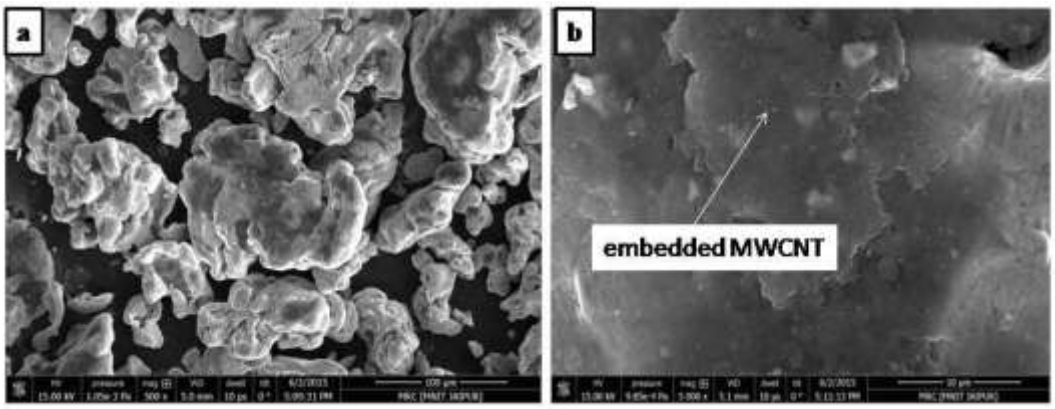


**Figure 4.3** SEM image of Fe-2wt.%MWCNT nanocomposite (a) morphology of powder after 2h milling and (b)At higher magnification embedded MWCNT.

### *4.3.2 XRD Analysis*

X-ray diffraction study is conducted to monitor the evolution of structural constituents in iron-MWCNT nanocomposites. Figure 4.4 shows the XRD spectra of

nanocomposites containing different quantity of MWCNT reinforcement. It can be seen in the spectrum of Fe-0.5 wt.% MWCNT that no characteristic peak of MWCNT presents in the said XRD spectrum. For iron- 1 wt.% MWCNT nanocomposite, a prominent peak is observed at $26.4^0$ in its XRD spectrum, which is indexed as CNT (002). It is therefore ascertained that MWCNT as reinforcing constituent persists in HEBM iron-1 wt.% nanocomposite. However, upon further increase in the amount of MWCNT (2 wt.%), the characteristic peak due to MWCNT cannot be observed in the concerned XRD spectrum. instead characteristic peaks of cementite ($Fe_3C$) are recorded in the above spectrum. The absence of MWCNT peak in XRD spectrum of HEBM iron - MWCNT powder mix may be due to two reasons. Either HEBM induced damage of graphitic structure of MWCNT has led to dissolution of carbon in the lattice of iron or mechano-chemical activation has led to synthesis of iron and carbon to give rise to the formation of iron carbide viz. cementite with orthorhombic crystal structure. When amount of MWCNT is small, only dissolution of carbon can take place and there may not be any CNT peak in corresponding diffractogram. It may be mentioned that the equilibrium solubility of carbon in iron is only 0.025 wt.% at $723^0$C and naturally this poses a question of how it is possible that there is no peak of CNT and at the same time any peak due to carbide is also absent. This can be explained only if it is surmised that ferrite so formed due HEBM of iron MWCNT mixture has remained supersaturated. Super saturation of ferrite with carbon is feasible under non-equilibrium situation as it prevails during high energy ball milling. However, the supersaturated solid solution is prone to cause precipitation of carbide under normal circumstances. The absence of carbide peak in the said XRD spectrum suggests that the carbon atoms are segregated at the dislocations which are produced aplenty within the iron crystals due to harsh ball milling condition. Such type of super saturation is reported in heavily cold deformed high carbon steels [13].Figure 4.5 demonstrates that the (110) peak of bcc iron in Fe-1 wt.% MWCNT undergoes a shift towards low angle side after 2h of high energy ball milling. Such shift of peak towards lower angle side implies that there has been an increase in lattice parameter; such increase in lattice parameter stems from dissolution of carbon in iron. However, when the MWCNT content is increased to 2 wt.%, the XRD spectrum shows peaks of cementite ($Fe_3C$) instead of MWCNT

peaks. This suggests that all the MWCNTs are now consumed for HEBM induced chemical reaction between iron and carbon. It is thus seen that at quite low MWCNT content, dissolution of carbon in iron results in the absence of MWCNT peak in the concerned XRD spectrum, whereas at significantly higher MWCNT content, formation of iron carbide appears to be the main reason of absence of reinforcement peaks in the X-ray diffractogram.

In contrast with XRD results for iron-1wt.% MWCNT nanocomposite ball milled with solid stearic acid as PCA, the XRD spectrum of similar Fe-1 wt.% MWCNT prepared by the same HEBM procedure but with the use of ethanol as PCA does not show any CNT peak in the XRD spectrum. Absence of any carbide peak in case of Fe-1wt.% MWCNT nanocomposite produced with solid stearic acid as PCA, rules out the possibility of occurrence of any interfacial chemical between iron and carbon. On the contrary, the absence of either peak in case of use of ethanol as the PCA verifies that chemical degradation of MWCNT has taken place due to reaction between ethanol and MWCNT exposed to $50^0$C. It is therefore conjectured that the conservation of tubular structure of MWCNT is realized in case of 1 wt.% MWCNT nanocomposites if HEBM is carried out for 2 h with solid PCA, viz. stearic acid.

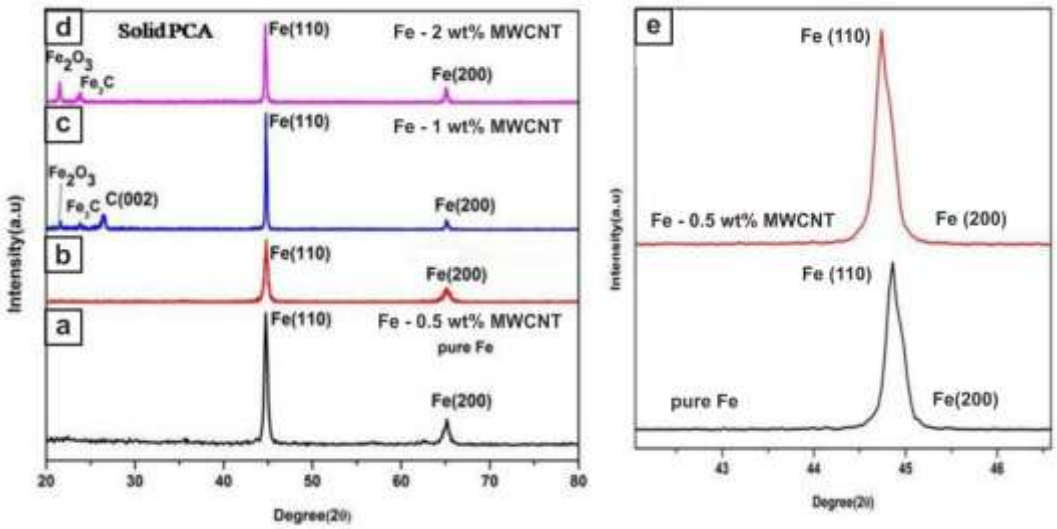


**Figure4.4**XRD spectra of the (a) pure iron (b) Fe - 0.5 wt.% MWCNT (c) Fe -1 wt.% MWCNT and (d) Fe-2 wt.% MWCNT nanocomposite after 2 h HEBM and (e) Shifting of (110) Fe peak to lower angle in case of Fe-0.5 wt.% MWCNT.

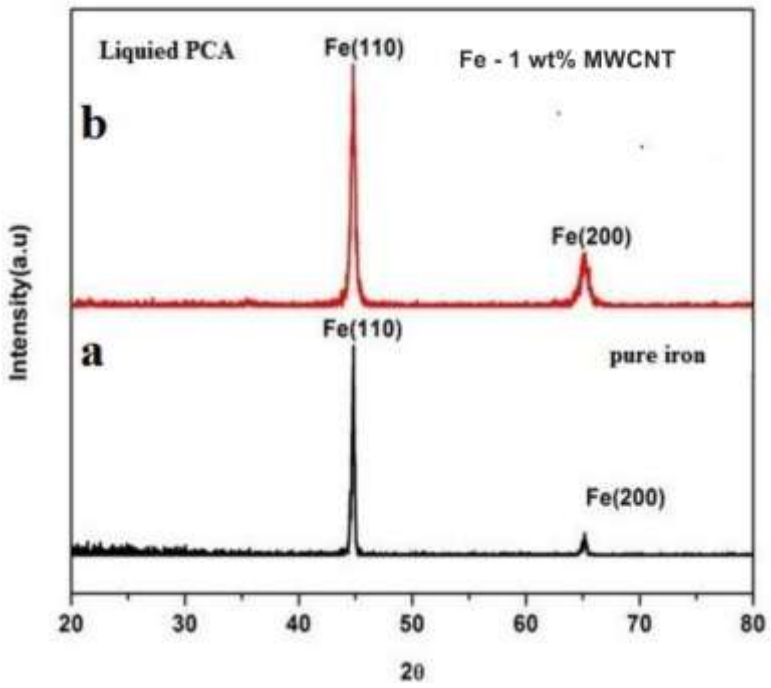


**Figure4.5**XRD spectra of (a) Pure iron and (b) Fe-1wt.%MWCNT nanocomposite after 2h HEBM by wet method; no CNT peak is observed.

### *4.3.3 Transmission Electron Microscopy*

The high-resolution transmission electron microscopic observation indicates that interfacial bonding attainable in Fe-MWCNT nanocomposite is quite good. The delineation of a smooth interface between Fe and MWCNT in high energy ball milled nanocomposite containing 1 wt.% MWCNT corroborates the results of X-ray diffraction. HRTEM photographs of iron- 1 wt.% MWCNT is presented in figure 4.6.

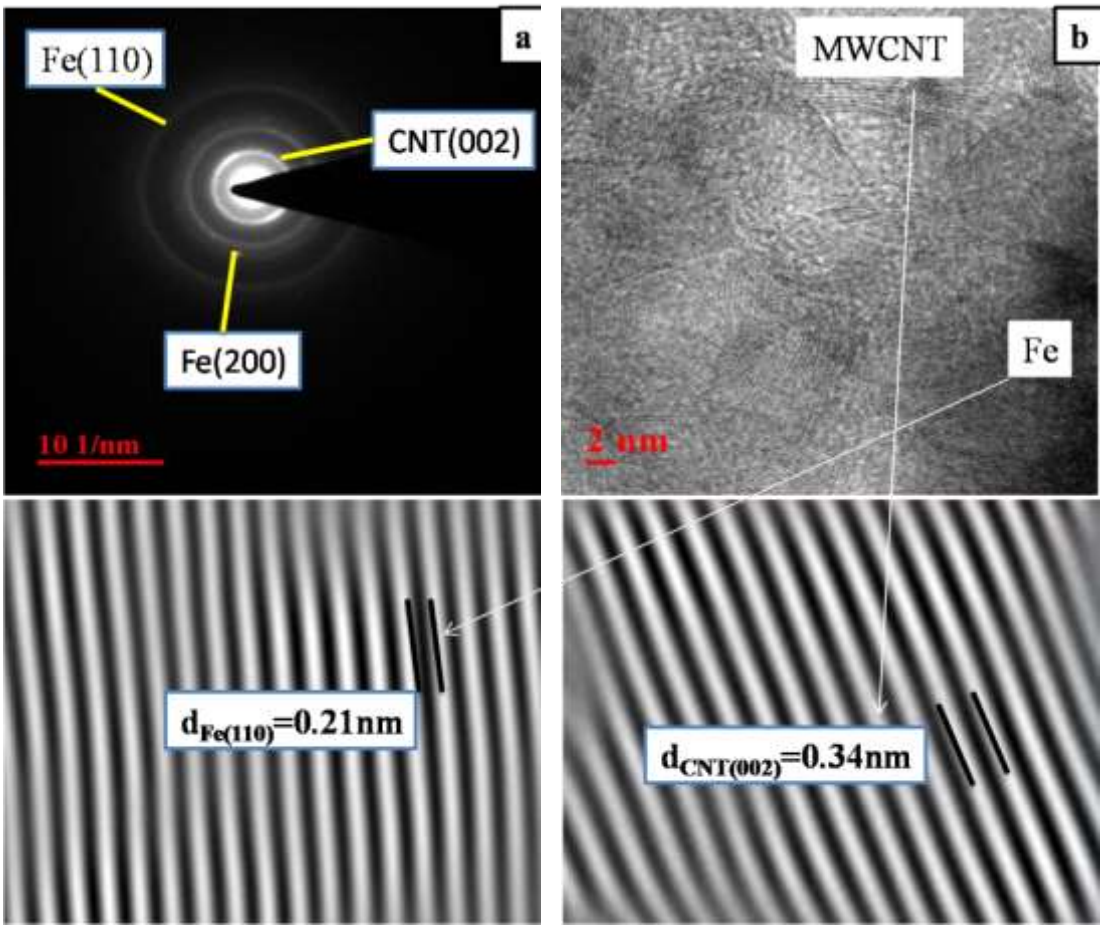


**Figure4.6** (a) SAED pattern of Fe-1 wt.% MWCNT nanocomposite (b) HRTEM image of Fe-1 wt.%MWCNT nanocomposite and corresponding lattice images show the d spacing of CNT and Ferrite.

High resolution image records the presence of both MWCNT and pure iron. The interplanar spacing, 0.34 nm of MWCNT characterizes (002) CNT and verifies that graphite structure of MWCNT is conserved. The corresponding SAED pattern presents continuous ring pattern of MWCNT. The evidence of ring pattern from (110) Fe implies that crystals of iron are very fine. In case of Fe- 2 wt.% MWCNT nanocomposite, the high-resolution image reveals the presence of cementite particles (figure4.7). The formation of cementite in high energy ball milled Fe-2 wt.% MWCNT nanocomposite has also been recorded in the corresponding XRD spectrum and is thought to be due to mechano-chemical activation during two h HEBM of Fe-MWCNT nanocomposite containing as high as 2 wt.% MWCNT. Besides (002) CNT rings, the SAED pattern of Fe-2 wt.%MWCNT also exhibits ring pattern of iron due to its fine crystal size. The diffused ring pattern of iron as

seen in figure 4.7 is suggestive of the fact that iron crystals are considerably strained. This strain originates from high amount of ball milling energy partitioned into iron particles. This increases the dislocation density in iron crystals. It is known that these dislocations can act as sites for segregation of carbon atoms[13]. Due to close proximity between iron and carbon atoms, 2p-3d hybridization occur [14] and a very good interfacial bonding is ensured. Thus, it is found that at low concentration of MWCNT, carbondissolves in iron during HEBM and intense ball milling at high MWCNT content (~2wt.%) leads to carbide formation. However, at 1wt.% MWCNT level, cementite is not found to form.

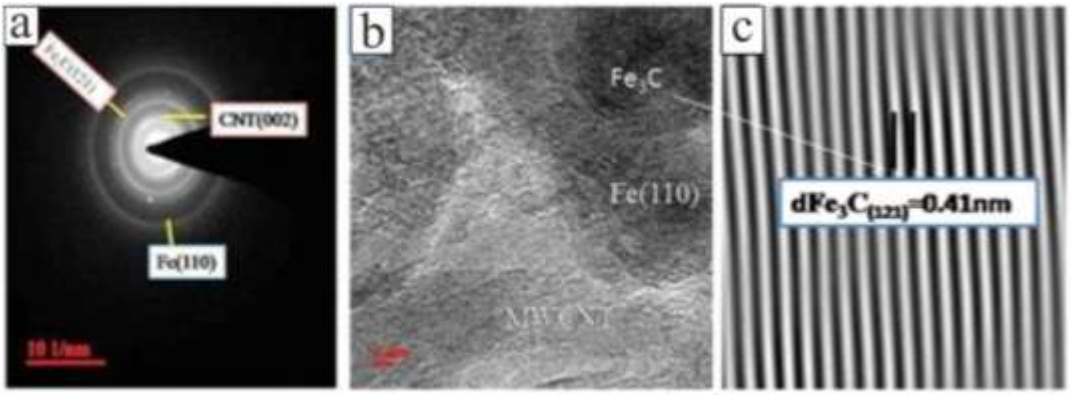


**Figure4.7**(a) SAED pattern of Fe-2 wt.% MWCNT nanocomposite b) HRTEM image of Fe-2 wt.% MWCNT nanocomposite shows Fe (110), CNT (002) and cementite (112) phase and (c) shows the corresponding d spacing of cementite ($Fe_3C$).

### *4.3.4 Raman Spectroscopy*

The Raman Spectra of pristine MWCNT and Fe-MWCNT nanocomposites are furnished in figure 4.8. It is apparent that pristine MWCNT records characteristic G (graphite) and D (defect) band at 1350 and 1552 $cm^{-1}$. The strong G and D peaks authenticate perfect graphite structure of MWCNTs. Another peak observed at 2700 $cm^{-1}$ has been assigned as $G^I$ band by previous workers [15, 16].While the change in size and shape of G and D bands (viz. widening and shortening) suggests introduction of defects in the graphite structure of MWCNT, the degradation in MWCNT structure is also associated with shift of position of G and D bands in Raman Spectra. Also, the ratio of intensities of D and G band i.e. $I_D/I_G$ gives the idea of the magnitude of damage in MWCNT structure if there be any. Raman

Spectroscopic results of HEBM nanocomposites are furnished in summarized form in Table 4.1.

It can be seen from Table4.1, that $I_D/I_G$ ratio of nanocomposite samples, high energy ball milled for 2h, increases with increase in MWCNT content; also, a shift of G band towards higher wave number may be noticed. These observations have the implication that MWCNT milled with iron has undergone considerable structural damage. Degradation of MWCNT structure under severe ball milling has been reported elsewhere [17]. Structural damage of reinforcing MWCNT is also substantiated by the change in size and shape D and G band in the present experiments. From the appearance of peaks of G and D band in ball milled nanocomposite samples it seems that complete amorphization of MWCNT has not taken place in the present experimental condition. The G' band is seen to have been flattened due to ball milling and this hints upon significant damage of MWCNT in 2wt.% nanocomposite after HEBM for 2 h.

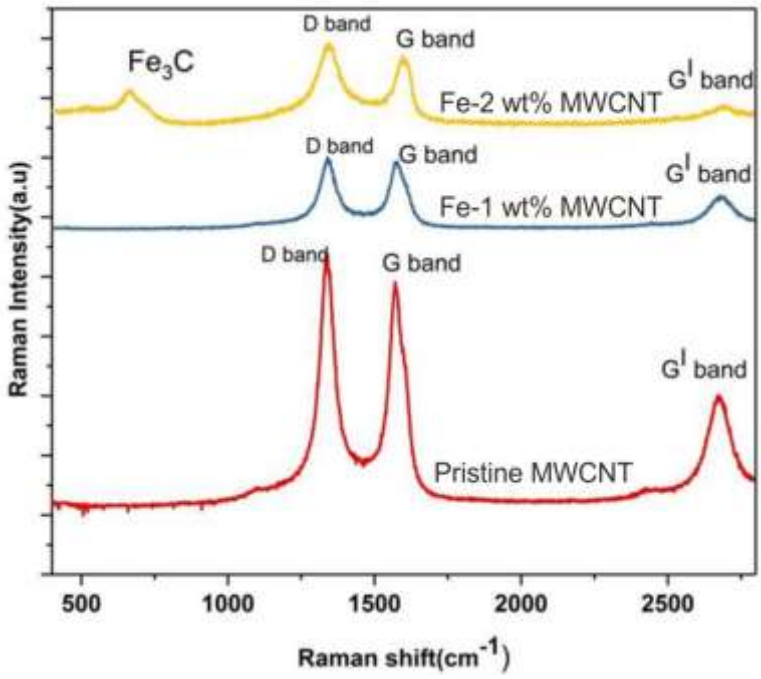


**Figure 4.8** Raman spectra of pristine MWCNT and of Fe-MWCNT nanocomposites containing different weight percent of MWCNT.

**Table 4.1**Summarized results of Raman Spectroscopy

| Sample Name | Raman Peak Shift ($Cm^{-1}$) | | $I_D/I_G$ |
|---|---|---|---|
| | D band | G band | |
| Pristine MWCNT | 1343 | 1571 | 0.98 |
| Fe-1 wt.% MWCNT | 1349 | 1575 | 1.02 |
| Fe-2 wt.% MWCNT | 1353 | 1589 | 1.09 |

## 4.4 Conclusions

The authors conclude that high energy ball milling with tailored process parameters can be effectively used to produce iron-MWCNT nanocomposite. Severe ball milling at high MWCNT content leads to chemical degradation of MWCNT. Mechano-chemical activation leads to the formation of iron carbide at the interface. A very good interfacial bonding is achievable after ball milling of iron-1 wt.% MWCNT nanocomposite for 2h.

## REFERENCES


[1] S. Iijima, Helical microtubules of graphitic carbon, Nature 354(1991)56-58.

[2] E.l-sherbiny, G.Sh,S.Wageh, S.M. Elhalafawy, A.A. Sharsha,Carbon nanotube antenna analysis and application: review, Advance in nanoresearch 1(2013) 13- 27.

[3] K.Rakrak,M.Zidour,H.Heireche,A. A. Bousahla, A. Chemi,Free vibration analysis of chiral double-walled carbon nanotube using non-local elasticity theory, Advancein nanoresearch 4(2016) 31-44.

[4] A. Chemi, H. Heireche, M. Zidour, K. Rakrak, and A. A.Bousahla,Critical buckling load of chiral double-walled carbon nanotube using non-local theory elasticity, Advance innanoresearch4( 2015) 193-206.

[5] M.H. Kazemi, M.A. Akhavan-Behabadi, and M. Nasr, Convective heat transfer of MWCNT / HT-B Oil nanofluid inside micro-fin helical tubes under uniform wall temperature condition, Advance in nano research 2(2014) 99-109.

[6] F.C. Dillon, A. Bajpai, S. A. Koo, S.Downes, Z.Aslam, N. Grobert, Tuning the magnetic properties of iron-filled carbon nanotubes, Carbon50(2012)3674-3681.

[7] M. B.Vishlaghi, A. Ataie, Investigation on solid solubility and physical properties of Cu–Fe/CNT nanocomposite prepared via mechanical alloying route, Powder Technology268(2014) 102–109.

[8] R. Paul,P. Kumbhakar,A. K. Mitra, A facile chemical synthesis of a novel photo catalyst: SWCNT/titania nanocomposite, Advance in nanoresearch 2(2013)71-82.

[9] M.R. Basariya, V. C. Srivastava, N. K. Mukhopadhyay,Microstructural characteristics and mechanical properties of carbon nanotube reinforced aluminum alloy composites produced by ball milling, Materials and Design 64(2014) 542–549.

[10] T. Peng,I. Chang, Mechanical alloying of multi-walled carbon nanotubes reinforced aluminum composite powder, Powder Technology266(2014) 7-15.

[11] W.W. Zhou, S. Bang, H. Kurita, T. Miyazaki, Y. Fan, A. Kawasaki, Interface and interfacial reactions in multi-walled carbon nanotube reinforced aluminummatrix composites, Carbon 96(2016) 919-928.

[12] H. J. Choi, J. Y. Shin, B. H. Min, J. Park, D. H. Bae, Reinforcing effects of carbon nanotubes in structural aluminum matrix nanocomposites, J Mater Res. 24(2009)2610-2616.

[13] J. Languillaume, G. Kapelski, B. Baudelet, Cementite dissolution in heavily cold drawn pearlitic steel wires, Acta mater. 45(1997) 1201-1212.

[14] K. S. Munir, M. Qian, Li. Yuncang, D. T. Oldfield, P.Kingshott, D.M.Zhu, C. Wen, Quantitative analysis of MWCNT-Ti powder mixtures using Raman spectroscopy: The influence of milling parameters on nonstructural evolution, Adv. Eng. Mater17 (2015) 1660-1669.

[15] D. Poirier, R. Gauvin, R. A. L. Drew, Structural characterization of a mechanically milled carbon nanotube /aluminum mixture, Composite part A 4 (2009) 1482-1489.

[16] J. Y. Suh, D. H. Bae, Mechanical properties of Fe-based composites reinforced with multi –walled carbon nanotubes, Mater. Sci. Eng. 582(2013) 321-325.

[17] H.J. Choi, J. H. Shin, D.H Bae, The effect of milling conditions on microstructures and mechanical properties of Al/MWCNT composites, Composites Part A43(2012) 1061–1072.

# *CHAPTER FIVE*

## *Development of A Novel MWCNT Reinforced Iron Matrix Nano Composite Through Powder Metallurgy Route*

In the present chapter, discussion is made about the structural evolution in iron-MWCNT synthesized by high energy ball milling. Nanocomposite of iron and MWCNT is produced under optimized condition of high energy ball milling (HEBM) of powder mix. The ball milling is carried out for different milling time and characterization of structure and assessment of structural stability are conducted by various techniques. Magnetic properties of the nanocomposite are measured by Vibrating Sample Magnetometer (VSM). The results have indicated that structural identity and hence characteristic properties of MWCNTs can be retained till 60 min of ball milling. The study also delineates partial destruction of C-C bonds of MWCNT due to high energy ball milling of powder mix. However, amount of carbon atoms released by bond disruption is rather small and heavy super saturation of iron with carbon and extensive precipitation of carbides during heating is untenable. The excellent interfacial structure so achieved has significantly improved the magnetic properties of iron-MWCNT nanocomposite.

## 5.1 Introduction

Unique mechanical and physical properties of carbon nanotubes (CNT) have attracted immense research in development of functional nanocomposite with CNTs as reinforcing material. Following success in development of useful polymer matrix-CNT nanocomposites, a great deal of research efforts has been exerted to harness the potential of CNTs as reinforcement in metal matrices [1-9]. Unlike polymer-CNT nanocomposite, mixing of CNTs in a metal matrix is quite difficult and so, the fabrication and processing of metal matrix-CNT nanocomposites has been a matter of concern. High aspect ratio and Vander-Waals forces of attraction among thin and long tubes of CNT are liable for intense tendency towards agglomeration; therefore, securing uniform dispersion of CNTs within metal matrices appears to be a challenge to the materials engineers. Liquid metallurgy and stir casting routes have not been successful owing to poor wettability of reinforcement [10].In liquid metallurgy processes, difference in density between MWCNT and metal matrix poses additional difficulties in achieving homogeneous dispersion of MWCNT [10]. Mechanical alloying route, which is essentially a high-energy ball milling (HEBM) process, has been successful in achieving more or less uniform dispersion of CNTs in Al-matrix [5, 7, 11-13]. This has stimulated wide usage of HEBM for synthesizing metal matrix-CNT nanocomposite [14-15].

That multiwall carbon nanotubes (MWCNTs) undergo considerable damage during high energy ball milling is well documented in literature [2]. Extensive ball milling may lead to shortening and even to amorphization of MWCNTs [9, 16-17]. The defects created during milling of MWCNTs deteriorate properties and hence continue to limit its application until the evolution of structural degradation during the course of ball milling of MWCNT is well understood. Moreover, there are reports of accelerated damage of MWCNTs when milled with metal powders like iron [18].

In spite of successful production of metal matrix nanocomposites through mechanical alloying route, the attainment of desired properties of nanocomposite is still not satisfactory. The major factor which prohibits the attainment of desirable properties in metal matrix nanocomposite is ascribed to poor bonding between CNT and matrix metal [4]. Theoretical studies with the aid of density function theory (DFT) have been conducted to demonstrate interfacial bonding characteristics of metal particles with CNTs [19-20].

Till date it has remained a research task to circumvent the challenges emanating from poor bonding of MWCNTs with most metals. Interestingly, transition metals with vacant 3d orbital (like iron) may be expected to hybridize with p-orbital of CNTs and in that case, a better interfacial bonding may be obtained [4].

So far, most of the research on CNT reinforced metal matrix nanocomposites has focused on improvement of mechanical properties. Reports of studies on magnetic behavior of Fe-nanoparticles filled CNTs or iron nanoparticles layered MWCNTs are also available in literature [21-27]. However, there is no recorded attempt to disperse MWCNT in iron matrix for the sake of enhancement of its physical properties.

With the understanding that MWCNTs subjected to high energy ball milling with metal powders are prone to suffer structural damage, it may be surmised that, a controlled damage of MWCNT, secured by optimal ball milling with iron may insure excellent interfacial bond, besides MWCNT being well embedded into the metal matrix.

Thus, in the present investigation, attempts are made to probe into the feasibility of achieving a good interfacial bonding between reinforcing CNTs and the iron metal matrix by way of tailored damage of outer layers of MWCNT, yet retaining its structural integrity; this insures harnessing the excellent potential of MWCNTs to enhance physical properties of nanocomposites. In order to attain this

goal, high energy ball milling of iron-MWCNT mixture is carried out for various milling time and the degree of damage in CNTs is monitored. By the use of various experimental techniques optimization of process parameters against the improvement of magnetic properties of nanocomposite is tried.

## 5.2 Experimental

The starting materials used for the present investigation consist of Fe-powder and multiwall carbon nanotube (MWCNT). Irregular shaped iron powder of size 325 mesh with purity higher than 99% has been procured from Sigma-Aldrich Company Co. Ltd. The MWCNT used for the current research has been purchased from Nanoshel Company. MWCNT was more than 98% pure; its diameter is about 10-20nmand length ranges from 3-8 μm. The size, shape and morphology of iron powder are observed under Field Emission Scanning Electron Microscopy (FESEM) and are shown in figure5.1.

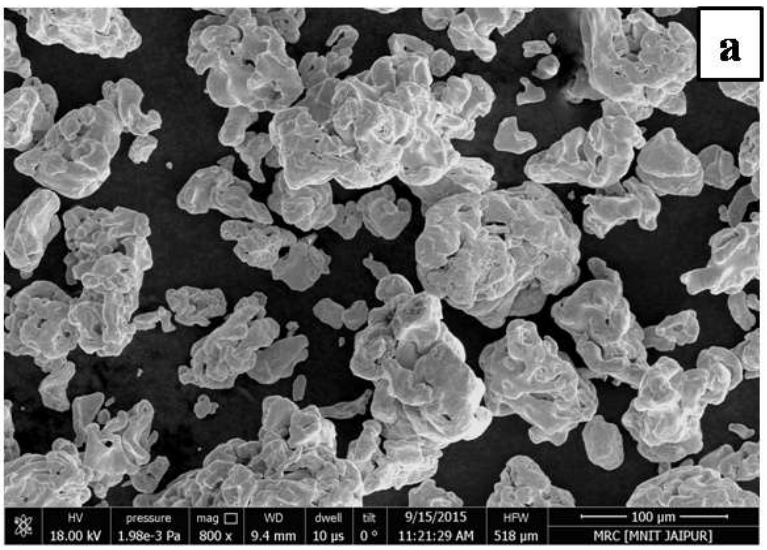


**Figure5.1** FEG-SEM micrograph of Fe powder

Transmission electron micrographs (TEM) of MWCNT used for the present investigation are shown in figure5.2 (a) &5.2(b).

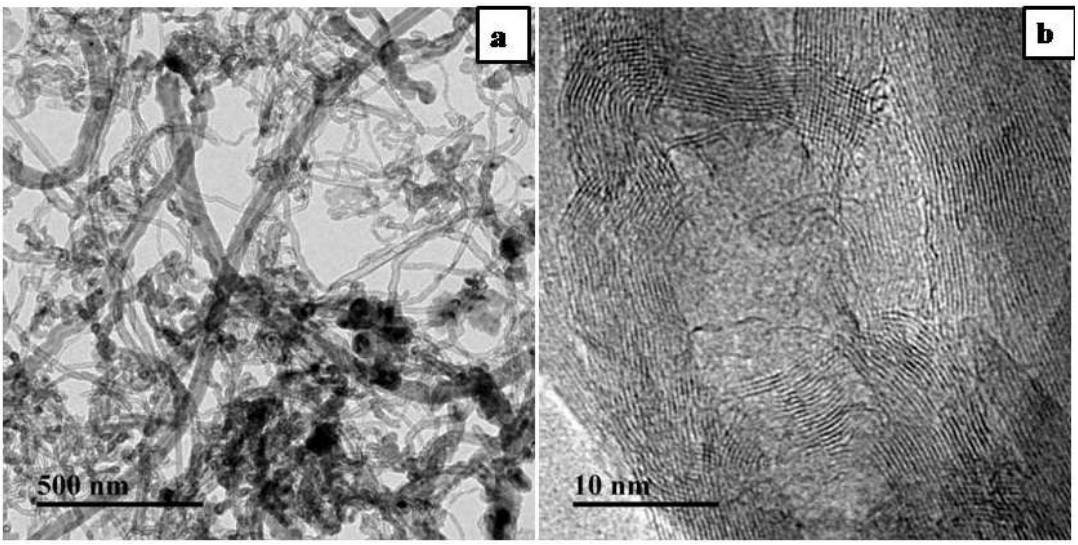


**Figure 5.2** (a) TEM image of MWCNT and (b) HRTEM image of MWCNT

It is seen from figure 5.2(a) that the long thin and tubular CNT's are clustered and also bent at some places; the walls of MWCNT is clearly discerned in figure 5.2(b) and the total number of walls of MWCNT is found to be around 10-12.

High energy ball milling of a mixture of thirty-gram iron powder and 2 wt.% MWCNT has been carried out in a Planetary Ball Mill by following the procedure described in earlier chapter. Thus, Samples milled under argon atmosphere were collected at regular intervals of milling viz.10, 20, 30, 40, 60 & 90 min for characterizing the Fe-based MWCNT nanocomposites. Evolution of structure of nanocomposite with progress in milling time has been studied by field emission scanning electron microscope of model, NOVA NANOSEM 450, at an accelerating voltage of 15KV. X-Ray Diffraction study was carried out in Xpert-Pro Pan Analytical model XRD system and the study was conducted within 2θ range of 20-100°for powder samples and at scan speed of$2^0$/min., step size 0.04° and counting time 30s. Microstructural characterization of the nanocomposites after different milling times has been carried out in high resolution transmission electron microscope (Tecnai $G^2$20 FEI S Twin). Powder samples, were prepared as per procedure described in Chapter 3.

XPS study was performed in Omicron Nanotechnology XPS system from Oxford Instruments (model ESCA+) by following the process described in Chapter 3. Fourier transform infrared (FTIR) spectrometer (Perkin Elmer Frontier) was used to obtain information about stretching vibration of different bonds present in HEBM nanocomposite from the corresponding FTIR spectra.

Raman spectroscopy was carried out at room temperature in AIRIX STR 500 CONFOCAL MICRO Raman Spectrometer. The procedure followed is same as described in Methodology chapter. Differential Scanning Calorimetric study was carried out in DSC404 F3 of NETZCH make to analyze the interaction, if any, between MWCNT and neighboring Fe powder particles during the course of high energy ball milling. Vibrating Sample Magnetometer(VSM) of model EZ9 of make Microsence Company was used at applied magnetic field from -20Oe to + 20Oe for the sake of studying the room temperature magnetic properties of nanocomposites obtained by milling for different times.

## 5.3 Results and discussion

### *5.3.1 Structural evolution study by Scanning Electron microscopy*

Field Emission Electron Microscopy study (FESEM) has revealed the dispersion behavior of MWCNT after high energy ball milling of Fe-MWCNT nanocomposite for various times. The representative micrographs in figure 5.3 (a-f) help to understand the structural evolution in Fe-MWCNT nanocomposite during the course of high energy ball milling.

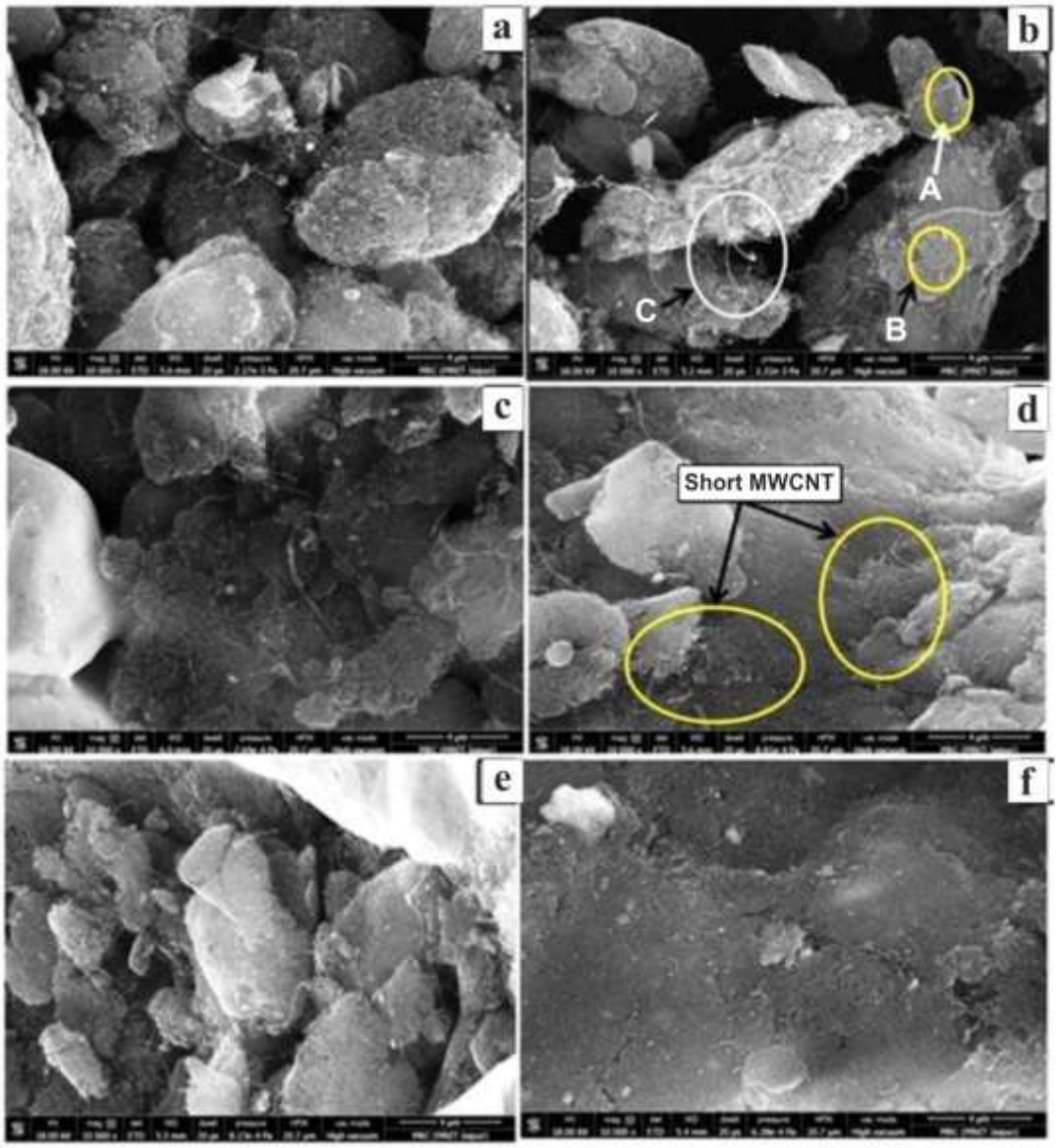


**Figure5.3**(a)SEM image of Fe-MWCNT nanocomposite milled for (a) 10 min (b) 20 min (c) 30 min (d)40 min (e) 50 min and (f) 1h

At the early stage of milling, say for 10 min., it can be seen that CNTs are just laid over the iron particles (figure 5.3a). It may be observed that after 20 min of milling MWCNTs are embedded only in some particles (as in A marked particle), whereas MWCNT is either partially embedded as in 'B' or not at all embedded as in 'C' (figure 5.3b). Such trend continues till 30 min of milling time when occasional embedding of CNT onto the iron matrix is noted (figure 5.3c). Cold welding of iron particles is also observed in the same photomicrograph; figure 5.3 (c)reveals that some iron particles are flattened, whereas some previously fractured smaller particles undergo cold welding. Further increase in milling time (≈ 40 min) has led

to perceptible flattening of some matrix particles, within which shorter MWCNT particles are well embedded (figure 5.3d); a few MWCNTs still remain to undergo bonding with the matrix**.** Still higher milling time viz.50 min, causes more deformation of matrix phase; also MWCNTs appear to have been ruptured and shortened to some extent. The short CNTs are found to be embedded over a large area of the matrix phase (figure 5.3d). FE-SEM photomicrograph of nanocomposite powder ball milled for 1h (figure 5.3e), gives evidence of formation of flat sheets, which cover the entire field of view. It is observed in figure5.3 (e) that the shortened CNTs are embedded quite well within the matrix phase, presumably with a firm interfacial bonding. The characteristic processes in mechanical alloying viz. fracturing, cold welding and deformation of experimental nanocomposite powders are seen to continue till 1hr in the instant milling process [28].

High energy ball milling of Fe-CNTs leads to appreciable reduction in sizes of MWCNTs and these MWCNT exhibit enhanced tendency to embed into the flattened matrix metal; these observations are consistent with previous research reports [1, 3, 12, 27-28]. In the present work we have attempted to engineer the microstructure of nanocomposite in such a way that Fe-CNT interface becomes very smooth and continuous; in fact, this is known to be a major constraint in the development of metal-MWCNT nanocomposite. Although it has been reported by some researchers that extensive high energy ball milling can completely destroy the tubular structure of CNTs and may even lead to amorphization [29], optimal ball milling conditions employed in the present study have been able to conserve the tubular structure of MWCNT quite well. The shortened MWCNTs are seen to be firmly embedded within the matrix (figure 5.3e). It further appears from the morphology of embedded MWCNTs that the bonding at metal interface has been rather good. High energy ball milling has produced ultra-small crystallites of metal powder; high aspect ratio of MWCNT is one of the impediments to secure uniformity in CNT distribution [12] in small crystals. On the other hand, when tubular structure of MWCNT is retained, the shortening of MWCNT in ball milling has become quite effective in achieving desirable uniformity in the distribution of CNT within the metal matrix. As stated earlier, the shape of pure iron particles used in this experiment is non-spherical in nature and the hardness of this pure iron is quite low (~ 20 BHN); moreover, the strain hardening exponent ‘n’ of BCC iron is

lower than that of the FCC metals like aluminum, nickel etc. This has helped in flattening of metal particles during ball milling and thus assisted the embedding of MWCNTs into them.

High energy ball milling causes deformation of iron powders which in turn generates appreciable dislocations within iron matrix. When the interaction energy between dislocations and C atoms exceeds the bond energy between carbon-carbon atoms in adjacent MWCNT, disruption of bonds in MWCNT may lend free carbon atoms to segregate at the nearby dislocations in iron in accordance with the need to lower the overall free energy of the system. This hypothesis owes its origin to similar observations in heavily cold deformed iron-carbon system (high carbon steels with a microstructure of alternate lamellae of ferrite and carbide) [30].

### *5.3.2. X-Ray Diffraction study*

XRD spectra of Fe-CNT nanocomposite milled for various times are shown in figure 5.4 (a-b). XRD results in figure 5.4 and figure 5.5 provide information about refinement of iron crystals which is useful to explain the impact of ball milling on physical properties of nanocomposite. The contemplated XRD study also helps to verify if MWCNT could retain its tubular structure under prescribed ball milling condition without unwanted formation of cementite ($Fe_3C$) by mechano-chemical synthesis of iron powder and MWCNT. The XRD spectra in figure5.4 (a) record the presence of diffraction peaks at $26.4^0$; this peak is assigned to (002) CNT. Persistent CNT peaks in XRD spectra of HEBM samples verifies that structural integrity of MWCNT is conserved in Fe-MWCNT nanocomposites ball milled up to 60 min. Moreover, the XRD spectra obtained in the present study do not show any characteristic diffraction peaks of iron carbide or other crystalline contaminating phase. Therefore the results of present XRD study exclude the formation of any kind of reaction products at the MWCNT- metal interface which would otherwise cause damage to the virgin MWCNT structure and would restrict the enhancement of mechanical and physical properties of iron-MWCNT nanocomposite due to MWCNT reinforcement. The diffraction peaks (figure5.4a-b) are seen to be of finite width; the usual line broadening in XRD peaks is ascribed to cumulative effect of reduction in crystallite size and generation of lattice strain.

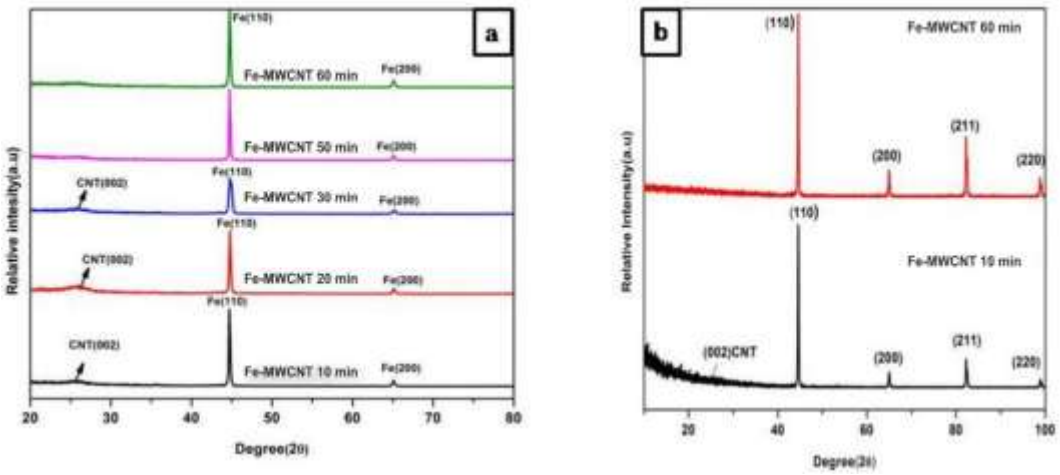


**Figure 5.4**(a) XRD Pattern of samples after milling for different times (b) XRD showing first four peaks.

The Williamson and Hall method is used to calculate the size of crystallite (L) and associated lattice strain (η) from XRD spectra; this is given by

$$b\cos\theta = \frac{k\lambda}{L} + \eta\sin\theta \ldots\ldots\ldots (1)$$

Where k is the Scherrer's constant, and $2\theta$ is the Bragg angle.

In order to determine the crystallite size and lattice strain we have taken four strong peaks in order of relative intensities (figure5.4b) to plot the curve of $b\cos\theta$ as a function of $\sin\theta$.Taking Scherrer's constant as 0.9 and securing a best fit for a straight-line relationship (vide equation1), $b\cos\theta\ vs.\sin\theta$curves for various milling times are derived and representative curves are furnished in figure5.5 (a-b).

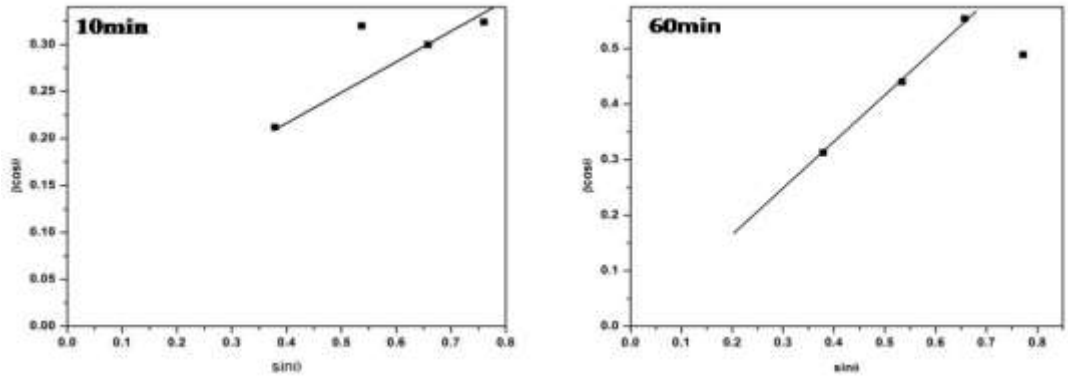


**Figure5.5**(a-b) Williamson and Hall plots of Fe-MWCNTs powder after milling for (a) 10 min and (b) 60 min.

Extrapolation of straight lines in figure5.5(a-b) yields the corresponding points of intersection with y-axis; from the read outs of Y-axis intercepts, crystallite sizes are obtained whereas, the slopes of individual $bcos\theta\ vs.\ sin\theta$ curve give the values of lattice strains in each milling time (equation 1). The calculated values of crystallite size and lattice strain are presented in Table 5.1.

**Table5.1**Crystal size and strain after 10 min and 60 min milling.

| **Values** | **10 min milling** | **60 min milling** |
|---|---|---|
| Crystallite size (nm) | 61 nm | 57 nm |
| Lattice strain | 0.0036 | 0.0018 |

The results show the expected trend of decrease in crystallite size with increasing milling time. It is also seen that the overall reduction in crystallite size is not very large within the range of milling time employed in present experimentation. The trend of variation of lattice strain is found to be decreasing with milling time. Although one may expect that increasing milling time would exhibit continuous rise in lattice strain due to higher energy being imposed on the system, the same is not observed in the instant case. Similar decrease in lattice strain at higher milling time for Al -MWCNT nanocomposite has also been reported by other workers [3]; the observed decrease in lattice strain had been attributed to possible occurrence of recrystallization of the heavily deformed metal matrix [3].

Although no other experiment was conducted to verify the factors responsible for the observed diminution of lattice strain at higher milling times, the above observation does suggest that either some kind of recovery mechanism has been operative at higher milling time or strain induced precipitation of carbide particles due to local super saturation of iron with carbon takes place at region adjacent to Fe-CNT interface.

Figure 5.4(a) further delineates that the increasing milling time has caused a marginal shift of the position of (110) ferrite peak towards lower value of 2θ. Such shift of peak is indicative of a change in lattice parameters and this can be explained only if it is presumed that some carbon atoms have entered into iron lattice; this could be possible if HEBM has led to damage of MWCNT to the extent that

disruption of some C-C bonds of MWCNT has taken place, and it has produced amorphous carbon atoms which can enter into the lattice of bcc iron; this may lead to the increase in lattice parameter of iron as manifested by the shift of peaks to lower angles. This means that, commensurate with the aim of the study, limited structural damage of MWCNT takes place after 1 h of high energy ball milling of Fe-MWCNT nanocomposite powder.

### *5.3.3 Fourier Transform Infrared Spectroscopy Analysis (FTIR)*

Fourier Transformation Infrared Spectroscopy (FTIR) study is conducted to get an idea about the possible changes in quality of bonding in Fe-MWCNT nanocomposites, ball milled for different times. Figure5.6 shows FTIR spectra of pristine MWCNT as well as Fe-MWCNT nanocomposites after milling for various times (10 -60 min).

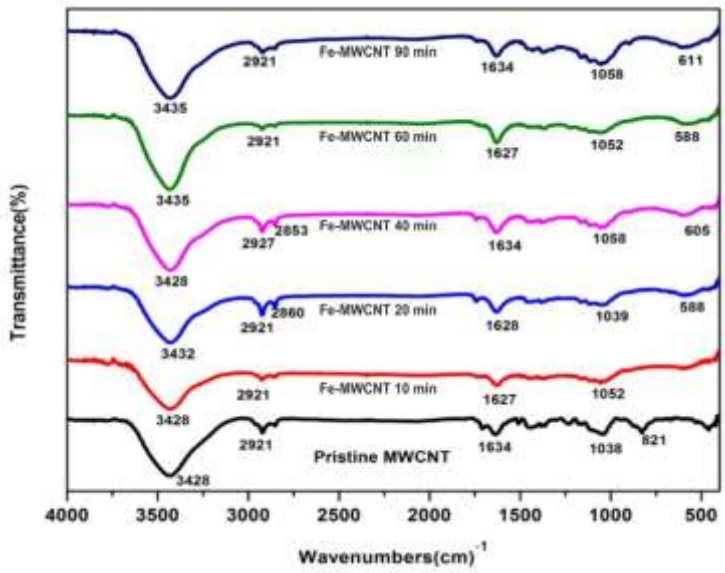


**Fig. 5.6** FTIR spectra of pristine MWCNT as well as Fe-MWCNT nanocomposites after milling for various times.

The peaks observed at around 3428 $cm^{-1}$are known to represent bending vibration of hydroxyl (OH) group, and may be due to partially adsorbed water in MWCNT and Fe-MWCNT nanocomposite samples. Expectedly, FTIR spectra do not show any perceptible change in intensity of peak due to bending vibration of hydroxyl group, owing mainly to aerial exposure of each sample before testing. The bands appearing at 2852 and 2921 $cm^{-1}$ are supposedly due to the C-H stretching in $CH_2$ and $CH_3$ group respectively [31]. Moreover, two prominent peaks of interest,

respectively at 1627-1634 $cm^{-1}$and 1038-1058 $cm^{-1}$are observed in FTIR spectra of pristine MWCNT and high energy ball milled (HEBM) Fe-MWCNT nanocomposite. While the first peak in the range 1627-1634 $cm^{-1}$characterises C=C stretching vibration, the second in the range 1038-1058 $cm^{-1}$corresponds to IR activated graphitic C-C stretching mode.

The peak observed at 821$cm^{-1}$in case of pristine MWCNT stems from Fe-O stretching vibration and it is characteristically different from the absorbing peaks of magnetite ($Fe_2O_3$) and magnetite ($Fe^{2+}Fe^{3+}{}_2O_4$) generally occurring at 570 $cm^{-1}$and 615 $cm^{-1}$respectively [32]. From the results of FTIR, it is observed that with the increase in milling time, the intensity of peak at 1634 $cm^{-1}$ which represents C=C stretching vibration decreases. Also, the peak due to Fe-O stretching vibration seen in pristine MWCNT, disappears in HEBM samples; instead, absorbing peaks around 570 - 615 $cm^{-1}$ are seen to appear in FTIR spectra of ball milled samples. Moreover, increasing milling time has shown a decrease in intensity of C-C stretching peak until 1 h of milling. It is interesting to observe that the intensities of absorbing peaks in the range of 570 - 615 $cm^{-1}$continually increase with increasing milling time. Decreasing intensities of C=C and C-C peaks with milling time hints upon disruption of C=C and C-C bonds in MWCNTs. Incidentally, the said decrease in intensities is associated with simultaneous increase in intensities of absorbing peaks. The implication of disappearance of F-O stretching vibration peak concurrent with appearance and subsequent enhancement of intensities of absorption peaks at 570 - 615 $cm^{-1}$ in FTIR spectra may be understood by surmising that disruption of bonds in MWCNTs makes carbon atoms available for combining with $Fe^{3+}$, may be through 2p-3d hybridization. While disruption of bonds gives way to iron-carbon bond formation and hence to enhancement of intensity of absorbing peak, the rate of disruption of single bond may lag behind the absorption rate of carbon atoms. This results in accumulation of C-C bond beyond 60 min of ball milling; this explains why the intensity of C-C stretching peak is seen to increase after 1h of high energy ball milling.

### *5.3.4 Differential Scanning Calorimetric study (DSC)*

DSC heating run is conducted for all the high energy ball milled iron-MWCNT nanocomposite samples; incidentally no peak has been detected in any of the DSC curves (figure5.7).

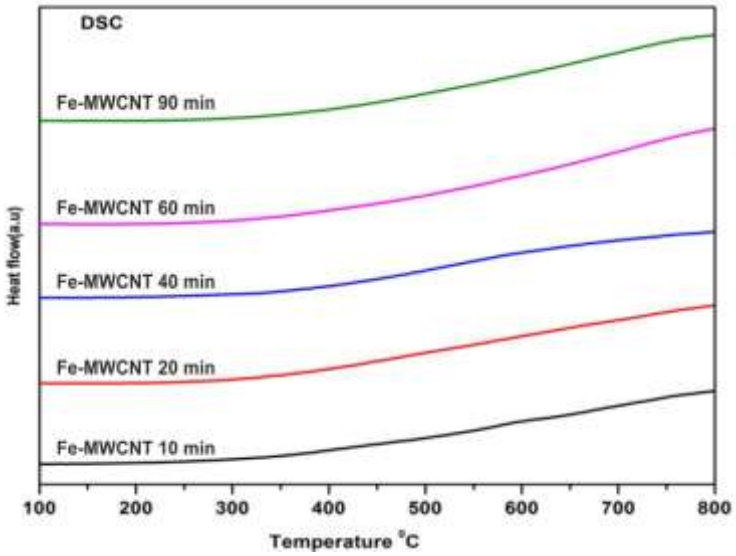


**Figure5.7** DSC heating curves of ball milled samples after milling for different times.

This clearly indicates that within the range of milling time employed in the present study, carbon dissolution in iron has not been as extensive as to be subsequently precipitated with a volume fraction that exceeds the detectable limit of XRD. The idea behind the design of present experiments was to preserve the structural integrity of MWCNT as best as possible with marginal damage at its outer layer, so that desired level of interfacial bonding is achieved. If a good number of carbon atoms is released during damage of MWCNT at its outer layers, and then gets dissolved in iron, a super saturated solid solution of carbon in iron adjacent to MWCNT reinforcement could have formed. In that case, DSC heating run should have envisaged the appearance of an exothermic peak at elevated temperature during heating run. However the absence of any formation peak in DSC heating runs lends indirect support to the other experimental findings that there is no objectionable reaction took place during fabrication of the present set of iron-MWCNT nanocomposite samples. Therefore in the present situation, one may anticipate a possible improvement of magneto-electric property of pure iron.

### *5.3.5 Study of structural stability of MWCNT by Raman Spectroscopy*

Since high energy ball milling envisages structural degradation of MWCNT and the damages caused to MWCNT can affect the properties of metal-MWCNT nanocomposite, Raman Spectroscopy of high energy ball milled Fe-CNT nanocomposites is carried out in the present study to gather more understanding about the possible damage of MWCNTs. Raman spectra. In figure5.8(a) show that the first order peaks of pristine MWCNT composed of D band (defect) G band (graphite) occur respectively or 1352 and 1555 cm-$^{1}$ respectively.

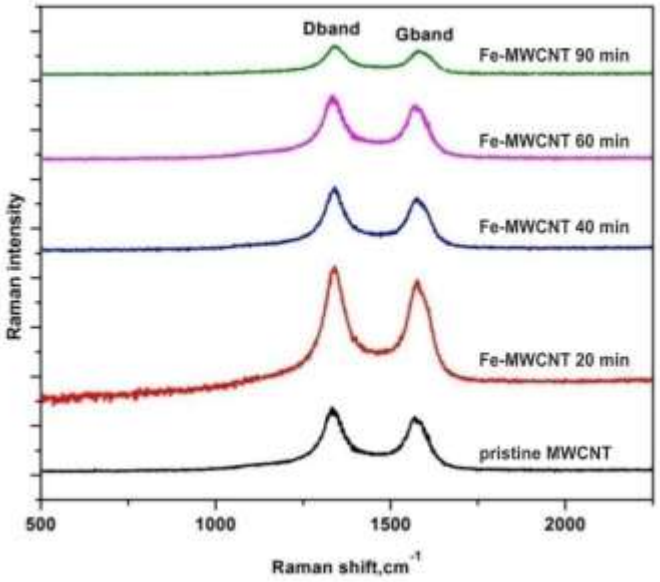


**Figure5.8** (a) Raman spectra taken from pristine MWCNT and differently milled Fe-2 wt.%MWCNT powder mixture.

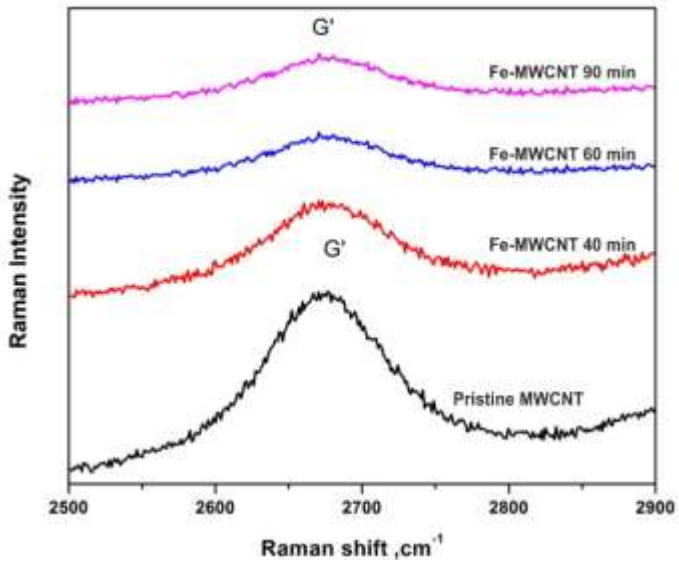


**Figure 5.8**(b) Shows G' band at higher wave number

Also, one more peak at 2700cm$^{-1}$ is observed in figure5.9 (b).Following a similar observation in a previous work, this peak is assigned as G' band [3, 4].The results of Raman Spectroscopy in figure8 (a) show that G band becomes shorter and wider with increasing milling time. While a sharp G band peak in pristine MWCNT characterizes its perfectly hexagonal graphite structure, the observed shortening and widening of G band in nanocomposites at higher milling time suggests that high energy ball milling has caused deterioration in graphite structure of MWCNT.

The results further record a continuous shift of G band to higher wave number and of D band to lower wave number with increasing milling time (figure8a). Such shift of D and G band characterizes enhancement of the defect density in iron-MWCNT nanocomposites. In a previous work with Al-CNT nanocomposite, a similar shift of G and D band was noticed and the concerned shifts were ascribed to the creation of defects in the structure of MWCNTs [33, 36].In this work, G' band is also seen to decrease with increase in milling time (figure5.9b). Diminution of intensity of G' band with increasing milling time hints upon a certain degree of amorphization.

The ratio of intensities of D band and G band, $I_D/I_G$, measures the quantum of structural damage in MWCNT. Summarized results of Raman Spectroscopy in Table 5.2 display the $I_D$ / $I_G$ ratios for different ball milling times. It can be seen that $I_D/I_G$ values in iron-MWCNT nanocomposites increase progressively with increasing time of milling. This observation affirms that higher milling time leads to enhanced damage in MWCNT structure. As reported in later section, microscopic studies have delineated that upon high energy ball milling; CNTs undergo bending, collapse of tubular structures at certain places and also become shorter in lengths. These are responsible for the observed enhancement of $I_D/I_G$ (Table 5.2).

**Table 5.2**Results of Raman spectroscopy showing peak shift and $I_D/I_G$ ratios of nanocomposites

| **Sample Name** | **Raman Peak Shift ($Cm^{-1}$)** | | **$I_D/I_G$** |
|---|---|---|---|
| | **D band** | **G band** | |
| Pristine MWCNT | 1355 | 1573 | 0.99 |
| Fe-2wt%MWCNT20 min | 1341 | 1579 | 1.02 |
| Fe-2wt% MWCNT 40 min | 1340 | 1585 | 1.05 |
| Fe -2wt% MWCNT60 min | 1336 | 1593 | 1.09 |

In consideration of present results of Raman spectroscopy study, it may be postulated that high-energy ball milling leads to damage of MWCNT to the extent where bonding potential between C atoms is significantly reduced. However, the persistence of prominent G and D bands till 1 h milling of Fe-MWCNT nanocomposite confirms that the structural integrity of MWCNT is conserved and reasons out the occurrence of complete amorphization of MWCNT.

### 5.3.6 *XPS-Study*

The present study has envisaged the availability of carbon atoms through controlled damage of MWCNT, so that iron - carbon bond formation by p-d hybridization becomes possible at the interface. So XPS study is employed as an aid to assess the degree of damage in MWCNT, due to high energy ball milling of MWCNT with iron powders. Representative X-ray Photo-electron spectra are shown in figure5.9 (a-b).

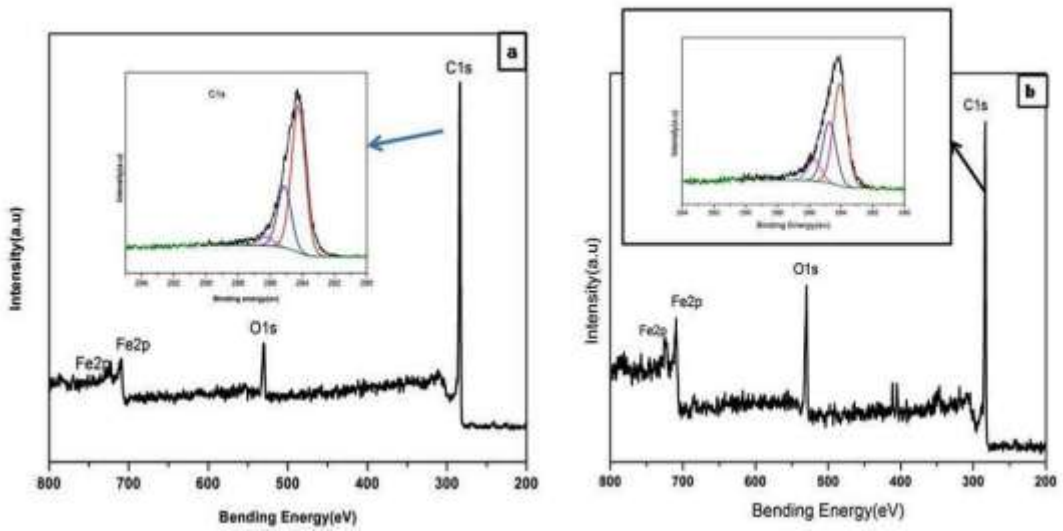


**Figure5.9** XPS Survey scan of Fe-MWCNT nanocomposite after (a) 10 min milling with inset image showing the patterns for C1s at the surface for different etching depths of Fe-MWCNT nanocomposite (b) 1h milling with inset image showing the patterns for C1s atthe surface for different etching depths of Fe- MWCNT nanocomposite (The insets are for etching times 0 to 15s).

Since C-C bond of CNT is of major interest of this study, the C1s spectra are shown in the insets of the corresponding spectrum. Deconvolution separates the peaks in terms of bonding energies and the amount of C-C bond retained after milling the Fe-MWCNT nanocomposite is furnished in Table.5.3.

**Table 5.3** Result of XPS study of C1s at the surface for different etching depths at various mills time

| Sample name | Bonding type | Relative atomic (%) | Bonding energy(eV) |
|---|---|---|---|
| Fe-MWCNT 10 min | C-C | 67.66 | 284.25 |
| Fe-MWCNT 20 min | C-C | 63.82 | 284.26 |
| Fe-MWCNT 40 min | C-C | 61.23 | 284.26 |
| Fe-MWCNT 60min | C-C | 55.60 | 284.05 |

From the results, it is clear that increasing milling time till 60 min has resulted in continuous reduction in the amount of C-C bond. The amount of C-C bond is reduced from 73% to 55% within 1h milling, which means that 20% of the

existing bonds are destroyed. The free bonds may now go for hybridization to insure a good interfacial bonding; alternatively, damage of MWCNTs in terms of disruption of C-C bonds may lead to a situation where some C-atoms may be weakly held on the hexagonal lattice of MWCNT. During high energy ball milling of Fe-CNT composite, the energy imposed onto the system is partitioned between iron particles and MWCNT. Volume fraction of iron is quite large; extensive deformation of iron particles is therefore, expected to introduce high density of dislocations in them. On the basis of previous reports on structural evolution in heavily cold drawn high carbon steel wires or hot forged cast iron [30, 37, 38], it is hypothesized that under situation of partial disruption of C-C bond in MWCNT, the interaction energy between the dislocations and the carbon atoms might become higher than the bond energies of loosely attached carbon atoms (after substantial loss of C-C bonds in MWCNT). In this circumstance, carbon atoms may get away from MWCNT and can join iron lattice by being segregated at the dislocations. Thus formation solid solution between iron and carbon is encouraged. This ensures excellent interfacial bonding between MWCNT and iron. This postulate appears to be more plausible on account of the previous observations, where high interaction energy between dislocations and carbon atoms led to collapse of cementite lattice and also where heavy cold compressive deformation of pearlitic steels had led to segregation of carbon atoms at the dislocations in ferrite [37, 38].

### 5.3.7 *Microstructural Characterization by Transmission Electron Microscopy (TEM)*

The evolution of structure of MWCNT during the course of high energy balling of Fe-MWCNT composite has been studied by Transmission electron Microscopy. As described earlier, the as received MWCNTs are seen to be agglomerated, bent at places and contain some defects (figure 5.10). These features of CNTs produced by CVD technique is quite common and are reported elsewhere [39-46]. Just after milling for 10 min, the MWCNT in composite mixture shows the onset of deformation. The deformation of individual CNTs is characterized by its up and down bending (figure5.10a).

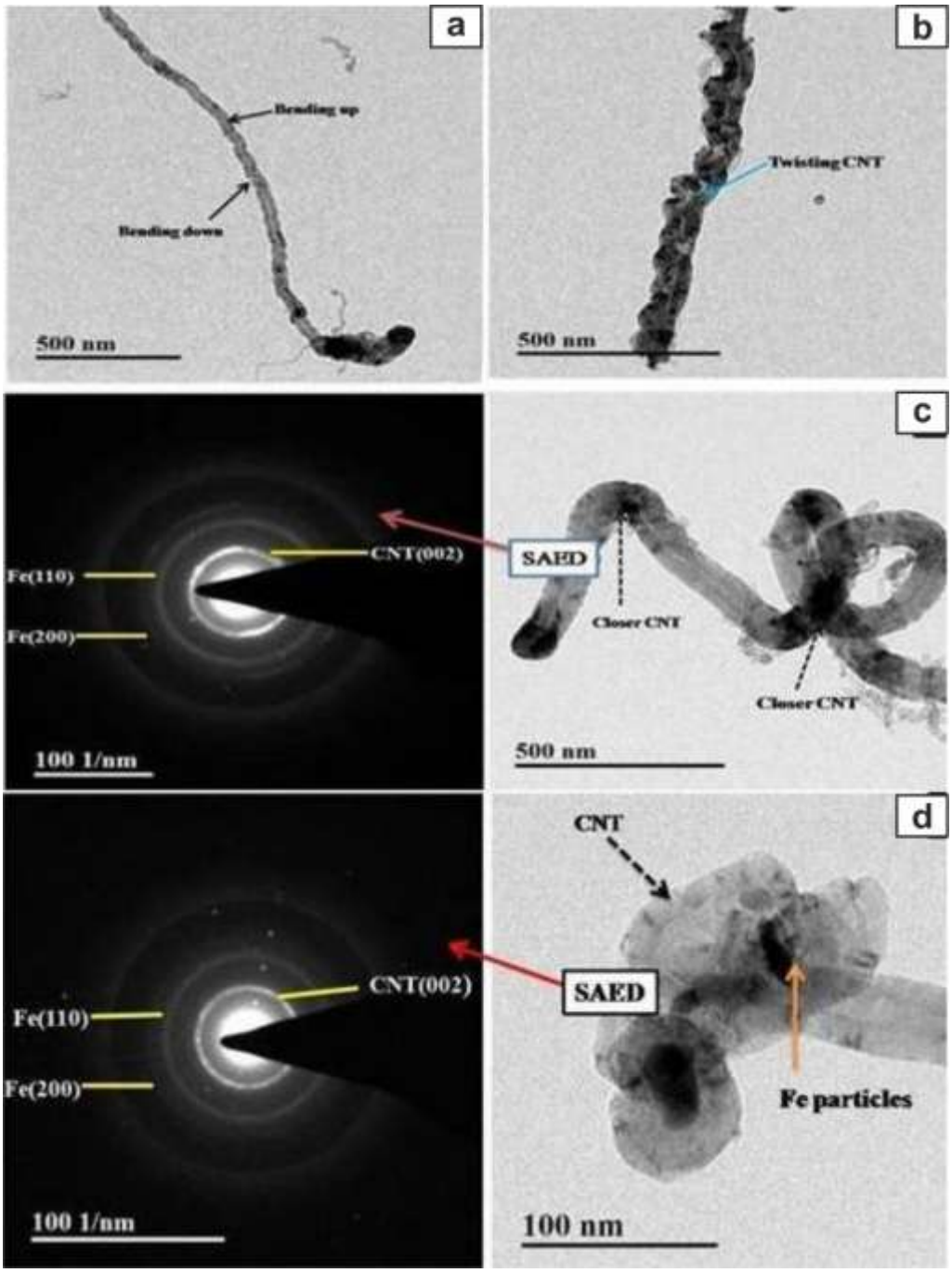


**Figure 5.10** TEM image of Fe-CNT nanocomposite after (a) 10 min milling (b) 20 min milling (c) 30 min milling and (d) 1h milling (Figs. 10c and 10d show corresponding SAED patterns).

The evolution of structural morphology of MWCNT with increasing higher milling time is depicted in figure5.10 (b) and 5.10 (c). It is known that hexagonal closed packed crystals of graphite are capable of twisting or tilting to accommodate

imposed strain on them [4]. It is seen that with increasing milling time, bending and twisting of MWCNTs are intensified. It is further observed that Multiwall CNTs have maintained its' structural identity without loss of tubular structure by bending at both sides of wall in the same direction figure 10 (a-c). With increase in milling time, deformation by localized bending of MWCNTs is seen to be intensified (figure5.10c); this results in closure of tubes at some places along the length of CNT (arrow marked region in figure5.10c).Mixing of metal particles with CNT and its consequent embedding on iron particles is also observed after 30 min of milling and beyond (figure5.10c). The electron diffraction pattern offigure5.10(c) reveals the concurrent presence of CNT and iron. When milling, time is increased to 60 min, the interfacial bonding seems to have been quite good with concurrent damage of MWCNT (figure5.10d).

High resolution electron micrograph taken from the powder samples of composite after 60 min of ball milling is shown in figure5.11.

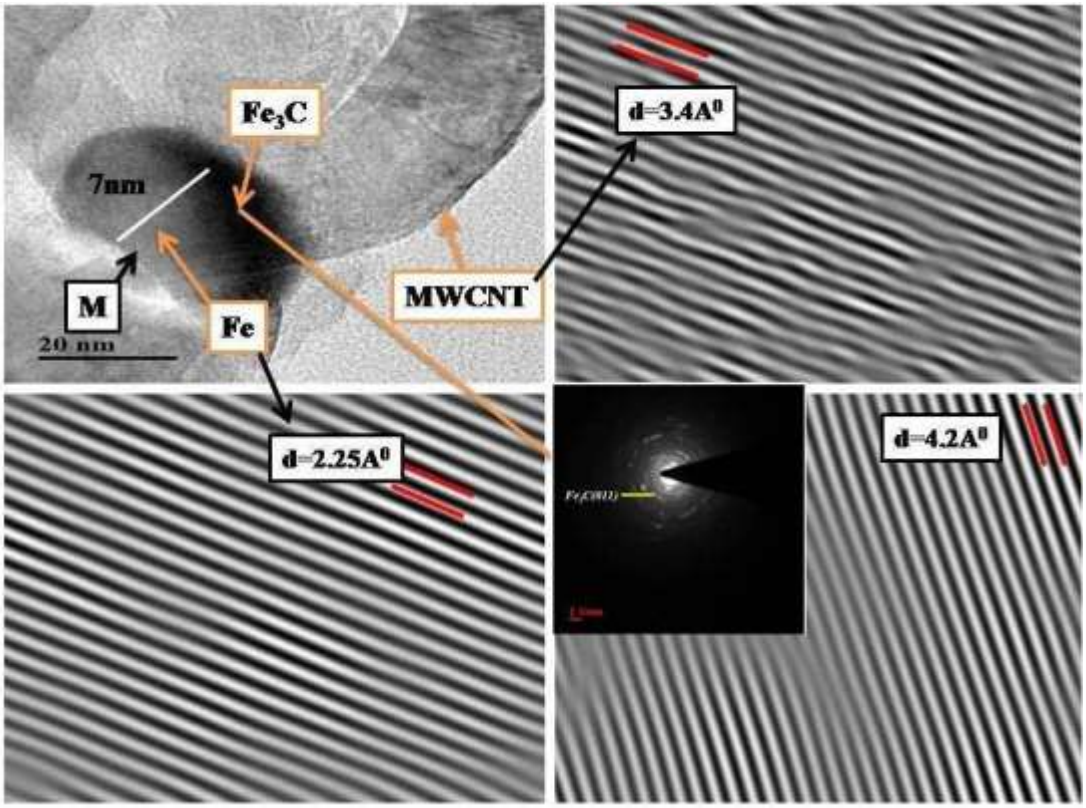


**Figure 5.11** HRTEM image of Fe-MWCNT nanocomposite after 1h milling.

It is evident from the micrograph that merger of outer layers of MWCNTs with crystals of iron takes place at the iron-CNT interface presumably because of the partial collapse of C-C bonds at the outer layers of MWCNT and consequent 3d-2p hybridized iron-carbon bond formation. The lattice image of the concerned sample verifies that there is a smooth interfacial transition between CNT and iron as shown by 'M' marked region.

Moreover, in such cases some new particles are seen to form in the adjacent regions. The particles are, in general, of ellipsoidal shape. Interestingly the ellipsoidal particles formed at the adjoining region are found of 7 nm size and the observed d-spacing verifies that the particles are orthorhombic cementite ($Fe_3C$).The SAED pattern shown in the inset of figure 5.11 verifies the presence of orthorhombic $Fe_3C$.

The general information conveyed by the HRTEM study is that milling up to 1 h can maintain the structural integrity of MWCNT and hence its characteristic physical properties. Bending with shorter wavelength (with increasing time) and collapse of tubular structure of MWCNT at various locations characterize degree of its damage caused by high energy ball milling.

Microscopic observation delineates that under present situation of ball milling, MWCNTs largely maintain its tubular structure and become embedded within the matrix metal with continues and smooth interface. This insures a good interfacial bonding between iron and MWCNT. Raman spectroscopic results ascertain the retention of MWCNT structure with some kind of damage caused to it but negate its complete amorphization till 1 h. milling. XRD results have also confirmed the preservation of MWCNTs in ball milled composite and rules out extensive formation of iron carbide by mechano-chemical synthesis of Fe and MWCNT. While FTIR results prove the loss of C-C bond at the expense of formation of Fe-C bonds, XPS study affirms the disruption of C-C bonds in ball milled samples by about 20%; but DSC study makes it clear that there is no super saturation of iron with carbon atoms after milling the composite powder for 1 h. All these entice one to hypothesize that a controlled damage of MWCNT secured by optimal high energy ball milling of Fe-CNT composite disrupts C-C bonds in

MWCNT; the consequent availability of carbon atoms and its' segregation at dislocations within nearby iron crystals make the system highly conducive to iron-carbon bond formation; this leads to a very good interfacial bonding; it therefore, bears the scope for improvement in magnetic properties of the MWCNT reinforced iron matrix composite.

### 5.3.8 *Study of magnetic property by Vibrating Sample Magnetometer (VSM)*

The magnetic properties of Fe-MWCNT nanocomposite produced by high energy ball milling for different milling times are studied by VSM. The results are shown in figure5.12

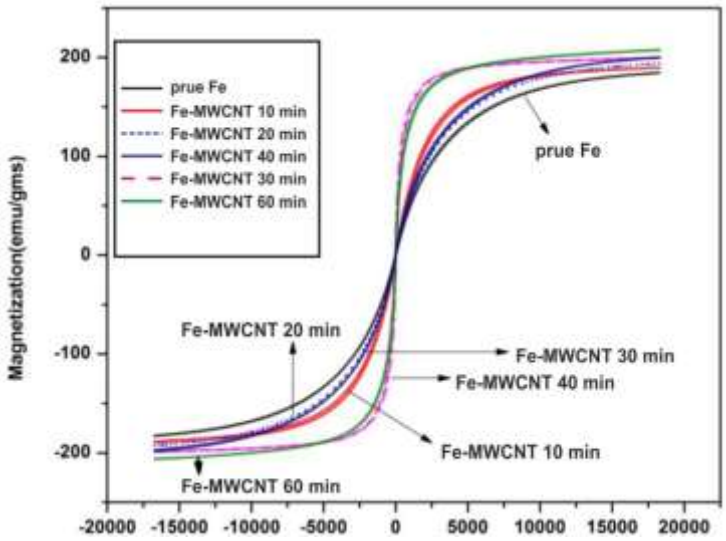


**Figure5.12**M-H curves of Fe-MWCNT nanocomposite for different milling times.

From the figures, it is apparent that saturation magnetization, coercivity and remnant magnetism vary with varying milling time; it is also seen that all the above magnetic properties are concurrently improved in Fe-CNT nanocomposite in order of increasing milling time. The curves in figure5.12 record a typical ferromagnetic behavior of the composite. The improvement in the magnetic properties of the composite are assessed against the pure iron used for production of composites. If pure iron is subjected to high energy ball milling, saturation magnetization generally decreases due to strain generated within the material, although its coercivity increases [47]. In the present case, saturation magnetization is found to have increased by 11% after 1 h milling. It is to be noted that MWCNT used in the present investigation has been prepared by CVD technique with iron as catalyst and

hence MWCNT used in the present investigation behaves ferromagnetic [23, 25, and 28]. The results of VSM study are furnished in summarized form in Table.5.4

**Table 5.4**Magnetic property of samples for different milling times

| **Sample Name** | **Saturation Magnetization,**(Ms) (emu/gms) | **RemanantMagnetization**(Mr)(emu/gms) | **Coercivity**(Hc) (Oe) |
|---|---|---|---|
| Pure Fe | 184 | 0.21 | 3.2 |
| Fe-MWCNT10min | 188 | 0.98 | 11.4 |
| Fe-MWCNT20min | 194 | 3.4 | 15.5 |
| Fe-MWCNT30 min | 198 | 4.7 | 13.5 |
| Fe-MWCNT 40min | 199 | 5.7 | 16.7 |
| Fe-MWCNT60min | 205 | 6.2 | 19.1 |

It is evident that saturation magnetization has increased in opposition to expected degradation of magnetic behavior of ball milled iron. From the results of other experiments in this work and from the foregoing discussion it is clear that MWCNT have effectively embedded within iron matrix and that the controlled damage of MWCNT has insured a good interfacial bonding with a high degree of cohesion.

As a matter of fact, the particle size of matrix iron ranges within 35-40nm for the ball milled composite. Thus, the nanocomposite is constituted by almost single domain magnetic material having coherent interface with MWCNT. Application of magnetic field can align the domain along the direction of field quite perfectly. In a coarse multiple domain, ferromagnetic material, the inevitable movement of domain boundaries along with intra-domain spin alignment exhibits magnetostriction; the magnetostriction resists domain alignment along the applied field to a much higher extent than a single domain magnetic material to orient itself along the field. It is further aided by the MWCNT, which itself gets aligned with the adjoining crystallites. Seemingly this is the reason for higher magnetic saturation value; higher

milling time ensures better interfacial bonding and hence smooth flux flow across the interface. Moreover, magnetic particles become finer at higher milling time and these result in a higher population density of single domain particles. The nanosized magnetic particles attached to the surface of MWCNTs enhance the magnetic susceptibility of MWCNT [48] this has a positive influence on the overall saturation magnetization value of iron-MWCNT composite. Another reason for high saturation magnetization might be the higher remnant magnetism for higher milling time. Upon withdrawal of the field, the domains become disorderly arranged to lower overall free energy; however, in CNT-reinforced nanocomposite the rotation of domain is resisted by impingement of domain boundaries with the MWCNT walls. Hence remnant magnetism is significantly high. Due to high remnant magnetism, overall saturation magnetism might have become significantly higher [49]. For the reason of more interfaces and high energy areas like dislocation tangles, the domains, once rotated in alignment with imposed field, cannot of its own, revert back to random configuration simply upon withdrawal of the imposed field without application of stronger reverse field. This explains the concurrent improvement in coercivity of the nanocomposite under investigation.

## 5.4 Conclusions

It is concluded that degree of damage caused to MWCNTs during high energy ball milling with iron powders is dependent on milling time and milling of iron-MWCNT composite for 60 min produces optimal damage to MWCNTs reinforcing iron matrix. Further, controlled high energy ball milling insures uniform distribution of reinforcing MWCNT in the iron matrix. It is also concluded that the damage of MWCNT takes place by partial destruction of C-C bonds of MWCNT; the available carbon atoms segregate at dislocations in nearby iron crystals. These carbon atoms are highly conducive to undergo 3d-2p hybridization and hence aids in achieving a smooth CNT-matrix interface. Such a good interfacial structure significantly improves the magnetic properties of nanocomposites in opposition to the expected degradation of saturation magnetization, which is commonly observed in high energy ball milled iron powders. Nevertheless, occasional presence of

carbide at the iron-MWCNT interface is inevitable in HEBM composite due presumably to high chemical affinity between iron and carbon.

## REFERENCES


[1] J. Z. Liao,M. J. Tan, Mixing of Carbon nanotubes (CNTs) and aluminum powder for powder metallurgy use, Powder Technol 208(2011) 42-48.

[2] K. S. Munir, M.Qian, Li Yuncang, D. T. Oldfield, P.Kingshott, D. M. Zhu,C. Wen, Quantitative analysis of MWCNT-Ti powder mixtures using Raman spectroscopy: The influence of milling parameters on nonstructural evolution, Adv. Eng. Mater.17 (2015) 1660- 69.

[3] D.Poirier, R.Gauvin, R. A.L, Drew Structural characterization of a mechanicallymilled carbon nanotube /aluminum mixture,Composite Part A 40 (2009) 1482- 89.

[4] J. Y.Suh, D. H.Bae, Mechanical properties of Fe-based composites reinforced with multi –walled carbon nanotubes, Mater. Sci. Eng.582 (2013) 321- 5.

[5] Z. Y.Liu, S. J.Xu, B.L.Xiao, P.Xue,W.G.Wang, Z. Y. Ma, Effect of ball - milling time on mechanical properties of carbon nanotubes reinforced aluminum matrix composites, Composite Part A (2012) 2161- 68.

[6] K. Morsi,A. Esawi, Effect of mechanical alloying time and carbon nanotubes (CNT) content on the evolution of aluminum (Al)-CNT composite powder, J. Mater Sci.42 (2007) 4954- 59.

[7] A. M. K.Esawi,K.Morsi,A.Sayed,M.Taher,S.Lanka, The influence of carbon nanotubes (CNT) morphology and diameter on the processing and properties of CNT –reinforced aluminum composites, Composite Part A 42 (2011) 234-43.

[8] S.Azadehranjbar, F.karimzadeh, M.H. Enayati, Development of NiFe-CNT and $Ni_3Fe$ –CNT nanocomposites by mechanical alloying, Adv. powder Technol 23 (2012) 338- 42.

[9] B.Munkhbayar, Md. J.Nine, J. Jeoun, M. B.Erden, H.Chung, H.Jeong, Influence of dry and wet ball milling on dispersion characteristics of the multi- walled carbon naotubes in aqueous solution with and without surfactant, Powder Technology 234 (2013) 132- 40.

[10] Z. Y.Liu, B.L. Xiao, W.G.Wang, Z. Y. Ma, Singly dispersed carbon nanotube/aluminum composites fabricated by powder metallurgy combined with friction stir processing, Carbon 50 (2012) 1843-52.

[11] R.P. Bustamante, R.E. Guel, I.A. Flores, W.M. Yoshida, M. F.PJ,R. MS, Novel Al-matrix nanocomposites reinforced with multi-walled carbon nanotubes, J Alloy. Compd 450 (2008) 323–6.

[12] A.Esawi, K.Morsi, A.Saye, M.Taher, S,Lanka, Effect of carbon nanotube (CNT) content on the mechanical properties of CNT-reinforced aluminum composites, Compos. Sci. Technol 70 (2010) 2237–41.

[13] H. J.Choi, J. Y.Shin, B. H.Min, J.Park, D. H. Bae Reinforcing effects of carbon nanotubes in structural aluminum matrix nanocomposites,J. Mater. Res. 24 (2009) 242610–6.

[14] K.Morsi,A. M. K.Esawi, S.Lanka, A.Sayed, M.Taher, Spark plasma extrusion (SPE) of ball milled aluminiumand carbon nanotube reinforced aluminum composite powder,Composite A38 (2010) 322-26.

[15] A.Esawi, K.Morsi, Dispersion of carbon nanotubes (CNTs) in aluminum powder. Composite A 38 (2007) 646-50.

[16] N.Pierard, A.Fonseca, J.F.Colomer, C. Bossuot, J.M.Benoit, G.V. Tendeloo, J.P.Pirard, J. B. Nagy, Ball milling effect on the structure of single –wall carbon nanotubes, Carbon 42 (2004) 1691-97.

[17] W.M.Tucho, H. Mauroy, J.C. Walmsley, S. Deledda, R. Holmestada, B.C. Hauback,The effects of ball milling intensity on morphology of multiwall carbon nanotubes,Scr. Mater 63 (2010)637- 40.

[18] Y.B. Li, B.Q. Wei, J. Liang, Q. Yu, D.H. Wu, Transformation of carbon nanotubes to nanoparticles by ball milling process, Carbon 37 (1999) 493-7.

[19] Y.He, J. Zhang, Y. Wang, Z. Yu, Coating geometries of metals on single-walled carbon nanotubes, Appl. Phys. Letter 96 (2010) 063108-3.

[20] S.Yuan, Y.Kong, F. Li. F.Wen, $Fe_4$ cluster adsorbed on single-wall carbon nanotubes: A density functional study, Comput. Mater.Science 42 (2008) 83-9.

[21] S.F.Boi, J.Guo, M.Lan, T.Yu, S.Wang, Y.He, J.Wen, G.Xiang,Tuning high magnetizations in foam-like carbon-based films completely filled with a-Fe, Carbon 101 (2016) 28-36.

[22] T. Peci, M. Baxendale, Length and a-Fe content control of self-organised ferromagnetic nano wires encapsulated by multiwalled carbon nanotubes by low flow-rate CVD, Carbon 98 (2016) 519-525.

[23] F. C.Dillon, A.Bajpai, A.Koos, S.Downes, Z.Aslam, N. Grobert, Tuning the magnetic properties of iron-filled carbon nanotubes, Carbon 50 (2012) 3674-81.

[24] F. S. Boi, G. Mountjoy, R.M.Wilson, Z. Luklinska, L.J.Sawiak, M. Baxendale, Multiwall carbon nanotubes continuously filled with micrometer-length ferromagnetic a-Fe nanowires, Carbon 64 (2013) 351-358.

[25] H.Kim, W.Sigmun, Iron particles in carbon nanotubes, Carbon 43 (2005) 1743–1748.

[26] C.Prados, P. Crespo, J.M.Gonzalez, A. Hernando, J.F. Marco, R.Gancedo, N. Grobert, M.Terrones,Hysteresis shift in Fe-filled carbon nanotubes due to γ-Fe, Phys. Rev. B. 65 (2002) 113405-4.

[27] S.Hudziak, A.Darfeuille, R.Zhang, T.Peijs, G.Mountjoy, G.Bertoni, M. Baxendale, Magnetoresistive phenomena on Fe-Filled carbon nanotube/ elastomer composites, Nanotechnology 21 (2010) 125505-8.

[28] C. Suryanaryana,Mechanical alloying and milling Prog, Mater Science 46 (2001) 1-184.

[29] M.T.Hassan, A. M.Esawi, S.Metwalli, Effect of carbon nanotube damage on the mechanical properties of aluminium–carbon nanotube composites, J Alloy, Compd 607 (2014) 215-22.

[30] M.H.Hong, W.T. Reynolds,Jr. T.Tarui, K. Hono, Atom Probe and TransmissionElectron Microscopy Investigations of Heavily Drawn Pearlitic Steel Wire,Metall, Mater. Trans. A30 (1999) 717-27.

[31] P.Gill, N. Munroe,Study of Carbon Nanotubes in Cu-Cr Metal Matrix Composites,J. Mater. Eng. Perform 21 (2012) 2467-71.

[32] L.Jiang, L.Gao, J. Sun, Production of aqueous colloidal dispersions of carbon nanotubes,J. Colloid Interface Science260(2003) 89–94.

[33] F.Zhao, H.Duan, W.Wang, J. Wang,Synthesis and characterization of magnetic Fe/CNT composites with controllable Fe nanoparticles concentration, Physica B 407 (2012) 2495-99.

[34] L.Jiang,G.Fan, Z. Li, X.Kai, D. Zhang, Z. Chen, S. Humphs, G.Heness, W. Y. Yeung,An approach to the uniform dispersion of a high volume fraction of carbon nanotubes in aluminum powder, Carbon 49 (2011) 1965-1971.

[35] P. Delhaes, M. Couzi, J.M.Trinquecoste, H.Hamidou, C.V.Guterl, A comparisonbetween Raman spectroscopy and surface characterization of multiwall carbon nanotubes, Carbon 44 (2006) 3005-13.

[36] S.Wang, R.Liang, B.Wang, C. Zhang, Load-transfer in functionalized carbon nanotubes/polymer composites, Chem.Phys. Letter 457 (2008) 371-75.

[37] J.Languillaume, G.Kapelski, B. Baudelet, Cementite dissolution in heavily cold drawn pearlitic steel wires, Acta Metall. Inc 45 (1997) 1201-12.

[38] N. R.Bandyppadhyay, M.K.Banerjee, P. P. Das, Hot Forging A Tool to Improve the Structure of White Cast Iron,Trans IIM 39 (1986) 486-91.

[39] A.N.Volkov, T.Shiga, D.Nicholson, J. Shiomi, L.V. Zhigilei, Effect of bending buckling of carbon nanotubes on thermal conductivity of carbon nanotube materials, J. Appl. Phys. 111 (2012) 053501-11.

[40] W.Z.Qian, W.Fei, W.Zhanwen, L.Tang, Y. Hao, L.Guohua, X. Lan, Production of carbon nanotubes in a packed bed and a fluidized bed, AICHE J 49 (2003) 619–25.

[41] H. Yu, Z.h.Li, G.Luo, F.Wei, Growth of branch carbon nanotubes on carbon nanotubes as support, Diamond Relat. Mater 15 (2006) 1447–51.

[42] T.Erik, T. Z. Ren, T.W.Chou, Advances in the science and technology of carbon nanotubes and their composites: a review, Compos. Sci. Techno. 61 (2001) 1899–1912.

[43] H. Kind, J.M.Bonard, C. Emmenegger, L.O.Nilsson, K.Hemadi, E. L.Maillard-Schaller, L.Forro, K. Kem, Patterned Films of Nanotubes Using Microcontact Printing of Catalysts, Adv. Mater 11 (1999) 1285-89.

[44] C.J. Lee, D.W. Kim, T.J. Lee, Y.C. Park, Y.H. Lee, W.B. Choi, N.S. Lee, G.S. Park, J.M. Kim, Synthesis of aligned carbon nanotubes using thermal chemical vapor deposition Chem, Phys. Letter 312 (1999) 461-68.

[45] P.C.Hidber, W.Helbig, E. Kim, G.M. Whitesides,Microcontact printing of palladium colloids: micron-scale patterning by electroless deposition of copper,Langmuir 12 (1996) 1375-1380.

[46] J.D. Harris, R.P.Raffaelle, T. Gennett, B.J. Landi, A.F.Hepp, Growth of multi-walled carbon nanotubes by injection CVD using cyclopentadienyliron

dicarbonyl dimer and cyclooctatetraene iron tricarbonyl, Mater.Sci. Eng B 116 (2005) 369-74.

[47] T.T. Bui, X.Q. Le, D.P.To, V.T. Nguyen, Investigation of typical properties on nanocrystalline iron powders prepared by ball milling techniques,Adv. Nat. Sci. Nanosci. Nanotechnol 4 (2013)045003-8.

[48] R. Tannenbaum, Magnetic carbon naotubes synthesis characterization and anisotrophic electrical properties,Georgia Institute of Technology United StatesJuly(2011).

[49] O.Boshko, O.Nakonechna, M.Dashevskyi, K.Lvanenko, N.Belyavina, S. Revo, Effect of the carbon naotubes on structure and magnetic properties of the Fe-Cu(4:1) composites,Adv. Powder Technol27 (2016) 1101-1108.

# *CHAPTER SIX*

## *Effect of MWCNT Content on The Structure and Properties of Spark Plasma Sintered Iron-MWCNT Composites Synthesised by High Energy Ball Milling*

In current chapter, discussion has been made about the structural evolution and phase evolution of iron-MWCNT composites. Their mechanical and physical properties are measured and discussed. Magnetic properties of the Fe-MWCNTs after varying the MWCNT (1, 2, 3 and 4 wt. %) nanocomposites are measured by Vibrating Sample Magnetometer (VSM). Study of the mechanical and electrical property after spark plasma sintering (SPS) with different weight percent of MWCNTs in Fe has also been done. The study delineates partial destruction of C-C bonds of MWCNT due to high energy ball milling of powder mix. However, amount of carbon atoms released by bond disruption is rather small and heavy super saturation of iron with carbon and extensive precipitation of carbides during heating is seen untenable.

## 6.1 Introduction

Owing to fascinating properties of carbon nanotubes, there has been growing interest in developing novel metal matrix- MWCNT composites. However, fabrication of metal matrix-MWCNT composite has remained a concern due to difficulties in achieving uniform dispersion of reinforcing MWCNT and good interfacial bonding. Of the several routes tried so far, mechanical alloying route has been found to provide a good uniformity in dispersion of MWCNT into the matrix. However mechanical alloying suffers from the problem of mechano-chemical synthesis between matrix metal and MWCNT.

Many researchers believe that any reaction product formed at the interface between metal matrix and MWCNT is deterring to the possible enhancement in properties of iron matrix composite due to reinforcing with MWCNTs. It is further believed by a school of thought that presence of interfacial reaction product is not a necessity to achieve good bonding at the interface between metal matrix and the reinforcing MWCNT [1-3]. However, there are others who claim that the formation of aluminum carbide at the interface of aluminum- MWCNT ensures better bonding by way of modifying the wettability angle. Transition metals find wide usage as structural materials in various industries. The vacant 3d orbital of transition metals bears the possibility of 3d-2p hybridization between metal and MWCNT graphitic structure; it is stated elsewhere that this enables to achieve good interfacial bonding. Moreover, many transition metals are strong carbide formers; thus, formation of transient metal-MWCNT composite by mechanical alloying route envisages formation of carbide at the interface and hence leads to structural degradation of MWCNT. Research reports of fabrication of Titanium- MWCNT composite without formation of interfacial carbide is documented in literature [4]. So far, most of the researchers in the field have concentrated in the study of the effect of interfacial reaction on the mechanical properties of metal-MWCNT composite. Besides being employed as structural material where mechanical properties are of major interest, iron as transition metal, is also very important in electromagnets as well as permanent magnets for engineering applications. Unlike in majority of transition metals, carbon is known to dissolve easily in iron and at the same time, it is

chemically affinitive to iron towards the formation of various types of carbides. Thus, it appears that mechanical alloying route if adopted for producing Fe-MWCNT composite can influence the interfacial bonding at matrix- reinforcement interface in different ways.

It is already demonstrated by the author that beyond a certain milling time, formation of $Fe_3C$ is inevitable in mechanical alloying of iron and MWCNT. But the milling time responsible for degradation of MWCNT with the formation of iron carbides can be different for different amount of MWCNT in iron matrix and hence it appears to be worth studying. Moreover, the impact of mechanical alloying route of fabrication of Fe-MWCNT composite on physical properties like magnetic and electrical properties have not been well studied.

Importantly, consolidation technique of composite powders is of extreme importance so far as the avoidance of structural degradation of reinforcement is concerned. Spark plasma sintering (SPS) technique is a very useful technique of consolidation of composite powders; this is because of its rapid rate of heating and cooling from the sintering temperature for a short holding time. Besides being able to achieve almost theoretical density by way of getting sintered under high pressure, the technique also inhibits grain growth in the sintered mass. However, in the case of iron-MWCNT composite, the chance of damage of MWCNT structure during SPS cannot be over ruled for reasons like high solubility of carbon in iron, possible phase transformation under pressure, carburizing of iron and ultimate formation of carbides.

In the present chapter, study on the effect of MWCNT content on the physical and mechanical properties of Fe-MWCNT composites fabricated by high energy ball milling followed by spark plasma sintering is reported.

## 6.2 Experimental methods

### *6.2.1 Materials*

The raw materials used in this study consist of Fe powder and multiwall carbon nanotube. Fe powder particles (purity ≥99%, -325 meshes, average particle

size 43 micron), are irregular in shape. MWCNTs purchased from Nanoshel (average diameter and length are 15-20nmand 10-26 µm, respectively), are used as the reinforcement. Figure 6.1(a, b)show the FE-SEM image of iron powder and MWCNTs; figure 6.1(c, d) show the HR-TEM images of the as-received CNTs used for the present experimentation.

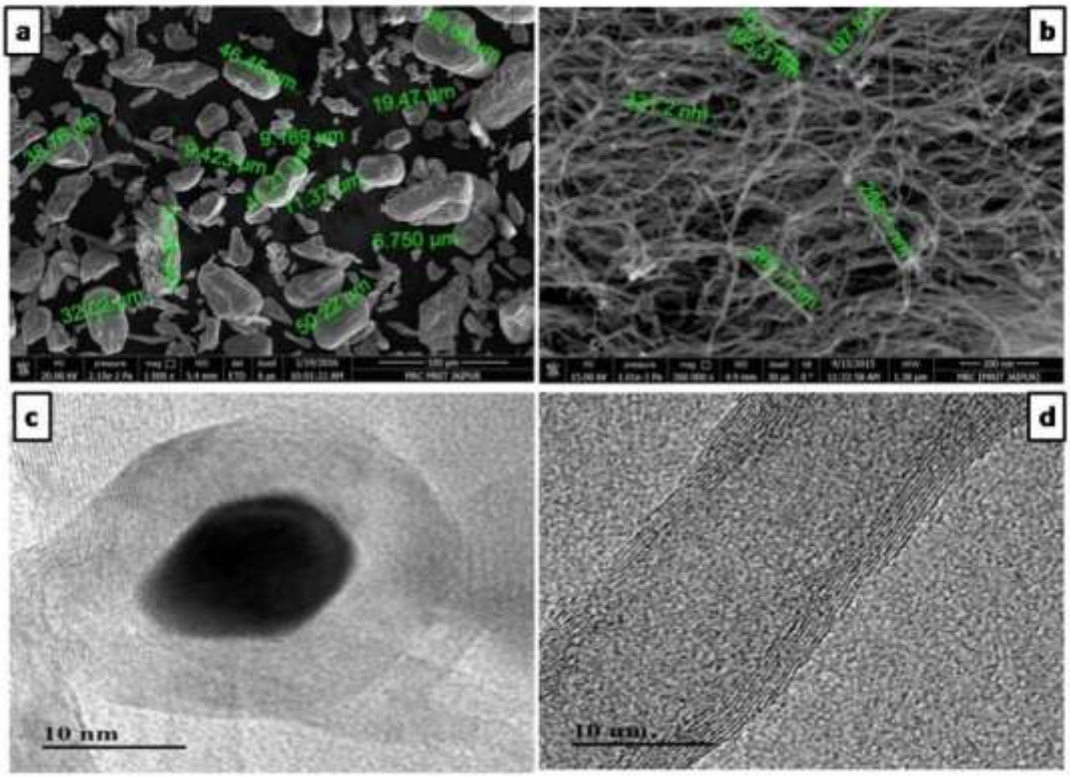


**Figure6.1** Typical micrographs of raw powders (a) SEM image of iron powder and major the particle size (b) SEM image of MWCNT (c) HR-TEM image of the open tip of MWCNT and (d) HR-TEM image of MWCNT

### *6.2.2 Mixing and Mechanical Alloying*

The iron powder (Fe) with the various weight percent of MWCNTs (1, 2, 3 and 4wt.%) are mechanically alloyed by utilizing Pulverisette-P6 high energy planetary ball mill (Fritsch, Germany); using the tungsten carbide vial and ball. Ball to powder weight ratio is maintained at around 6:1. Stearic acid is used as the process controlling agent (PCA) to prevent excessive cold welding on the surface of the ball and vial and also to provide reducing media during the milling. The milling is carried out for varying periods up to 50 min in a planetary ball mill at 200 RPM. The mechanically milled powders Fe-MWCNTs with various weight present of

MWCNTs (1, 2, 3 and 4 wt.%) were sintered by spark plasma sintering method by the following the technique describe in Chapter 3.

X-ray diffractometer (XRD, Philips X'Pert with Cu Kα radiation) was utilized to analyze the constituent phases in the nanocomposite powder(Fe-MWCNT).The measurement technique has been same as that narrated in Chapter3.Microstructures of polished samples were observed under optical and field emission scanning electron microscope (FESEM).Transmission electron microscope (TecnaiF-20) was used for detailed microstructural study. Vibrating Sample Magnetometer(VSM) of model EZ9 of make Microsence Company was used to study the magnetic property of the composites. Micro hardness characterization of the sintered composites was carried out by UHL VMHT (WalterUhlGmbh, Germany) micro hardness tester at a load of 300gf with dwell time of 15 sec. Average of ten consistent readings was taken as the representative hardness value. The compressive test of Fe-MWCNTs composite was done in Instron testing machine under a constant cross head speed with an initial strain rate of0.05 $s^{-1}$at room temperature. To conduct the compressive tests, the samples were prepared with a cylindrical form with a height and diameter 5×5 mm.

XPS study was performed in Omicron Nanotechnology XPS system from Oxford Instruments (model ESCA+). The method used is described in Chapter 3. Also, Fourier transforms infrared spectrometer (Perkin Elmer Frontier) was used to obtain information about stretching vibration of different bonds present in the experimental composites.

Raman spectroscopy was carried out at room temperature in AIRIX STR 500 CONFOCAL MICRO Raman Spectrometer by following the process described in Chapter3. The DC electrical conductivity of Fe-MWCNT nanocomposite pellets are measured using electrometer (B 1500A Agilent Technology). Silver paste is applied on the cross-sectional faces of the pellets prior the electrical measurements. Standard two-probe set up is used for these measurements.

## 6.3 Results and Discussion

### *6.3.1 X-ray diffraction study*

XRD spectra of sintered Fe-MWCNTs composites containing varying weight percent of MWCNTs (1, 2, 3, and 4wt.%) are shown in figure 6.2(a). The results of XRD reveal the presence of peaks of iron and MWCNTs. The absence of any peak of $Fe_3C$ in X-ray diffractogram of the experimental composites verifies that, there has not been any unwanted product of chemical reaction between iron powder and MWCNT either during ball milling operation or during spark plasma sintering. The XRD peaks due to MWCNT are indexed as (002) plane of which has the interplaner spacing of 0.34nm; this observation confirms that the crystallinity of MWCNT is conserved. Thus, XRD results suggest that neither perceptible mechano chemical synthesis nor chemical reaction between carbon in MWCNT and iron metal has taken place. It is to be noted that in accordance with the objective of the present study the structural identity of MWCNTs could be satisfactorily retained in iron matrix.

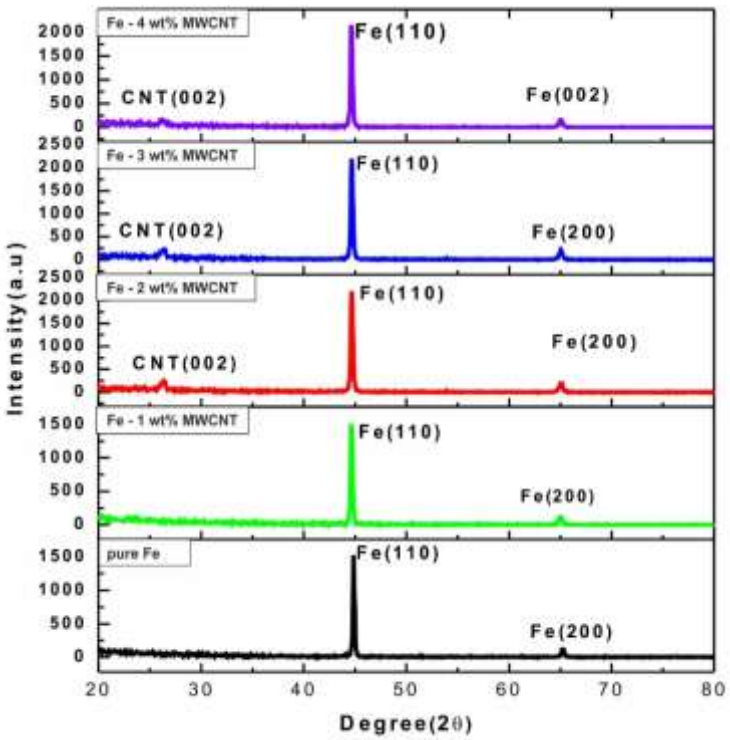


**Figure6.2**(a) XRD Pattern of Fe-MWCNTs nanocomposite with increasing wt.% MWCNT in Fe

There is however varying opinion on the role of formation of carbide at the metal matrix interface. The better interfacial bonding is achieved without any carbide forming at the interface, has demonstrated that formation of $Al_4C_3$carbide at the Al-MWCNT interface can reduce the wettability angle and hence insures a better bonding[5].

It is known that, for achieving the best combination of mechanical and physical property in Fe-MWCNT nanocomposite, well uniform dispersion of MWCNT in Fe matrix with a good interfacial bonding is mandatory. In our case SPS temperature has been deliberately kept at a low level to avoid the dissolution of carbon in iron crystals from adjoining MWCNTs. Low temperature and high pressure chosen for spark plasma sintering can help to obtain homogenous microstructure with small pore content and no measurable second phase. Reportedly vacant 3d orbital in transition metal like iron is conducive to3d-2p hybridization, which when takes place ensures a good interfacial bonding. However, such observation cannot be authenticated by XRD study.Never the less, present XRD study, within the limit of detection of phases by the concerned instrument, reasons out any contamination to take place at interface.

It is apparent from figure 6.2(b) that increasing MWCNT content from 1wt.%-4wt.%has caused appreciable shift of (110) XRD peak of iron towards lower angle side. This has the implication that there has been increase in lattice parameter of iron. Lattice parameter of iron can increase only when carbon goes in solution in iron either during HEBM or during SPS.

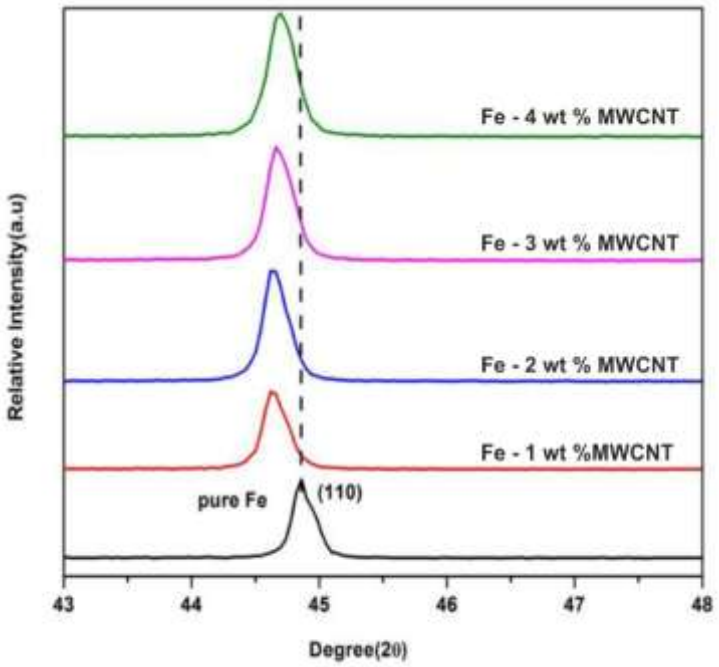


**Figure 6.2**(b) Shift of XRD Peaks (110) to low angle sides with increasing weight percent of MWCNT.

In view of high solubility of carbon in iron at higher temperature, the process parameters in spark plasma sintering are extremely important to avoid extensive dissolution of carbon in iron. Imperatively, high thermodynamic feasibility of bonding between iron and carbon goes to degrade MWCNT structure unless the sintering parameters are properly controlled. It is evident from iron - carbon equilibrium diagram [6] that about 0.02wt.% of carbon is soluble in iron at $650^0$C. Since in SPS both heating and cooling are done very fast, precipitation of carbide from ferrite may be sluggish. So XRD carried out at room temperature of SPS samples (figure 6.3) does not record any carbide peak. This means that neither iron-carbide is formed due to mechano-chemical synthesis between iron and carbon nor there has been so much dissolution of carbon during SPS as to cause unavoidable carbide precipitation during cooling from sintering temperature (figure6.3).

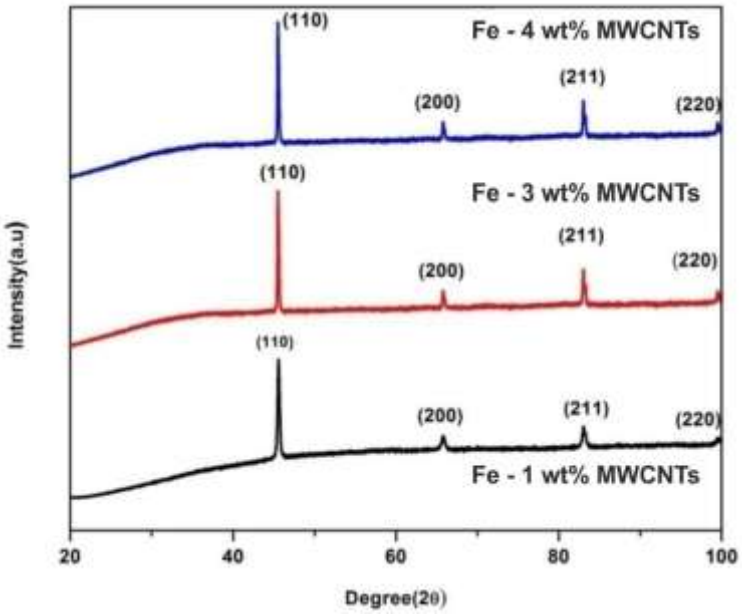


**Figure6.3**XRD patterns of samples after SPS; four major peaks of iron for use to constructWilliamson and Hall plots for Fe -MWCNT composites.

We also try to get idea about the lattice stain and crystal size after SPS of samples containing varying amounts of MWCNT in Fe. It is observed that with increasing MWCNT content there is an increase in size of crystal with concurrent reduction in residual strain(Table6.1). The Williamson and Hall method commonly used to calculate the size of crystallite(L) and associated lattice strain(η) from XRD spectrum is of the form $B\cos\theta=k\lambda/L+\eta\sin\theta$..... (1)

Where k is the Scherer's constant, B is the FWHM and 2θ is the Bragg angle. Williamson and Hall plots of composites with different wt.% of MWCNT in Fe is shown in figure 6.4.

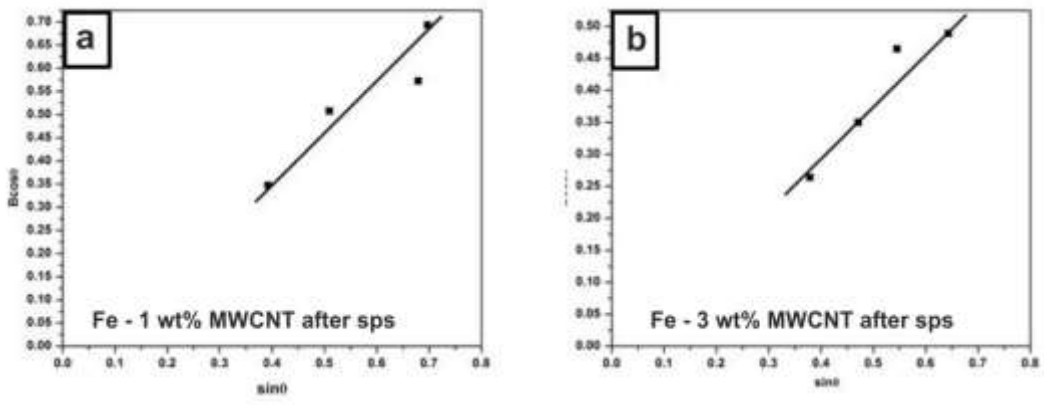

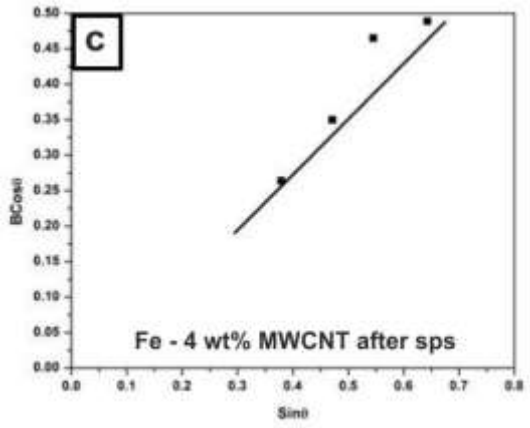


**Figure 6.4**(a-c) Williamson and Hall plots of Fe-MWCNT composites of varying concentration ofMWCNT.

The summary of results is presented in Table 6.1. From results in Table 6.1, it is noticed that there is reduction in strain at higher MWCNT content and this is ascribed to the aggregation of MWCNT; the agglomerated regions contain very small sized pores inside them. These pores accommodate residual strain. Increment in crystal size is indicative of the fact that in line with earlier observation [7],the curly MWCNT has form 2Dchannel network on the flattened metal matrix surface during ball milling; cylindrical MWCNTs having formed the 2D network restricts radial plastic flow of iron crystallites. Cold welding of particles, an important step in mechanical alloying can however continue along vertical direction; hence increase of crystallite size after 50 min of HEBM followed by SPS of experimental composite samples is noticed (Table 6.1).

**Table6.1**Crystal size and strain of iron-MWCNT composites with different wt.% of MWCNT

| **Values(After SPS)** | **Fe -1 wt.%MWCNT** | **Fe-3wt.%MWCNT** | **Fe-4 wt.% MWCNT** |
|---|---|---|---|
| Crystallite size (nm) | 43 nm | 51 | 58 nm |
| Lattice strain | 0.0023 | 0.0019 | 0.0017 |

### *6.3.2 Raman spectroscopy*

As discussed in the preceding section, the presence of carbide in Fe-MWCNT could not be detected in the XRD study. Reported that the formation of carbide at the interface in an aluminum graphite system is helpful in insurance of strong interfacial bonding between MWCNT and matrix metal by way of reducing wettability angle by about $80^0$[7, 13].But mere absence of $Fe_3C$ peak in the XRD spectra of Fe-MWCNT composite cannot guarantee that HEBM followed by SPS have not caused any damage of MWCNT. The traceability of a diffraction peak of a phase in XRD spectrum also depends upon the detection limit of the XRD instrument employed for the study. Incidentally, formation of interfacial carbide in metal-MWCNT composite implies certain damage of MWCNT either during ball milling or during sintering. It may be noted that the pristine MWCNT used for the present investigation is curled with disorder at places; also presence of amorphous carbon at the surface of carbon nanotube produced by CVD technique has been reported by[5]. Raman Spectroscopy is a very effective tool to assess the damage of MWCNT in a metal matrix composite; the same is therefore employed to probe into the impact of HEBM plus SPS on the structural integrity of MWCNT in Fe matrix composite. The Raman spectroscopy of pristine MWCNT and Fe-CNT composite produced by SPS is shown in figure6.5.

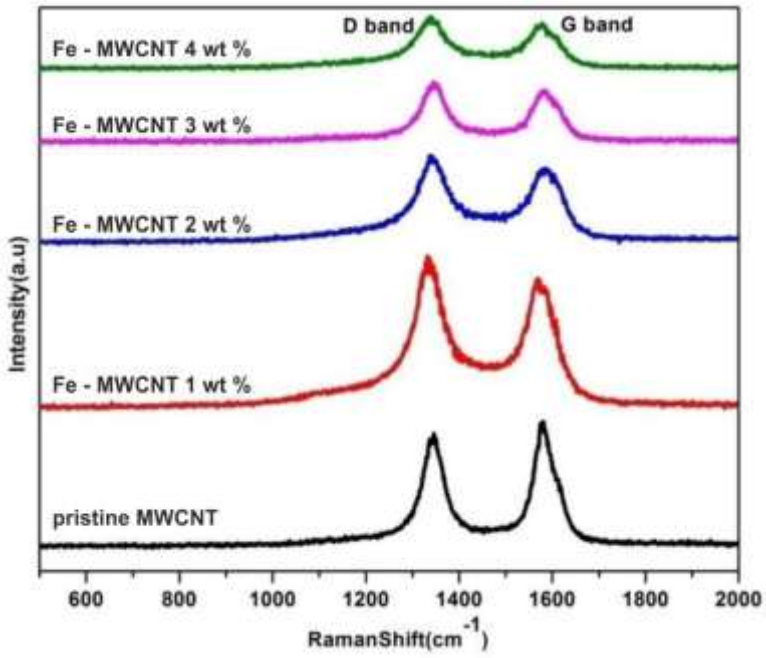


**Figure6.5** Raman spectra of pristine and iron-MWCNT composites of different MWCNT content. The figure shows the relative changes in first order D and G bands of MWCNT.

The characteristic G band and D band of pristine CNT are found to occur at 1353 and 1575 $cm^{-1}$ respectively with $I_D/I_G$ ratio 0.99. This signifies that MWCNT possess perfect graphite structure. From the result of Raman spectroscopy, it is observed that there is only a small change in $I_D/I_G$ ratio (1.02 to 1.09), with increase in MWCNT content. Also, it is found that there is a small shift in D and G band towards higher wave number. $I_D/I_G$ provides information about the structural degradation of MWCNT; also change in size, shape and position of D and G bands give us information about structural integrity of MWCNT in a composite. Present results of Raman spectroscopy tend to establish that increasing MWCNT content in experimental composites have not in general, given rise to massive amorphization of MWCNT. Nevertheless, the broadening of G band with its concurrent shortening in the case Fe-4wt% MWCNT composite suggests that at 4wt.% MWCNT level it becomes more prone to damage. This is further corroborated by characteristic change in G' band shown in figure 6.6. Beyond 3wt.% MWCNT, G' band is significantly flattened and this indicative of appreciable structural damage in Fe-4wt.% MWCNT composite. This adds further credence to the observation that increasing the MWCNT content to as high an amount as 4wt.% makes MWCNT suffer from appreciable structural degradation at the interface.

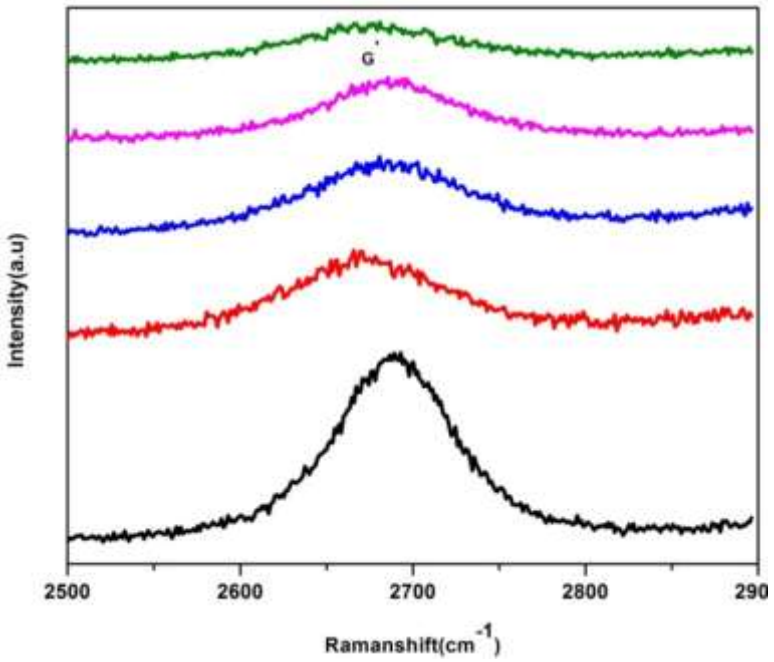


**Figure6.6** Shows G' band at higher wave number

**Table6.2** Raman spectra characteristics for different wt.% of MWCNT in Fe

| Sample Names | Raman Peak Shift ($Cm^{-1}$) | | $I_D/I_G$ |
|---|---|---|---|
| | D band | G band | |
| Pristine MWCNT | 1353 | 1575 | 0.99 |
| Fe-1wt.% MWCNT | 1348 | 1573 | 1.03 |
| Fe-2wt.% MWCNT | 1347 | 1577 | 1.04 |
| Fe-3wt.% MWCNT | 1339 | 1579 | 1.08 |
| Fe-4wt.% MWCNT | 1336 | 1582 | 1.09 |

### *6.3.3 SEM study of composite powder after HEBM*

The scanning electron microstructures of Fe-MWCNTs composites after 50 min of high energy ball milling are shown in figure6.7.It is revealed from figure6.7, that the matrix phase is somewhat flattened after 50 min ball milling; it further appears that the reinforcing MWCNTs are physically damaged by way of getting shortened. These short CNTs are seen to have been embedded well into the matrix. This observation of flattening of matrix particle along with physical damage of MWCNTs is in line with earlier observation[8].

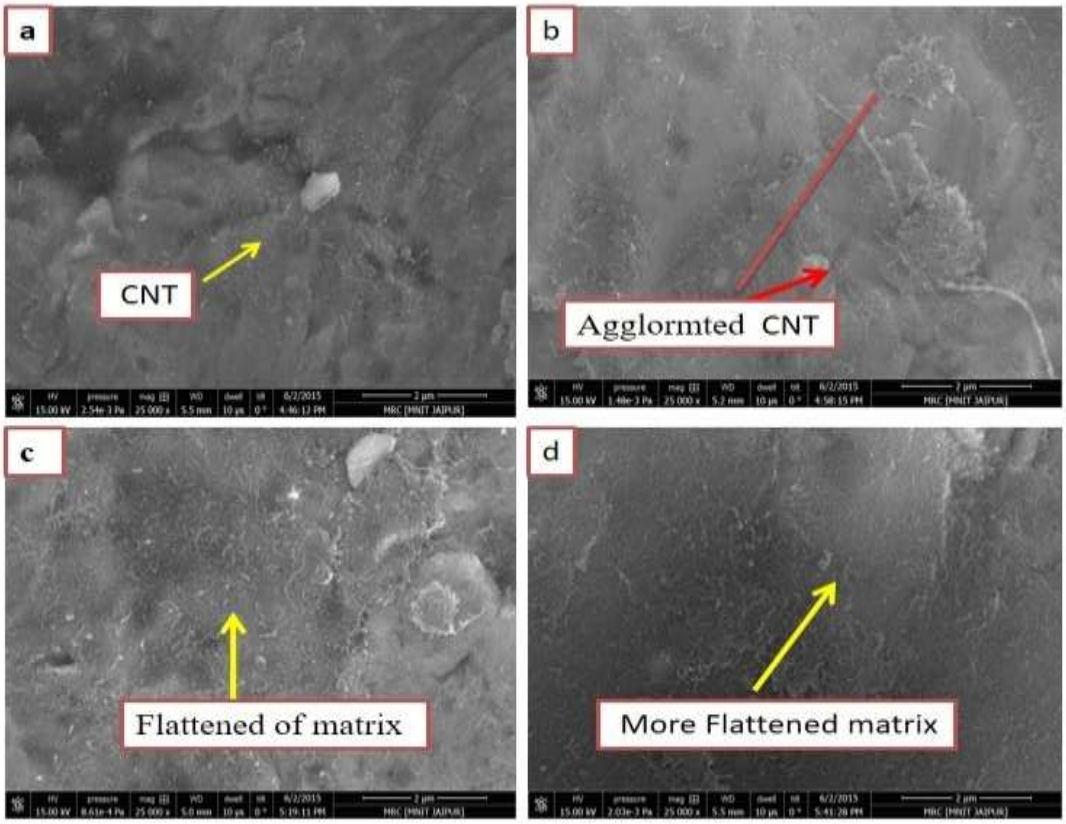


**Figure6.7**(a-d) SEM image of iron – MWCNT composites of different compositions after 50 min of milling (a) 1 wt.% of MWCNT(b) 2wt.% of MWCNT (c) 3 wt.% of MWCNT (d) 4 wt.% of MWCNT

Mechanical alloying route of powder processing involves repeated impact deformation of matrix particles followed by cold welding; thus continued milling is expected to lead to flattening of these particle; during the initial period of ball milling, the MWCNTs are laid over the matrix phase and further milling makes them firmly embedded. It is known that structural integrity in Fe-MWCNT nanocomposite depends upon the size and shape of matrix powder as well as geometrical parameters of MWCNT. In the present investigation MWCNTs of high aspect ratio and curly morphology has been used (figure 6.1 (b)). Therefore, it is but natural that harsh ball milling condition will lead to flattening of matrix particle with consequential shortening of MWCNTs and these observations corroborate the reports of earlier researchers [9].Also, there are large numbers of reports which claim that high energy ball milling leads to amorphization. However, the objective of the present study is to conserve the structural integrity of MWCNT as far as practicable, without sacrificing the quality of dispersion and interfacial bonding of reinforcing MWCNT. The microstructural observation made in figure 6.7 verifies that optimal ball milling condition practiced in this investigation has enabled to retain the required structure of MWCNT which can ensure the expected enhancement of physical and mechanical properties of iron-matrix composite reinforced by MWCNT.

It is observed in Figure 7(a) that the MWCNT are embedded more or less uniformly within the flattened matrix particle. Fe-2wt.% MWCNT composite shows regions where MWCNTs are not embedded; the same picture also shows a number of regions where MWCNTs are agglomerated. It is clear from the figure7(c) and 7(d) that increasing the amount of MWCNT leads to an increase in the agglomerated areas. However, at higher MWCNT content, the MWCNT could not embed well at many places (figure 7(c)& 7(d)). The agglomerated regions are normally present at the boundary of the particles. It is further observed that even if MWCNT is shortened, the tubular structure MWCNT remains intact. At smaller concentration of MWCNT, the distribution of MWCNT within the matrix is more or less uniform. However, as we increase the MWCNT content the same ball milling parameters cannot ensure equivalent effect in composite of higher reinforcement content.

With increasing amount of MWCNTs, potential for its survival from mechanical damage is increased. The ball milling energy is partitioned between matrix and MWCNT. The presence of long MWCNT of high aspect ratio together with Vander Waals force of attraction result in higher tendency for agglomeration. Agglomeration leads to non-uniformity of distribution of MWCNT. Also, due to such situation neither distribution of MWCNTs is very uniform nor the interfacial bonding has been as good as in relatively lower MWCNT containing composites. The load transfer from Matrix to MWCNT takes place by shear at the interface. Increasing percentage of MWCNT of high aspect ratio gives rise to increase in interfacial area. Due to low density and slender morphology, the increase in volume percent per weight percent addition of MWCNT is quite high. Hence the stress on MWCNT due to shared HEBM force is appreciably lower. Thus, physical damage of MWCNT is less at high wt.% for the same ball milling condition.

### *6.3.4 Optical Microstructural study*

Optical microstructures of Fe-MWCNTs composite with varying MWCNT content are shown in figure6.8. At lower MWCNTs content~ 1wt.%, a homogenous microstructure with negligible agglomeration of MWCNT is observed. The black particle, in figure 8(a) is the MWCNTs which are seen to be distributed uniformly throughout the matrix. When the MWCNT content is increased to 2wt.%, it is observed that the microstructure of the composite comprises of a homogenous structure with MWCNT decorating the crystal boundary; some regions with high population of MWCNTs are also seen in figure 8(b). It is known that at higher concentration of MWCNT, agglomeration of MWCNT takes place. Entanglement of MWCNT is stated to be due to high aspect ratio and Vander Waal's force of attraction among MWCNTs. Samples with MWCNT content higher than 2wt.%, exhibits more agglomerated regions of MWCNT with directional arrangement of MWCNTs at places. The general observation from optical micrograph hints upon the fact that Fe-MWCNT composite powder subjected to SPS is amenable to producing homogenous microstructure. However, MWCNTs are seen to form a network at the crystal boundary; with increasing MWCNTs content intensive agglomeration of MWCNTs take place and in sample containing 4wt.% MWCNTs

agglomerated regions assume directional arrangement(figure8(d)). It has been previously demonstrated that directional arrangement of MWCNTs in a metal matrix is promoted by SPS. It further appears from the optical microstructures that, after SPS, the MWCNTs have embedded well into the matrix.

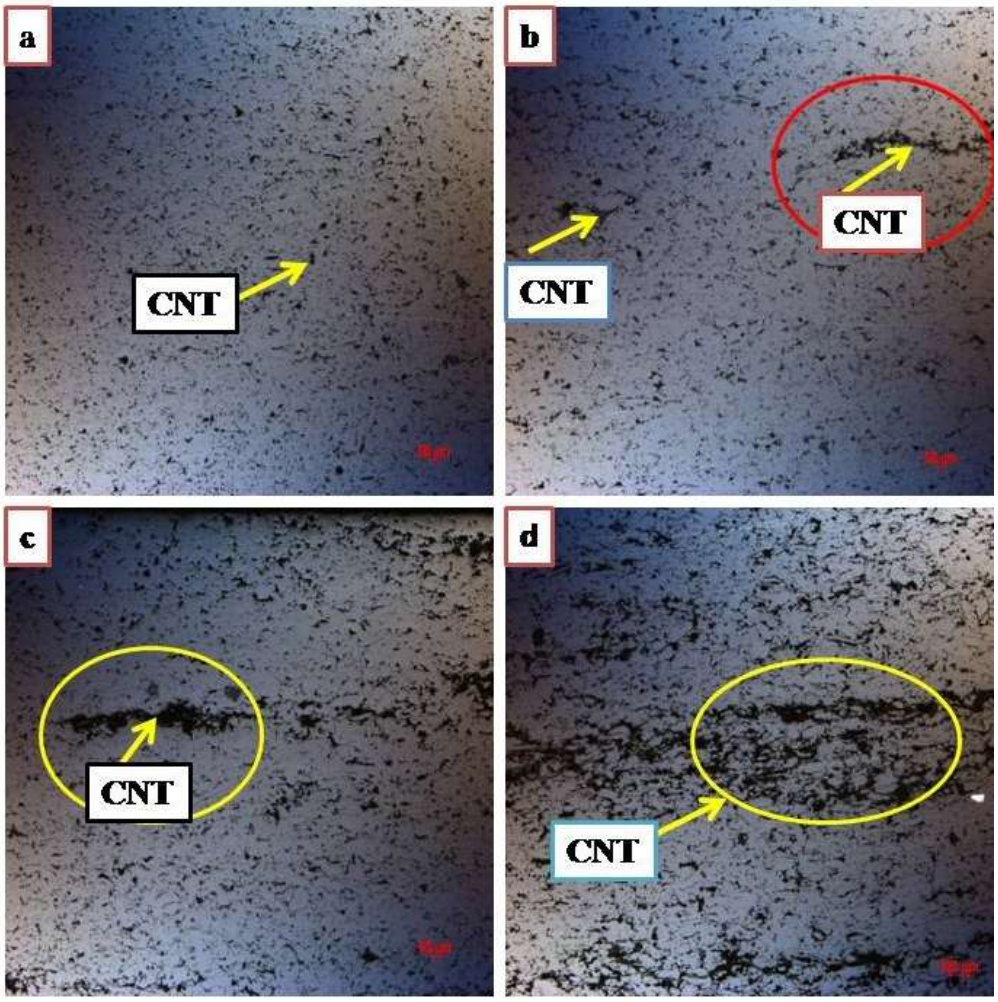


**Figure6.8**(a-d) Optical mircogarhs of composites after SPS (a)Fe-1 wt.%MWCNT (b) Fe-2 wt.% MWCNT (c) Fe-3 wt.% MWCNT(d) Fe-4 wt.%MWCNT

### *6.3.5 FTIR Analysis for assessment of bonding quality in composites*

FTIR study has been carried out for SPS samples with varying MWCNT content to yield qualitative information about different types of vibration and characteristic frequency so that bonding between MWCNT and matrix can be understood. It is seen from FTIR spectra in figure6.9that there is a number of peaks at different wave number; the peaks observed between 3412 $cm^{-1}$to 3464 $cm^{-1}$ correspond to bending vibration for hydroxyl group due to absorbed water in samples. It is rather unexpected that there will be FTIR peak corresponding to

hydroxyl group as SPS is carried out attemperature650$^0$C where moisture should be eliminated from the sample; it is presumed that absorption of moisture has taken place during testing and it may come from the binder KBr which is prone to moisture pick up; this may account for the presence of hydroxyl group in FTIR spectra. Two other peaks at around1630 cm$^{-1}$ and 1120 cm$^{-1}$ characterize C=C stretching vibration and IR active C-C stretching graphite mode respectively; another peak at 620 to 649 cm$^{-1}$seen in FTIR spectra corresponds to absorption peak hinting upon iron–carbon bond formation. It may be noted that the intensity of peak corresponding to C-C vibration undergoes very small change; concurrently, the absorption peak survives; this indicates that ball milling followed by SPS has led to the formation of iron – carbon bond at interface of matrix and MWCNT.

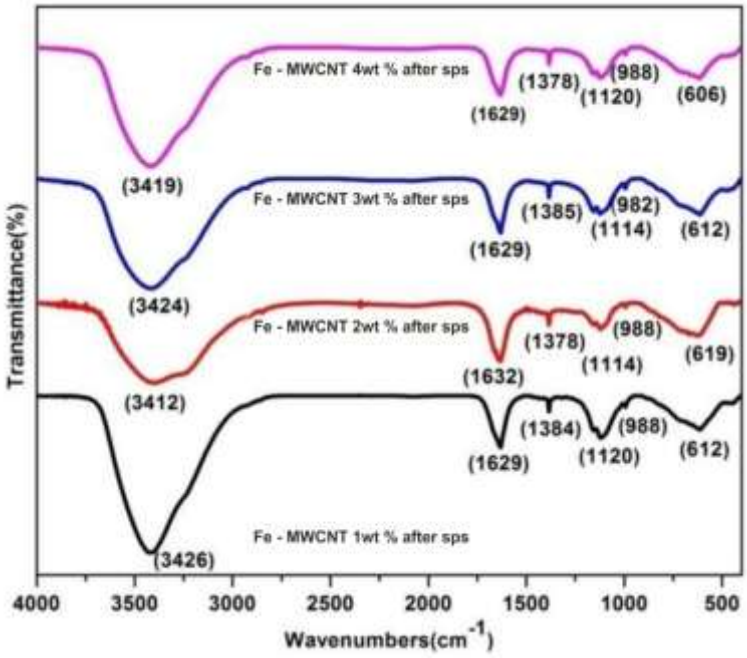


**Figure6.9** FTIR spectra of composites with different percentage of MWCNT in iron matrix.

### *6.3.6 Scanning Electron Microscopy (SEM) of Spark Plasma Sintered Samples*

SEM pictures of composite samples (figure 6.10) show that the pore content in SPS samples is very small. Moreover, no phase other than MWCNTs is found to be present within the matrix. The MWCNTs are seen to be present at the grain boundaries and in this regard our observation is similar to those of others[10].It is also observed that increase in MWCNT content gives rise to more entanglements and clustering of MWCNT; the array of clustered MWCNTs exhibits directionality

in the microstructure. Such directional arrangement of MWCNTs within metal matrix of SPS sample has been reported by number previous investigations [10-11]. The tendency of out word flow of composite powder during SPS within a closed die leads to directional arrangements of MWCNTs at higher concentration of MWCNT in the composites. The metal flow radially and rigid MWCNTs embedded within it remain unaffected expect for orienting themselves along the direction of plastic flow of metal so as to give way to the plastic deformation.

The regular arrangement of MWCNTs prohibits grain growth. During SPS, recrystallization of existing grains takes place. Grain size measurements results indicate that grain size decreases with increase in MWCNT content. The higher volume of metallic material under pressure of SPS behaves like a constrained elastic continuum, subjected to compressive stress. Higher volume fraction of metal at low MWCNT content takes up high load and experiences more recrystallization. Grain growth is inhibited because of restricted grain boundary sliding due to MWCNTs being present as network. Also, the excess MWCNTs are distributed within the grains. Hence grain growth during recrystallization processes is also restricted by the short MWCNTs which are finely distributed at the grain interiors. High magnification photograph in figure 6.10(d) verify that the black constituents at the grain boundaries are MWCNTs.

It is known that during MA (mechanical alloying) repeated collision of metal powder leads to plastic deformation of powder particles; these particles become flattened, continually cold welded and then fracture to smaller sized particles. While milling with MWCNTs, the refinement of particles is in general noticed. However, if the MWCNT content is increased to high volume fraction, the total surface area of MWCNT will quite high and this will increase the area of contact with metal particles. Importantly, the impact force due to high energy ball milling of Fe-MWCNT composite is to be partitioned between metal powder and reinforcement. The transfer of applied force from metal to reinforcement takes place by shear stress along the powder –MWCNT interface. Whenever MWCNTs content is increased the total length of MWCNTs is increased. This implies that the proportional contact area between MWCNT and metal powder also becomes quite high. This implies that a greater portion of applied force is shared by the MWCNT, which is very rigid.

However, like graphite crystals, MWCNTs can tilt or twist to accommodate increased strain and in this process of twisting or tilting they may get damaged when the milling is extensive. But in the present case the structural identity of MWCNTs are appreciably conserved. Due to impedance from increased wt.% fraction of MWCNTs, the particle refinement is limited and hence the crystallite size remains higher. This explains why in XRD studies of SPS samples we see the crystallite size higher. Also, due to larger crystallite size, the residual strain of as milled powder has been lower for samples with higher MWCNT content. After SPS, there is strain relaxation. Quite obviously the residual strain in metal powder is less for samples with higher MWCNT content. During SPS, the compressive force applied on the sample tends to cause radial flow of material which is constrained by the die wall as well as by the surrounding MWCNT network. The situation leads to directional arrangements of MWCNTs along the radial direction.

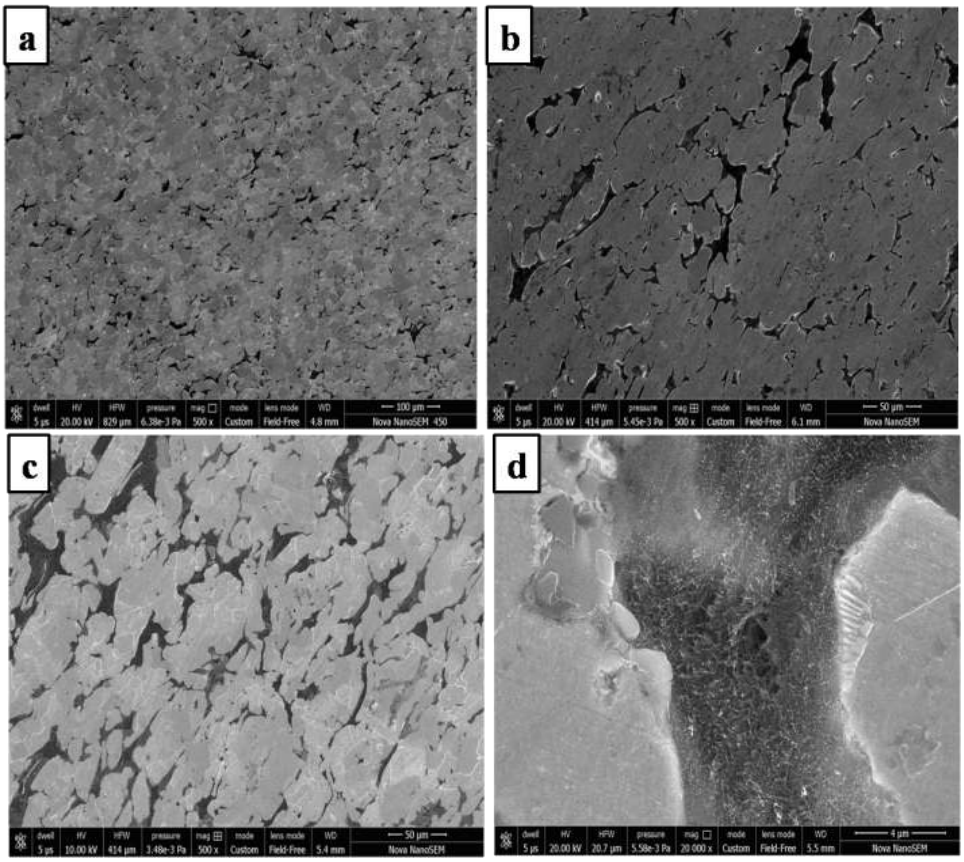


**Figure 6.10** SEM microstructure of Fe-MWCNTs composites after SPS (a) Fe-1wt.% MWCNTs (b)Fe-2wt.%MWCNTs (c) Fe- 3wt.% MWCNTs and (d) higher magnification photo graph delineating MWCNT at grain boundaries.

The SEM image further delineates that new grains are formed after SPS within the prior grains bound by the MWCNTs. The evolution of the grain structure in SPS samples is quite prevalent in Fe-MWCNT composites. SPS has been carried out under 50Mpa pressure at $650^0$C which is above the recrystallization temperature of pure iron. Pressure applied during SPS has been shared by metal and by the MWCNT. The force shared by metal is responsible for its plastic deformation. Since the deformation temperature is above the recrystallization temperature, the recrystallization of iron particles take place during SPS and SEM micrographs show that new grains have been formed within the pre-existing grains. It is known that higher amount of deformation leads to lower recrystallized grain size. In case of very low percentage of MWCNT the relative proportion of load to be shared by metal is high and hence its deformation is comparatively higher. This leads to appreciable recrystallization.

### *6.3.7 Hardness Analysis*

Figure 6.11presents the micro hardness values of Fe-MWCNT composites of varying MWCNTs content.

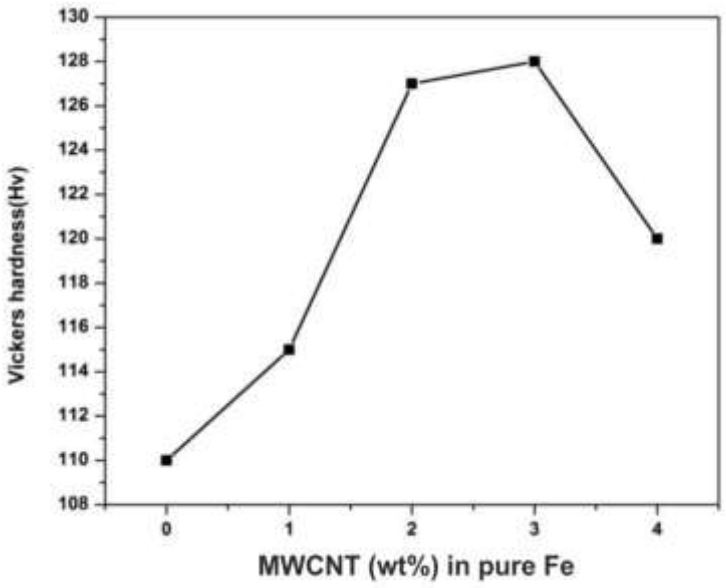


**Figure6.11**Vickers hardness of Fe-MWCNT nanocomposite with different MWCNT content after sintered at $650^0$C.

From figure6.11 it is evident that reinforcement of iron with MWCNTs remarkably improves the microhardness values. The microhardness values increase quite steeply at low MWCNT content (up to 2 wt.%), and then the rise in hardness value becomes rather slow[12].Finally, there is fall in hardness value at 4wt.%MWCNTs in iron matrix. HEBM of Fe-MWCNT composite followed by SPS leads to appreciable structural refinement. Also, partial damage of MWCNT walls due to ball milling and sintering at higher temperature like $650^0$C envisages dissolution of carbon in iron. Both structural refinement and solid solution hardening due to carbon are capable of improving hardness values. Although to avoid dissolution of carbon in iron, the SPS temperature was kept low and both heating and cooling were quite fast, some dissolution of carbon cannot be reasoned out due to high thermodynamic driving force for dissolution of carbon in bcc iron at least by 0.02 wt.%. Also, dislocations are generated in iron crystals adjoining to MWCNTs due to mismatch in co-efficient of thermal expansion. Moreover, effect of plastic deformation of ferrite before and after SPS may persist. The dislocation has strong interaction with carbon atom. When this interaction energy exceeds the C-C bond energy in MWCNT, it may break away and carbon atoms may segregate at the dislocations. All these are responsible for increase in hardness.

It is known that there are many defects in MWCNTs product by CVD route, and it is also evident in figure 6.1(d)of the present study. Thus carbon atoms at this defect site of MWCNT can be responsible for mechno-chemical synthesis, thereby forming carbide of iron; it is pertinent to mention that hexagonal carbide of composition of $Fe_3C$is more probable to form due to its good lattice matching at the matrix –MWCNT interface. Formation of carbide insures better interfacial bonding at high volume percent of MWCNTs. However, agglomeration starts to take place at higher MWCNT concentration and this reduces effective aspect ratio; it has been demonstrated earlier that yield strength is dependent upon aspect ratio of reinforcement and volume fraction of MWCNTs. The aggregation of MWCNTs reduces contact between matrix and reinforcement. Moreover, as reported earlier, extensive entanglement of MWCNTs affects spark discharge effect which has the adverse effect on the properties of composite; because of entanglement, effective aspect ratio of MWCNT is reduced and naturally contact area between the metal

matrix and MWCNTs is reduced. This finally leads to reduction in hardness of the composite.

### *6.3.8 Study on compressive strength of the composites*

The compressive strength of the composites determined at constant cross head speed, is shown in figure 6.12. From the results of compressive testing is evident that increasing MWCNT leads to higher compressive strength [12].As stated earlier that the interfacial bonding in the present experiments has been quite good. This means that composite hardening could be realized to the best possible extent. Experimental limitation could not enable to fracture the specimens with 3 wt.% MWCNT and above. It is important to notice that at lower MWCNT content compressive strain is quite high and is about 35%. It is obvious because at low MWCNT content the plastic flow of soft iron is quite easy due to less constraint from the reinforcement. Raising the MWCNT content to 2 wt.% is seen to enhance compressive strength quite appreciably without much sacrifice in compressive strain which is seen to be higher than 25%. Moreover, from the trend of the curves for composites at higher MWCNT content (3 and 4 wt. %), it is evident that both compressive strength and compressive strain increase substantially. This hint upon the fact structural fineness insured in the composites where there is no constraint out of decohesion between matrix and reinforcement has helped in enhancement of the toughness of the composites, as measured by area under the stress- strain curve

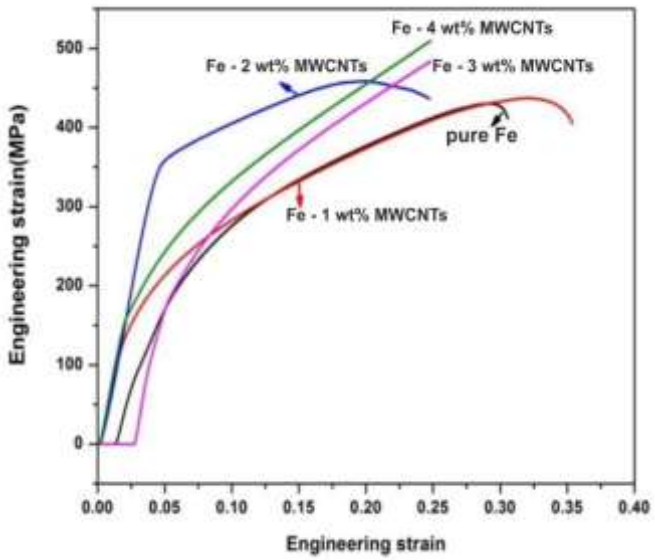


**Figure6.12** Compressive stress strain curves of iron-MWCNT composites

### *6.3.9 XPS Analysis*

High energy ball milling of Fe-MWCNTs composite is expected to cause structural damage of MWCNTs. There are reports demonstrating that HEBM of MWCNT in association with metal accentuate damage to MWCNTs. It may be noted that there is a possibility of 3d-2p hybridization for such transition metals-MWCNT composites which have unfilled 3d orbitals. Thus, it is expected that HEBM of Fe-MWCNTs may give rise to a better interfacial bonding due to 3d-2p hybridization. However, for this phenomenon to take place, easy availability of carbon atoms is required. As stated earlier, the MWCNTs used for the present investigation contain defects and amorphous carbon at its interface. Thus, either HEBM induced disrupted C-C bond or the existing defects in MWCNTs may aid in better interfacial bonding. It is therefore of interest to know the quality of C-C bonding in milled powder. At the same time, during sintering there may be chemical reaction between metal matrix and MWCNT. In case of titanium alloys formation of carbide of the interface was considered detrimental to interfacial bonding. It was anticipated that formation of carbide will damage the MWCNT structure at the interface and will reduce the expected enhancement of properties. On the other hand, demonstrated that in Al-graphite system, formation of interfacial carbide reduces the wetting angle and hence insure strong bonding. Whatever be the outcome, the formation of carbide during SPS will certainly damage the outer wall of MWCNTs which is manifested by a loss in C-C bond [13-14].

Results of XPS study carried out to assess the damage in MWCNTs are shown in XPS spectra in figure6.13; C1s spectra, the one of major interest is shown in the inset of representative spectra.

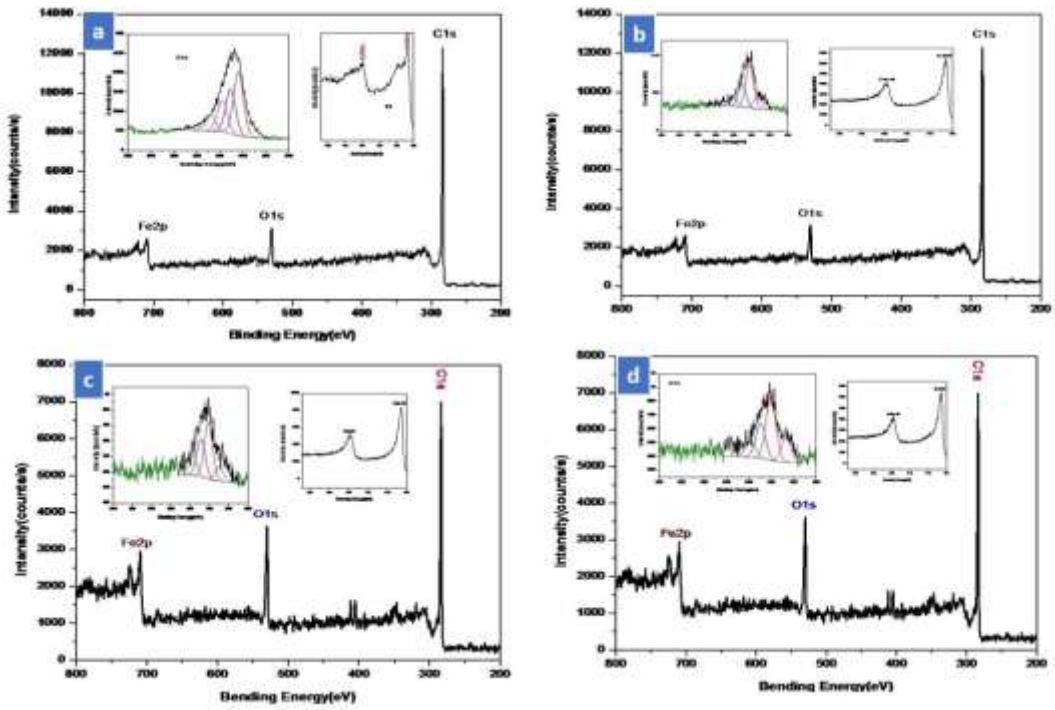


**Figure6.13**(a-d)XPS Survey scan of composites of different percentages of MWCNTs (a)Fe-1wt.%MWCNT(b) Fe-2 wt.% MWCNT (c) Fe-3wt.%MWCNT and (d)Fe-4wt.% MWCNTs and inset images showing the patterns for C1s at the surface for different etching depths of Fe-MWCNT nanocomposite and Fe2p orbital's.(The insets are for etching times 0 to 15s).

Peaks are separated in terms of bond energy by deconvolution of C1s spectra. The amount of C-C bonds remaining in SPS samples of various MWCNTs is shown in figure6.13. From the data, it is seen that the amount of C-C bond increases with increase in wt.% of MWCNT. It is also noted that C-O and C=O bond is less than 8% for all the composites and remains more or less constant. Thus, the variation of C-C bond should have some correspondence with the volume present of MWCNTs. It is obvious that C-C bond will increase with increasing MWCNT content. But it is to be noted that for increase in MWCNT content by each 1%, the relative increase in amount of C-C bond decrease at higher MWCNT content. This hints upon the fact that more structural damage of MWCNTs is caused at higher MWCNT content. Amount of bond should increase with increase in MWCNT; however, the fabrication process adopted in this work may lead to damage of MWCNT and reduces the amount of C-C bond. In normal expectation, one must foresee for increasing correspondence of increase in amount of bond with increasing percentage of MWCNT. A reverse trend is however noted. This indicates that as the

MWCNTs is increased to higher values relative decay of bond becomes increased and so consistent increase in C-C bond is not observed. It is known that at higher MWCNT content, relative contact area is more and hence higher probability of damage of MWCNT results. Again, the energy applied during milling is partitioned between MWCNT and iron; as compared to lower MWCNT content, composite of higher MWCNT content secures higher load on the MWCNT and hence more C-C bond breakage takes place. The abundance of loosely held carbon atoms after considerable loss of C-C bonds may get away from MWCNTs and join the dislocations in iron which is plastically deformed. On the contrary pure mechano-chemical synthesis may lead to formation of $Fe_3C$ which may show prevalence of Fe-C bonds rather than C-C bonds. During SPS, the dislocations are partly annihilated due to recrystallization and more carbon atoms can go in solution at higher MWCNT content. This may also reduce the C-C bond. When the material is cooled, there might be precipitation of carbide. The conjecture is subjected to verification by high resolution transmission microscopy.

**Table 6.3Different types of bonds, energies and amount derived from XPS study**

**Table6.3.1**Bonding types, bond energy and relative amounts in Fe-1 wt.% MWCNT composite

| **Bonding Type** | **Bonding Energy( eV)** | **Relative atomic (%)** |
|---|---|---|
| | | **Milled MWCNT** |
| C-C | 284.6 | 45.01 |
| C-O | 285.79 | 5.3 |
| C=0 | 286.89 | 2.31 |

**Table 6.3.2**Bonding types, bond energy and relative amounts in Fe-2 wt.% MWCNT composite

| **Bonding Type** | **Bonding Energy( eV)** | **Relative atomic (%)** |
|---|---|---|
| | | **Milled MWCNT** |
| C-C | 284.25 | 53.71 |
| C-0 | 285.85 | 5.6 |
| C=0 | 286.78 | 2.31 |

**Table 6.3.3**Bonding types, bond energy and relative amounts in Fe-3 wt.% MWCNT composite

| Bonding Type | Bonding Energy( eV) | Relative atomic (%) |
|---|---|---|
| | | Milled MWCNT |
| C-C | 284.26 | 59.32 |
| C-O | 286.05 | 5.3 |
| C=0 | 286.95 | 2.2 |

**Table 6.3.4**Bonding types, bond energy and relative amounts in Fe-4 wt.% MWCNT composite

| Bonding Type | Bonding Energy( eV) | Relative atomic (%) |
|---|---|---|
| | | Milled MWCNT |
| C-C | 284.07 | 63.32 |
| C-O | 286.05 | 5.3 |
| C=0 | 286.95 | 2.2 |

### *6.3.10 Conductivity Analysis*

Figure 6.14shows the electrical conductivity of Fe-MWCNTs composite with varying percentage of MWCNTs. The inset shows the values of conductivity at various MWCNT content.

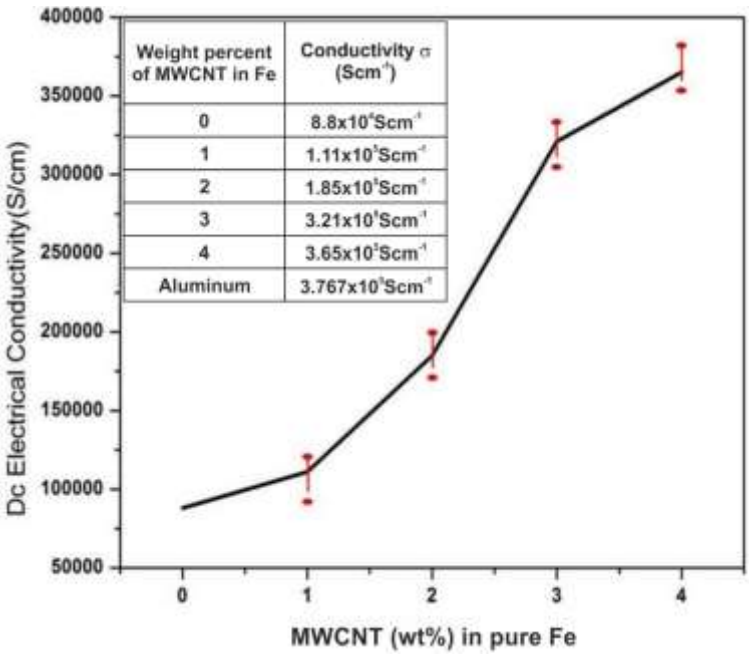


**Figure 6.14** Variation of electrical conductivity (σ) vary with MWCNT content

It is observed that conductivity of iron increases substantially after reinforcing with MWCNTs. The curve in figure6.14 indicates that the increase in conductivity is initially slow, followed by a rapid rise till 3 wt.% beyond which a slower rise in conductivity is noted. It is found that the initial conductivity of pure iron processed identically with the composite is nearly same as that of the reference conductivity. This is indicative of the fact that after SPS, the pore content has been negligible and theoretical density is almost reached. The Fe-MWCNTs composite reinforced with 4wt.%MWCNT has achieved the highest conductivity $3.65 \times 10^5 Scm^{-1}$which is very close to that of EC grade aluminum. It further appears that although there is a considerable improvement in conductivity due to reinforcing iron with MWCNTs, the quantum of rise is not as high as can be achievable in polymer matrix-MWCNT composite. It is known that MWCNT can carry high electric current density of $4x10^9$ $A/cm^2$; improvement in electrical conductivity is influenced by electron transport through MWCNT. It is known that high aspect ratio of MWCNT provides efficient electron conduction path and so addition of MWCNT increases the conduction with addition of MWCNT. Increasing MWCNT at its low content makes the aspect ratio additive and so it increases quite rapidly till 3wt.%MWCNT. Moreover, homogenously distributed MWCNTs help to achieve a compact structure; the interfacial bonding is quite strong and a smooth interface is possible in case of Fe-MWCNTs composite presumably due to 3d-2phybridization. This implies that electron moving through matrix iron crystals can easily tunnel through the barrier at the metal-MWCNT interface; the magnitude of barrier for tunneling of electron is greatly lessened by the sound interfacial structure. Another most important point to consider is the network structure of MWCNT around iron crystal. This creates a very effective conduction channel for electron due mainly to high current density of MWCNTs. Thus, the strategy of conserving MWCNT structure with tailored damage at outer walls to form a smooth transition at the interface makes the composite as good an electrical conductor as aluminum. However, this material is much stronger at the equivalent conducting level and may be considered to be a better overhead conductor.

When the reinforcement content is increased to 4wt.% the improvement in conductivity slows down. This is ascribed to two factors. First, high MWCNT content leads to objectionable degree of agglomeration of MWCNT. The entanglement of MWCNT reduces the effective total length of MWCNT available for charge transport. This leads to a reduction in aspect ratio of MWCNT. Therefore, conduction path become less effective and so electron conduction is affected. Also, due to agglomeration, some pores may be entrapped in the structure. These pores may curtail the conduction path or the way incoherently scatter electrons and so increase resistivity. Thus, overall improvement in conductivity becomes rather small.

### *6.3.11 Magnetic property Analysis*

Figure 6.15 presents the result of test for magnetic properties of Fe-MWCNTs nanocomposite.

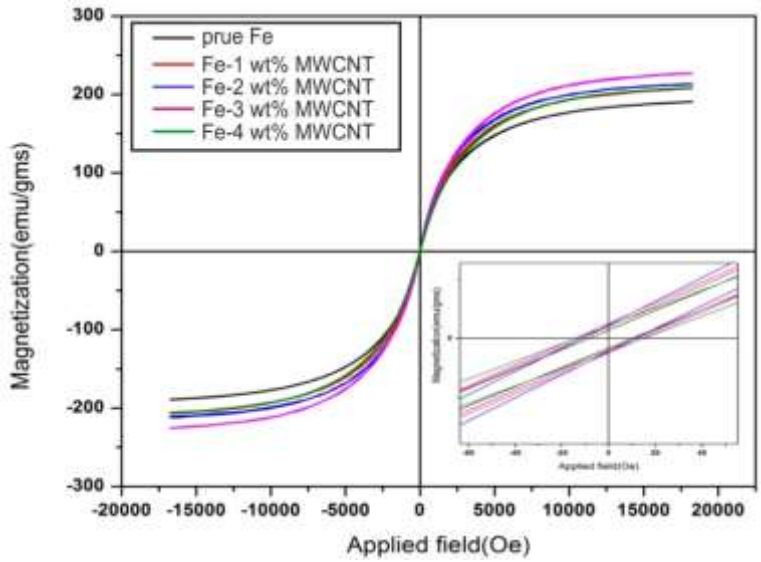


**Figure6.15**Magnetization curve Fe-MWCNT samples at different weight percent of MWCNT inFe at room temperature (inset expanded views of the respective M-H loops close to origin.)

The samples are seen to exhibit ferromagnetic nature (figure 6.15). Moreover, the result of VSM study is summarized in Table6.4.

**Table 6.4** Magnetic properties of iron-MWCNT composites.

| Sample name | Saturation Magnetization(Ms)(emu/gms) | Remanent Magnetization (Mr)(emu/gms) | Coercivity (Hc) (Oe) |
|---|---|---|---|
| Pure Fe | 190.55 | 0.21 | 3.2 |
| Fe-1 wt.% MWCNT | 207.15 | 0.306 | 6.66 |
| Fe-2 wt.% MWCNT | 213.47 | 0.471 | 11.34 |
| Fe-3 wt.% MWCNT | 227.01 | 0.681 | 12.07 |
| Fe-4 wt.% MWCNT | 217.46 | 0.72 | 14.11 |

The results of VSM testing demonstrate that the saturation magnetization of Fe-MWCNT composite increases up to 3wt.%MWCNTs and that there is a decrease in saturation magnetization at a MWCNT level of 4wt.%.Remnant magnetization and coercivity properties are seen to increase continuously with increasing MWCNT content in the composite(figure 6.15).

In general saturation magnetization of ball milled pure iron undergoes degradation due to the strain created with concurrent enhancement in coercivity [15].However, MWCNT reinforced iron composite has shown improvement in saturation magnetization by 20%; it may be noted that MWCNT used in the present investigation is produced by CVD technique with iron as catalyst; in such situation MWCNTs behave like ferromagnetic although MWCNT is reported to be diamagnetic on many pervious occasion[16-18].Microstructural analysis has revealed that MWCNTs are uniformly distributed in SPS samples and the interfacial bonding is also quite good. The magnetic behaviors of the Fe- MWCNT composite are explained by considering two different issues. First, the ball milled particles are very small, in the range of 35-40 nm. After SPS there is no effective grain growth due to the presence of MWCNT. Thus, in the composite, the iron behaves almost like a single domain magnetic material and hence upon application of magnetic field the domain alignment along the applied field becomes very easy. Inter domain boundary constraints are not there. Moreover, there are reports which demonstrate

that MWCNTs when decorated by magnetic particle onto its surface or within the tube can align with applied field rather easily [19]. We know that in a multiple domain ferromagnetic material, the rotation of domain along with intradomain spins alignment exhibits magnetostriction which restricts domain alignment along the applied field. This behavior does not happen for single domain particles. Due to efficient alignment of domain, the saturation magnetization is quite high. The existence of MWCNT at the crystal boundary plays a positive role. It aids in enhancing remnant magnetism. Upon withdrawal of the field, the domains normally tend to assume random orientation. However, the required rotation of domain for this purpose is resisted by the enclosing MWCNTs which are aligned with applied filed. Thus, more number of parallel spins is available to cause the increase in remnant magnetism. Due to higher remnant magnetism, overall saturation magnetization become higher [20].This phenomenon is more intense for nanocomposite of higher MWCNTs content and therefore increasing MWCNT content has positive role in increasing saturation magnetization. Due to the constraint of strong interface, the domains once aligned, cannot simply revert back to their earlier configuration upon mere withdrawal of the field without application of a reverse field and so the coercivity is constantly improved.

The second factor for the observed variation in magnetic properties of nanocomposite is no less important. It has been reported by a number of pervious workers that tethering the nanotube surface with magnetic particles improve magnetic susceptibility. It is expected that decoration of MWCNTs with metal ion would alter its surface functionality which can impact its physical properties. Binding metal ions on MWCNT surface can make the combination become ferromagnetic. It is demonstrated elsewhere that oxidized nanotubes can more effectively bind metal ion at the surface [15].

It is further known that in a ball milled Fe-MWCNT nanocomposite, MWCNT are firmly embedded in the metal matrix. The bonding becomes quite strong in SPS sample. During SPS, the vacant 3d orbital of the iron envisages 3d-2p hybridization with MWCNT and therefore ensures a very good interface. Moreover,

in our case, XPS result has shown the presence of C=O and C-O bond up to amounting 8% and this remains constant at all MWCNT concentration.

This means that MWCNT is oxidized to some extent. Moreover, we notice that C-C bond is also disrupted more with increasing MWCNT content. FTIR results have shown the presence of absorption peaks of maghemite as 606-619$Cm^{-1}$ at the expense of reduction of intensity in C-C stretching bond; but this implies that 3d-2p coordination between MWCNT and iron takes place. The existence of maghemite is also authenticated by XPS study where $Fe2p_{3/2}$ and $Fe2p_{1/2}$ peaks occur and are known to be due to X-$Fe_2O_3$.Also from O1s spectrum the existence of C=O bond and Fe-O bond are verified. While FTIR spectroscopy confirms the presence of absorption peak $Fe^{3+}$,the simultaneously decreasing peak intensity of C-C bond indicate coordinate reaction. Further, XPS confirms oxidation of MWCNT. Similarly, decoration of MWCNT surface by iron is also observed in TEM (figure 6.16(c)).

The bond disruption in MWCNT makes carbon atoms free, which undergoes reaction with $Fe_2O_3$ and forms C-O bond; it helps to attach $Fe_2O_3$ onto the surface of MWCNT. Therefore, the magnetic material is finally tethered at the surface of MWCNT. It is reported earlier that $Fe^{3+}$ ion bonding at the surface of MWCNT increase the saturation magnetization by about 10-12 emu/g.

As we increase the MWCNT content, the above phenomena is increased and stronger ferromagnetic behavior is exhibited. Thus, in SPS samples, not only the matrix has a strong magnetic property, the reinforcement is also appreciably ferromagnetic. Moreover, the interface is smooth and continuous at atomic level of magnitude which ensures smooth flux flow. Thus, saturation magnetization is quite good for these composites. However, we notice that saturation magnetization decreases at 4wt.%MWCNT. It may be noted that mechno-chemical activation during ball milling followed by SPS is amenable to the formation of iron carbide. The propensity of carbide formation increases with increasing MWCNT content in the composites. During ball milling bond disruption takes place. The loosely bonded

carbon atoms produced by disruption of bonds have the access to the segregate at the dislocations which are created within the ball milled iron that undergoes heavy cold deformation. Subsequently, during SPS, these carbon atoms may precipitate out in the form of $Fe_3C$ or ε-carbide. Again, direct formation of these carbides is equally probable. Notwithstanding if either one or both the events take place, the SPS relieves internal strain and stable structure is formed. It is known that ε-carbide (hexagonal structure) maintains definite Bagariatsky orientation relationship with iron and being hexagonal can have minimum lattice mismatch. But presently, $Fe_3C$ formation, instead of ε-carbide is confirmed in HR-TEM. In either case the interface is incoherent and is similar to high angle grain boundary. The presence of second phase constituent at the metal-MWCNT interface is not good so for as physical properties are concerned. Thus, formation of interfacial cementite in 4wt.%MWCNTcompositemight have adverse effect on the quality of interface and this has interfered with unidirectional spin alignment. Moreover, this restricts attachment of magnetic particles on MWCNT. Hence it will harm the magnetic property of the composite. The formation of carbide along with higher tendency for agglomeration may also be responsible for lowering of saturation magnetization. However, loss of orientation after withdrawal of field is resisted by higher density of reinforcing MWCNT. It is for this reason the coercivity of composite containing 4wt.%MWCNT is higher at higher remnant magnetization level although the saturation magnetism has gone down.

### *6.3.12 Transmission Electron Microscopic Study*

Figure 6.16(a) displays the bright field image of Fe-MWCNT composite showing ferrite grains with embedded MWCNTs. The corresponding SAED shown in the inset in figure 6.15 exhibits diffused diffraction spots indicating presence of strain. The pattern is indexed to be B=Z= $[\bar{1}33]$.

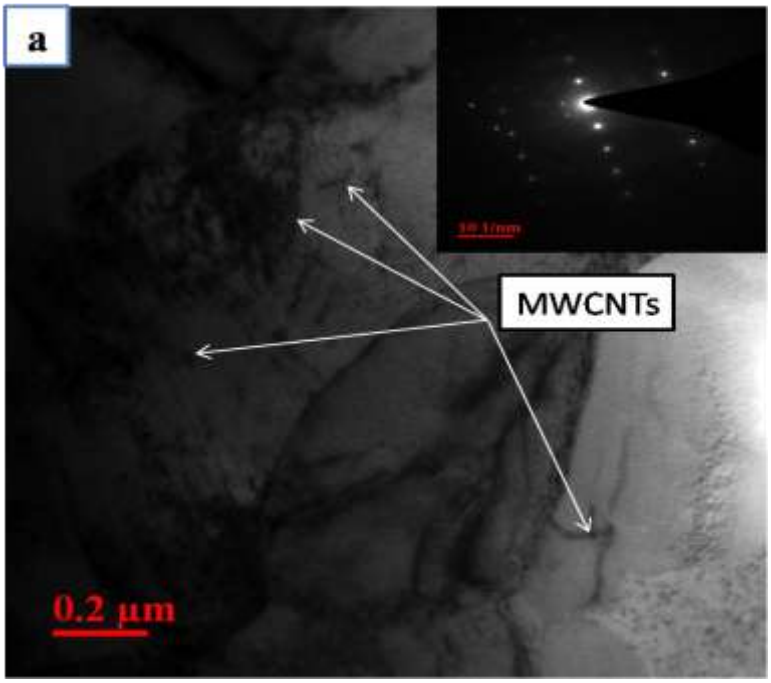


**Figure 6.16**(a)Bright field image of Fe-3wt.%MWCNT composite; inset SAED with zone axis Z= [$\bar{1}$33]

This hints upon the fact that there has been some strain at the interface of MWCNT and iron matrix probably due to lattice mismatch. The same microstructure gives the evidence of deformed grain structure, which is seen to be retained even after SPS. Traces of dislocations probably formed due to mismatch in coefficient of thermal contraction between iron matrix and the reinforcing MWCNT.

Figure6.16 (b) reveals uniform distribution of MWCNT within the matrix. The micrograph is taken from the cross section of SPS sample; so, the majority of MWCNTs have the out of plane orientation. Again, MWCNTs are seen to form 2D network in a SPS sample.

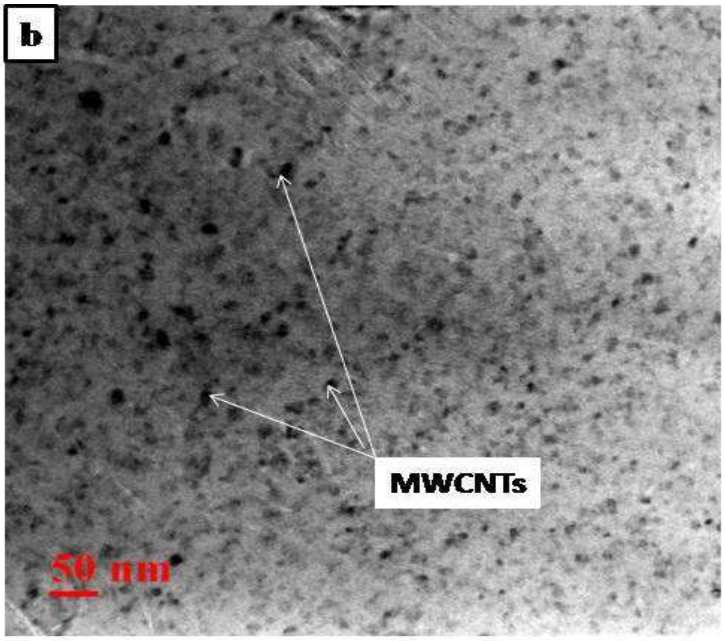


**Figure 6.16**(b) Bright field image of Fe-3 wt.%MWCNT composite MWCNT with mostly out of plane orientation.

High resolution image in figure6.16(c) shows that interface between MWCNT and matrix is quite clear. No contamination is seen at the interface and also, we do not see the formation of carbide at Fe-MWCNT interface. Special care was taken to conduct SPS under such condition that carbide formation at the interface can be avoided.

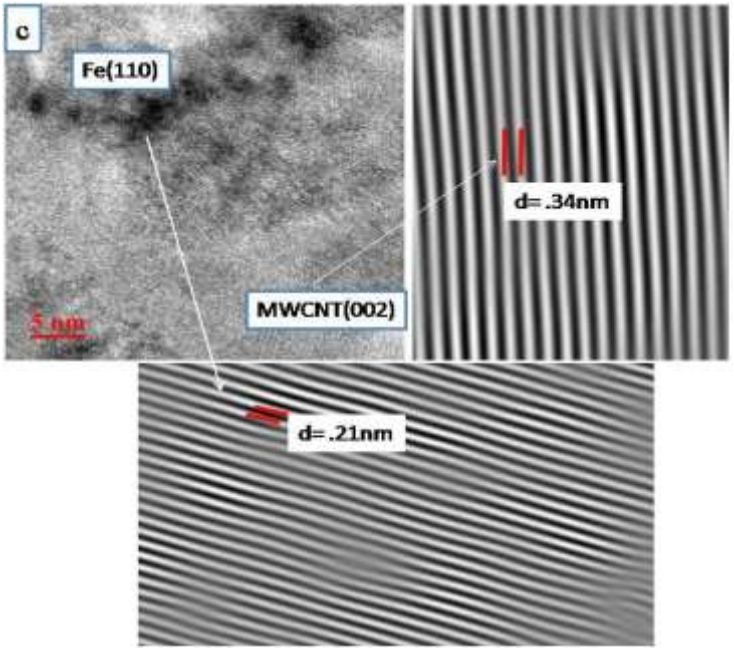


**Figure6.16**(c) High resolution image showing that iron is present at the interface of MWCNT (corresponding d spacing of iron and MWCNT)

From the nature of the interface it appears that interfacial bonding has been quite good. It is conjectured that during HEBM, mechano-chemical activation has led to 3d-2p hybridization which is possible due to vacant 3d orbital in iron and harsh ball milling has led to disruption of C=C bond.

It is known that carbon is highly soluble in iron and that ball milling and sintering operation makes the composite system vulnerable to formation of carbide. Keeping this in view, HEBM was conducted under optimal condition and SPS was carried out at comparatively lower temperature where the solubility of carbon in bcc iron is quite small. Even if some carbon has gone into solution at the sintering temperature due to its high thermodynamic driving force for dissolution, the fast cooling after SPS has prohibited the formation of carbide either at the interface or at the nearby grain boundaries of ferrite. HRTEM image of the same sample from some other location shows that iron particles are present at the surface of MWCNT (figure6.16c).

In case of iron-4wt.% MWCNT composite the HRTEM image (figure 6.17) delineates that dissolved carbon is seen to have precipitated at the ferrite-MWCNT interphase boundary. Also, the inter wall distance of MWCNTs is formed to be 0.35 nm a value close to the reported theoretical value. This indicates that structural integrity is still conserved in iron-4wt.% MWCNT by during the entire processing.

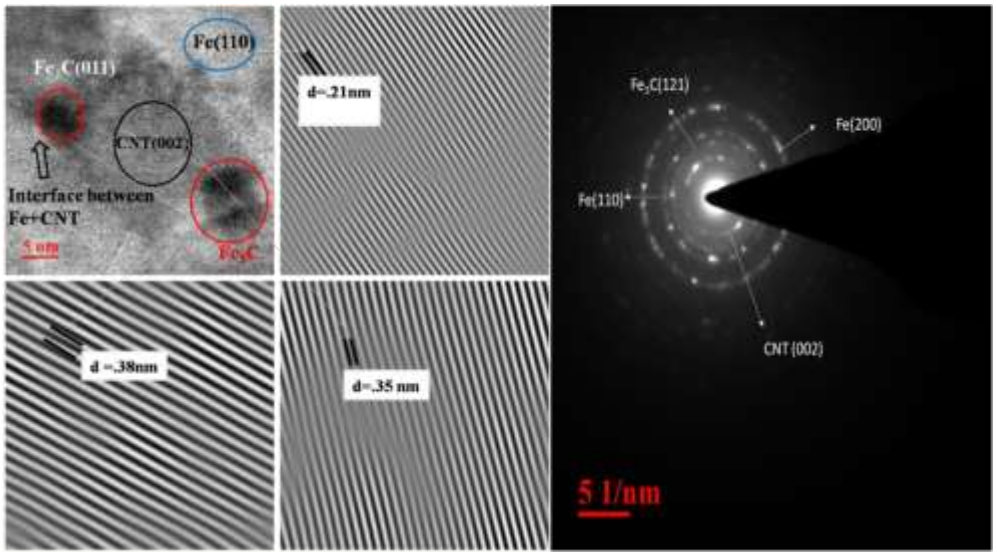


**Figure6.17** HRTEM image of Fe-4wt.% MWCNT showing carbide at the interface and corresponding SDAE pattern of Fe-4wt.% MWCNTs.

The SADP corresponding of figure6.17 shows spotty ring pattern around the continuous ring. The continuous ring pattern is indexed as MWCNT, whereas the spotty ring pattern is due to nanoscale iron particles. It therefore appears that besides monolithic bonding at MWCNT-matrix interface, the HEBM plus SPS composite also experiences attachment of metal particle on MWCNT. This is further supported by HRTEM in figure6.16(c), which clearly shows iron particles (<10nm size) tethering MWCNT. This has been possible due to 3d-2p hybridization. SPS results have already demonstrated that only iron is present in the material and that there was considerable loss of C-C bonds in MWCNTs.

Upon increasing the MWCNT content to 4wt.%, considerable agglomeration of MWCNTs is seen to take place.Figure6.18(a) shows extensive agglomeration of MWCNTs at many places in the structure; high resolution HRTEM image of the same area is shown in figure6.18(b).

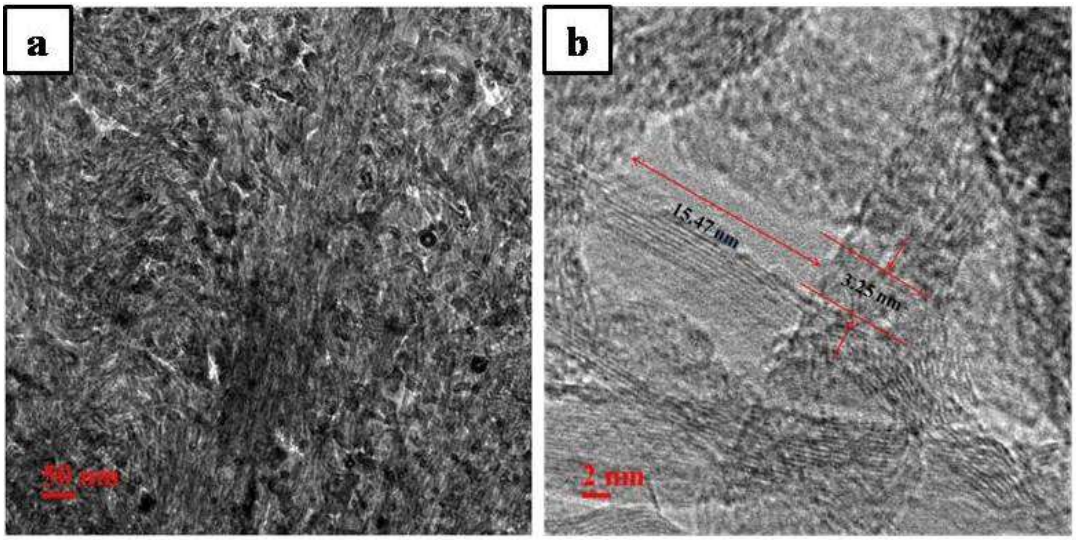


**Figure 6.18** TEM image of Fe-4 wt.% MWCNT (a) agglomerated MWCNTs (b) nano sized pore in Fe-MWCNTs.

It is seen that nanosized pores are present within the entangled MWCNTs. These types of pores in agglomerated MWCNTs are also reported to be the cause of deterioration of mechanical and physical properties. In our case we find that hardness of composite has decreased beyond 3wt.%MWCNT. Also, the saturation magnetization is found to have been significantly decreased in 4wt.%MWCNT.

## 6.4 Conclusions

The fabrication of iron-MWCNT composites can preserve the crystallinity of MWCNT as evidenced by visible (002) CNT peak in XRD spectra of the composites, till 3 wt.% MWCNT in the composites, no contamination takes place at the interface of MWCNT and iron crystals. Increase in amount of MWCNT leads to an increase in size of crystallites with concurrent reduction in residual strain the MWCNT content to as high an amount as 4wt.% makes MWCNT suffer from perceptible structural degradation at the interface. High energy ball milling leads to flattening of matrix particle along with visible physical damage viz. shortening of MWCNTs. Physical damage of MWCNT is less at high weight percent of MWCNT for the same ball milling condition. Fe-MWCNT composite powder subjected to SPS produces homogenous microstructure. With increasing MWCNTs content agglomeration of MWCNTs take place and in sample containing 4wt.% MWCNTs agglomerated regions assume directional arrangement High energy ball milling followed by Spark Plasma Sintering has leads to the formation of iron – carbon bond at interface of matrix and MWCNT. Spark Plasma Sintering leads to directional arrangement of MWCNTs within metal matrix. Recrystallization of existing grains takes place during Spark Plasma Sintering. Grain size measurements results indicate that grain size decreases with increase in MWCNT content. Reinforcement of iron with MWCNTs appreciably improves the microhardness values of the composites. The microhardness values increase quite steeply at low MWCNT content (up to 2 wt.%), then the rise in hardness slows down. Increasing MWCNT content in composites gives rise to higher compressive strength of the material higher degree of structural damage of MWCNTs is caused at higher MWCNT content of composites. As the MWCNTs is increased to higher values relative decay of bond becomes increased. It is observed that conductivity of iron increases significantly after reinforcing with MWCNTs. The increase in conductivity is initially small, becomes more intense till 3 wt.% beyond which a slower rise in conductivity is caused. The saturation magnetization of Fe-MWCNT composite increases up to 3wt.%MWCNTs;its saturation magnetization decreases at a MWCNT level of 4wt.%.Remnant magnetization and coercivity properties increase continuously with increasing MWCNT content in the composite. Traces of dislocations, formed due to

mismatch in the coefficient of thermal contraction between iron matrix and the reinforcing MWCNT, remain present in the microstructure of SPS sample. Under high resolution microscopy it is ascertained that there is carbide formation at Fe-MWCNT interface in 3wt.% MWCNT composite after Spark Plasma Sintering. In case of iron-4wt.% MWCNT composite the HRTEM image carbon initially dissolved in ferrite is precipitated at the ferrite-MWCNT interphase boundary. Nano sized pores are produced in 4wt.% MWCNT composite within the agglomerated MWCNTs

## REFERENCES


[1] S. Wang, R. Liang, B. Wang, C. Zhang, Dispersion and thermal conductivity of carbon nanotube composites, Carbon 47 (2009) 53-57.

[2] Z.Y. Liu, B.L. Xiao, W.G. Wang, Z.Y. Ma, Developing high performance aluminum matrix composites with directionally aligned carbon nanotubes by combining friction stir processing and subsequent rolling, Carbon 62 (2013) 35-42.

[3] X. Feng, J.H. Sui, Y. Feng, W. Cai, Preparation and elevated temperature compressive properties of multiewalled carbon nanotube reinforced Ti composites, Mater. Sci. Eng. A 527 (2010) 1586-1589.

[4] F.C. Wang, Z.H. Zhang, Y.J. Sun, Y.L, Z.Y. Hu, H. Wang, A.V. Korznikov, E. Korznikova, Z.F. Liu, S.Osamu, Rapid and low temperature spark plasma sintering synthesis of novel carbon nanotube reinforced titanium matrix composites, Carbon 95 (2015) 396-407.

[5] H. Kwon, M. Estili, K. Takagi, T. Miyazaki, A. Kawasaki, Combination of hot extrusion and spark plasma sintering for producing carbon nanotube reinforced aluminum matrix composites, Carbon 47(2009)570-577.

[6] H.S. Avener, Introduction to physical metallurgy,McGraw Hill Eduction (India) 35 (2013).

[7] Z.Y. Liu, S.J. Xu, B.L. Xiao, P. Xue, W.G. Wang, Z. Y. Ma, Effect of ball-milling time on mechanical properties of carbon nanotubes reinforced aluminum matrix composites, Composite Part A 43 (2012) 2161–2168.

[8] L. Wang, H.Choi, J.M. Myoung, W. Lee, Mechanical alloying of multi-walled carbon nanotubes and aluminium powders for the preparation of carbon/metal composites, Carbon 47 (2009) 3427-3433.

[9] S.E. Shin, Y.J. Ko, D.H. Bae, Mechanical and thermal properties of nanocarbon-reinforced aluminum matrix composites at elevated temperatures, Composites Part B 106 (2016) 66-73.

[10] H. Kwon, D.H. Park, J.F. Silvain, A. Kawasak, Investigation of carbon nanotube reinforced aluminum matrix composite materials, Composites Science and Technology 70 (2010) 546–550.

[11] M. K. Mani, G. Viola, M. J. Reece, J.P. Hall, S. L. Evans, Fabrication of carbon nanotube reinforced iron based magnetic alloy composites by spark plasma sintering, Journal of Alloys and Compounds 601 (2014) 146–153.

[12] J.Y. Suh, D.H. Bae Mechanical properties of Fe-based composites reinforced with multi-walled carbon nanotubes, Materials Science & Engineering A 582 (2013) 321–325.

[13] T. Laha Synthesis and characterization of plasma spray formed carbon nanotube reinforced aluminum composite, Materials Science and Engineering A 381 (2004) 249–258.

[14] K.S. Munir, M.Qian, Li. Yancang,T.D. Oldfield,P.Kingshott, D.M. Zhu, C.Wen, Qantitative analyses of MWCNT-Ti powder mixtures using Raman spectroscopy the influence of milling parameter on nanostructural evolution, Advance Engineering Material17( 2015) 1660-1669.

[15] T.T. Bui, X.Q. Le, D.P. To, V.T Nguyen, Investigation of typical properties on nanocrystalline iron powders prepared by ball milling techniques,Adv. Nat. Sci. Nanosci. Nanotechnol.4(2013) 045003-8.

[16] F.C Dillon, A. Bajpai, A. Koos, S. Downes, Z. Aslam, N.Grobert,Tuning the magnetic properties of iron-filled carbon nanotubes, Carbon50 (2012) 3674-81.

[17] H. Kim,W. Sigmund, Iron particles in carbon nanotubes, Carbon 43 (2005)1743–1748.

[18] C. Suryanaryana, Mechanical alloying and milling, Prog. Mater Science 46 (2001) 1-184.

[19] R.Tannenbaum, Magnetic carbon naotubes synthesis characterization and anisotrophic electrical properties, Georgia Institute of Technology United States July 2011.

[20] O. Boshko, O. Nakonechna, M.Dashevskyi,K. Lvanenko, N.Belyavina, S.Revo, Effect of the carbon nanotubes on structure and magnetic properties of the Fe-Cu(4:1) compoites, Adv. Powder Technol 27(2016) 27 1101-1108.

# *CHAPTER SEVEN*

## *Effect of Silver Doping on The Structure and Properties of Spark Plasma Sintered Iron-x wt.% MWCNT Composites (x= 1, 2, 3 and 4 wt.%) Synthesised by High Energy Ball Milling*

In the present chapter, discussion is made about the fabrication of iron-MWCNT-Ag composites by high energy ball milling. Fixed quantity of silver amounting to 0.1 weight percent has also been added for every batch, of Iron – MWCNT-Ag composite. Even at a relatively low temperature of spark plasma sintering, $700^0$C, carbon atoms cannot diffuse into the iron crystals. Silver atoms have adhered to the surface of MWCNT and it is likely the sintering pressure (60MPa) and temperature ($700^0$C) have enabled silver atoms to tether to the MWCNT surface. Silver protects the MWCNT from chemical damage during spark plasma sintering.

In this chapter discussion is also made about the structural, phase evolution and evaluation of physical property of Fe-MWCNTs-Ag composites. The saturation magnetization of silver doped Fe-MWCNT composite increases by 25% over that of pure iron for the composite containing 3wt.%MWCNTs however, it drops at 4 wt.% MWCNT composite due to pores existing within the agglomerated MWCNTs. Remnant magnetization and coercivity properties increase continuously with increasing MWCNT content in the composite.

The DC electrical conductivity of Fe-MWCNTs-Ag composite is higher than that of aluminum after doping of silver, with increasing the weight percent of MWCNTs.

## 7.1 Introduction

In order to harness the potential of metal-MWCNT composites, evolution of suitable fabrication technique which can secure excellent interfacial bonding with uniform dispersion of reinforcing MWCNT within the matrix metal has emerged as a challenge in materials engineering. It is now agreed by most of the research workers that high energy ball milling is most suitable to produce a good metal matrix composite with MWCNT as reinforcement[1-4].However, the above mentioned mechanical alloying route suffers from the risk of physical and structural damage of MWCNT. Moreover, in many cases, where matrix metals are chemically affinitive to carbon, the formation of metal carbide at the interface between matrix metal and MWCNT has become a matter of concern [5-7]. Although varying opinions regarding beneficial or detrimental effect of interfacial carbide on the bonding quality at the interface are documented in literature, it is no denying that presence of carbide at the interface is a signature of structural damage of MWCNT, which, undoubtedly, deprives from accruing the full advantage due to the usage of MWCNT as reinforcement. To alleviate with this difficulty which may emanate from structural damage of MWCNT, surface treatment has also been tried by a number of workers.

In the previous chapters, the author has demonstrated considerable improvement in mechanical and physical of MWCNT reinforced iron matrix composite can be achieved if the fabrication process parameters (viz. HEBM and SPS parameters) are suitably optimized. However, the author has experienced that longer milling time and higher MWCNT content make conservation of MWCNT structure difficult. The author has also experienced that the formation of interfacial carbides adversely affects the physical properties of the composites. There are reports of improvement in properties of the nickel matrix composites where silver coated MWCNT is used as reinforcement. In Chapter 7, the author has demonstrated significant enhancement of electrical conductivity with improved magnetic properties of iron-MWCNT composites**.**

On the basis of understanding that unique electrical property of MWCNT can be utilized to improve the conductivity of the excellent magnetic material, that is

iron, and based on the information that silver coated MWCNT as reinforcement can considerably improve the electrical conductivity of nickel matrix composite, it appears of worth to probe into the effect of silver doping on the electrical and magnetic properties of iron-MWCNT composites produced through high energy ball milling followed by spark plasma sintering. Hence attempt has been made to study the structural aspects of iron-MWCNT composites of varying concentration of MWCNT under optimized processing conditions during ball milling and sintering; further, in this investigation effort is also exerted to understand the role of silver doping in influencing the structure and properties of Fe-MWCNT composites.

## 7.2 Experimental methods

### *7.2.1 Materials*

The raw materials used in this study consist of Fe powder and multiwall carbon nanotube. Fe powder particles (purity ≥99%, -325 mesh, average particle size 43 micron), are irregular in shape. MWCNTs purchased from Nanoshel (average diameter and length are 15-20 nm and 10-26 µm, respectively), are used as the reinforcement. Silver powder of spherical shape (purity≥99.9 average particle size 3-8micron)is used 0.1 wt.%doping in Fe-MWCNT nanocompoite. Figure 7.1(a, b)show the FE-SEM images of iron powder and silver powder. Figure7.2(a, b) HR-TEM of MWCNTs used for the present experimentation.

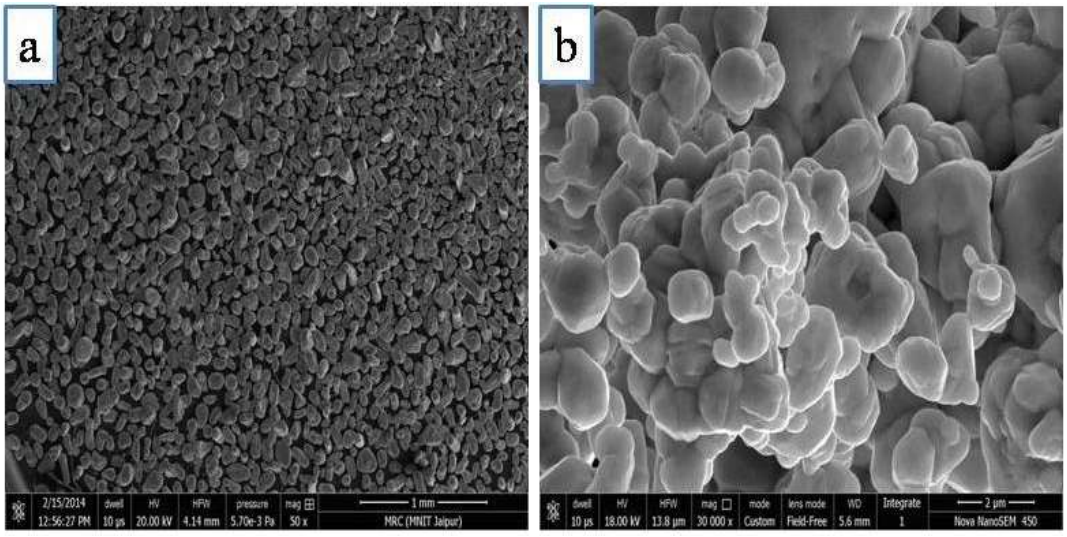


**Figure7.1** Typical micrographs of raw powders (a) SEM image of iron powder and (b) SEM image of silver powder.

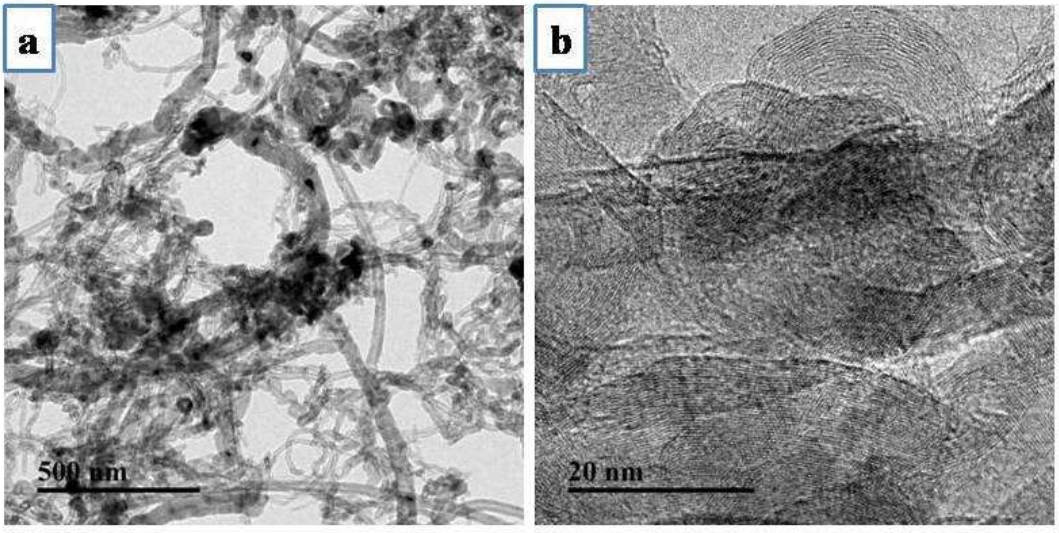


**Figure 7.2** (a) TEM image of MWCNT and (b) HR-TEM image of MWCNT

### *7.2.2 Mixing and Mechanical Alloying*

The iron powder (Fe) with the various weight percent of MWCNTs (1, 2, 3 and 4wt. %) are mechanically alloyed by utilizing Pulverisette-P6 high energy planetary ball mill (Fritsch, Germany); using the tungsten carbide vial and ball. For every batch, a fixed quantity of silver amounting to 0.1 wt.% has also been added to the mixture. The process of ball milling has been similar to what is described in Chapter 6. The mechanically milled powders of silver doped Fe-MWCNTs composite containing various weight present of MWCNTs (1, 2, 3 and 4 wt. %) but at fixed0.1 wt. % of silver were sintered by spark plasma sintering method by the following the technique described in Chapter 6.However the sintering temperature was kept at $700^0$C and the pressure applied has been 60 MPa.

X-ray diffractometer (XRD, Philips X'Pert with Cu Kα radiation) was utilized to analyze the constituent phases in the nanocomposite powder (Fe-MWCNT).The measurement technique has been same as that narrated in Chapter6.Microstructures of polished samples were observed under optical and field emission scanning electron microscope (FESEM).Transmission electron microscope (TecnaiF-20) was used for detailed Microstructural study. Vibrating Sample Magnetometer(VSM) of model EZ9 of make Microsence Company was used to study the magnetic property of the composites. Fourier transforms infrared spectrometer (Perkin Elmer Frontier) was used to obtain information about

stretching vibration of different bonds present in the experimental composites by following the same technique used in Chapter 6. Raman spectroscopy was carried out at room temperature in AIRIX STR 500 CONFOCAL MICRO Raman Spectrometer by following the process described in Chapter 6. The DC electrical conductivityof Fe-MWCNT nanocomposites pellets are measured using electrometer (B 1500A Agilent Technology).Silver paste is applied on the cross-sectional faces of the pellets prior the electrical measurements. Standard two-probe set up is used for these measurements.

## 7.3 Results and Discussion

### *7.3.1 X-ray diffraction study*

XRD spectra of silver doped Fe-MWCNTs composites containing varying weight percent of MWCNTs (1, 2, 3, and 4wt.%) and high energy ball milled for 50 min are shown in figure 7.3(a).The results of XRD reveal the presence of peaks of iron and silver. At higher percentage of MWCNT (~4wt. %) prominent peak of MWCNT is noted. From the existence of CNT peak, it transpires that MWCNT has maintained its crystallinity and have not undergone any structural degradation. On the contrary, the composites without silver doping exhibited cementite peaks at higher weight percent of MWCNT. It thus appears that doping of iron- MWCNT composites with silver aids in restoring the crystallinity of MWCNT even under harsh ball milling conditions. The absence of such peak of $Fe_3C$ in XRD spectra further authenticates that the experimental composites do not have any unwanted product of chemical reaction at the interface between iron powder and MWCNT during ball milling operation. The similar observation of absence of cementite peak in XRD spectra of composites after SPS (figure.7.3b) also suggest that unlike undoped composites, no damage of MWCNT structure takes place during spark plasma sintering.

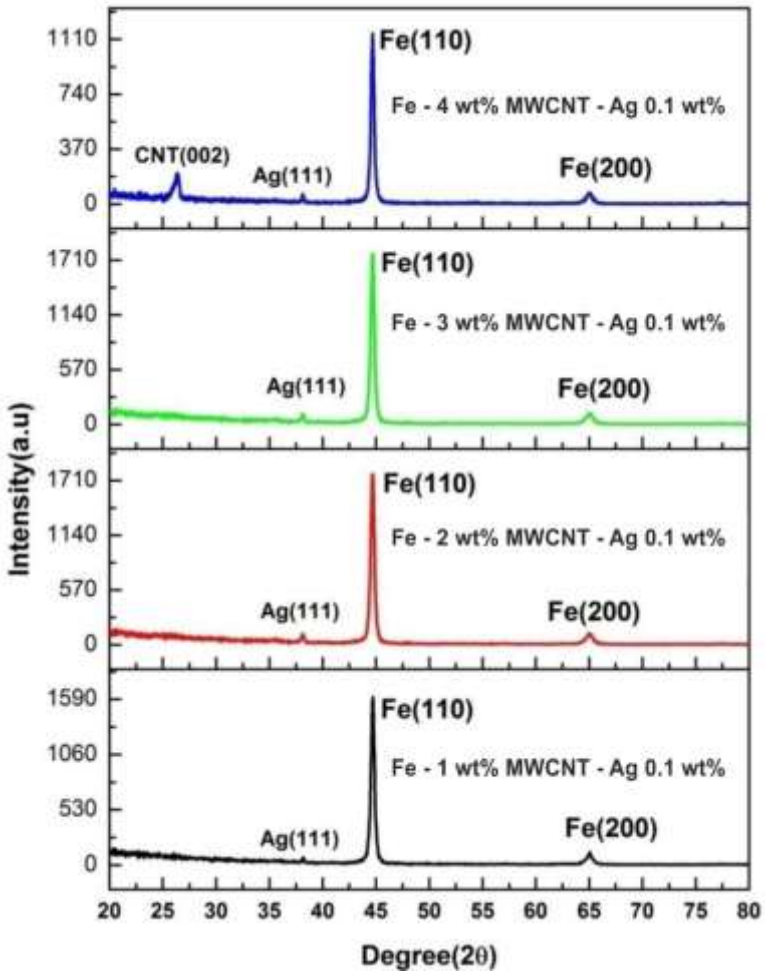


**Figure7.3** (a) XRD Pattern of Fe-MWCNTs-$Ag_{0.1}$ nanocomposite with increasing wt. % of MWCNT in Fe

It is known that, uniform dispersion of MWCNT with in metal matrix coupled with sound interfacial bonding is needed to maximize benefit of reinforcement with MWCNT.SPS temperature is kept at a level so that the dissolution of carbon in iron crystals is avoidable. It is apparent from figure7.3b that for increasing the MWCNT content from 1wt.% - 4wt.%, there has not been appreciable shift of (110) XRD peak of iron towards lower angle side. This is suggestive of the fact the fabrication technique, adopted in case of silver doped composites acts in opposition to usual expectation of dissolution of carbon in iron during milling or sintering which was quite observed in undoped composites.

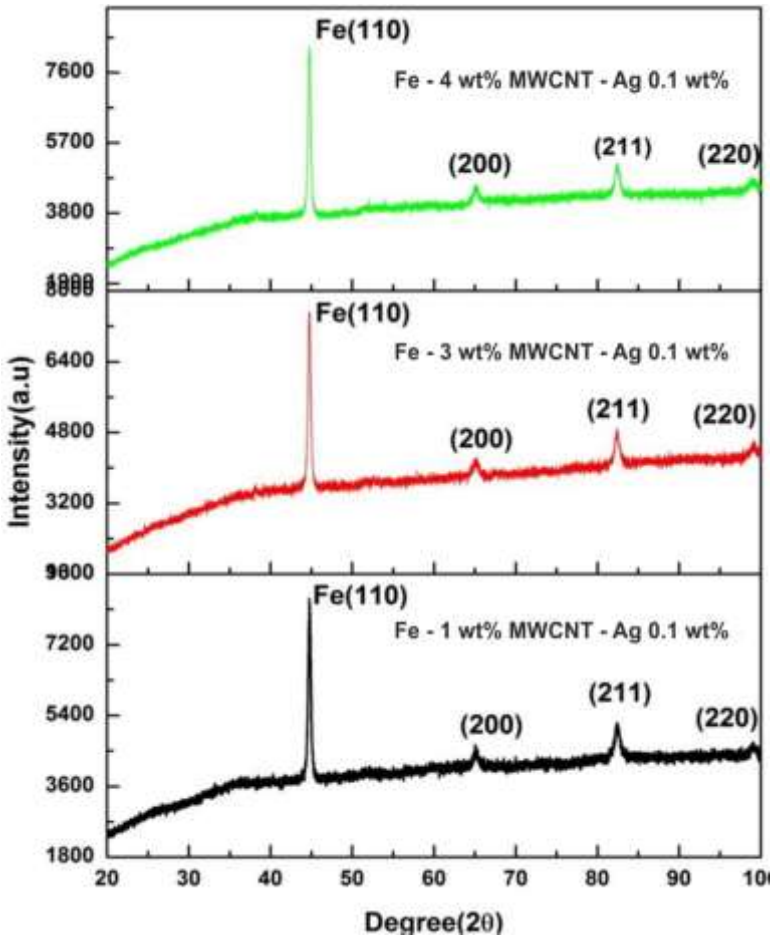


**Figure 7.3** (b) XRD pattern of samples after SPS; four major peaks of iron for use to construct Williamson and Hall plots for Fe -MWCNT composites.

As observed in previous cases, the increase in crystallite size along with reduction in lattice strain is noted in case of silver doped composites after HEBM (Table7.1). The corresponding

Williamson and Hall plots of composites with different wt.% of MWCNT in Fe are shown in figure7.4.

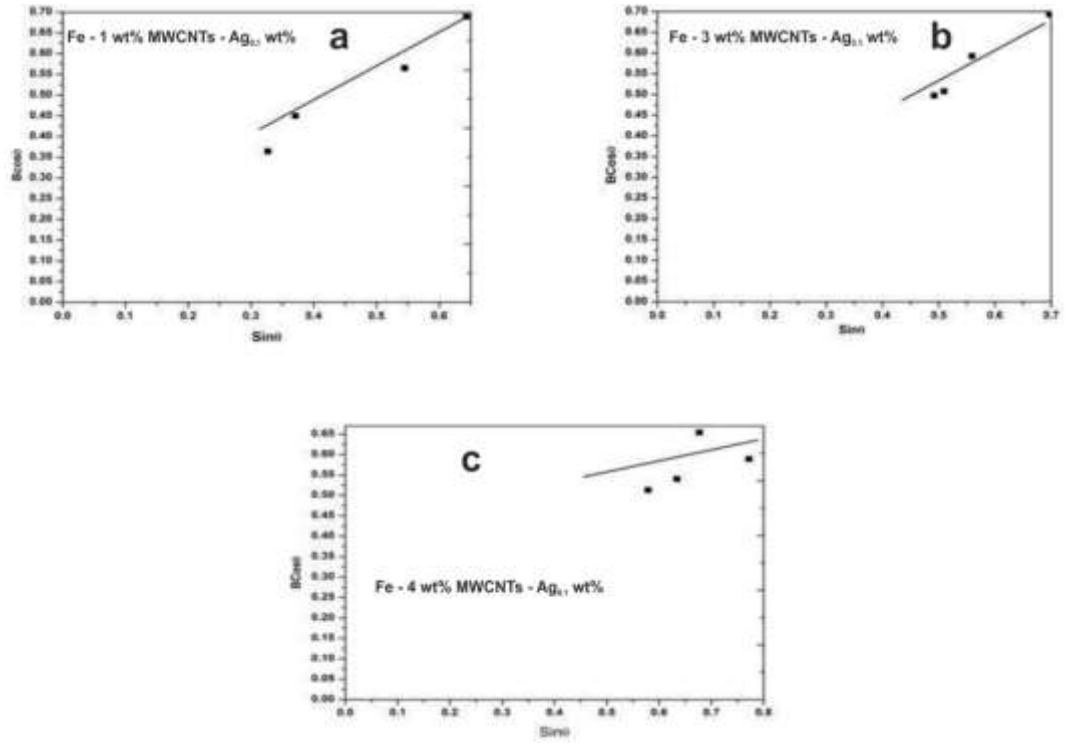


**Figure 7.4** (a-c) Williamson and Hall plots of Fe+MWCNT+$Ag_{0.1}$ composites of varying concentration of MWCNT

The summary of results presented in Table 7.1 shows the characteristic reduction in lattice strain at higher MWCNT content; as explained in the previous chapter, this is ascribed to the aggregation of MWCNT; the agglomerated regions contain very small sized pores inside them which help in strain relaxation. In line with previous explanation about increment in crystal size the curly MWCNTs are presumed to have formed 2Dchannel network on the around metal particles, thereby restricting flow of material in radial direction and allowing usual cold working in the third dimension. Thus crystallite size as measured by XRD appears to be higher for higher amount of MWCNTs.

**Table 7.1**Crystal size and strain of iron-MWCNT composites with different wt.% of MWCNT in Fe-MWCNT-$Ag_{0.1}$

| **Values (After SPS)** | **Fe-1wt.% MWCNT-Ag $_{0.1}$** | **Fe-3wt.% MWCNT-Ag $_{0.1}$** | **Fe-3wt.% MWCNT-Ag $_{0.1}$** |
|---|---|---|---|
| Crystallite size (nm) | 42 nm | 47 | 55 nm |
| Lattice strain | 0.0026 | 0.0023 | 0.0019 |

### *7.3.2 SEM study of doped composite powder*

The representative SEM image of silver doped iron-MWCNT composites are shown in figure 7.5 it appears from figure 7.5(a) that the high energy ball milling for 50 min has led to plastic deformation of metal particles which have exhibited a prominent tendency to flattening. The flattening tendency of doped composite can be monitored from a close examination of figure 7.5(a-d); it is evident from the figure that with increase in MWCNT content, the tendency towards flattering decreases.

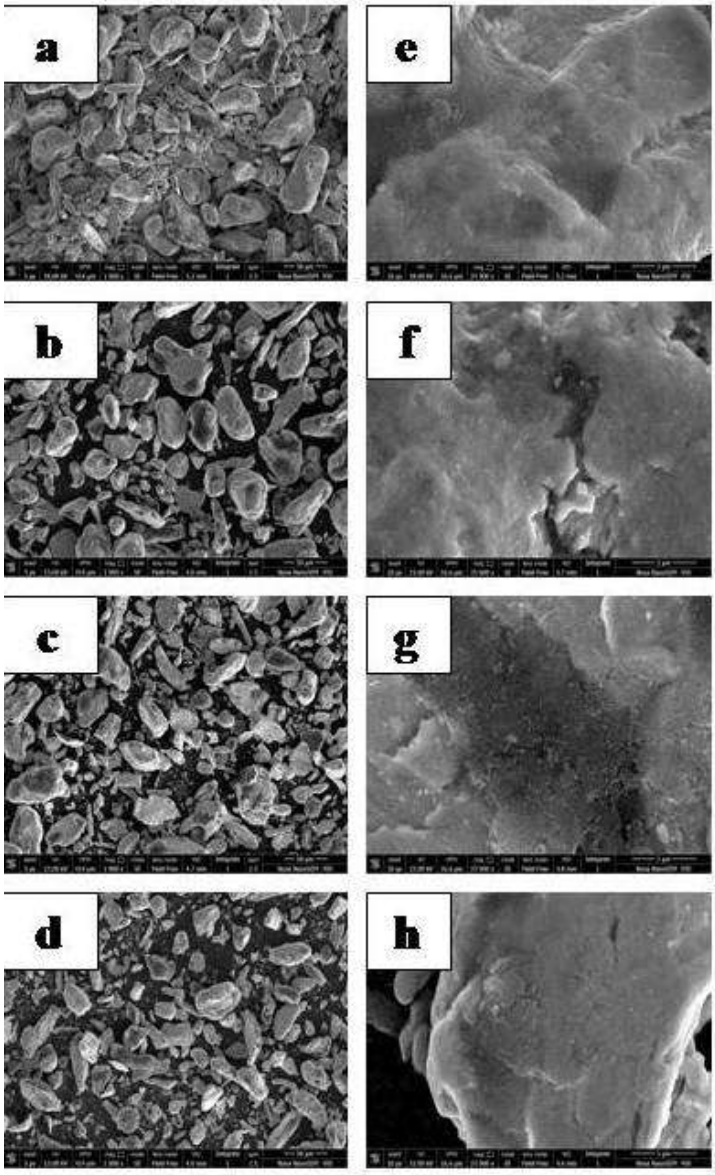


**Figure 7.5** SEM microstructure of composite with varying weight percent with silver doping of composite(a)Fe-1 wt.%MWCNT-$Ag_{0.1}$(b)Fe-2 wt.%MWCNT-$Ag_{0.1}$(c)Fe-3 wt.%MWCNT-$Ag_{0.1}$ (d)Fe-4 wt.%MWCNT-$Ag_{0.1}$(e-h).SEM image at higher magnification of Fe-MWCNT-Ag composite after varying wt.%of MWCNTs.

Figure7.5 (d) makes it clear that for a composite containing 4 wt.% MWCNT, the particles have not flattered to any appreciable extent. This observation is similar to that for undoped composites (vide chapter 6). The decreasing tendency towards flattening of particles implies less plastic deformation of metal during HEBM; it is understood that ball milling energy is partitioned between metal and MWCNT. When MWCNT content is increased by 1wt.%; there is an increase in volume percentage of more than 3%. Since aspect ratio is quite high for MWCNT, its available area to share ball milling force is also quite high. Thus at higher MWCNT content, much higher amount of imposed ball milling energy is sustained by MWCNT. As a result, amount of load on metal particle is decreased to a significant extent. So, deformation of metal particle becomes less and hence the reduced tendency towards flattering. At the same time, increasing MWCNT leads to more agglomeration. It is observed in figure7.5(e) that the MWCNT is very uniformly dispersed within the matrix. However as amount of MWCNT is increased its population density becomes appreciably high (figure7.5 f, g). It is found that the MWCNTs are, in general, embedded well into the matrix and become noticeably shortened after ball milling. Therefore the tendency for agglomeration of MWCNT is enhanced at a higher MWCNT content and can be clearly observed in figure 7.5(g) and 7.5(h). As explained earlier, such agglomeration of MWCNT takes place due to its high aspect ratio and the Vander Waal's forces of attraction among them [5,8,9].

### *7.3.3 Optical Microstructural study*

The optical microstructures of the silver doped Fe-MWCNT composites are shown in figure7.6 (a-d); from the figure, it is apparent that for a low concentration of 1wt.% MWCNT, the reinforcing nanotubes are uniformly dispersed throughout the matrix. The MWCNT network is found to be present at the crystallite boundaries. However, at this low concentration of 1 wt.%, the network is not continuous. The MWCNTs are also noticed to be embedded within the crystals. Spark plasma sintering has been carried out at $700^0$C under 70 MPa pressure. During sintering the iron particles have undergone hot working and recrystallized grains

within the individual crystallite are discernible in the microstructures. The feature of recrystallization of grains is noticed at all concentration of MWCNT (figure 7.6a-d).

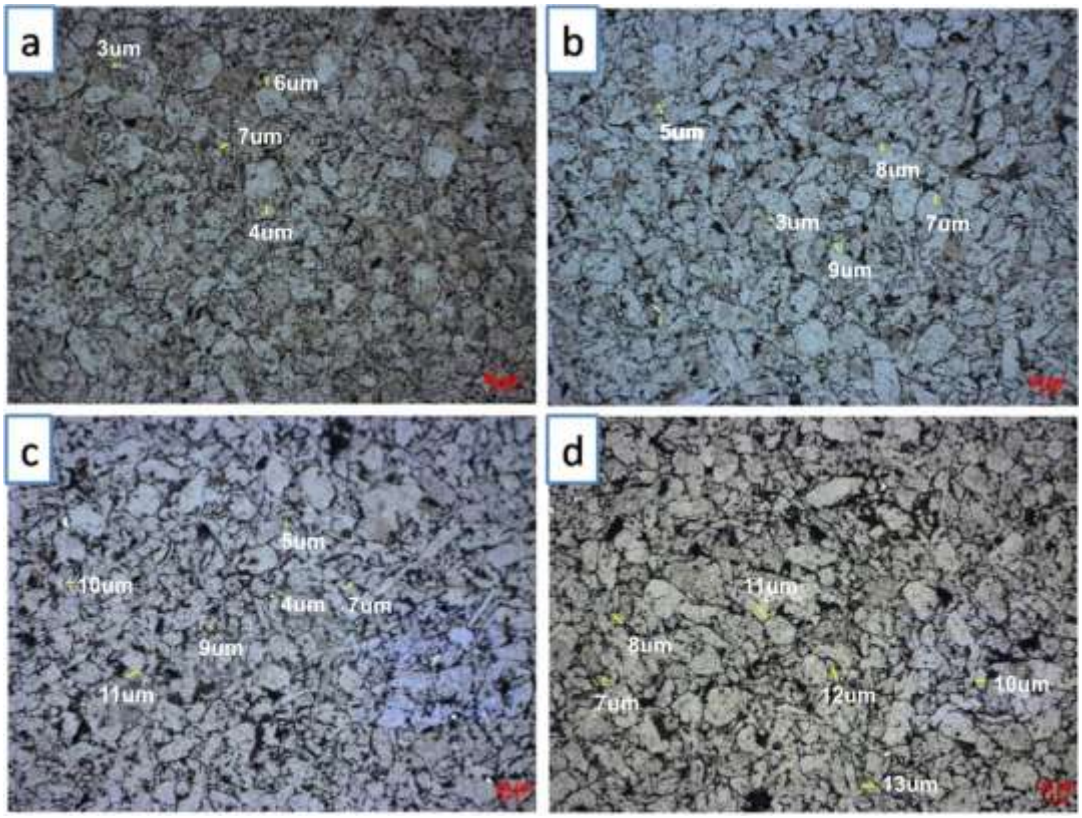


**Figure 7.6** Optical microstructure after SPS (a) Fe-1 wt.%MWCNT-$Ag_{0.1}$ (b) Fe-2wt.% MWCNT-$Ag_{0.1}$(c) Fe-3 wt.%MWCNT-$Ag_{0.1}$(d) Fe- 4 wt.%MWCNT-$Ag_{0.1}$

However, when the MWCNT content is low (~1wt. %), the deformation of matrix can be higher; this results in smaller recrystallized grains. Increasing MWCNT content means more surface area of contact and high magnitude of load transfer. This leads to less share of energy by the metal; so the amount of deformation of metal at the sintering temperature is rather low. Thus, the recrystallized grain size should be higher in case of higher MWCNT concentrations. Upon examination of size of the recrystallized grains in the doped composites of various MWCNT content it can be seen that the size of the recrystallized grain is higher at higher MWCNT content. When the MWCNT contents is increased in amount, the high aspect ratio and curly nature of MWCNT makes then organized in such a fashion that they form a continuous network around the crystal boundary. At the higher concentration of MWCNT, figure 7.6(d) exhibits thick MWCNT area at

the crystal boundary triple points. These are the regions of high degree of agglomeration of MWCNTs. It has been observed in the previous chapter that agglomerated MWCNTs enclose nanopores within them. These pores have considerable influence on the physical properties of the composites. When the MWCNT content is low, the amount of deformation of metal is quite high; so it has been possible to achieve grains of size 3-5μ and even less at places. On the contrary, it can be noticed that average grain size can be as high as 10-12μ at 4 wt.%MWCNT content. It is already mentioned that at high MWCNT content, deformation of metal matrix is less; this is manifested by elongated morphology of most of the iron crystals in microstructure of 4wt.% MWCNT containing composites.

### *7.3.4 Scanning Electron microscopic study of spark plasma sintered composite*

The SEM images of silver doped iron-MWCNT composites after being spark plasma sintered are shown in figure 7.7(a-c). It is seen from the SEM images that an extremely dense structure without any pores are obtainable in Fe-MWCNT composites after SPS. The HEBM powders are consolidated by spark plasma sintering.

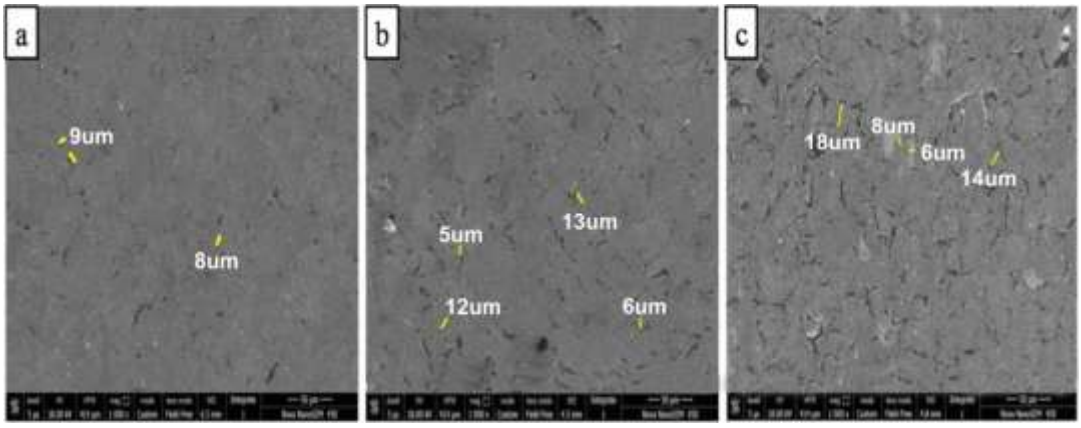


**Figure 7.7** SEM image after spark plasma sintering (a) Fe-1 wt.%MWCNT-$Ag_{0.1}$ (b) Fe-2wt.%MWCNT-$Ag_{0.1}$ (c) Fe- 4 wt.%MWCNT-$Ag_{0.1}$

The microstructures further authenticate that the sintering parameters used for this experiment are adequate to produce the desirable consolidation. In composite with low MWCNT content (~1wt. %), it is observed that the reinforcing phase remains present at the crystal boundary and tend to form network; the network is not found to be continuous due to paucity in the amount of available MWCNT. A close observation of the microstructure makes it apparent that the original grains are

recrystallized. Since the original grains are enclosed by MWCNT, their plastic deformation at sintering temperature has led to the formation of recrystallized grains. It is further observed that the MWCNTs are well embedded into the matrix and seemingly the tubular structures of MWCNTs are conserved. For the 2 wt.%MWCNT composite, the network appears to have become continuous all through; similar to 1wt.% MWCNT composites, the reinforcing phase is present around the original grains which undergo recrystallization during SPS. It is noted that there are scanty regions, mainly the triple points at the grain boundaries, where agglomerated MWCNTs are present. In this respect, the observation is similar to that in the case of undoped composites. However, for higher MWCNT containing composites, the number of areas of agglomerated MWCNT is found to have increased. Due to the availability of higher amount of MWCNT, they become more amenable to entanglement due to reasons explained in preceding chapters. The traces of recrystallized grains, though observed, are seen to be far less; in magnitude as compared to low MWCNT containing composites (figure 7.7c).The reason for such observation could be assigned to less plastic deformation of matrix phase taking place during SPS. The higher MWCNT content lends more area of contact between matrix and reinforcement; because load transfer between metal matrix and MWCNT takes place by shear stress at the interface, there will always be more load to be shared by reinforcing MWCCNT.

The SEM image further delineates that new grains are formed after SPS within the prior grains bound by the MWCNTs. The evolution of the grain structure in SPS samples is quite prevalent in Fe-MWCNT composites. SPS has been carried out under 50Mpa pressure at $650^0$C which is above the recrystallization temperature of pure iron. Pressure applied during SPS has been shared by metal and by the MWCNT. The force shared by metal is responsible for its plastic deformation. Since the deformation temperature is above the recrystallization temperature, the recrystallization of iron particles take place during SPS and SEM micrographs show that new grains have been formed within the pre-existing grains. It is known that higher amount of deformation leads to lower recrystallized grain size. In case of very low percentage of MWCNT the relative proportion of load to be shared by

metal is high and hence its deformation is comparatively higher. This leads to appreciable recrystallization.

### *7.3.5 FTIR Analysis for assessment of bonding quality in composites*

The results of FTIR study for silver doped Fe-MWCNT composites in high energy ball milled (~50 min) condition as well as after spark plasma sintering of ball milled powder are shown respectively in figure 7.8(a) and 7.8(b); the observed peaks at 3432 -3436 $cm^{-1}$ in HEBM samples is ascribed to bending vibration of hydroxyl group due to absorption of water in the sample (figure 7.8a). This peak occurs at 3415$cm^{-1}$ in SPS sample. It appears unusual that the samples after sintering at $700^0$C would record peak corresponding to bending vibration of hydroxyl group.

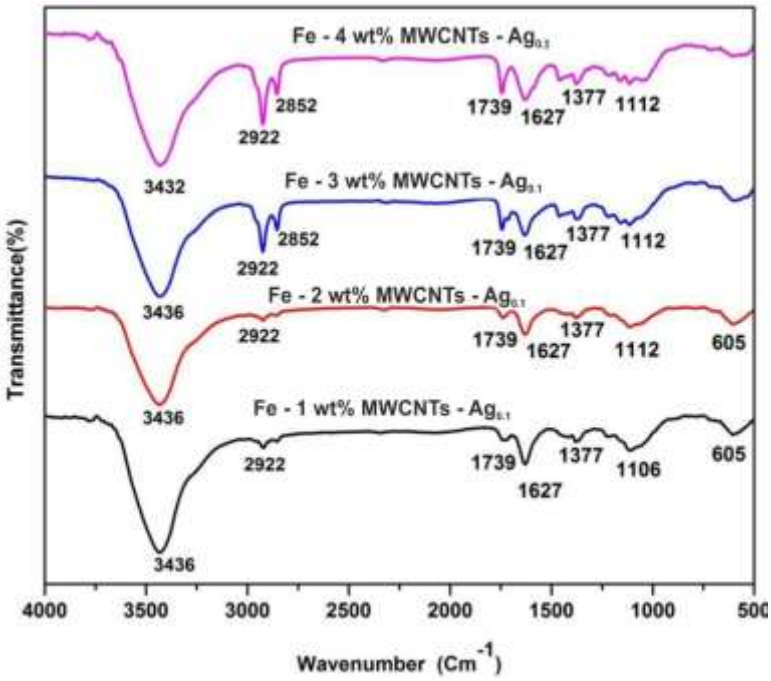


**Figure 7.8** (a) FTIR spectra after high energy ball milling

It is surmised that the sample preparation technique is responsible for moisture absorption by KBr, which is used as a binder and is known to absorb moisture. The peaks of interest pertaining to the present study occur at 1627 and 1112-1106 $cm^{-1}$ in the HEBM samples. It is reported earlier that the peak at 1627$cm^{-1}$ originates from C=C stretching vibration whereas the other peak near 1112$cm^{-1}$is due to IR active C-C stretching mode. In fact, no major change in peak intensities is noticed in either case. The absorption peak at 605$cm^{-1}$ is due to iron –carbon bond

formation. It is conjectured that in the doped composites, the quality of C-C bonds in MWCNT does not experience too much degradation, rather the existence of absorption peak at 605cm$^{-1}$ where intensity is independent of MWCNT content indicates that there has been minimal disruption of C-C bonds to create Fe-C bonding by 3d-2p hybridization [10-11]. From the results of XRD and Raman spectroscopy it has appeared that MWCNT structure is far better conserved in doped composites as compared to the undoped composites at high weight fraction of MWCNT. FTIR results of HEBM also corroborate the above observation. These observations hint upon the fact that silver atoms tether the surface of MWCNT in such a manner that the atomic layers of silver behaves as a coating on MWCNT. In fact, improvement of properties has been reported in nickel matrix composite reinforced with silver coated MWCNT [12]. It is quite possible that high energy ball milling makes silver atoms segregate at the iron-MWCNT incoherent interface similar to high angle grain boundaries. Segregation of silver at the grain boundaries is commonly observed in many function materials. The FTIR study on the composite samples after SPS is shown in figure 7.8(b).

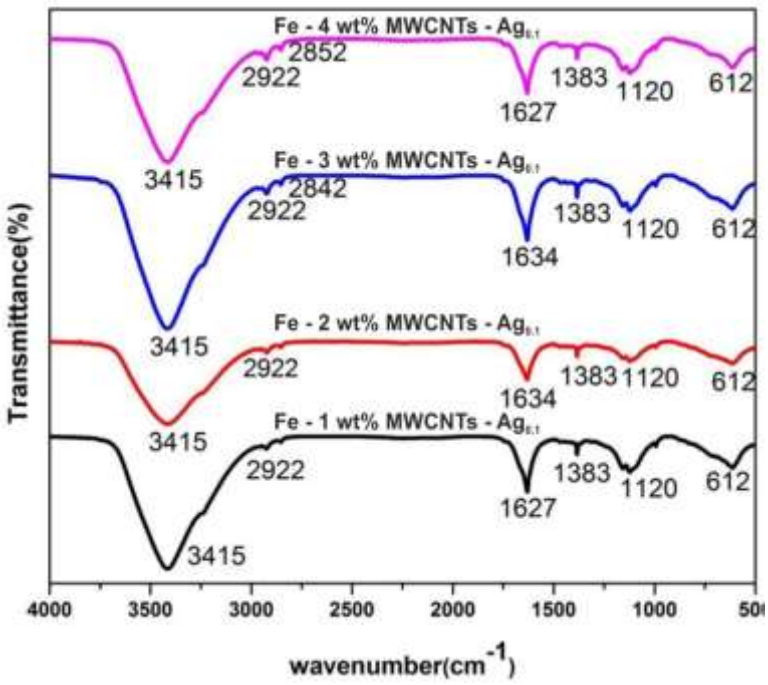


**Figure 7.8** (b) FTIR spectra of composites after spark plasma sintering

It is observed that FTIR spectra are qualitatively same as those for HEBM composites. This means that spark plasma sintering has not led to a change in quality of bond vis-a-vis extra damage to MWCNT and therefore SPS can be considered to be very suitable consolidation process in the iron-MWCNT composites.

### *7.3.6 Raman Spectroscopy*

XRD study of silver doped Fe-MWCNT composite has hinted upon the fact that structural degradation of MWCNT is insignificant. However the degradation of MWCNT can be assessed by XRD study only within the detection limit of the instrument. Since Raman spectroscopy is a very important tool to assess the structural damage of MWCNT even in a metal matrix, the silver doped composites after HEBM were also subjected to Raman spectroscopy study to monitor the structural condition of MWCNT within the composite. The results of Raman spectroscopic study is shown in figure 7.9. The shift of position of peaks and the $I_D/I_G$ ratio are tabulated in Table 7.2. It is evident from figure 7.9 that very sharp and undistorted D and G band peaks are present in composites containing up to 3 wt.% MWCNT. This observation is also with the appearance of $G^I$ band. All these suggest that there has been minimal damage of MWCNT in silver doped composites. When the MWCNT is increased to 4 wt.%, the D and G band peaks are found to have somewhat shortened and widened. Concurrent widening of $G^I$ band in also noticeable. These are the indication of small amount of structural damage of MWCNT. The results shown in Table 7.2 are also supportive to these. It is found that $I_D/I_G$ ratio increases to 1.11 at 4wt.% MWCNT; also, there are appreciable shift in D and G band peaks especially at higher MWCNT level. It may be mentioned that in the case of un-doped composite, prominent cementite peaks were detected in Raman spectra; but no such peak is observed in the doped composite. It may therefore be conjectured that in the case of silver doped composite there is no mechano-chemical synthesis between iron and carbon and hence no carbide has formed

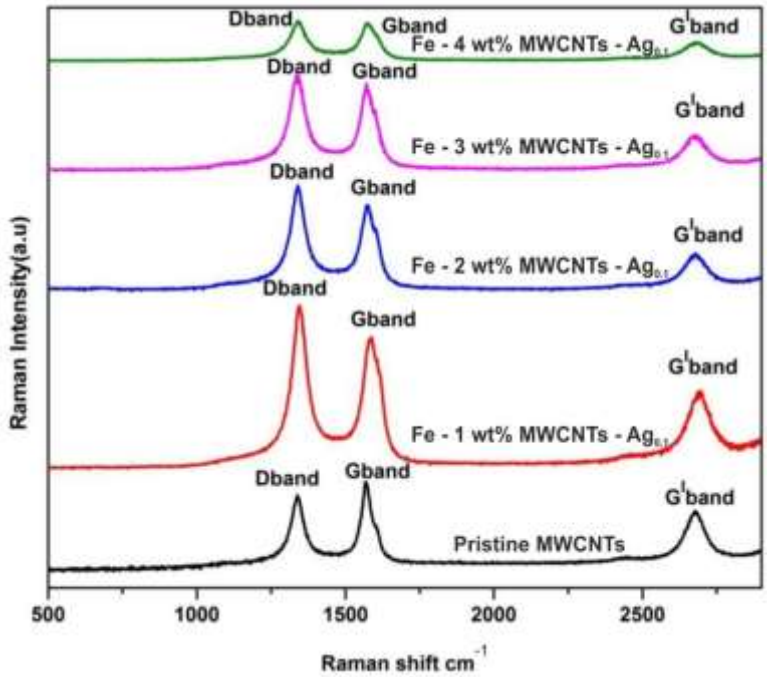


**Figure 7.9** Raman spectra of pristine and iron-MWCNT-$Ag_{0.1}$composites of different MWCNT content. The figure shows the relative changes in first order D and G bands of MWCNT.

**Table 7.2**Position of D and G bands along with $I_D/I_G$ ratios in Raman spectra after 50 min milling of high energy ball milling

| Sample Name | Raman Peak Shift ($Cm^{-1}$) | | $I_D/I_G$ |
|---|---|---|---|
| | D band | G band | |
| Pristine MWCNT | 1353 | 1575 | 0.99 |
| Fe-1wt.% MWCNT | 1345 | 1579 | 1.05 |
| Fe-2wt.% MWCNT | 1351 | 1585 | 1.07 |
| Fe-3wt.% MWCNT | 1359 | 1589 | 1.09 |
| Fe-4wt.% MWCNT | 1365 | 1597 | 1.11 |

### *7.3.7 Study of Magnetic properties of silver doped composite*.

The magnetic properties of silver doped composites of varying MWCNT content is shown in Figure 7.10.

**Table 7.3** Magnetic properties of Fe-MWCNT-Ag nanocomposite

| Sample name | Saturation Magnetisation (Ms)(emu/gms) | Remanent Magnetisation (Mr)(emu/gms) | Coercivity (Hc)(Oe) |
|---|---|---|---|
| Pure Fe | 184.41 | 0.19 | 3.7 |
| Fe-1wt.%MWCNT | 213.17 | 0.211 | 5.11 |
| Fe-2wt.%MWCNT | 223.37 | 0.351 | 9.34 |
| Fe-3wt.%MWCNT | 230.07 | 0.653 | 13.06 |
| Fe-4wt.%MWCNT | 214.31 | 0.92 | 17.21 |

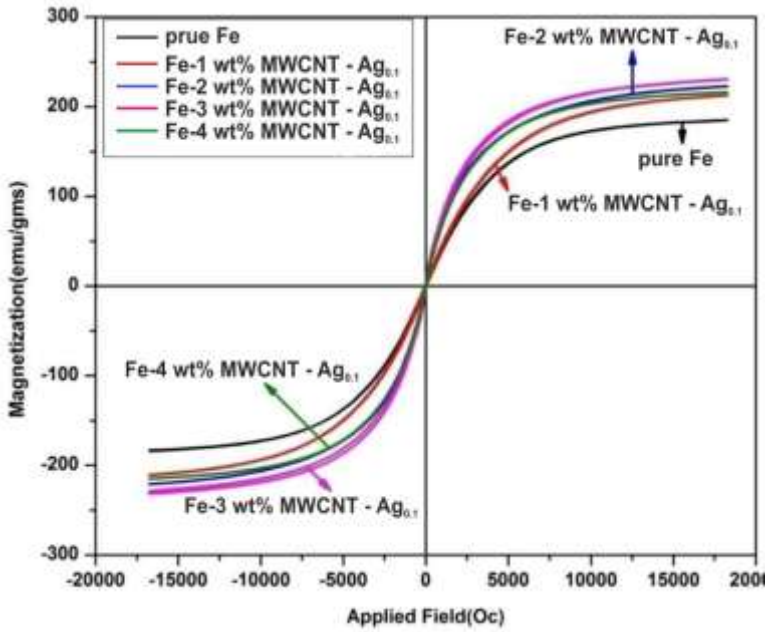


**Figure 7.10** Hysteresis loop Fe-MWCNT-Ag with different wt. % of MWCNTs

From the figure, it is evident that the materials behave ferromagnetic. The summarized results of VSM testing are presented in Table 7.3; there is a 25% increase in saturation magnetization over that of pure iron where the composite contains 3 wt.%MWCNT.

However, further increase in the MWCNT content to 4 wt.%, has led to a substantial reduction in saturation magnetization even through the value of saturation magnetization in 4 wt.% MWCNT composite is still far more than the usual saturation magnetization value of pure iron. It is further evident from Table 7.3 that both remnant magnetism and coercivity of the composites increase continuously with increasing MWCNT content. In opposition to usual observation of diminution

of saturation magnetization in high energy ball milled pure iron, the saturation magnetization of Fe-MWCNT composite after HEBM has significantly increased.

There can be number reasons which could be assigned to the observed increased in saturation magnetization. Firstly the particle size obtained by the processing route practiced in this investigation is very small. The size of the crystal attained in the composite is far less than the normal domain size of a ferromagnetic material. The MWCNT restores the fine size of the crystal by inhibiting the movement of grain boundaries under application of external field; those single domains or micro magnets quite easily align along the applied field. This is so possible because unlike a multi domain magnetic material, magneto restriction does not resist the tendency of micro magnets (domains) to align along the applied field. Since in the doped composites, the interface is absolutely contamination free, also since the reinforcing phase MWCNT used in this investigation behaves ferromagnetic, there is no resistance to aligning of micro magnets along the applied field. The tethering of silver at the surface of MWCNT has protected the MWCNT; also, it has ensured a contamination free continuous interface between matrix and MWCNT. This could be the reason why the saturation magnetization attainable in silver doped Fe-3 wt.% MWCNT is higher than its un-doped counterpart, where the formation of cementite at the interface could not be avoided. The presence of higher amount of MWCNT has been additive towards the finally attainable value of saturation magnetization due to the fact that the MWCNTs produced by CVD technique with iron as catalyst have behaved like ferromagnetic materials. But upon withdrawal of the field, the automatic reversal to random configuration of the domains is improbable due to the resistance, arising from the rigid MWCNT distributed uniformly within the matrix. This enhances both values of remnant magnetism and coercivity.

The drop in saturation magnetization is iron- 4 wt.%MWCNT composite may be due to extensive agglomeration of MWCNT, which not only reduces the effective aspect ratio but also contains pores inside them. The pore acts as discontinuity and interferes with the passage of magnetic flux. This lessons the effective field strength and hence the reduction in saturation magnetization.

### *7.3.8 Transmission electron microscopy*

The transmission electron microscopy carried out with silver doped iron-MWCNT composite shows that the MWCNT are in general uniformly distributed throughout the matrix and that the reinforcing MWCNT is very well embedded into the matrix. The uniform dispersion of MWCNT without much agglomeration is shown in figure 7.11a.

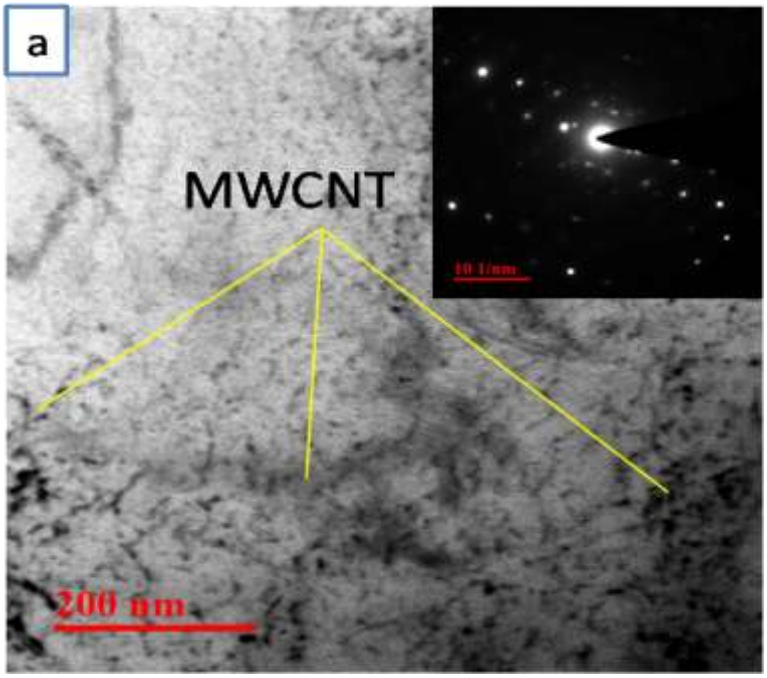


**Figure 7.11**(a) Tem image of Fe-1 wt.% MWCNTs - Ag0.1

The inset in the same TEM image shows the SAED pattern indexed as B= Z= [$\bar{1}$11].Besides uniform distribution of MWCNT, the bright field image in figure 7.11(a) also delineate some dislocations in SPS sample; this is supposed to have been created while being cooled from the sintering temperature, $700^0$C, due principally to the mismatch in coefficient of thermal contraction of iron matrix and MWCNT. Sub grain type structure of size 100nm or less is discerned in the same image. This influences the mechanical and physical properties of the composites. The HRTEM image of the same area is shown in figure 7.11(b). HRTEM image exhibits a clean interface. There is no sign of the presence of any contaminating phase at the iron-MWCNT interface.

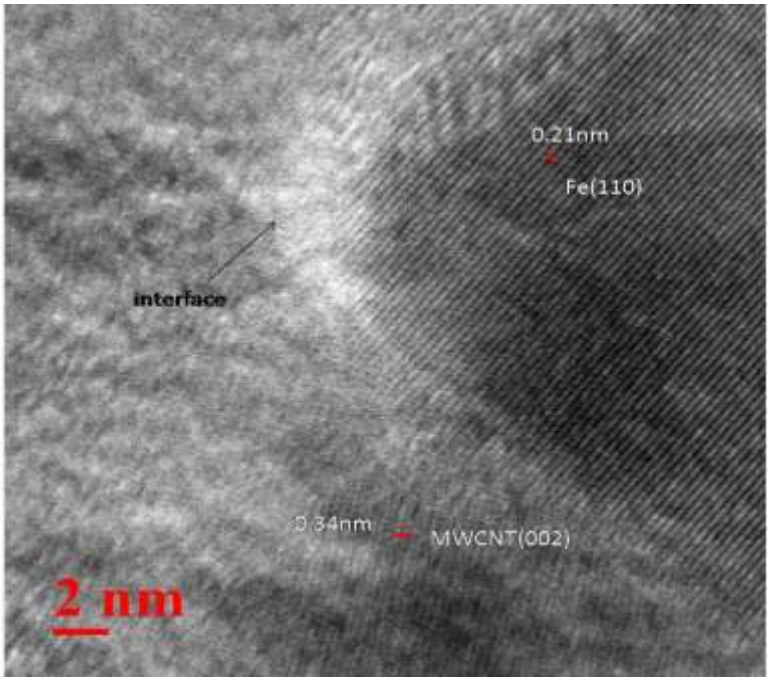


**Figure 7.11(b)** HR-TEM image of Fe -1wt.%MWCNTs -Ag0.1 composite

A similar observation can be made in the interface of Fe-3 wt.%MWCNT composites (figure7.12). The observations made in XRD, Raman or FTIR studies have indicated that MWCNT structure is better conserved in silver doped composites and have not revealed the presence of $Fe_3C$ at the interface.

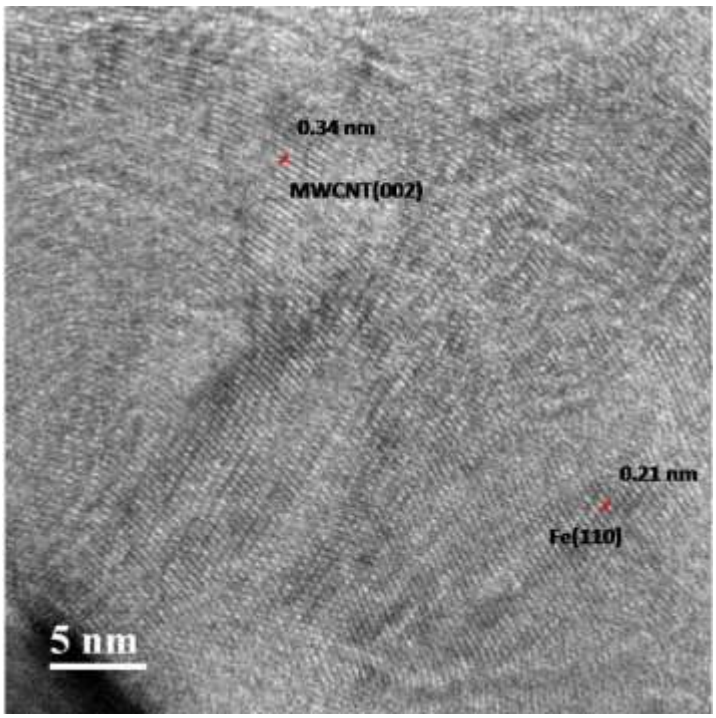


**Figure7.12**HR-TEM image of Fe-3 wt.%MWCNTs - $Ag_{0.1}$ nanocomposite

The HRTM study on silver doped composite verifies that MWCNT does not degrade to form contaminating phase at the interface. Thus it is conjectured that silver has positive influence in the conservation of MWCNT structure. The elemental mapping by EDS attached to TEM is presented in figure 7.13.

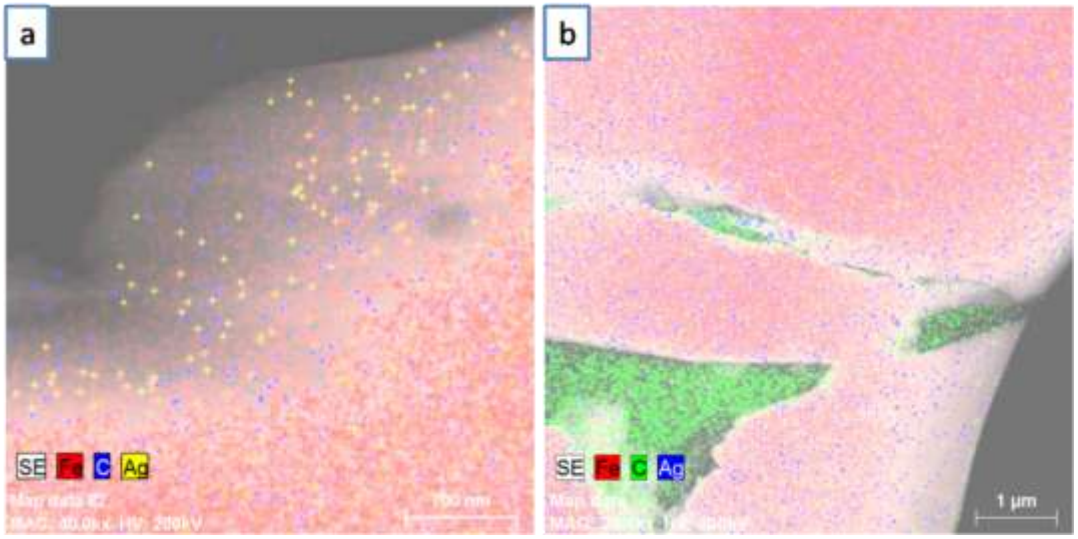


**Figure 7.13** EDX analysis (a) Fe–1 wt.% MWCNTs -$Ag_{0.1}$ and (b) Fe–3 wt.% MWCNTs -$Ag_{0.1}$

It is seen from elemental map that silver has decorated the surface of MWCNT; most likely silver atoms have adhered to the surface of MWCNT and it is likely the sintering pressure (60MPa) and temperature ($700^0$C) have enabled silver atoms to tether to the MWCNT surface. This makes silver behave as a coating on MWCNT. In fact, silver coating on MWCNT has been successfully accomplished by previous investigators by other method [12]. The silver around the surface of MWCNT protects from chemical relation with iron. Moreover, presence of silver as a layer insures a far better bonding. That this is so, can be verified from the elemental mapping which clearly shows that silver has diffused both in iron as well as in MWCNT.

### *7.3.9 Conductivity Analysis:*

Figure7.14shows the electrical conductivity of silver doped Fe-MWCNTs composite with varying percentage of MWCNTs. The inset shows the experimentally obtained values of conductivity at various MWCNT content

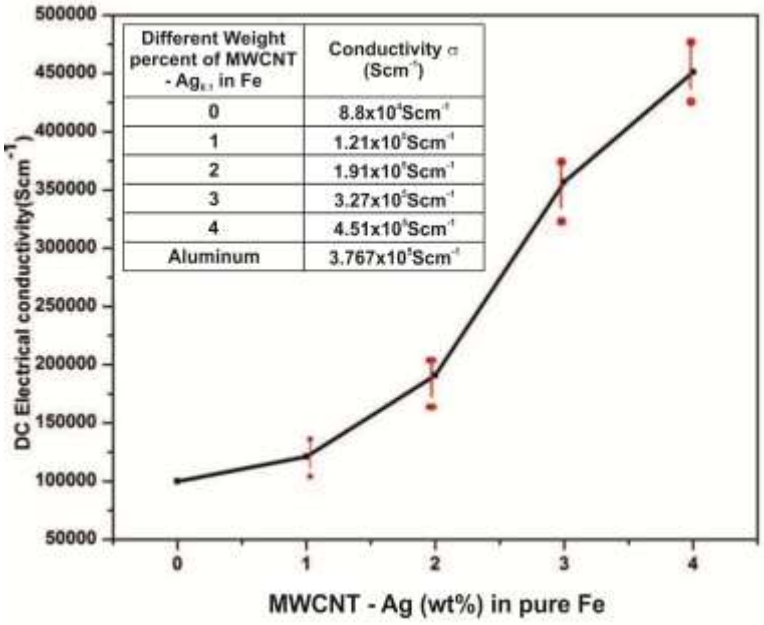


**Figure7.14.** Variation of electrical conductivity (σ) of silver doped Fe-MWCNT composites with MWCNT content

It is observed that doping of silver in the experimental composites have improved the conductivity of the composites quite significantly. It appears from figure7.14 that the electrical conductivity of iron continually increases with increasing MWCNT in the silver doped alloys. The curve infigure7.14 indicates that the increase in conductivity is initially slow, followed by a rapid rise till 4wt.%. It is to be noted that the measured conductivity of identically processed pure iron is very similar to that of the reference conductivity. This suggests that the parameters used for SPS, have been quite adequate to achieve the density of the consolidated mass near to its theoretical value; this further verifies that the pore content in the sintered material is negligibly small to affect the electrical conductivity; this is also corroborated by the microscopic observation which did not detect pores within the composites. Noticeably, the conductivity of Fe- 4wt.% MWCNT composite has attained the highest value of electrical conductivity, $4.51x10^{5}Scm^{-1}$; this is a value which is higher than the electrical conductivity value of electrical grade aluminum. Comparing this value with un-doped composite of same amount of MWCNT it can be seen that silver doping has a positive effect on conductivity of the composites. The point mapping in TEM study(Figure 7.13) has shown that silver is present at the surface ofthe MWCNTs. HEBM can make the silver atoms to adhere to the

MWCNT as if, it has been coated over the surface of dispersed MWCNTs. Thus it protects the MWCNT which does not undergo structural degradation to any greater extent. By being tethered at MWCNT surfaces, silver prevents the formation of iron carbide at the interface. This is proved by the XRD observation which does not record any cementite peak even at high concentration of MWCNT. It may be mentioned that Fe-MWCNT composites, processed by HEBM followed SPS, suffer from structural degradation to the extent that cementite formation takes place quite significantly. The absence of cementite in XRD spectra suggests that silver prevents the formation of cementite at the interface and a clean interface is responsible for enhanced physical and mechanical properties. MWCNTs can carry electric current density, of as high as $4x10^9$ A/cm$^2$; this means that electrical conductivity of a metal-MWCNT composite may be enhanced by transportation of electrons through MWCNT. It is observed in the microstructures that MWCNTs are present in the matrix in the form of network along the crystal boundaries. This type of network acts as a conducting channel and coupled with high current capacity of MWCNT, the conductivity of a composite reinforced with MWCNT increases appreciably. Importantly, the MWCNTs behave as if they are coated with the highest conductivity metal, silver. Thus, electron transport becomes highly efficient. Moreover the silver present within the matrix in close proximity of uniformly dispersed MWCNT far reduces the tunneling distance for electron transport and so there is a considerable improvement in conductivity due to doping in MWCNT reinforced iron. In the low concentration of MWCNT, the network cannot become continuous. So, the improvement in conductivity may not be very high.When the concentration of MWCNT becomes such as to form a continuous network around grains, the conductivity increases remarkably. This seems to be reason for a steep rise in conductivity beyond 2 wt.% MWCNT. Optical and scanning electron microstructures have also shown that network of MWCNT becomes quite continuous in 3 wt.% MWCNT composites. The rise in conductivity is less steep for 4wt.% MWCNT composite than that with 3 wt.% MWCNT. This is attributed to agglomeration of MWCNT at the grain boundary triple points. The agglomerated MWCNTs are seen to have contained nano sized pores (Chapter6) which impede the electron transport by acting as the centers for incoherent scattering of electrons and

so increase resistivity. Thus, overall improvement in conductivity becomes rather small.

### 7.4 Conclusions:

It is concluded that silver doping in iron-MWCNT composites can conserve the structure of MWCNT better than the undoped alloy and that in silver doped composites; no contamination takes place at the interface of MWCNT and iron crystals. High energy ball milling helps to flatten the matrix at low MWCNT content; increasing MWCNT in doped composites do not show much tendency towards flattening. Seemingly, silver protects the MWCNT from chemical damage. Physical damage of MWCNT takes place by HEBM. High energy ball milling followed by Spark Plasma Sintering does not form chemical synthesis product in silver doped composites.

Conductivity of iron increases remarkably in silver doped composite; the conductivity of silver doped iron-4 wt.% MWCNT composites can achieve conductivity value higher than that of aluminum. It is further concluded that the saturation magnetization of silver doped Fe-MWCNT composite increases by 25% over that of pure iron for the composite containing 3wt.%MWCNTs;however, it drops at 4 wt.% MWCNT composite due to pores existing within the agglomerated MWCNTs. Even after drop the value of saturation magnetization remains significantly higher than pure iron. Remnant magnetization and coercivity properties increase continuously with increasing MWCNT content in the composite

HRTEM image of silver doped composites further proves that there cannot be chemical contamination at the matrix-reinforcement interface. Silver atoms tether the surface of MWCNT and act as a coating over the MWCNT. This type of functionalization produces good interfacial bonding which improves the physical properties.

## REFERENCES


[1] D. Poirier, R. Gauvin, R. A.L. Drew, Structural characterization of a mechanically milled carbon nanotube/aluminum mixture, CompositesPart A 40 (2009) 1482-1489.

[2] A. Esawi,K. Morsi, Dispersion of carbon nanotubes (CNTs) in aluminum powder, CompositesPart A 38 (2007) 646-650.

[3] R. George, K.T Kashyap, R.Rahul, S.Yamdagni, Strengthening in carbon nanotube/aluminium (CNT/Al) composites,Scripta Mater 53, (2005) 1159-63.

[4] R. B. Perez, I.E Guel, W.F. Antunez, M. M. Yoshida, P.J.Ferreira, R. S. Martinez, Novel Al-matrix nanocomposites reinforcedwith multi-walled carbon nanotubes, J Alloys Compounds. 450 (2008) 323 - 6.

[5] W. Zhou, S. Bang, H. Kurita, T. Miyazaki, Y. Fan, A. Kawasaki, Interface and interfacial reactions in multi-walled carbon nanotube reinforced aluminum matrix composites, Carbon 96 (2016) 919-928.

[6] W. Zhou, T. Yamaguchi, K. Kikuchi, N. Nomura, A. Kawasaki, Effectively enhanced load transfer by interfacial reactions in multi-walled carbon nanotube reinforced Al matrix composites, ActaMaterialia 125 (2017) 369-376.

[7] Z.Y. Liu, S.J. Xu, B.L. Xiao, P. Xue, W.G. Wang, Z.Y. Ma, Effect of ball-milling time on mechanical properties of carbon nanotubes reinforced aluminum matrix composites,Composites Part A 43 (2012) 2161–2168.

[8] S.M. Uddin, T. Mahmud, C. Wolf, C. Glanz, L. Kolaric, C. Volkmer, H. Höller, U.Wienecke, S. Roth, H.J. Fech, Effect of size and shape of metal particles to improve hardness and electrical properties of carbon nanotube reinforced copper and copper alloy composites, Composites Science and Technology 70 (2010) 2253–2257.

[9] H.S. Kim, W. Park, M. Kang, H.J. Jin,Multiple light scattering measurement and stability analysis of aqueous carbon nanotube dispersions, J PhysChem Solids 69 (2008) 69 1209–12.

[10] P. Delhaes, M. Couzi, M. Trinquecoste, J. Dentzer, H. Hamidou, C. Vix-GuterA comparison between Raman spectroscopy and surface characterizations of multiwall carbon nanotubes, Carbon 44 (2006) 3005–3013.

[11] J.H. Lehman, M. Terrones, E. Mansfield, K.E. Hurst, V. Meunier, Evaluating the characteristics of multiwall carbon nanotubes, Carbon 49 (2011) 2581 – 2602.

[12] D. Lee, J. Sim, W. Kim, C.Moon, W.Cho, S.Baik, Enhanced electrical conductivity and hardness of silver-nickel composites by silver-coated multi-walled carbon nanotubes, Nanotechnology 26 (2015) 295705-14.

# *CHAPTER EIGHT*

## *Effect of Fabrication Process on Structure and Properties of Iron-x wt.% MWCNT Composites (x=0.5,1,2 and 3 wt.%)*

In the present chapter, discussion is made about the fabrication of iron-MWCNT composites by high energy ball milling which bears the potential danger of deterioration of the graphitic structure of MWCNT; this is because of the possible interactions between iron matrix and carbon atoms of MWCNT. Iron -MWCNT system has high sensitivity for its constituents to interact with each other. Even at a relatively low temperature of spark plasma sintering, $650^0$C, carbon atoms can diffuse very well into the iron crystals and form solid solution.

In this chapter discussion is also made about the structural and phase evolution Also evaluation of mechanical and magnetic properties of Fe-MWCNTs composites of varying weight percent of MWCNT are done after high energy ball milling. Magnetic properties of the Fe-MWCNTs after varying the MWCNT (0.5 1, 2 and 3 wt.%) and ball milling time up to 2 h are measured by Vibrating Sample Magnetometer (VSM).

## 8.1 Introduction

It is known that high ball milling of MWCNT with metal powder leads to degradation of MWCNT structure. Fabrication of iron-MWCNT by high energy ball milling bears the potential danger of deterioration of the graphitic structure of MWCNT owing principally to the possible interactions between iron matrix and the carbon atoms of MWCNT. It is demonstrated in the previous chapter that high energy ball milling of Fe-2 wt.% MWCNT is susceptible to objectionable interfacial reaction beyond one hour of ball milling. The effect of MWCNT content on the structural integrity of MWCNT vis-a-vis properties of iron-MWCNT composite has been reported in the previous chapters. It is revealed from the above study that there is a limiting value of MWCNT content, ~3 wt.% beyond which high energy ball milling of iron-MWCNT composite for one hour leads to appreciable damage of the MWCNT structure. It is observed by the present author and also by the other investigators [1-8], that higher milling time leads to better dispersion of MWCNT and can enable to get rid of severe agglomeration tendency at higher concentration of MWCNT.

It therefore appears prudent to investigate the role of higher milling time onto the structural integrity of reinforcing MWCNT in iron matrix. Since it is observed in the previous chapter that for a particular milling time, the concentration of MWCNT determines the propensity of structural damage in MWCNT, it is required to carry out detailed investigation into the effect of MWCNT content onto the structural stability and hence the properties of the composites for a higher ball milling time of 2 h.

Moreover it is known and also observed by the author that spark plasma sintering method of consolidation of composite powder produced by high energy ball milling is a very useful technique; not only does it ensure the achievement of near theoretical density by being sintered under pressure,but also the rapid heating and cooling coupled with the short residence time at comparatively low sintering

temperature are equally aiding to the retention of structural stability of MWCNT and inhibition of grain growth. However, iron -MWCNT system is altogether a different one due to the high sensitivity of its constituents to interact with each other. Even at a low temperature of spark plasma sintering, carbon atoms can diffuse very well into the iron crystals and form solid solution. Moreover, high thermodynamic driving force for dissolution of carbon in iron under an ambience of high carbon potential may induce damage of MWCNT during spark plasma sintering process. Thus, after ball milling, the powder of composite subjected to SPS, is no less free from the risk of further structural and hence property degradation. In fact, there is no report of systematic study to understand if spark plasma sintering causes further damage to the structure of the composites after it has been subjected to high energy ball milling for a period of 2h.

The present chapter reports the results of investigation on the effect of MWCNT content on the structure of iron matrix composites; it further estimates the quality of structures retained in composites after spark plasma sintering of the high energy ball milled composite powders. Finally, the properties of the composites produced by HEBM followed by SPS are characterized and then correlated with its microstructures.

## 8.2 Experimental Procedure

### *8.2.1 Materials*

The raw materials used in this study consist of Fe powder and multiwall carbon nanotube. Fe powder (purity ≥99%, -325 mesh, particle size 43 micron), are irregular in shape and MWCNTs purchased from Nanoshel (with diameter and length are 16-20 nm and 3-8 μm, respectively), are used as the reinforcement. Figure 1 shows the FE-SEM and figures 2(a-b) shows the TEM and HR-TEM microstructure of the as-received CNTs used for the present experimentation.

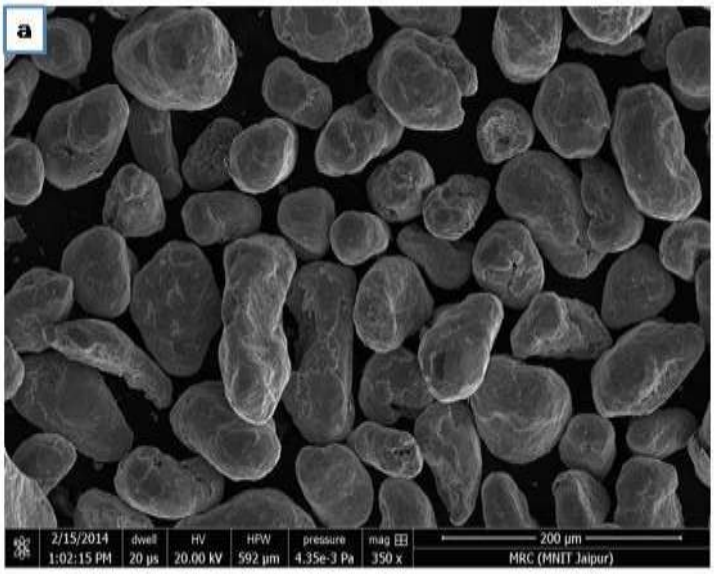


**Figure8.1** SEM image of the pure iron used as raw material.

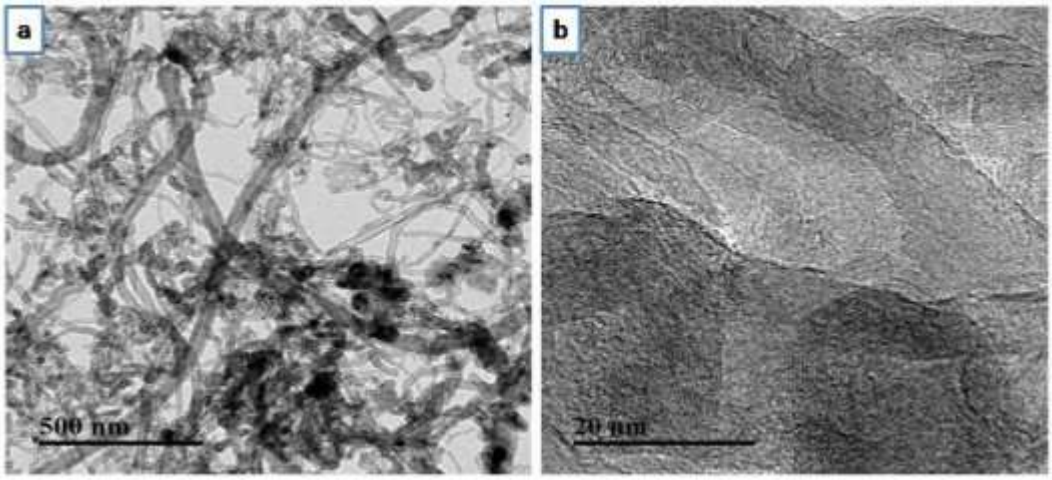


**Figure 8.2** (a) TEM image of MWCNT and (b) HR-TEM of WMCNT.

### *8.2.2 Mixing and Mechanical Alloying*

The iron powder (Fe) with various weight percent of MWCNTs (0.5, 1, 2 and 3 wt.%) are mechanically alloyed by utilizing Pulverisette-P6 high energy planetary ball mill (Fritsch, Germany) by using the tungsten carbide vial and ball. Ball to powder weight ratio is maintained at around 6:1. Stearic acid is used as the process control agent (PCA) to prevent excessive cold welding on the surface of the ball and vial and also to provide reducing atmosphere during the milling. The milling is carried out for two h in a planetary ball mill at 200 RPM. The mechanically milled powders Fe-MWCNTs with various weight present of

MWCNTs (0.5, 1, 2, and 3wt. %) were sintered by spark plasma sintering method using a Dr. Sintered (Model SPS -625 at IIT Kharagpur). The sintering procedure has been same as described in Chapter 3.The milled powders of Fe-MWCNT are sintered by SPS at $700^0$C. The holding time at the sintering temperature, the heating rate, and applied load are 10 min, $100^0$C/min and 60MPa, respectively. After spark plasma sintering, the sintered samples of diameter and height around20mm x 5mm arepolished by SiC paper to take out surface contamination of the sintered sampleafter then find out the mechanical and physical properties of Fe-MWCNTs nanocomposites.

X-ray diffractometer (XRD, Philips X'Pert with Cu Kα radiation) was utilized to analyze the constituent phases in the composite powder (Fe-MWCNT).The measurement procedure is same as described in Chapter3. Microstructures of polished samples are studied by optical microscopy and field emission scanning electron microscope (FESEM).Transmission electron microscope (TecnaiF-20) was used for the detailed structural study of Fe-MWCNT composite. HRTEM is used to observe the finer details in Fe-CNT composite. Vibrating Sample Magnetometer (VSM) of model EZ9 of makingMicrosence Company was used at the applied magnetic field from -20Oe to + 20Oe to study the room temperature magnetic behavior of the composites. Micro hardness characterization of the sintered composites was carried out by UHL VMHT (Walter Uhl Gmbh, Germany) micro hardness tester. The load of 300gf and dwell time of 15 sec is applied to take the hardness of the Fe-MWCNTs composite. An average of ten consistent results was taken as the representative hardness values. The compressive test of Fe-MWCNT composites is carried out at room temperature in an Instron (Model 8800)testing machine under a constant cross head speed with an initial strain rate of 0.05 $s^{-1}$.To conduct the compressive test, the samples are prepared in a cylindrical form with a height and diameter 5mm×5 mm.

XPS study was performed in Omicron Nanotechnology XPS system from Oxford Instruments (model ESCA+). The aluminum source was used for XPS study under high vacuum with monochromatic Al-Kα radiation at source energy of 1486.7

eV and a 124-mm hemispherical electron analyzer. Also, Fourier transform infrared spectrometer (Perkin Elmer Frontier) was used to obtain information about stretching vibration of different bonds present in HEBM nanocomposite from the corresponding FTIR spectra.

Raman spectroscopy was carried out at room temperature in AIRIX STR 500 CONFOCAL MICRO Raman Spectrometer. Raman spectra of nanocomposites milled for various times were recorded under Argon Ion laser excitation at 514nm at a very low power (< 1mW) to avoid excessive heating.

## 8.3 Results and Discussions

### *8.3.1 Scanning electron microscopy*

Scanning electron micrographs in figure 8.3 show the structure of iron-MWCNT composites of varying MWCNT content after being subjected to high energy ball milling for 2h.SEM photograph of iron 0.5 wt.% MWCNT powder reveals that considerable deformation of powder particles has taken place. It is observed from figure 8.3(a,b,c,d) that the tendency of flattening due to plastic deformation decreases with increasing MWCNT content of composites. Powder particles of Fe-3 wt.% MWCNT composites are not flattened much due to ball milling for 2 hrs. SEM photographs (figures 8.3e,f,g,h) at high magnification help to study the dispersion behavior of high energy ball milled Fe-MWCNT composites as function of MWCNT content.

It is clear from figure3(e) that for a low MWCNT content, ~0.5wt.%, MWCNTs are embedded well into the matrix metal and are more or less uniformly distributed. It is apparent from figures 8.3 (g)& (h), that with increase in the amount of MWCNT, the quality of dispersion of reinforcing MWCNT into the matrix metal becomes degraded. AlthoughFe-1 wt.% MWCNT (figure8.3f) exhibits reasonably good dispersion even at higher population density of MWCNT, the agglomerated regions are prominent at places. Moreover, the particles of composite with MWCNT content more than 1 wt.% cannot embed into the matrix metal as good as the composites of lower MWCNT content.

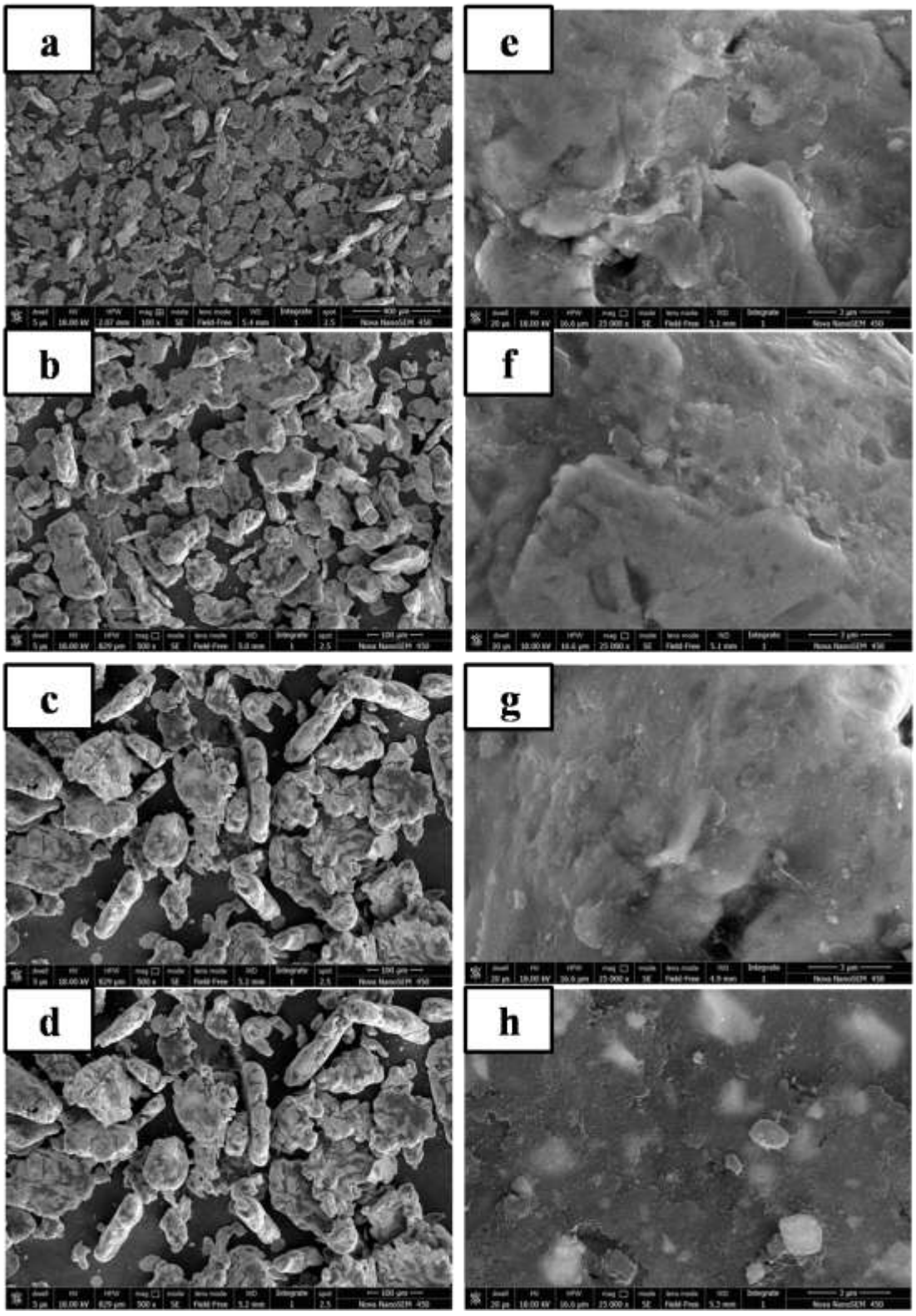


**Figure 8.3** SEM images of Fe-MWCNTs composites with varying weight percent of MWCNT in matrix Fe.(a)Fe-0.5 wt.%MWCNT(b)Fe-1wt.%MWCNTs(c)Fe-2 wt.%MWCNTs(d)Fe-3 wt.%MWCNTs and (e-h**)**SEM image at higher magnification of Fe-MWCNT composite after 2h milling.

The MWCNT used for the present investigation are curly with a high aspect ratio(figure8.2); this together with Vander Waal's forces of attraction among MWCNTs is known to increase the tendency for agglomeration of nanotubes; this tendency is enhanced at higher concentration of MWCNTs(figure8.3g, h). Because of the specific morphology, MWCNT forms a 2D network surrounding the powder particles during high energy ball milling. The soft iron powders of low strain hardening exponent can undergo deformation and flattening so long as the resistance to radial plastic flow matrix material is low at low reinforcement content. With increasing MWCNT content, the force imposed onto the system under HEBM is partitioned more to the MWCNTs; thus metal powders receive less energy for deformation. Also 2D network at higher density of MWCNT are more resistive to plastic flow in radial direction. This explains why the degree of flattening is found to be less in 3 wt.% MWCNT composite. Also at higher concentration, MWCNTs are very prone to agglomeration. This along with less plastic deformation of iron powders restricts MWCNT to satisfactorily disperse and embed into the matrix. However, high magnification SEM photographs in figure 8.3(e-h)delineates a good interfacial bonding of MWCNT embedded into the matrix metal.

### *8.3.2 Transmission electron metallography of powder composite*

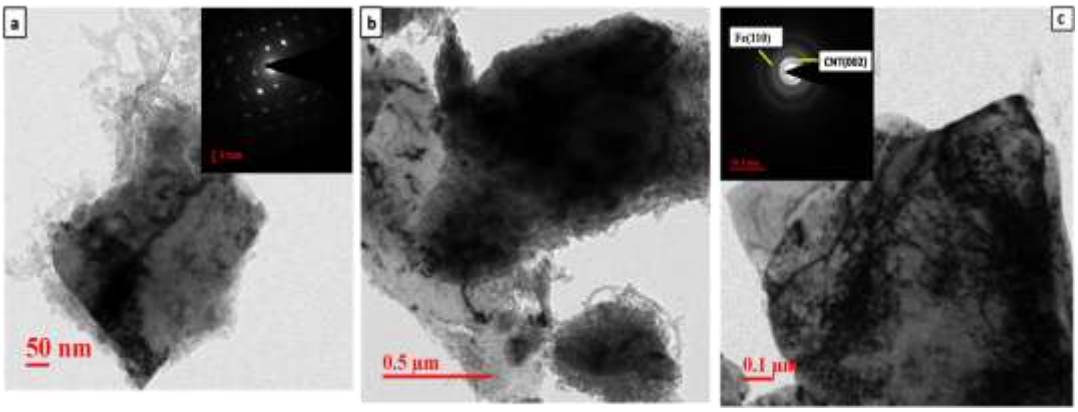


**Figure 8.4** TEM image of powder samples after 2h HEBM (a) Fe-0.5 wt.%MWCNTs (b) Fe-2 wt.% MWCNTs and (c) Fe-3 wt.% MWCNTs

Transmission electron microscopic studies of HEBM iron-MWCNT composite powders have revealed that the powder particles are surrounded by a network of MWCNT [figure(8.4a–c)].In case of 0.5 wt.%MWCNT composite, MWCNTs are found to be embedded well within the particles. Also it appears from

TEM photograph, that the particles are deformed with a lot of dislocations present within them (figure4a-c). The SAED pattern in the inset of figure8.4(a) shows (110) reflection from matrix and the spots are seen to be highly streaked. This is indicative of a huge strain within the deformed particles. A higher resolution TEM picture demonstrates a good dispersion of MWCNT with adequate interfacial bonding (figure8.4b).figure8.4(c) demonstrates that when MWCNT content is high (~2 wt.%), the MWCNTs are agglomerated at various places within the powder particles, which besides being surrounded by MWCNT network, also exhibits some MWCNTs well embedded into the matrix metal.

### *8.3.3 Optical microscopy of Spark Plasma Sintered samples*

The optical microstructures of spark plasma sintered samples are shown in Figure 8.5 (a-c). It is evident from the microstructures that MWCNTs form network structure at the particle boundaries. Individual particle is comprised of several grains.

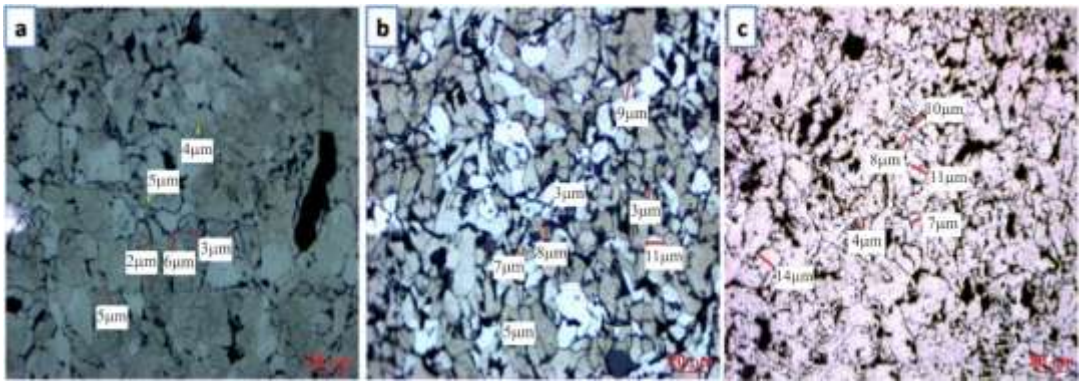


**Figure 8.5**Optical microstructure after SPS (a) Fe- 0.5 wt.% MWCNTs (b) Fe-1 wt.% MWCNTs and (c) Fe-2 wt.% MWCNTs; the microstructures show that grain size increases with increasing percentage of MWCNTs.

In this work, SPS has been deliberately carried out at a low temperature with rapid rate of heating and cooling so as to conserve the structure of MWCNTs. SPS is carried out in a closed die at a pressure of 50 MPa at $650^0$C. Due to deformation of iron particles at high temperature, extensive recrystallization has taken place and very fine grains are resulted. The same general feature is observed in figure8.5 (b) and figure8.5(c). However, it is apparent that at higher MWCNT content intensive network is formed. Evidence of recrystallized grains are noticed in both figure 8.5(b) and figure8.5(c). The grain size variation of composites after spark plasma sintering

is shown in figure8.6. It is seen from the figure that the grain size increases with increase in MWCNT content. As evident from the optical microstructures, MWCNTs form network at the grain boundaries of powder particles. While subjected to high pressure during SPS, the iron particles deform; however deformation is constrained by network of MWCNT.

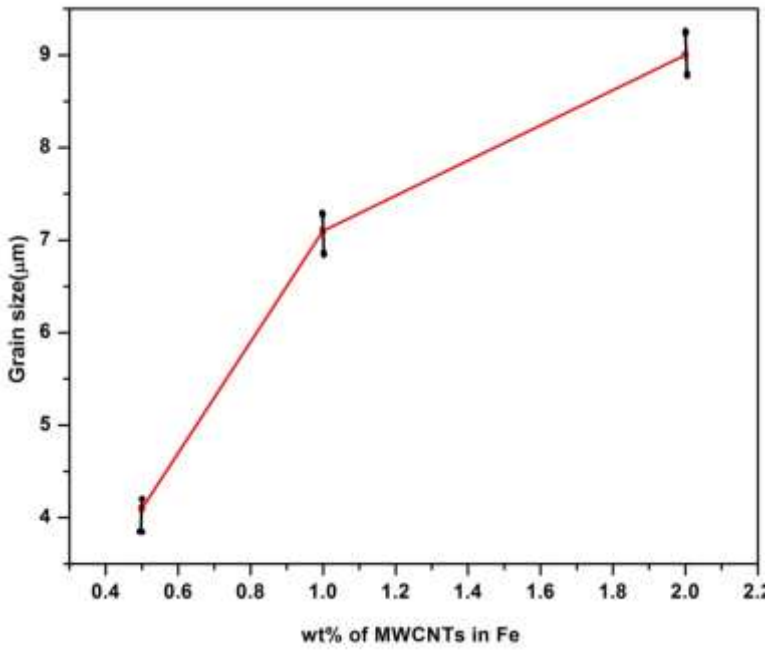


**Figure 8.6** Effect on grain size of weight percent of MWCNT in matrix (Fe)

Since, sintering temperature is higher than the recrystallization temperature of matrix metal, the grains are recrystallized and fine recrystallized grain structure is formed. At higher MWCNT content, the deforming force is partitioned more to the ultra-strong MWCNTs; thus higher MWCNT content shares higher deforming force applied during SPS. As a result, less deformation is experienced by iron matrix. Since deformation of iron is less at higher MWCNT content, the number of effective nuclei for recrystallization is small. As a result, there crystallized grain size is higher at higher MWCNT level. The thick network in high MWCNT composite is indicative of high degree of agglomeration and entanglement of MWCNTs. This reduces the effective aspect ratio of MWCNT and also leaves small sized pores within the agglomeration of MWCNTs.

### *8.3.4 Microstructural Analysis of SPS Samples by Scanning Electron Microscopy*

The SEM photographs of SPS samples are shown in figure 8.7(a-c); in general, the SEM observation corroborates the results obtained in optical microscopy. Black constituents are seen to decorate the grain boundary.

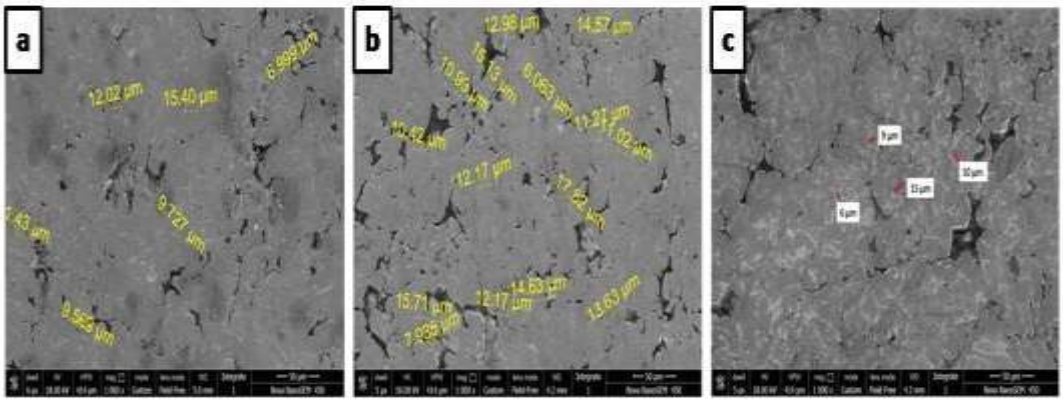


**Figure 8.7** SEM micrographs after SPS (a) Fe-1 wt.% MWCNTs (b) Fe-2 wt.% MWCNTs and (c) Fe-3 wt.% MWCNTs

The grain sizes measured from SEM pictures are similar to the observations obtained from optical micrographs. At high concentration of MWCNT, grain size is found to be higher than that for the lower MWCNT content. The amount of black constituents increases with increase in MWCNT. It is observed at high magnification that massive agglomeration of MWCNT tales place. Massive network is seen in iron-2wt.% MWCNT composite sample. Interestingly, a lamellar structure is noticed at the grain boundary triple points of composites of high MWCNT content. When the MWCNT content is higher, the lamellar structure at the grain boundary triple points is found to be more prevalent. For example, a much higher amount of lamellar constituent is observed in iron-3 wt.% MWCNT composite sample. Alternate bands of white constituents are observed at the grain boundary triple points in 3wt. % MWCNT composites. Seemingly these are the MWCNTs aligned in specific directions with good chemical bonding at the interface with iron matrix.

From the appearance of the lamellar structure observed at high magnification(figure8.7d-8.7e) it seems that some new phases with threaded morphology have formed onto the directionally aligned MWCNT phase.

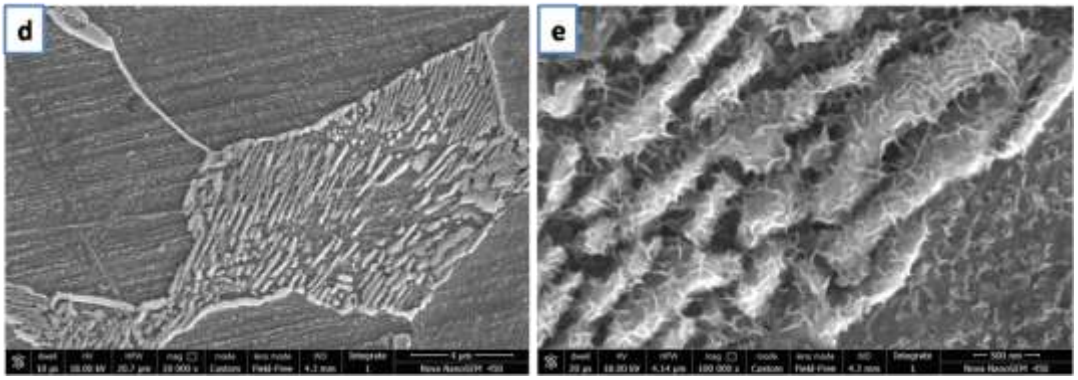


**Figure 8.7**SEM shows the (d) pearlite like lamellar structure and (e)shows the same at higher magnification.

Carbon is known to be austenite stabilizer. Close contact between MWCNT and iron is envisaged in iron-3 wt.% MWCNTs; when subjected to sintering temperature, $650^0$C, under 50 MPa pressure, transformation of BCC iron to austenite of closed packed FCC structure seems plausible at the so called subcritical temperature; austenite can hold high amount of carbon in solid solution. Upon cooling from sintering temperature, this austenite of high carbon content gives rise to discontinuous precipitation of cementite onto the residual MWCNT. This leads to the formation of ferrite; since all MWCNTs could not be destroyed; discontinuous precipitation of cementite takes place at the ferrite/ MWCNT boundaries and on the existing MWCNTs. However a detailed study for the formation of such pearlite like phase mixture of peculiar morphology of carbon rich phases as seen in figure 8.7(e) is required to gather proper understanding. As stated earlier, the black regions are constituted by agglomerated MWCNTs which contain micro voids within the agglomerates.

### *8.3.5. XRD Studies*

X–ray diffractogram of powder sample of Fe-MWCNT composites are shown in figure 8.8(a).The spectra are seen to record increasing tendency of formation of $Fe_3C$ with increasing MWCNT content. The prominent peak of $Fe_3C$ in Fe-3 wt.% MWCNT composite suggests that the tubular structure of MWCNT is damaged when it is high energy ball milled with iron for 2 h.

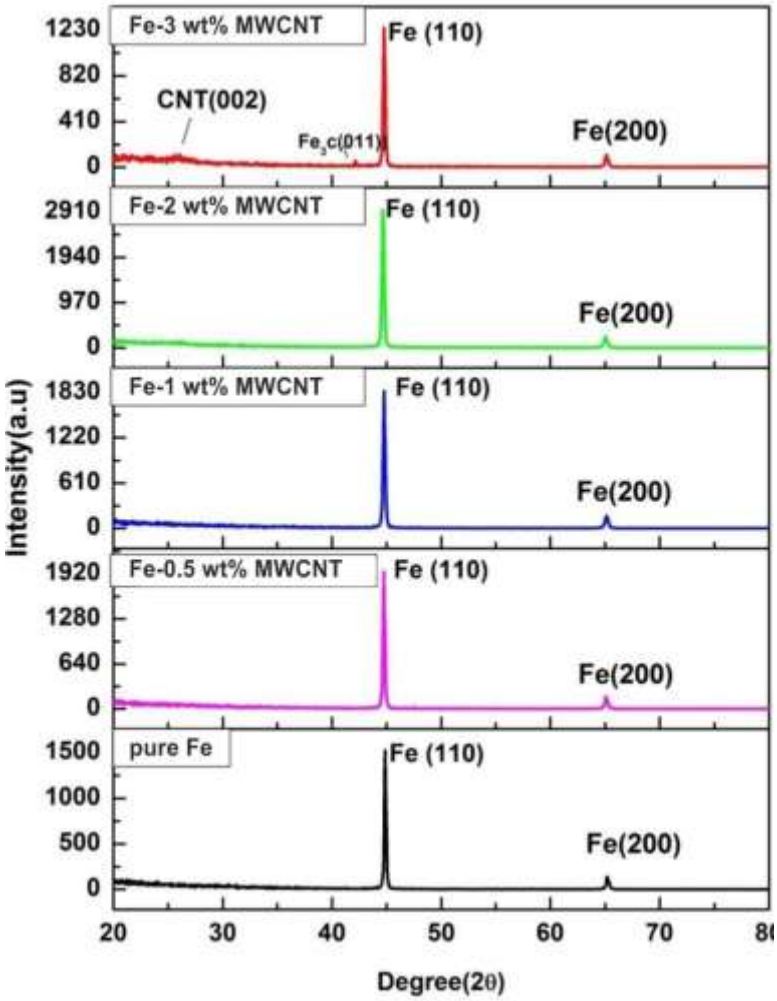


**Figure 8.8 (a)** XRD pattern of different weight percent of MWCNTs in Fe.

It is observed from Table 8.1 that HEBM of iron matrix composites of increasing MWCNT content gives rise to a shift of major XRD peak of iron, (110) towards low angle side.

**Table8.1**. shows the peak (110) shifting in Fe-MWCNTs after 2h milling

| **Samples Name** | **Initial peak of Fe and Fe-MWCNTs nanocomposites** | **Peak Shifting** |
|---|---|---|
| Pure Fe (110) | 2θ=44.7606019 | ZERO |
| Fe-0.5 wt% MWCNTs(110) | 2θ=44.7058824 | 0.0136 |
| Fe-1 wt% MWCNTs(110) | 2θ=44.7047923 | 0.0547 |
| Fe-2 wt% MWCNTs(110) | 2θ = 44.701956 | 0.0562 |
| Fe-3 wt% MWCNTs(110) | 2θ=44.7705622 | (0.0099)shifting in higher angle side |

This shift of XRD peak is indicative of increase in lattice parameter of iron till 2wt.% MWCNT; beyond 2wt.% MWCNT, the XRD peak is seen to be shifted towards high angle side. Iron has high affinity for carbon. It is further envisaged that high energy ball milling can destroy MWCNT structures and can produce amorphous carbon. The carbon atoms so released, can diffuse into iron lattice and form carbon rich solid solution; in fact, high supersaturation in heavily deformed iron is reported elsewhere [5]. Higher is the MWCNT content of composites, greater is the availability of carbon atoms for dissolution in iron. As a result, degree of super-saturation is increased. This explains the observation that higher degree of peak shift takes place with increasing amount of MWCNT in composites. However, when MWCNT content is increased to as high as 3wt.%, the (110) Fe peak is found to be shifted to higher angle side.

The corresponding X –ray diffractogram records prominent $Fe_3C$ peak. This suggests that high energy ball milling leads to damage of MWCNT and hence releases the carbon atoms which diffuse in iron lattice and form iron rich solid solution. At certain values of MWCNTs, super-saturation can no longer be permitted and cementite precipitation takes place. When all the carbon atoms come out of solution by way of precipitating cementite, the lattice parameter is to decrease as evidenced by the shift of (110) peak towards right. When the same composites are subjected to spark plasma sintering, their XRD plots become significantly different. Appearance of $Fe_3C$ peak is evident at 2 wt.% MWCNT and for 3wt.% the concerned peaks become much stronger than that noticed in powder sample of composite. This means that SPS has led to further damage of MWCNT structure. The XRD spectra of samples after SPS are shown in figure 8.8 (b).

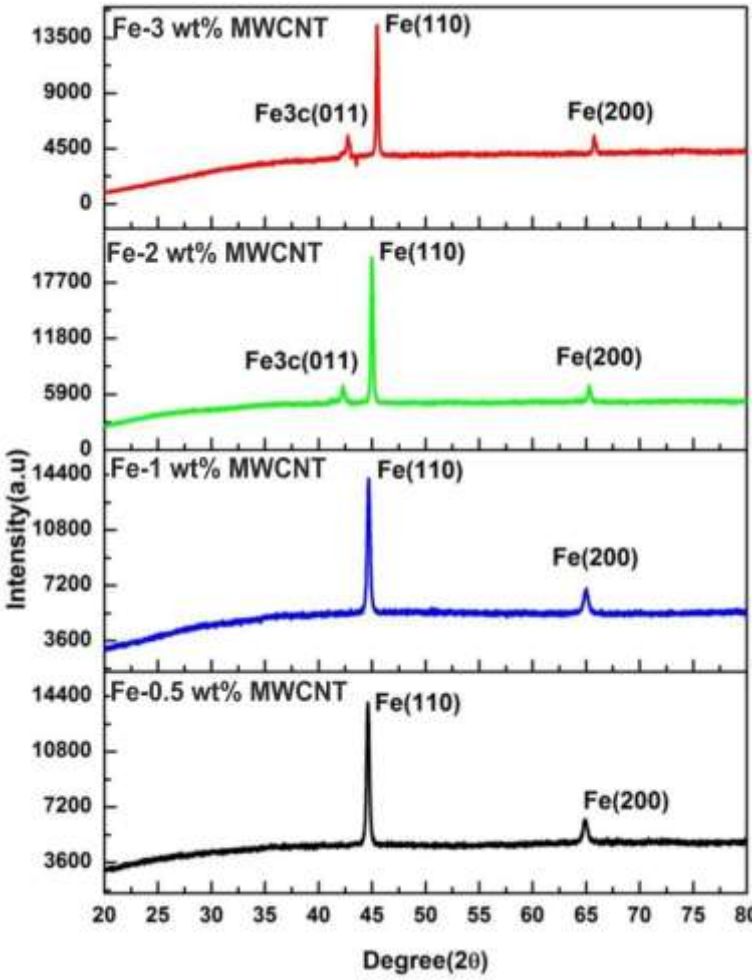


**Figure 8.8**(b) XRD pattern of different weight percent of MWCNTs in Fe after SPS.

It is revealed from the said spectra that distinct peaks of cementite start appearing in composites containing of 2wt.% MWCNT. For a 3 wt.% MWCNT composite the peaks of cementite is significantly enlarged. The results of XRD after SPS show that the reaction between iron and MWCNT does not take place when the MWCNT is 1 wt.% or less. For 2wt.% or more MWCNT content, the powders of composite after ball milling contained carbon rich phase and $Fe_3C$, whereas $Fe_3C$ content is very high for 3wt.%MWCNT. XRD of SPS sample follows the same trend with appearance of strong $Fe_3C$ peak. This tends to indicate that during SPS the damage of MWCNT takes place. It is unlikely that holding for a short time can dissolve cementite in the matrix. From the results of Table 8.2, it is observed that there is considerable shift of (110) Fe peak from the corresponding peak positions in HEBM powder composites.

**Table 8.2**. XRD Peaks (110) shifting after SPS.

| Samples Name | Initial peak of Fe and Fe-MWCNTs nanocomposites | Peak Shifting |
|---|---|---|
| Pure Fe (110) | 2θ = 44.746922 | zero |
| Fe-0.5 wt.% MWCNTs(110) | 2θ = 44.6511628 | 0.0957 |
| Fe-1 wt.% MWCNTs(110) | 2θ = 44.5827633 | 0.1641 |
| Fe-2 wt.% MWCNTs(110) | 2θ = 44.4719562 | 0.2749 |
| Fe-3 wt.% MWCNTs(110) | 2θ =44.765432 | (0.0865 )shifting higher angle side |

This means that SPS has led to further damage of MWCNT and carbon atoms diffuse into the matrix phase. Because the carbon atoms occupy the dislocations in matrix phase of powder composites, dislocation becomes immobile and substructure remains conserved after SPS. High pressure and temperature during SPS lead to breakage of bonds in MWCNT and the amorphous carbon so generated can diffuse easily into the matrix phase and get segregated at dislocations.

However at higher MWCNT levels $Fe_3C$ was present in the microstructures of HEBM powders; SPS of the powders has led to release of extra amount of carbon, which could undergo chemical reaction with iron, forms cementite which is finally precipitated on to the existing cementite or may be even separately.

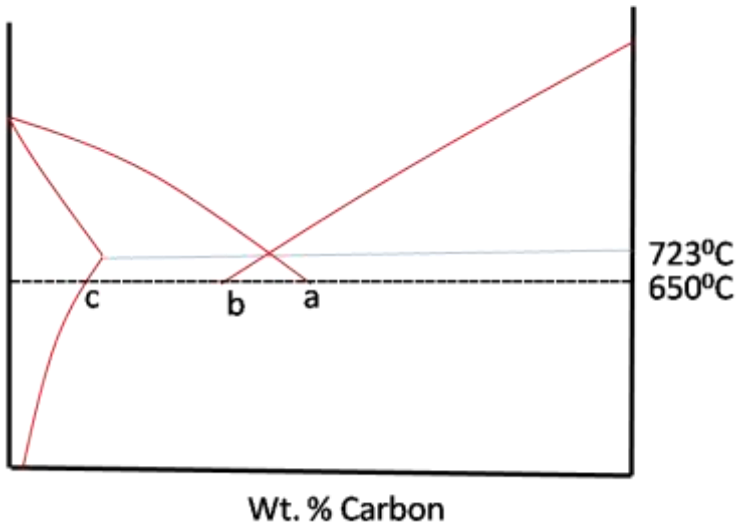


**Figure 8.8** (c) Equilibrium diagram of Fe-C system

High compressive forces and the high temperature during SPS may aid in the transformation of ferrite plus cementite to FCC austenite of higher carbon content. It is evident from the equilibrium diagram in figure8.8(c)that increasing carbon content beyond 'c' makes it possible to form austenite whose equilibrium carbon content is given by the point 'a'; any carbon content of iron between 'c' and 'a' leads to separation of phases into ferrite of composition 'c' and austenite of composition 'a'. However beyond a concentration of 'b', austenite rejects carbon and attains a composition 'b'. Formation of competitive austenite is possible at $650^0$C due to the reason that carbon is an austenite former and local supersaturation in excess of 'a' shall produce austenite. Evenif the temperature is less than the equilibrium transformation of ferrite to austenite. When cooled, austenite undergoes discontinuous precipitation of carbide mainly on the existing MWCNT and alternate lamellae of ferrite and cementite are formed. This is evident in scanning electron micrograph of 3 wt.% MWCNT composite (figure8.7d& 8.7e). Thus it appears that during SPS degradation of MWCNT takes place mainly by dissolution of carbon in iron till 2 wt.% MWCNT beyond which supersaturation becomes intolerable and precipitation of carbide takes place.

### *8.3.6 Raman spectroscopy*

When subjected to high energy ball milling with metal powders, MWCNTs are known to suffer intensive damage [9].However, in the case of high energy ball milling of MWCNT with iron, structural degradation of MWCNT may be quite severe. This is because of the proneness of reaction between iron and carbon. Carbon has a high solubility in iron at high temperature and can remain supersaturated under non equilibrium situation. Super saturation is relieved by formation of carbides which are metastable phases in iron-carbon system. Raman spectroscopy is a useful tool to understand the possible destruction of MWCNT structure; so it has been employed for the above stated purpose and the results are shown in figure 8.9(a).

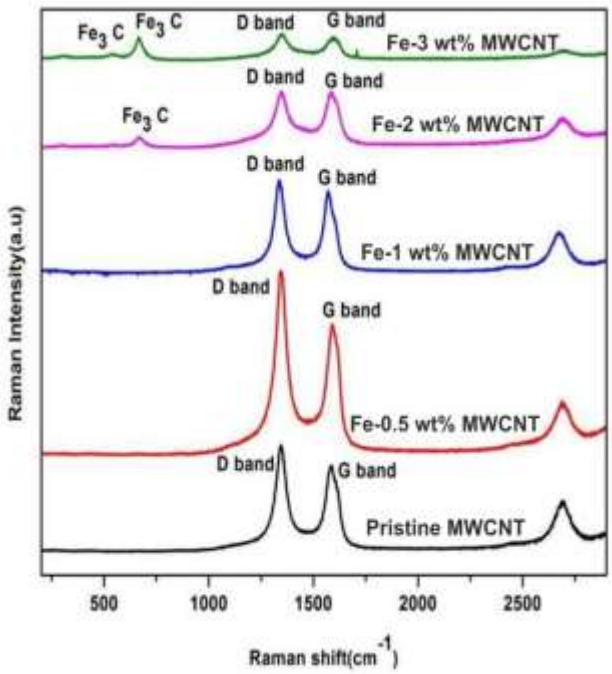


**Figure 8.9** (a) Raman spectra of powder samples after 2h high energy ball milling with different weight present of MWCNTs in matrix (Fe).

Raman spectrum of pristine MWCNT records first order peaks of D and G bands at 1352cm$^{-1}$and 1555cm$^{-1}$respectively, which authenticate the presence of perfect graphitic structure of MWCNT. Another peak at 2700 cm-$^{1}$assigned as G' elsewhere, is also observed in Pristine MWCNT and the iron matrix-MWCNT composites. It is well known that any defect in MWCNT on account of harsh ball milling with metal powders directly influences the sp2 bonding and hence both the vibration of atoms in rings and tangential stretching vibration of sp2 bonded carbon atoms in MWCNT. These give rise to the change in the shape, size and position of the D and G bands. The influence of defects on D and G band leads to a rise in intensity ratio, $I_D/I_G$ of D and G band. It can be seen from Raman spectra of HEBM composite powders that almost perfect graphitic structure is conserved in 0.5 wt. % MWCNT composite. Increasing the MWCNT content leads to a small shift of G band along with marginal rise in $I_D/I_G$ ratio. The position of D and G band along with $I_D/I_G$ ratio of various composites are shown in Table.8.3. The presence of sharp G and D bands are indicative of the fact that only a small structural damage has taken place till 1wt.% of MWCNT in the composites. Incidentally, increasing the

MWCNT content to 2wt.%makes it apparent that D and G bands are considerably shortened with appreciable shift in their positions.

**Table 8.3** Position of D and G bands along with $I_D/I_G$ ratios in Raman spectra after 2h high energy ball milling.

| Sample Name | Raman Peak Shift ($Cm^{-1}$) | | $I_D/I_G$ |
|---|---|---|---|
| | D band | G band | |
| Pristine MWCNT | 1343 | 1571 | 0.98 |
| Fe-0.5 wt.% MWCNT | 1347 | 1575 | 1.02 |
| Fe-1 wt.% MWCNT | 1353 | 1579 | 1.05 |
| Fe-2 wt.% MWCNT | 1359 | 1585 | 1.11 |
| Fe-3 wt.% MWCNT | 1363 | 1589 | 1.13 |

$I_D/I_G$ ratio has significantly increased to suggest that a good amount of damage is caused to MWCNTs. This observation is supplemented by the perceptible widening of G' band; this bears the signature of amorphisation taking place within the composite. Interestingly, Raman peaks characterizing cementite phase ($Fe_3C$)is seen to appear in the Raman spectrum of 2 wt.% MWCNT composite. It means that damage of MWCNTs has led to the formation of amorphous carbon which, apart from diffusing within iron crystals to produce carbon rich solid solution of iron, reacts with iron to form cementite. Increasing MWCNT content to 3wt.% aggravates the situation. There is the appearance of strong peaks of $Fe_3C$ with substantial shortening and widening of D and G bands. At the same time G' band is significantly distorted by broadening. All these observations together with the fact that there has been appreciable rise in $I_D/I_G$ (~1.13) ratio ascertains that high energy ball milling of 3 wt.% MWCNT composite for 2hleads to significant destruction of the graphitic structure of MWCNTs. While mechano- chemical synthesis of iron and carbon to form $Fe_3C$ cannot be ruled out, the gradual increase in lattice parameter as demonstrated by XRD analyses makes one believe that the damage of MWCNTs is envisaged in the form of breakage of C-C bonds in MWCNTs, which releases carbon atoms; they diffuse into the iron matrix and finally precipitates out cementite when a definite degree of supersaturation is exceeded.

Corroborating the XRD results, the Raman spectroscopy of spark plasma sintered samples demonstrate that additional damage of MWCNT takes place over and above what occurs during HEBM. In consideration of size, shape and positional change of D and G band along with the observed $I_D/I_G$ ratios, it becomes apparent that SPS has led to further damage of MWCNTs in composites While structure of MWCNT is conserved better till 1wt.% MWCNT composite, there is always some damage of MWCNT structure as demonstrated by the characteristics of Raman Spectra and its results, presented in Table 8.4. Damage of MWCNT structure is much intensified at higher MWCNT content ~2wt.% to 3 wt.%. The ball milled powder of ~2wt.% to 3wt.% MWCNT composites are seen to be comprised of $Fe_3C$ particles with structurally degraded MWCNTs. After sintering, the Raman spectra show much stronger peaks of cementite with concurrent changes in size and shape of D and G bands(figure8.9b). For 3 wt.% MWCNT composite, the G band has become very small and wide with G' band featuring a great deal of amorphisation of MWCNTs.

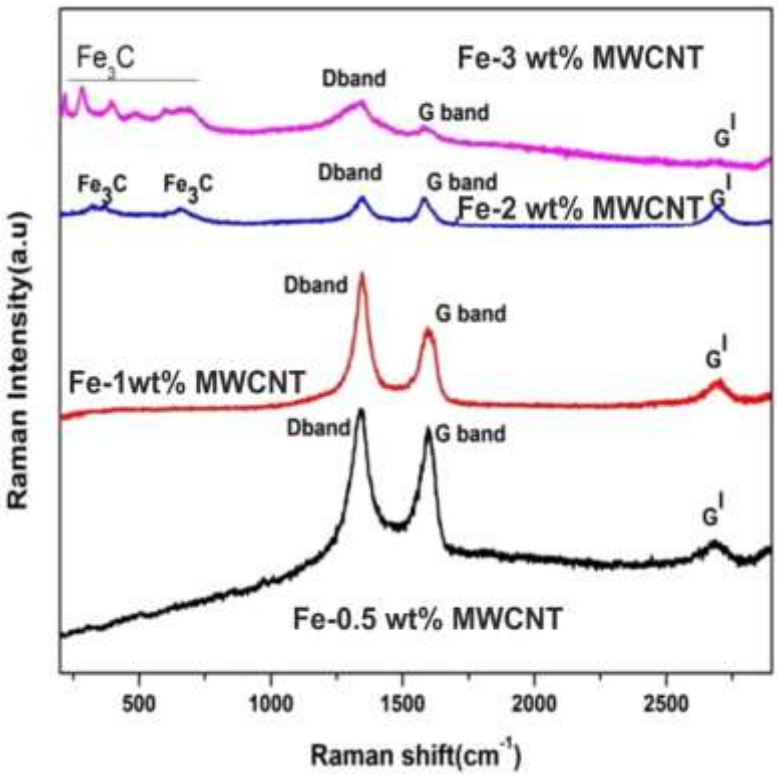


**Figure 8.9** (b) Raman spectra of samples(Fe-MWCNTs) with different weight present of MWCNT in Fe after spark plasma sintering.

**Table 8.4** Position of bands and $I_D/I_G$ ratios in Raman spectra after SPS.

| Sample Name | Raman Peak Shift ($Cm^{-1}$) | | $I_D/I_G$ |
|---|---|---|---|
| | D band | G band | |
| Fe-0.5 wt.%MWCNT | 1349 | 1577 | 1.03 |
| Fe- 1 wt.%MWCNT | 1357 | 1581 | 1.07 |
| Fe- 2 wt.% MWCNT | 1365 | 1589 | 1.14 |
| Fe-3 wt.%MWCNT | 1371 | 1593 | 1.17 |

This is further supported by a very high value of $I_D/I_G$ ratio of 1.19 in case of sintered Fe-3wt.%MWCNT composite. The appearance of stronger $Fe_3C$ peaks in SPS sample of Fe-MWCNT composite implies that amorphous carbon is produced aplenty during SPS. SPS was carried out at 50MPa and $650^0$C. Thus the damage caused to MWCNT and consequent enhancement in cementite formation is thought to be due to thermo mechanical effect imposed on partially damaged MWCNT with presence of $Fe_3C$ in its close vicinity. The formation of carbide takes place at the interface for being energetically cheaper. Thermo mechanical exposure of MWCNT during SPS makes them amenable for producing more carbon atoms which react with iron to form cementite. One more possibility viz. formation of high carbon austenite at the SPS temperature cannot be ruled out. In the event this happens, the post SPS cooling will effect decomposition of austenite through a discontinuous precipitation reaction akin to pearltic transformation. The Microstructural features in SEM of 3 wt.% MWCNT composite are supportive to this conjecture. Under static pressure at temperatures above the recrystallization temperature, mechano-chemical synthesis as is common in HEBM is unlikely to occur in case of SPS; rather SPS may accentuate parameters to cause amorphization. Higher wt.% of MWCNT implies that higher amount of load is shared by MWCNTs. Also the interfacial area for reaction to take places increases in proportion to increase in MWCNT content. Hence overall quantity of carbide is increased as observed in Raman spectroscopy. During SPS, the system is initially comprised of the intimately bonded CNT with supersaturated iron. When such entity is subjected to high temperature and pressure, there will be more thermodynamic urge for the formation of metastable cementite phase. If the binding energy between carbon atoms in MWCNT is exceeded by the energy of interaction between iron and carbon atoms, the dictate of thermodynamics

will entice carbon atoms to get detached from neighboring carbon atoms and will insure its' bonding with iron atoms. This happens because both the applied pressure and sintering temperature are responsible for lowering bonding potential between any two carbon atoms in MWCNT. When carbon content in iron is very high, the consequential structural instability ultimately leads to precipitation of cementite.

### *8.3.7 Assessment of quality of bonding by FTIR Analysis*

FTIR studies for iron-MWCNT composites in HEBM condition as well as after SPS are carried out to obtain hints about the possible changes in bonding quality. The FTIR spectra of both the milled powder sample and those of the samples after SPS are presented in figure8.10a and8.10b.

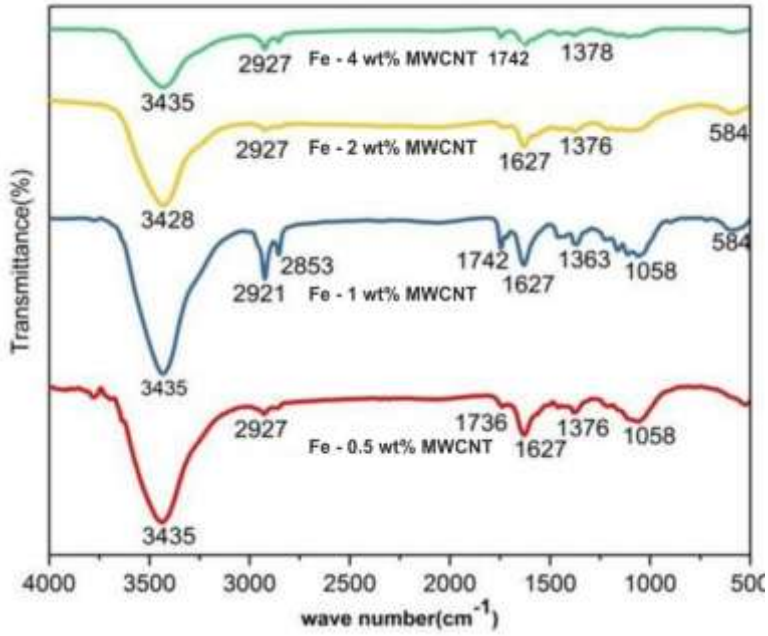


**Figure 8.10** (a) FTIR spectra Fe/MWCNTs with various wt.% percent of MWCNTs in Fe after 2h HEBM.

FTIR spectra of powder samples record peaks at 1627 $cm^{-1}$ and 1058 $cm^{-1}$; while the peak at 1627 $cm^{-1}$ originates from C=C stretching vibration, the IR activated graphitic C-C stretching vibration mode gives rise to the other peak at1058 $cm^{-1}$. The peak at 584 $cm^{-1}$ represents absorbing peaks of Maghemite ($Fe_2O_3$) and magnetite ($Fe_3O_4$) [$Fe^{2+}Fe^{3+}{}_2O_4$][10-11]. The normally observed peak due to Fe-O stretching vibration in pristine MWCNT is absent in FTIR spectra obtained from Fe-MWCNT composites of varying MWCNT content. It may be noted from figure8.10a, that increasing MWCNT content to the level of 2 wt.% has led to

diminution in the intensity of C=C peak; its intensity is further reduced significantly at 3wt.% MWCNT. Almost similar observation can be made for the 1058 $cm^{-1}$peak which characterizes C-C stretching vibration; in this case, it is found that up to 1 wt.% MWCNT in iron matrix composite, this peak is visible, whereas it becomes drastically reduced by increasing the MWCNT beyond 1wt.%.It may be specifically mentioned that for 3wt.% MWCNT in composite, no C-C stretching peak is observed in concurrence with noticeably reduced intensity of C=C peak. At the same time, one would observe that the absorption peak is almost eliminated at 3 wt.% MWCNT composite.

The reduction in intensity of C=C or C-C peaks hints upon the destruction of concerned bonds in MWCNT and simultaneous presence of absorption peak implies that amorphous carbon produced out of destruction of C=C or C-C bond goes to form Fe-C bond, may be by 3d-2p hybridization [12],between iron and carbon atoms. However, absence of absorption peak with almost elimination of C-C peak leads to the conjecture that when MWCNT content is as high as 3 wt.%, the damage of MWCNT becomes so severe that mechano-chemical synthesis of iron and carbon takes over and forms $Fe_3C$ instead of carbon rich solid solution in iron. Formation of $Fe_3C$ is in fact proved by the results of Raman spectroscopy and X-Ray diffraction study. FTIR spectra of HEBM composite powders after SPS are shown in figure8.10(b).

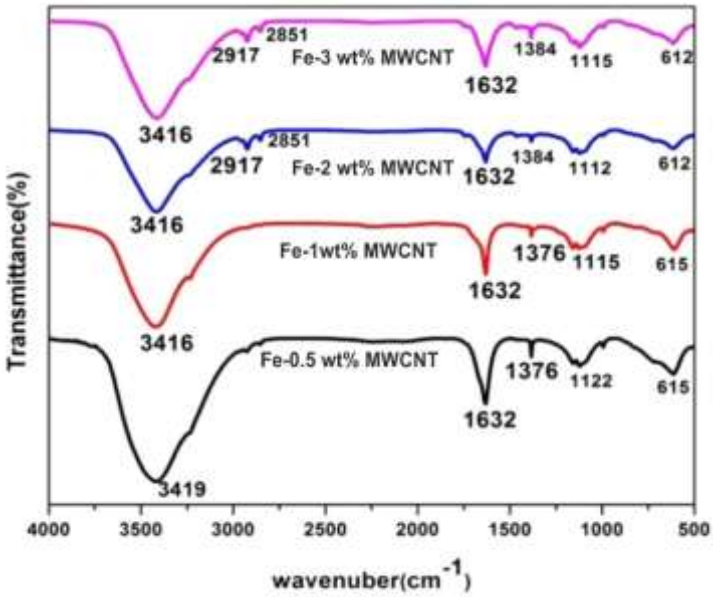


**Figure 8.10** (b) FTIR spectra of Fe-MWCNTs nanocomposites after SPS.

The revelation of reduction in intensity of peak at 1627 $cm^{-1}$ (C=C stretching vibration) till 2 wt.% MWCNT describes the damage of MWCNT structure. The slightly larger peak at 3wt.% MWCNT is at variance with other observation and may be due to variation in experimental condition. The appearance of a peak at 1112 $cm^{-1}$- 1122 $cm^{-1}$with simultaneous disappearance of peak due to C-C stretching vibration at 1054 $cm^{-1}$ is attributed to C-O stretching. Fe-C bonding is characterized by the absorption peaks at 612 $cm^{-1}$ 615 $cm^{-1}$ due to magnetite ($[Fe^{2+}\ Fe^{3+}{}_2O_4]$) and is at the loss of C-C bonding; this makes oxygen atoms available and creates a condition of formation of C-O bond. Stretching vibration of this bond has been responsible for the appearance of peaks at 1112 $cm^{-1}$- 1122 $cm^{-1}$.

### *8.3.8 Hardness test results*

Figure8.11shows the hardness values of iron-MWCNT composites of varying MWCNT content after spark plasma sintering. The curve in figure8.11shows an increase in the hardness value with increase in MWCNT amount till 2 wt.%. Beyond 2 wt.% a slight drop in hardness value is observed.

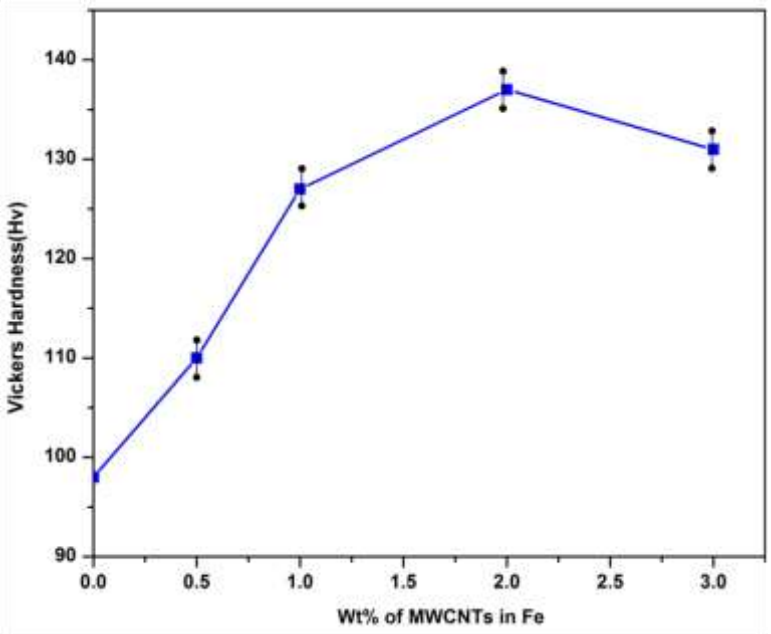


**Figure 8.11**Vickers hardness values of the sintered samples (Fe-MWCNT) composites after spark plasma sintering.

Reinforcing iron with MWCNT leads to significant improvement in strength properties. It is known that MWCNT has very high strength. The increment in hardness values in MWCNT reinforced iron matrix composites can be attributed to

various hardening mechanisms like refinement of matrix grains, dispersion strengthening due to nanotubes, solid solution hardening due to carbon dissolution in iron, dispersion strengthening due to fine scale carbide formation, strain hardening due mismatch in coefficient of thermal contraction of MWCNT and iron matrix during post SPS cooling which is quite fast [13-16]. In the instant case, the grain size is seen to increase with increasing MWCNT for reasons stated earlier. Therefore improvement in hardness is due to the other factors. As observed by an experiment there has been considerable damage of the structure of MWCNT and that the extent of damage is increased due to increase in amount of MWCNT. This has certainly reduced the capacity of dispersion strengthening due to MWCNT as it increases in amount.

Rather it continuously decreases the strength enhancement effect of MWCNTs reinforcing a metal matrix. In consideration of present experimental observation, solid solution hardening due to formation of carbon rich solid solution and dispersion hardening due to MWCNT and cementite formation are the chief hardening mechanisms; with increasing amount of MWCNT**,** both the carbon content of solid solution and the formation of cementite increases till 2 wt.%MWCNT with continuous damage of MWCNT. While the first two factors realize gain in hardness, the hardening effect due to MWCNT gets weakened rather than increasing the hardness at its higher concentration. So increasing MWCNT leads to combined enhancement of hardening due to solid solution and cementite with concurrent loss in the effectiveness of MWCNT in dispersion hardening. However, it has been observed that when MWCNT content is 3 wt.%, the carbon super saturation is fully relieved and cementite content increases which remains the main hardening agent. At the same time degeneration of tubular structure of MWCNT is quite significant. So dispersion hardening due to MWCNT decreases while hardening is enhanced only due to higher cementite content; concurrently solid solution hardening is also decreased. This leads to overall reduction in hardness value at 3 wt.% MWCNT. Moreover, it is found by metallographic study that MWCNTs at higher concentration exhibits higher tendency for agglomeration. Agglomerated MWCNT regions suffer from the problem of overall reduction in

effective aspect ratio and also contain many small sized voids within the entangled CNTs. This has the adverse effect on hardening. These are the reasons for the observed reduction in hardness at higher MWCNT content.

### *8.3.9 Compressive Test*

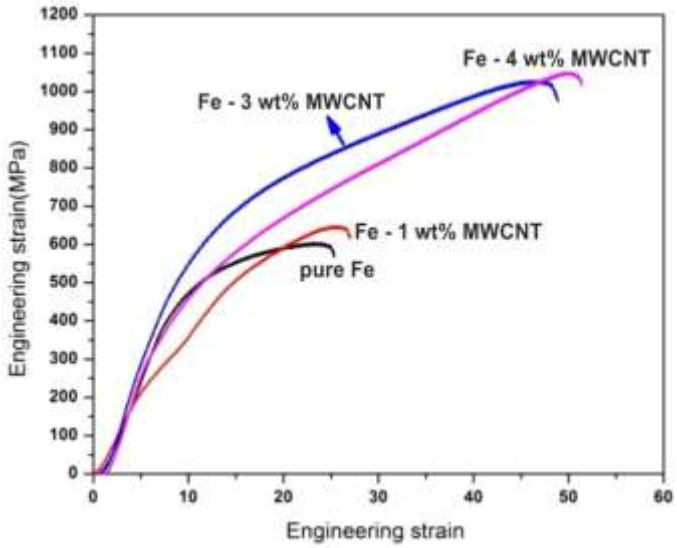


**Figure8.12** Compressive stress vs. strain curves of pure iron and Fe-MWCNTs composites after SPS

**Table 8.5** Results of compressive tests

| Sample Name | Compressive Strength[MPa] |
|---|---|
| Pure Fe | 595 |
| Fe-1 wt.% MWCNTs | 645 |
| Fe-3 wt.% MWCNTs | 1027 |
| Fe-4 wt.% MWCNTs | 1045 |

The results of compressive tests show that the strength of the composites increases with increasing MWCNT content (figure8.12) Corresponding values of compressive strength of the composites are presented in Table 8.5; it is seen that there is a steep rise in compressive strength beyond 1 wt. % MWCNT. At 3 or 4 wt.% MWCNT level the composite shows a rise in compressive strength by more than 100%. At the same time the strain is also quite high(figure8.12). More than 50% strain is recorded by the composites of higher MWCNT content. The

simultaneous improvement in strength and deformation strain can be ascribed to the fineness of microstructures. As noticed in microstructure studies, the MWCNTs become shorter and firmly embedded into the matrix. The enhancement of strength owes its origin to dispersion strengthening due to MWCNT and also strengthening due to nanosized precipitates of cementite. At the same time fine grains along with fineness of other structural constituents raise the ductility under compression. Due to fine distribution of MWCNT within the matrix, the propagation of cracks if formed during straining will greatly inhibited. This is the cause of the observed strain in composites of higher MWCNT content.

### *8.3.10 Magnetic behavior of iron-MWCNT composites*

Hysteresis loops in figure8.13 demonstrates ferromagnetic behavior of Fe-MWCNT composites.

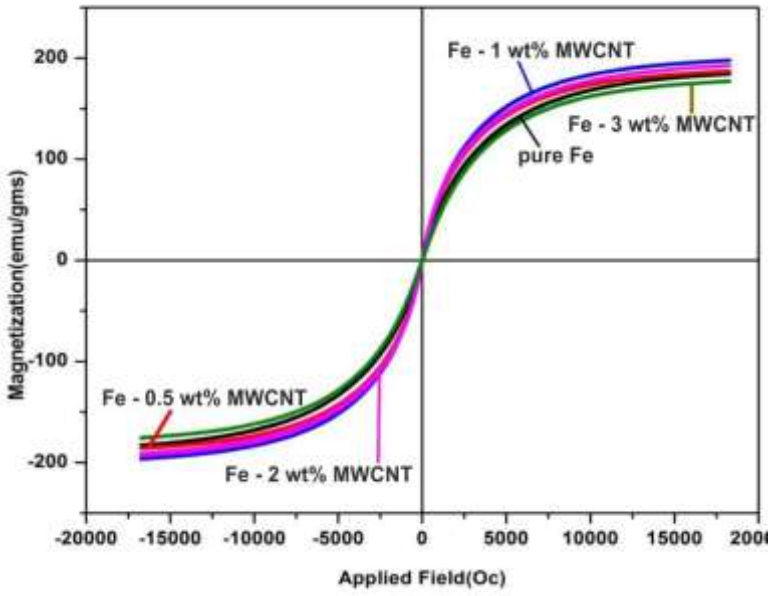


**Figure 8.13** Hysteresis loops of (Fe-MWCNTs) nanocomposites with different weight percentof MWCNTs in Fe after HEBM at room temperature.

The VSM test results are presented in Table 8.6. It is apparent that the saturation magnetization of the composites is increased up to 1 wt.% MWCNT beyond which it is seen to decrease. It is a general observation that ball milling of pure iron leads to deterioration of saturation magnetization due mainly to the internal strain created by ball milling [11].

**Table 8.6.**Magnetic properties of Fe-MWCNT nanocomposites

| Samples Name | Saturation Magnetization,(Ms)(emu/gms) | RemanentMagnetization (Mr)(emu/gms) | Coercivity( Hc) (Oe) |
|---|---|---|---|
| Pure Fe | 184 | 0.21 | 3.2 |
| Fe-0.5wt.%MWCNT | 187 | 0.30 | 4.26 |
| Fe-1wt.%MWCNT | 197 | 0.47 | 7.23 |
| Fe-2wt.%MWCNT | 192 | 0.49 | 8.12 |
| Fe-3wt.%MWCNT | 177 | 0.59 | 10.23 |

In contrast, in our experiments with Fe-MWCNT composite, an improvement in saturation magnetization is noted up to 1wt.% MWCNT. There is overall improvement of 7% in saturation magnetization in the experimental composites. Beyond 1 wt.% MWCNT, the saturation magnetization goes below that of the pure iron. On the other hand, coercivity and remnant magnetism continuously increases with increasing MWCNT content. It is pertinent to remember that the strain may be fully relieved in the SPS samples.Although MWCNTs are reported to behave as diamagnetic many where [17-18], the MWCNT used in this investigation are produced by CVD technique by the use of iron as catalyst. In such cases MWCNTs become ferromagnetic. Microstructural studies have indicated that MWCNTs are well embedded into the matrix. HEBM composite powders envisaged more or less uniform distribution. The TEM observation of SPS sample gives evidence of fine scale distribution MWCNTs in the matrix of iron. It is demonstrated earlier that if the surface of multiwall carbon nanotube is adhered by the magnetic particles, it increases the magnetic susceptibility of the above MWCNT [19]. In the present case, the MWCNTs have very good interfacial bonding even without the formation of iron carbide at the interface. High resolution micrograph shows an interface region which is clean and smooth. Such type of interface is as good as a sheath of iron over the surface of MWCNT. This improves magnetic susceptibility. At the same time MWCNTs are themselves ferromagnetic. It is seen that MWCNT forms network around the crystallites. The presence of CNT at the crystal boundaries is beneficial for improving remnant magnetism. Once the magnetic field is withdrawn, domain alignment along the applied field gets destroyed. However presence of MWCNT restricts domain boundary rotation and as a result remnant magnetism is increased. Higher weight percent of MWCNT implies higher

population density of MWCNT within the iron matrix and so the effectiveness in restricting the domain boundary movement to assume random orientation after withdrawal of externally applied magnetic field is increased. Higher remnant magnetism is helpful to obtain high saturation magnetization, although it can be seen from the results of Table 8.6 saturation magnetization starts to decrease when MWCNT content in composite is 2 wt.% or above. Due to the presence of uniformly distributed MWCNT, the domains after being favorably aligned along the externally applied field cannot revert back to their original random configuration due to the restriction of domain boundary movement by the MWCNTs, unless a reverse field is applied. Thus coercivity is improved.

### *8.3.11 TEM Analysis*

Transmission electron microstructure of iron-1wt. % MWCNT composite shows that MWCNTs are embedded well within the matrix phase and that MWCNTs have conserved their tubular structure(figure8.14).

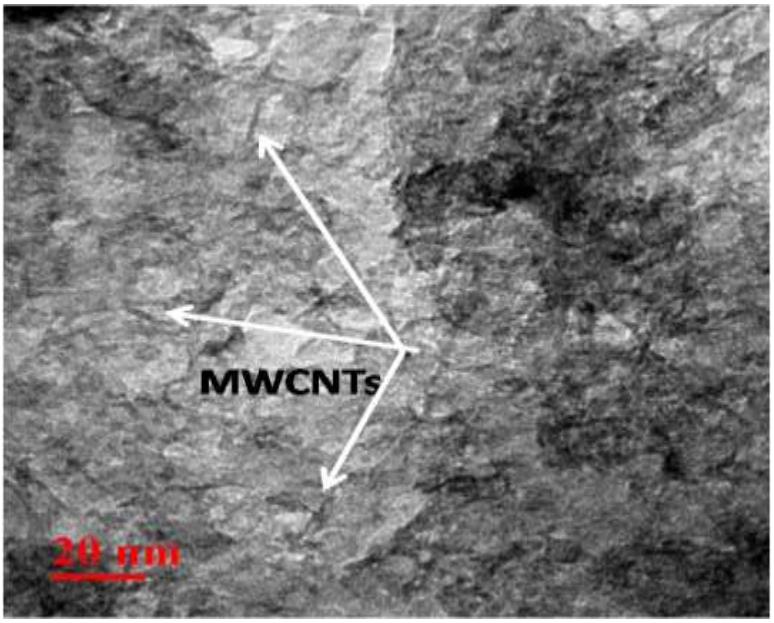


**Figure 8.14** Bright field image of 1wt.%MWCNT composite showing embedded MWCNTs.

It is further revealed from the same photograph that small sub grain like structure is formed; it is also discerned that MWCNTs are present at the boundaries of the crystal. For such a low amount of MWCNT in composite (~1wt. %), the interface between the matrix and MWCNT is found to be quite clean and no other phase is seen to have formed at the interface (Figure8.15).

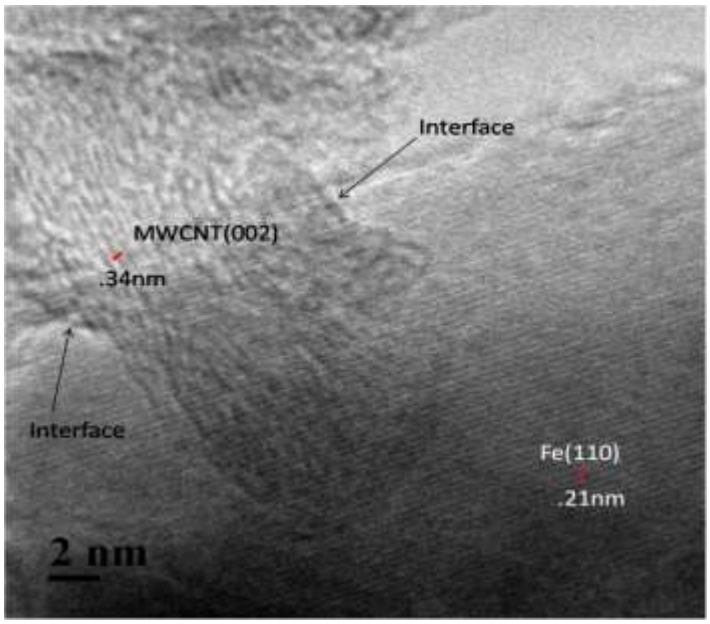


**Figure 8.15** High resolution transmission electron metallography of Fe-1wt.% MWCNTs nanocomposite; shows a clean interface.

However, at some other place of the same foil, formation of cementite adjacent to MWCNT is also noticed in HRTEM photograph. It shows the inter planer spacing of the phase to be around 0.38nm which is similar to (011) of orthorhombic cementite (figure 8.16).

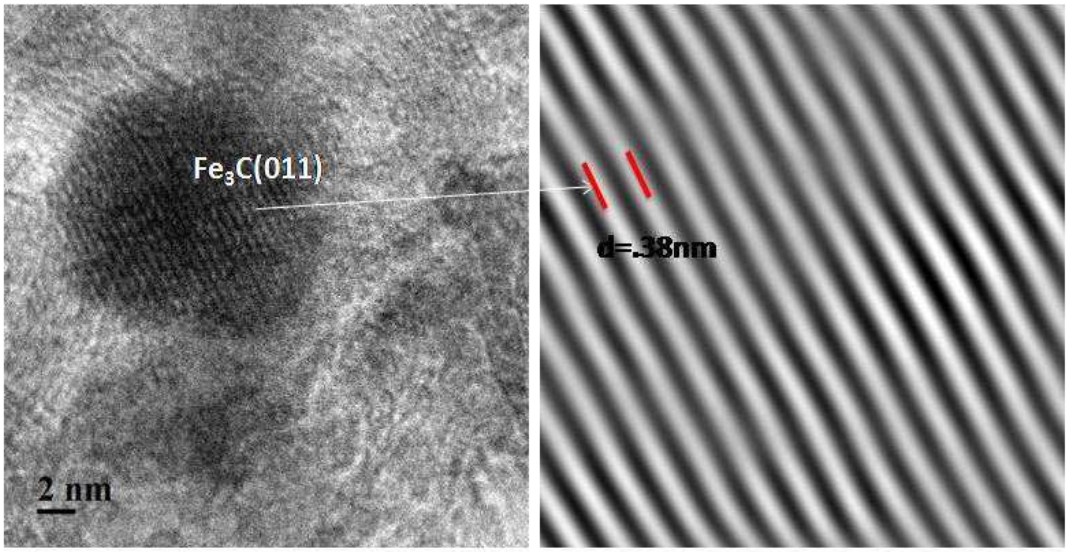


**Figure 8.16** HRTEM of Fe- 1 wt.%MWCNT composite giving evidence of cementite formation

The above observation is further supported the evidence available in figure8.17 which clearly delineates that cementite is formed at interface between iron matrix and reinforcing MWCNT. The identification of phases is done by the inter planar spacing measurement from the corresponding lattice images.

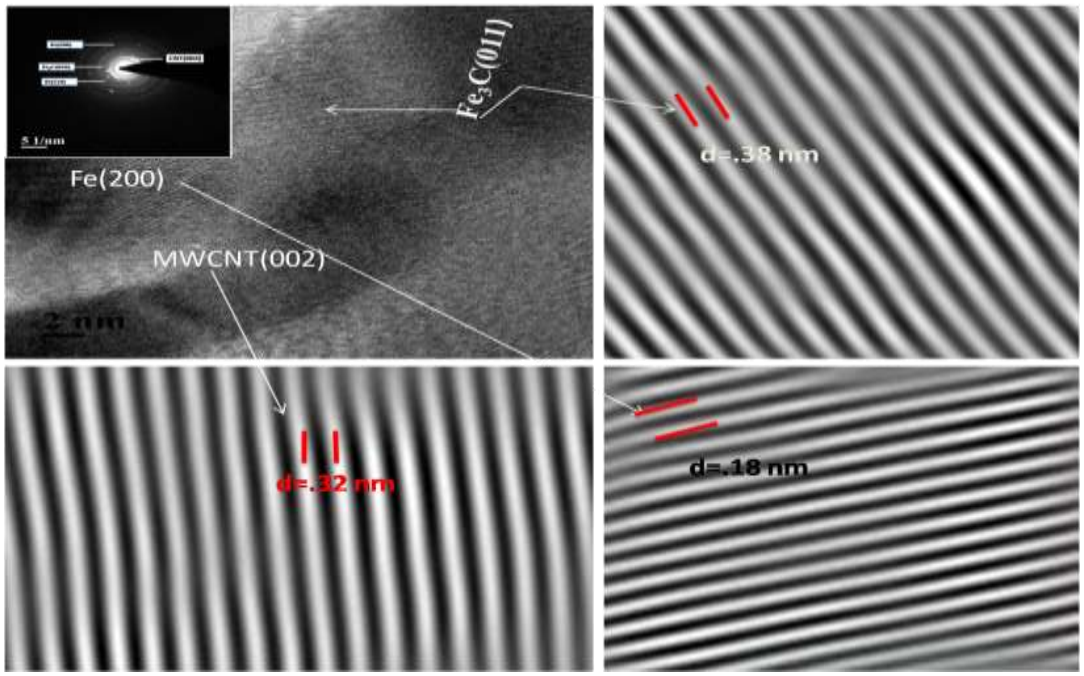


**Figure 8.17**HRTEM of Fe- 1wt.%MWCNT composite showing cementite at the iron-MWCNT Interface. Inset shows the SAED which exhibits cementite reflections. (Corresponding d spacing)

It is known that carbon can extensively dissolve in iron and during sintering at $650^0$C; the carbon atoms of MWCNT can react with iron to form $Fe_3C$. However for this composite (1wt.%MWCNT), no cementite peak could be traced in XRD spectrum, rather there is the evidence of large amount of carbon remaining dissolved in iron. From the present microscopic observation it may be stated that the MWCNTs conserve its crystalline structure in most of the regions. However, there are some places where very small sized $Fe_3C$ is formed in SPS sample and the quantity might be below the detection limit of XRD. Thus SPS has led to some degradation in MWCNT unlike in case of other transition metal matrix. As expected, the carbide is formed at the MWCNT-iron interface. Heavy dissolution of carbon in iron may be responsible for precipitation of $Fe_3C$ during the post SPS cooling. Although it is expected that super saturation of carbon in ferrite may be relieved through precipitation of carbide in accordance with equilibrium diagram of iron

carbon system, in reality it has not been so due to paucity of time (sintering time was kept very low and cooling rate was high).Nevertheless minor quantity of carbide formation could not be avoided; besides, high resolution TEM image and the cementite reflections noted in SAED in the inset of Figure 8.17(a)confirms the presence of carbide in the microstructure.

It appears from the HRTEM image of iron-3wt.%MWCNT that the interface between iron matrix and MWCNT is highly diffused(figure8.18a); this suggests that MWCNT has undergone a good degree of damage at the outer wall; nevertheless, the image verifies that amorphisation of MWCNT with its complete destruction of graphitic structure is not possible; HRTEM image records the wall thickness of MWCNT to be 0.33nm, which is quite close to the theoretically reported value of 0.34nm.Although multiwall structures are seen, mostly they are strained at many places and are seen to lose contrast; this means that MWCNT structure is destroyed at the outer walls. The concerned HRTEM in figure18(a) shows MWCNT adjacent to the matrix. The arrow marked region denotes that MWCNT is considerably damaged at the interface leading to amorphisation which is also evident from Raman spectroscopic result.

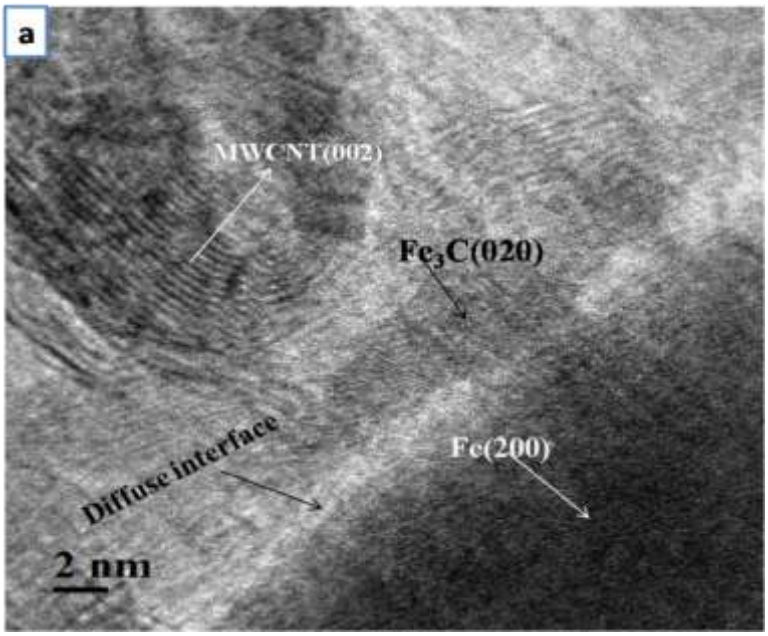


**Figure 8.18** (a) HR-TEM image of iron-3 wt.% MWCNT composite showing structural damage at the interface.

The EDS analysis(figure8.18b) also confirms that there has been negligible amount of oxygen and that MWCNT structure has degraded and carbon atoms have diffused into the iron rich region(arrow in point mapping).

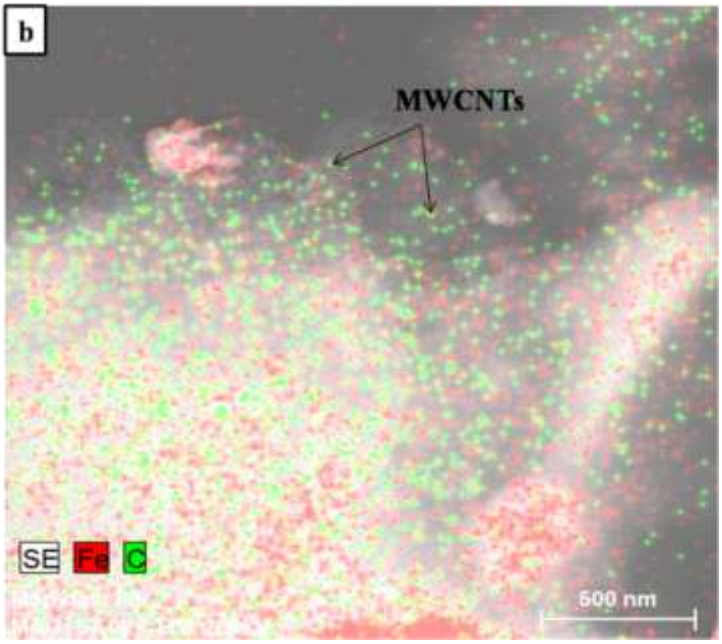


**Figure 8.18** (b) EDS analysis of Fe-3wt.% MWCNT

Figure 8.19 makes it evident that at higher MWCNT concentration interfacial reaction is inevitable. The image clearly discerns that precipitation of carbide has taken place at the interface between MWCNT and ferrite.

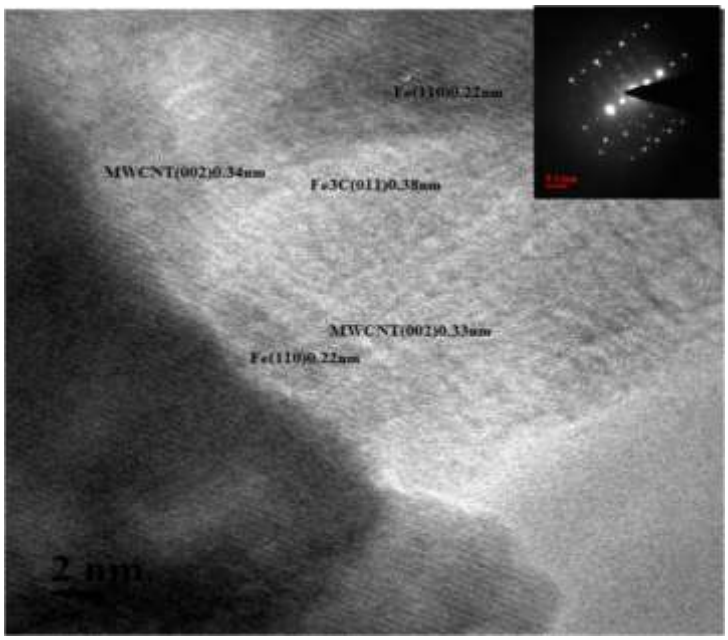


**Figure 8.19** HRTEM image of Fe- 3 wt.% MWCNT composite showing interfacial carbide.(Inset shows the SAED) which exhibits both ferrite and cementite reflections

As stated earlier, that at 3 wt.%MWCNT level, MWCNT goes in solution in ferrite and during cooling fine scale precipitation of $Fe_3C$ becomes unavoidable. SAED in the inset of figure8.19 shows both ferrite and cementite reflections. The ferrite reflections are indexed as B=Z= ( $\bar{1}$2 2)

## 8.4 Conclusions

From the foregoing results and discussions the following conclusions are drawn: High energy ball milling of iron-MWCNT composites for 2h tends to cause flattening of iron matrix by plastic deformation; tendency towards flattening is lessened with increasing amount of MWCNT. The reinforcing MWCNTs are well embedded into iron matrix after 2h milling; increasing MWCNT content degrades quality of dispersion of MWCNT and increases the tendency for agglomeration of MWCNT. The matrix particles are strained and contains appreciable amount of dislocations after ball milling for 2h. The MWCNT forms a 2D network around the particles of plastically deformed iron matrix.

Spark plasma sintering leads to recrystallization of grains leading to the formation of smaller grains. The grain refinement by recrystallization is less for composites of higher MWCNT content. The grain size increases with increasing MWCNT content. At high MWCNT content the microstructure of spark plasma sintered composites exhibit lamellar structure at the grain boundaries; degradation of MWCNT during SPS leads to formation of high carbon FCC phase at the sintering temperature; this undergoes discontinuous precipitation during post SPS cooling and leads to the formation of lamellar structure.

High energy ball milling for two h leads to the formation of cementite in the microstructure of composites with MWCNT content above 2 wt.%; spark plasma sintering leads to further damage of MWCNT structure and aggravates cementite formation from 2 wt.% MWCNT and higher in iron matrix. The degradation of MWCNT structure produces amorphous carbon which dissolves into iron and leads to an increase in its lattice parameter. Beyond a definite degree of super saturation at high MWCNT content, precipitation of cementite takes place. Increasing MWCNT content from 2 to 3 wt.% leads to a significant structural degradation of MWCNT.

Formation of cementite is aggravated due to SPS even at the level of 2 wt.% MWCNT. Structural degradation of MWCNT manifests by the formation of iron carbide. Hardness of iron-MWCNT composite increases with increase in MWCNT content; a marginal fall in hardness takes place at 3 wt.% MWCNT. At high MWCNT content contribution from MWCNT decreases due to structural degradation and agglomeration of MWCNTs after ball milling followed by SPS.

Compressive strength of the composites increases continually with increasing MWCNT content; the increase in strength is more than 100% at 2wt. % MWCNT or more. The tolerable compressive strain is higher than 50% at a level of compressive strength of 1045 MPa in the case of iron -3wt.% MWCNT composite. Saturation magnetization increases by about 7% over that of pure iron by reinforcing with MWCNT. The increase continues till 1 wt. % MWCNT beyond which it starts to decrease. The saturation magnetization attains the value below that of pure iron in case of 3 wt.% MWCNT composite.

Remnant magnetization and coercivity continuously increase above the values for pure iron with increasing reinforcement content. MWCNT structure in experimental composites is mostly conserved after two h HEBM followed SPS. Due to excellent bonding, the interface between matrix and MWCNT for 0.5 wt.% MWCNT content remains free from contamination or any reaction product viz. carbide of iron. Increasing the MWCNT content leads to very fine scale precipitation of cementite at the iron-MWCNT interface; moreover the bonding for composites of all composition has been quite good. SPS leads to disruption of bonds in MWCNT and the carbon atoms so released diffuse into iron crystals.

## REFERENCES


[1] R. George, K.T. Kashyap, R. Rahul, S. Yamadagni, Strengthening in carbon nanotube/ aluminum (CNT/Al) composites, Scripta Mater 5 (2005) 1159–1163.

[2] R. Perez-Bustamante, I. Estrada Guel, W. Antunez-Flores, M. Miki Yoshida, P.J. Ferrira, Novel Al-matrix nanocomposites reinforced with multi-walled carbonnanotubes, J. Alloys Compd. 450 (2008) 323–326.

[3] A.M.K. Esawi, K.Morsi, A. Syed, A. Gawad, P. Borah, Fabrication and properties of dispersedcarbon nanotube-aluminum composites, Mater. Sci. Eng. A 508 (2009)167–173.

[4] L.Wang, H. Choi, J.M. Myoung, W. Lee, Mechanical alloying of multi-walled carbon nanotubes and aluminum powders for the preparation of carbon/metal composites, Carbon 47 (2009) 3427–3433.

[5] D. Poirier, R. Gauvin, R.A.L. Drew, Structural characterization of mechanically milled carbon nanotube/aluminum mixture, Compos. A.Appl. Sci. Manuf. 40 (2009) 1482–1489.

[6] R.P.Bustamante, C. D G. Esparza, I. E. Guel, M. M. Yoshida, Microstructural and mechanical characterization of Al-MWCNT composites produced by mechanical alloying, Mater. Sci. Eng. A 502 (2009) 159–163.

[7] A.M.K. Esawi, K.Morsi, A. Syed, M. Taher, S. Lanka, The influence of carbon nanotube (CNT) morphology and diameter on the processing and properties of CNT reinforced aluminum composites, Compos. A: Appl. Sci. Manuf. 42 (2011) 234–243.

[8] J.Stein, B. Lenczowski, N. Frety, E. Anglaret, Mechanical reinforcement of a high performance aluminium alloy AA 5083 with homogenously dispersed multi-walled carbon nanotubes, Carbon 50 (2012) 2264–2272.

[9] P. Delhaes, M. Couzi, M. Trinquecoste, J. Dentzer, H. Hamidou, C. Vix-Guter, A comparison between Raman spectroscopy and surface characterizationsof multiwall carbon nanotubes, Carbon 44 (2006) 3005–3013.

[10] L. Jiang,L. Gao, J.Sun. Production of aqueous colloidal dispersions of carbon nanotubes, J. Colloid Interface Science 2003; 260: 89–94

[11] B.Hea, M. Wang, W. Sun, Z. Shen, Preparation and magnetic property of the MWNT-$Fe2^{+}$ composite, Materials Chemistry and Physics 95 (2006) 289–293.

[12] J.Y. Suh, D.H. Bae, Mechanical properties of Fe-based composites reinforced with multi-walled carbon nanotubes, Materials Science & Engineering A 582 (2013) 321–325.

[13] S. Huang, O. Van der Biest, L. Li, J. Vleugels, Properties of NbC–Co cermets obtained by spark plasma sintering, Mater. Lett. 61 (2) (2007) 574–577.

[14] W. Chen, U. Anselmi-Tamburini, J. Garay, J. Groza, Z.A. Munir, Fundamental investigations on the spark plasma sintering/synthesis process. Effect of dc pulsing on reactivity, Mater. Sci. Eng.: A 394 (1) (2005) 132–138.

[15] W. Tian, K. Vanmeensel, P. Wang, G. Zhang, Y. Li, J. Vleugels, O. Vander Biest, Synthesis and characterization of Cr 2 AlC ceramics prepared by spark plasma sintering, Mater. Lett. 61 (22) (2007) 4442–4445.

[16] K. Vanmeensel, A. Laptev, J. Hennicke, J. Vleugels, O. Van der Biest, Modelling of the temperature distribution during field assisted sintering, Acta Mater. 53 (16) (2005) 4379-4388.

[17] F.C Dillon, A.Bajpai, A.Koos,S. Downes, Z.Aslam, N. Grobert, Tuning the magnetic properties of iron-filled carbon nanotubes, Carbon 50 (2012) 3674-81.

[18] H. Kim, W. Sigmund, Iron particles in carbon nanotubes, Carbon 43 (2005) 1743–1748.

[19] T. Muhl, D. Elefant, A. Graff, R. Kozhuharova, A. Leonhardt, I. Monch, M. Ritschel, P. Simon, S. Groudeva-Zotova, C.M. Schneider, Magnetic properties of aligned Fe-filled carbon nanotubes, journal of Applied physics93 (2003) 7894-7896.

# *CHAPTER NINE*

## *Conclusions*

**The author wishes to draw the final conclusions as follow**

[1] High energy ball milling with tailored process parameters can be effectively used to produce iron-MWCNT composite.

[2] Severe ball milling at high MWCNT content leads to chemical degradation of MWCNT. Mechano-chemical activation leads to the formation of iron carbide at the interface.

[3] A very good interfacial bonding is achievable after ball milling of iron-1 wt.% MWCNT composite for two h.

[4] It is concluded that degree of damage caused to MWCNTs during high energy ball milling of iron -2 wt.% MWCNT powder mix is dependent on milling time and milling of iron-2 wt.% MWCNT composite for 60 min produces optimal damage to MWCNTs reinforcing iron matrix.

[5] Controlled high energy ball milling insures uniform distribution of reinforcing MWCNT in the iron matrix.

[6] Damage of MWCNT takes place in general by partial destruction of C-C bonds of MWCNT; the available carbon atoms segregate at dislocations in nearby iron crystals. These carbon atoms are highly conducive to undergo 3d-2p hybridization and hence aids in achieving a smooth CNT-matrix interface.

[7] A good interfacial structure improves the magnetic properties of Fe-2 wt.% MWCNT nanocomposites in opposition to the expected degradation of saturation magnetization, which is commonly observed in high energy ball milled iron powders.

[8] Presence of carbide at the iron-MWCNT interface is unavoidable in HEBM Fe-2 wt.% MWCNT composite due to high chemical affinity between iron and carbon.

[9] The fabrication technique comprised of controlled HEBM for 50 min followed by SPS at $650^0$C and 50 MPa pressure employed for production of iron-MWCNT composites of varying MWCNT content can preserve the crystallinity of MWCNT as evidenced by is visible (002) CNT peak in XRD spectra of the composites.

[10] Till 3 wt.% MWCNT in the composites, no contamination takes place at the interface of MWCNT and iron crystals when processed as above.

[11] Increase in amount of MWCNT leads to an increase in size of crystallites with concurrent reduction in residual strain.

[12] Composite with MWCNT content as high an amount as 4 wt.% makes MWCNT suffer from perceptible structural degradation at the interface.

[13] High energy ball milling leads to flattening of matrix particle along with visible physical damage viz. shortening of MWCNTs. Physical damage of MWCNT is less at high weight percent of MWCNT for the same ball milling condition.

[14] Fe-MWCNT composite powder subjected to SPS produces homogenous microstructure. With increasing MWCNTs content agglomeration of MWCNTs take place and in sample containing 4 wt.% MWCNTs agglomerated regions assume directional arrangement.

[15] Recrystallization of pre-existing grains takes place during Spark Plasma Sintering. Grain size measurement results indicate that grain size decreases with increase in MWCNT content.

[16] Reinforcement of iron with MWCNTs appreciably improves the microhardness values of the composites. The microhardness values increase quite steeply at low MWCNT content (up to 2 wt.%), then the rise in hardness slows down.

[17] Increasing MWCNT content in composites gives rise to higher compressive strength of the material.

[18] As the MWCNTs is increased to higher values relative decay of C-C bond in MWCNT becomes increased.

[19] It is observed that conductivity of iron increases significantly after reinforcing with MWCNTs. The increase in conductivity is initially small, becomes more intense till 3 wt.% MWCNT beyond which a slower rise in conductivity is caused.

[20] The saturation magnetization of Fe-MWCNT composite increases up to 3 wt.% MWCNTs; its saturation magnetization decreases at a MWCNT level

of 4 wt.%. Remnant magnetization and coercivity properties increase continuously with increasing MWCNT content in the composite

[21] Some dislocations are created due to mismatch in coefficient of thermal contraction between iron matrix and the reinforcing MWCNT.

[22] Under high resolution microscopy it is ascertained that there is carbide formation at Fe-MWCNT interface in 3 wt.% MWCNT composites after Spark Plasma Sintering.

[23] Nano sized pores are produced in 4 wt.% MWCNT composites within the agglomerated MWCNTs

[24] Silver doping in iron-MWCNT composites can conserve the structure of MWCNT better than the undoped alloy

[25] In silver doped composites, no contamination takes place at the interface of MWCNT and iron crystals.

[26] High energy ball milling tends to make matrix particle flattened at low MWCNT content; increasing MWCNT in doped composites do not show much tendency towards flattening.

[27] Silver protects the MWCNT from chemical damage. Physical damage of MWCNT takes place by HEBM.

[28] High energy ball milling followed by Spark Plasma Sintering does not for mchemical synthesis product in silver doped composites.

[29] Conductivity of iron increases remarkably in silver doped composite; the conductivity of silver doped iron-4 wt.% MWCNT composites can achieve conductivity value higher than that of aluminum.

[30] The saturation magnetization of silver doped Fe-MWCNT composite increases by 25 % over that of pure iron for the composite containing 3 wt.% MWCNTs; however, it drops at 4 wt.% MWCNT composite due to pores existing within the agglomerated MWCNTs. Even after drop the value of saturation magnetization remains significantly higher than pure iron. Remnant magnetization and coercivity properties increase continuously with increasing MWCNT content in the composite

[31] HRTEM image of silver doped composites proves that there cannot be chemical contamination at the matrix-reinforcement interface. Silver atoms

tether the surface of MWCNT and act as a coating over the MWCNT. This kind of functionalization produces a very good interfacial bonding for which the physical properties are greatly improved.

[32] The reinforcing MWCNTs are well embedded into iron matrix after two h milling; increasing MWCNT content degrades quality of dispersion of MWCNT and increases the tendency for agglomeration of MWCNT.

[33] The matrix particles are strained and contains appreciable amount of dislocations after ball milling for two h. The MWCNT forms a 2D network around the particles of plastically deformed iron matrix.

[34] At high MWCNT content (~3 wt.%), the microstructure of spark plasma sintered composites (after 2 h HEBM) exhibits lamellar structure at the grain boundaries; degradation of MWCNT during SPS leads to the formation of high carbon FCC phase at the sintering temperature; this undergoes discontinuous precipitation during post SPS cooling and leads to the formation of lamellar structure.

[35] High energy ball milling for two h leads to the formation of cementite in the microstructure of composites with MWCNT content above 2 wt.%; spark plasma sintering leads to further damage of MWCNT structure and aggravates cementite formation from 2 wt.% MWCNT and higher in iron matrix.

[36] The degradation of MWCNT structure produces amorphous carbon which dissolves into iron and leads to an increase in its lattice parameter. Beyond a definite degree of super saturation at high MWCNT content, precipitation of cementite takes place.

[37] Hardness of iron-MWCNT composite increases with increase in MWCNT content; a marginal fall in hardness takes place at 3 wt.% MWCNT. At high MWCNT content contribution from MWCNT decreases due to structural degradation and agglomeration of MWCNTs after ball milling followed by SPS.

[38] Compressive strength of the composites increases continually with increasing MWCNT content; the increase in strength is more than 100 % at 2 wt.% MWCNT or more. The tolerable compressive strain is higher than 50%

at a level of compressive strength of 1045 MPa in the case of iron -3 wt.% MWCNT composite.

[39] Saturation magnetization increases by about 7% over that of pure iron by reinforcing with MWCNT. The increase in saturation magnetization of 2hrs milled samples continues till 1 wt.% MWCNT beyond which it starts to decrease. The saturation magnetization attains the value below that of pure iron in case of 3 wt.% MWCNT composite.

[40] Due to excellent bonding, the interface between matrix and MWCNT for 0.5 wt.% MWCNT content remains free from contamination or any reaction product viz. carbide of iron even after 2h milling followed by sintering.

[41] SPS of 2 h ball milled composite leads to disruption of bonds in MWCNT and the carbon atoms so released diffuse into iron crystals.

# List of publications from research work

**International Conference publication**

1. **Akshay Kumar, U.Pandel, M.K.Banerjee "**Production of Iron –Multiwall Carbon Nanotubes (CNT) Composite by Mechanical Alloying''International Journal of Engineering Technology Science and Research Vol.4 (2017) ISSN 2394 – 3386.

2. **Akshay Kumar, M.K.Banerjee, U.Pandel"**Effect on Mechanical Properties of Fe-MWCNTNanocomposites after Vary the Weight present of MWCNTs prepared by High Energy Ball Milling" International Journal of Engineering Technology, Management and Applied Sciences. Vol. 5(2017) ISSN 2349-4476

**Under review in international journal**

1. **Akshay Kumar, U. Pandel M.K. Banerjee**" Effect of High Energy Ball Milling on the structure of iron –multiwall carbon nanotubes (MWCNT) composite" Advances in Materials Research, ***under review***

2. **Akshay Kumar, M.K. Banerjee, U. Pandel**Development of a novel MWCNT reinforced iron matrix Nanocomposite through powder metallurgy route.(to be submitted)

**PATENT**

**Akshay Kumar, M.K. Banerjee,U.Pandel"A Metal Matrix Nanocomposite (Conducting Magnet) and Process of Synthesis of Nanocomposite by High Energy Ball Milling**" (51) International classification :B02C23/06 (31) Priority Document No :NA (32) Priority Date :NA (33) Name of priority country :NA (86) International Application No Filing Date :NA :NA (87) International Publication No: NA (61) Patent of Addition to Application Number Filing Date :NA :NA (62) Divisional to Application Number Filing Date :NA :NA (71).

# ABSTRACT

The thesis entitled **"Development of Technology for Production of Iron-MWCNT Carbon Nanotubes Composite as a Conducting Magnetic Material"** deals with development of technology for production of MWCNT reinforced iron matrix composites with improved physical and mechanical properties. The work contemplates to evolve means to accrue the potential benefit of reinforcing iron matrix with MWCNTs having fascinating physical and mechanical properties. The major constraints in meeting the challenges of introducing MWCNTs within iron matrix, are duly identified through extensive literature survey. Noting that high energy ball milling, also referred as mechanical alloying, is the proven technique for production of metal matrix-MWCNT composites; the optimization of ball milling parameters is attempted. Varying concentration of MWCNTs with different process control agents are used for the preparation of iron matrix composites by initially fixing two hours as the milling time. Structural and property characterization of high energy ball milled composites has shown that beyond 1 wt.% MWCNT in iron, high energy ball milling (HEBM) leads to structural damage and chemical synthesis of iron and carbon and forms iron carbide. However, within the limit of 1 wt.% MWCNT containing composite, the uniform dispersion of reinforcement and its good interfacial bonding has been achieved.

Noting that the milling time of two hours is deterring to conservation of MWCNT structure at its higher concentration, studies have been conducted to optimize the milling time for iron-2 wt.% MWCNT composites such that structural integrity of MWCNT can be maintained without affecting the soundness of interfacial bonding and the uniformity of dispersion of MWCNT within iron matrix. Iron matrix-2 wt.% MWCNT composite has been subjected to high energy ball milling for various periods of time and the effect of milling time on retention of structural integrity of MWCNT and as well on its magnetic property has been examined. It is noticed that structural degradation of MWCNT can be avoided till 60 min of HEBM. It is verified that controlled HEBM leads to optimal damage at the surface of MWCNT which makes carbon atoms available for undergoing 2p-3d hybridization. Moreover, it can be found that ball milling for more than one hour leads to significant damage of MWCNT. However, ball milling for 1h ensures 11% improvement in saturation magnetization over the theoretical value for pure iron along with appreciable hike in remnant magnetism and coercivity.

It has been observed that high energy ball milling for 1h with the parameters fixed here has been successful in making MWCNT in Fe-2 wt.% MWCNT survive from severe damage due to harsh milling conditions. With this background further study is conducted to find the effect of amount of MWCNT on the structural stability and attainable mechanical and physical properties of the consolidated composites. The consolidation of powder composite is done by spark plasma sintering method which is known to be quite effective in conserving the MWCNT structure. It is observed that highly dense compact is obtainable by spark plasma sintering; when its process parameters are controlled, the interfacial reaction between iron and the carbon of MWCNT can be minimized. There is increase in hardness and compressive strength of the composites with increasing MWCNT content; also, magnetic properties are greatly improved till 3 wt.% beyond which degradation in saturation magnetization is noticed. There has been a great improvement in electrical conductivity with increasing MWCNT and it is possible to attain electrical conductivity of iron based composite equal to electrical grade aluminum with magnetic properties far better than pure iron. This result has stimulated to study the effect of silver doping on structure and properties of these composites. It is found that silver protects the MWCNT structure from physicochemical damage due to ball milling by forming a tethered layer on the MWCNT surface. The electrical conductivity becomes appreciably better than aluminum and concomitantly, remarkable improvement of magnetic properties is achieved. To understand the exact role of spark plasma sintering of high energy ball milled powders at different level of MWCNT content, similar experimentation is carried out in a more aggressive environment by increasing the milling time to two hours. The results show improvement in mechanical properties but magnetic properties have been degraded beyond 1 wt.% MWCNT. It is further observed from XRD, Raman spectroscopy, XPS and FTIR that structural degradation is enhanced over the ball milled materials during spark plasma sintering (SPS). This means that SPS aggravates the damage of MWCNT at its higher concentration mainly by forming iron carbide at the interface. HRTEM study has been supportive to all other observations; it is therefore concluded that iron-MWCNT composites can be effectively fabricated by HEBM plus SPS route by proper control of process parameters and finally these can create a material whose conductivity is greater than aluminum and magnetic properties are far superior to pure iron. The question finally remains to answer is 'should we call it a conducting magnet!'

# CONTENTS

# LIST OF FIGURES

# LIST OF TABLES

# LIST OF ABBREVIATIONS

| | |
|---|---|
| MMC | Metal Matrix Composite |
| MA | Mechanical Alloying |
| MWCNT | Multi Wall Carbon Nanotube |
| SWCNT | Single Wall Carbon Nanotube |
| HEBM | High Energy Ball Milling |
| SPS | Spark Plasma Sintering |
| XRD | X-Ray Diffraction |
| FE- SEM | Field Emission SEM Scanning Electron Microscopy |
| TEM | Transmission Electron Microscopy |
| XPS | X- Ray photoelectron Spectroscopy |
| VSM | Vibrating Sample Magnetometer |